Electronic Supplementary Information

Oxygen transfer reactivity mediated by nickel perfluoroalkyl complexes using molecular oxygen as a terminal oxidant

Shubham Deolka,[a] R. Govindarajan,[a] Eugene Khaskin,[a] Serhii Vasylevskyi,[a] Janet Bahri,[a] Robert R. Fayzullin,[b] Michael C. Roy,[a] and Julia R. Khusnutdinova*[a]

[a]Okinawa Institute of Science and Technology Graduate University, 1919-1 Tancha, Onna-son, Okinawa, 904-0495, Japan

[b] Arbuzov Institute of Organic and Physical Chemistry, FRC Kazan Scientific Center, Russian Academy of Sciences, 8 Arbuzov Street, Kazan 420088, Russian Federation

Table of Contents

Synthetic procedures

All reactions were performed using standard Schlenk or glovebox techniques under a dry nitrogen or argon atmosphere if not indicated otherwise. All chemicals unless noted otherwise were purchased from major commercial suppliers (TCI, Sigma-Aldrich and Nacalai Tesque) and used without purification. Anhydrous solvents were dispensed from an MBRAUN solvent purification system and degassed prior to use. Anhydrous deuterated solvents were purchased from Eurisotop and stored over 4 Å molecular sieves. $[Ni(MeCN)_2(C_2F_5)_2]$[1] and $[Ni(MeCN)_2(C_3F_7)_2]$[2] were prepared according to the literature procedures. The ligand **L3** was previously reported in the literature and was prepared according to the published procedures.[3 4 5-6] All the metal complexes were prepared under a nitrogen atmosphere in a glovebox, except some cases described in the procedures. Specification of syringe filters used in this study is 32 mm nylon membrane with 0.45 μm pore size. Labeled oxygen gas cylinder was purchased from TAIYO NIPPON SANSO with > 98 atom% ^{18}O.

Instrumentation: NMR spectra were measured on JEOL ECZ600R 600MHz, JEOL ECZ400S 400 MHz and Bruker Avance III Neo 500 MHz (CryoProbe) spectrometers. The following abbreviations are used for describing NMR spectra: s (singlet), d (doublet), t (triplet), br, s (broad singlet), vd (virtual doublet), vt (virtual triplet), br (broad). A typical Evans method magnetic moment measurement was done in coaxial tube containing the solvent and the internal standard.[7]

Electrospray Ionization Mass Spectrometry (ESI-MS) measurements were performed on a Thermo Scientific ETD apparatus. Elemental analyses were performed using an Exeter Analytical CE440 instrument. FT-IR spectra were measured using an Agilent Cary 630 with an ATR module in an argon-filled glovebox. The following abbreviations are used for describing FT-IR spectra: s (strong), m (medium), w (weak), br (broad). Absorbance UV/vis spectra were collected using an Agilent Cary 60 instrument.

X-band EPR spectra were recorded using X-band JEOL JES-X330 instrument. For low temperature measurements, liquid nitrogen-cooled cryostat was used and the samples were measured in 5 mm diameter quartz tubes; for room temperature samples, 50 μL quartz capillary tubes were used. Simulation of the experimental spectrum were done using the Easyspin package v. 5.2.35[8] in Matlab R2016b.[9] "Pepper" and "Garlic" functions were used for anisotropic and isotropic spectra simulation, respectively; least-square fitting procedure was utilized to optimize simulation parameters (esfit function, Levenberg-Marquardt algorithm).

Electrochemical grade tetrabutylammonium tetrafluoroborate ($^nBu_4NBF_4$) from Sigma-Aldrich was used as the supporting electrolyte in anhydrous MeCN as a solvent. Cyclic voltammetry and control potential electrolysis experiments were performed on an ALS CHI 660E electrochemical workstation. The electrochemical measurements were done under an N_2 blanket. A platinum disk electrode (d = 1.6 mm) was used as a working electrode. A non-aqueous Ag-wire reference electrode assembly was filled with 0.01M $AgNO_3$ in 0.1 M $^nBu_4NClO_4$/MeCN solution as a reference electrode. A Pt-wire was used as an auxiliary electrode. The reference electrode was calibrated against $FeCp_2$ (Fc), where the Fc/Fc^+ couple vs $Ag/AgNO_3$/MeCN.

Qualitative Fluoride test paper for fluoride: 20 mg/L detection limit for fluoride anion purchased from MACHEREY-NAGEL.

Gel permeation chromatography (GPC) measurements were performed using Shimadzu Prominence-i HPLC setup equipped with Shodex KD-804 column operating at 40 °C with LiBr DMF solution (20 mM) as the mobile phase at 1 mL/min flow rate. The calibration curve was

obtained by PEG analytical standards (Mw: 1,000, 8,000, 40,000, and 128,000) supplied by Sigma-Aldrich.

Synthesis of 1

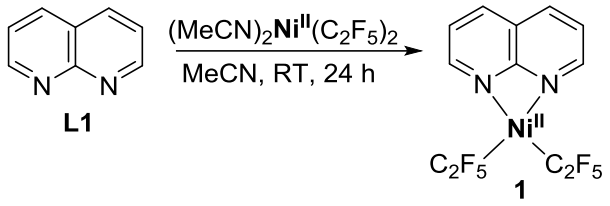

Scheme S1. Synthesis of **1**.

Inside the glovebox, a 20 mL vial equipped with a magnetic stirring bar was charged with $(MeCN)_2Ni(C_2F_5)_2$, (607.7 mg, 1.604 mmol) and **L1** (208.8 mg, 1.604 mmol), MeCN (4 mL) were added to give a yellow color solution. The reaction was left to stir at room temperature for 24 hours. Further, the reaction mixture was passed through a syringe filter to another 20 mL vial. Later the solvent was removed under vacuum and the desired complex was extracted with THF (20 mL) to obtain the yellow solution in a 100 mL flask. The solvent was removed under vacuum to obtain the yellow powder, which was further washed with cold pentane (5 x 2 mL). The powder was dried under vacuum for 24 hours to yield complex **1** as a yellow solid (395.3 mg, 0.926 mmol, 58% yield). Crystals suitable for X-ray diffraction study were grown by vapor diffusion method in THF/cyclohexane mixture, where cyclohexane slowly diffused to the THF solvent.

^{1}H NMR (600 MHz, CD_2Cl_2, 23 °C) δ 8.66-8.36 (m, 4H, CH_{Naph}), 7.77-7.56 (br m, 2H, CH_{Naph}). ^{1}H NMR (400 MHz, CD_3CN, 23 °C) δ 9.06-8.66 (br m , 2H, CH_{Naph}), 8.62-8.27 (br m, 2H, CH_{Naph}), 7.80-7.41 (br m, 2H, CH_{Naph}). The broadened NMR signals did not resolve at low temperature. (see below).

^{13}C{^{1}H} NMR (151 MHz, CD_2Cl_2, - 38 °C) δ 157.54 ($C_{q\ Naph}$), 151.66 (CH_{Naph}), 138.48 (CH_{Naph}), 125.08 (CH_{Naph}), 120.39 ($C_{q\ Naph}$). The C_2F_5 peaks could not be identifies due to broadening present even at low temperature and low signal intensity due to splitting.

^{19}F NMR (565 MHz, CD_2Cl_2, - 38 °C) δ -81.56, -106.39.

HRMS (ESI) calculated for $[M\text{-}C_2F_5]^+$ $C_{10}H_6F_5N_2Ni$: 306.9799; found, 306.9803.

FT-IR (ATR, solid): 2980 (s), 2867 (br, m), 1614 (s), 1502 (s), 1416 (s), 1298 (m), 1169 (s), 1083 (s), 904 (s), 797 (s), 730 (s) cm^{-1}.

UV-vis (MeCN), λ, nm (ε, $M^{-1}\cdot cm^{-1}$) : 307 (1715), 302 (1750), 254 (1965), 207 (16639).

Elemental Analysis: Expt (Calc): [$C_{12}H_6F_{10}N_2Ni$]: C 34.01 (33.76), H 1.79 (1.42), N 6.58 (6.56).

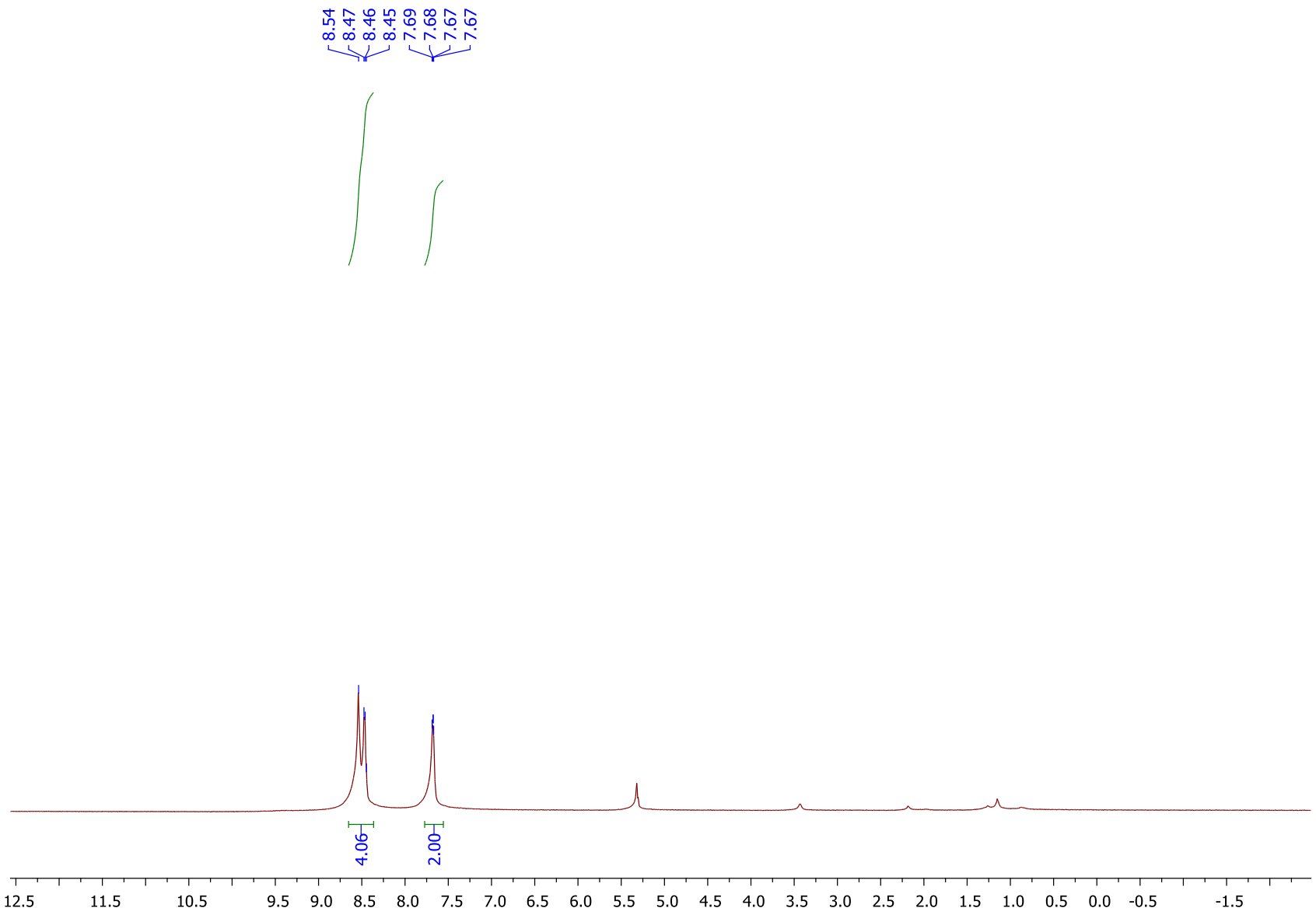

Figure S1. ^{1}H NMR spectrum of **1**· in CD_2Cl_2 at 23 °C.

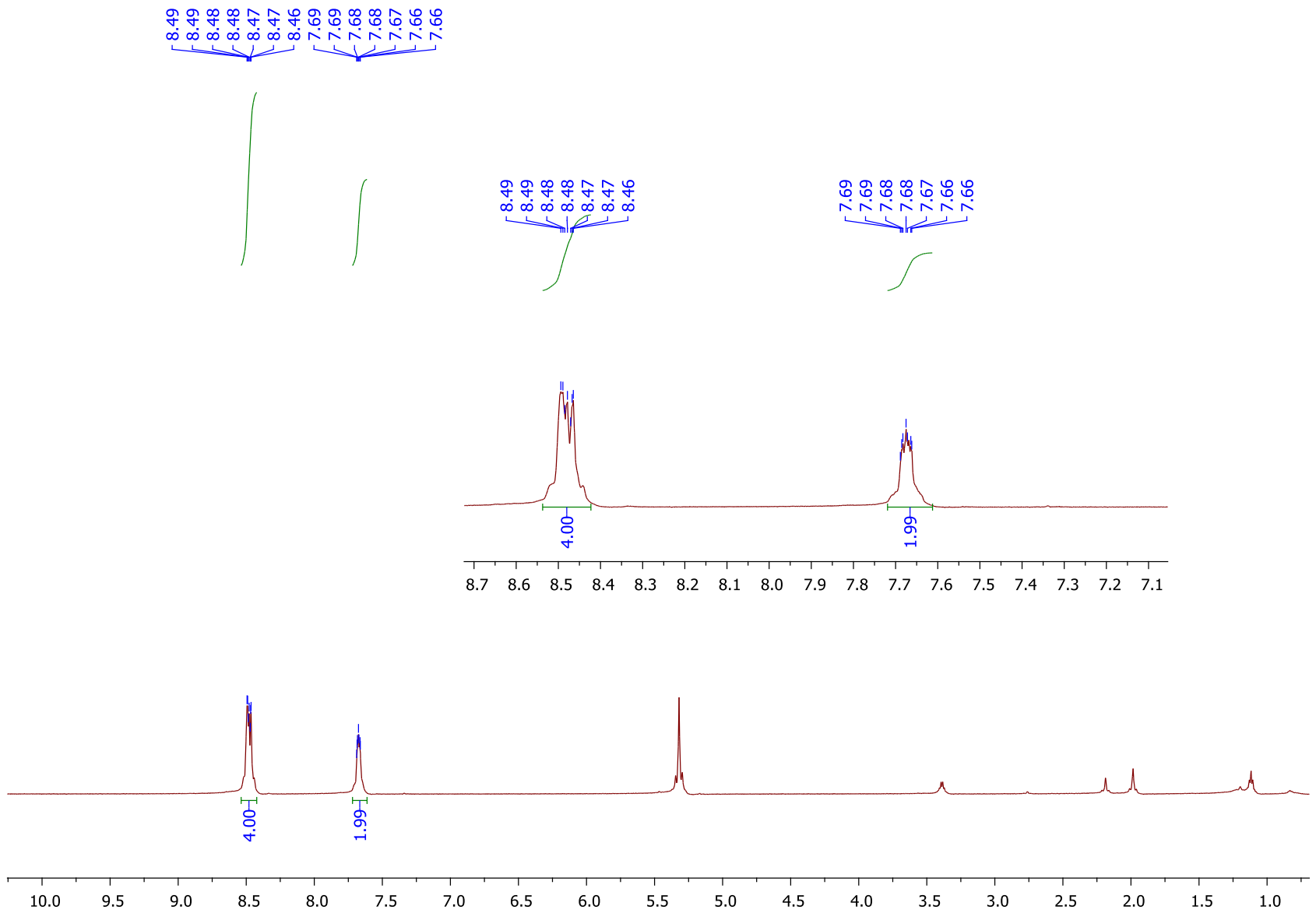

Figure S2. ^{1}H NMR spectrum of **1**· in CD_2Cl_2 at -38 °C.

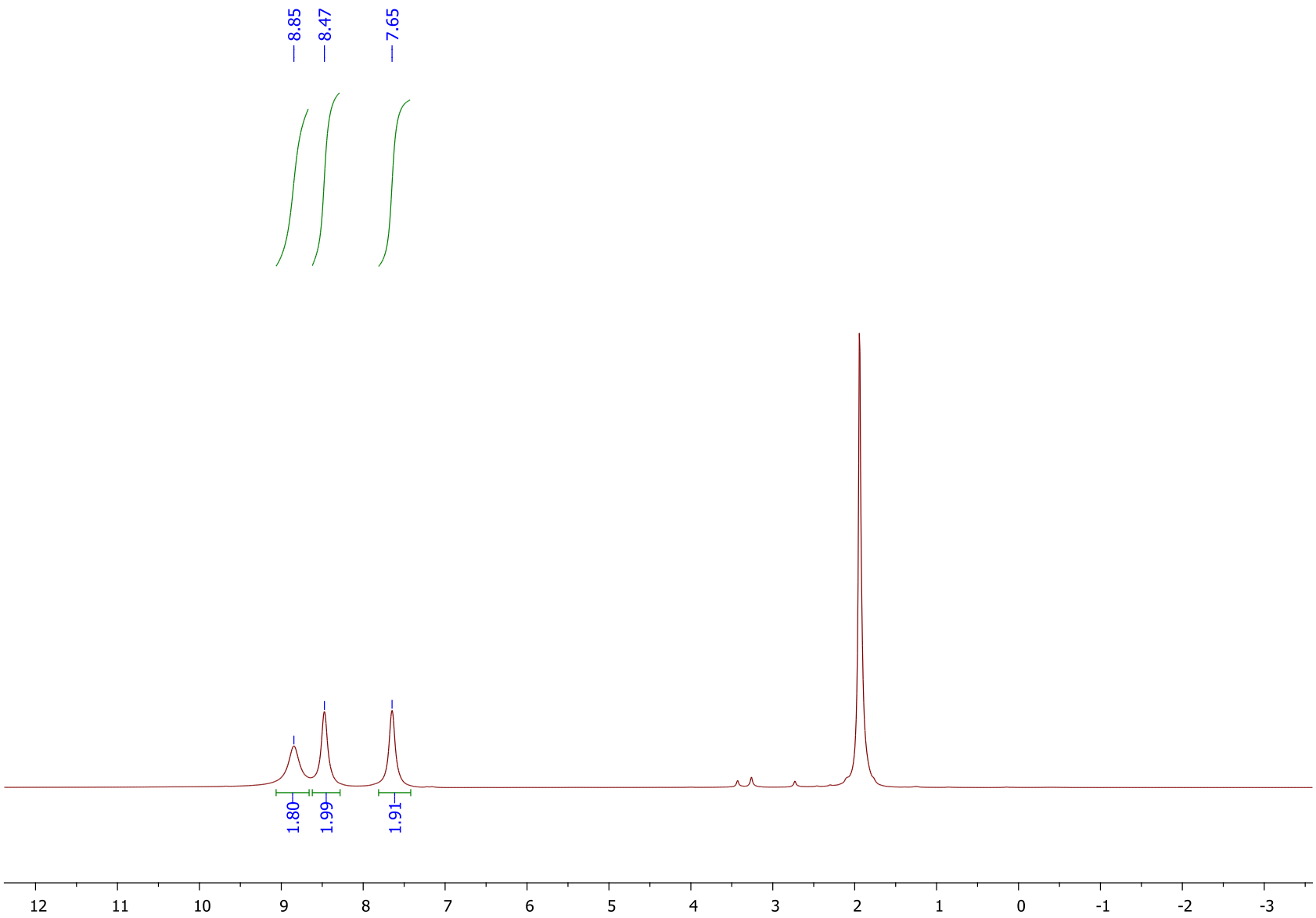

Figure S3. ^{1}H NMR spectrum of **1**· in CD_3CN at 23 °C.

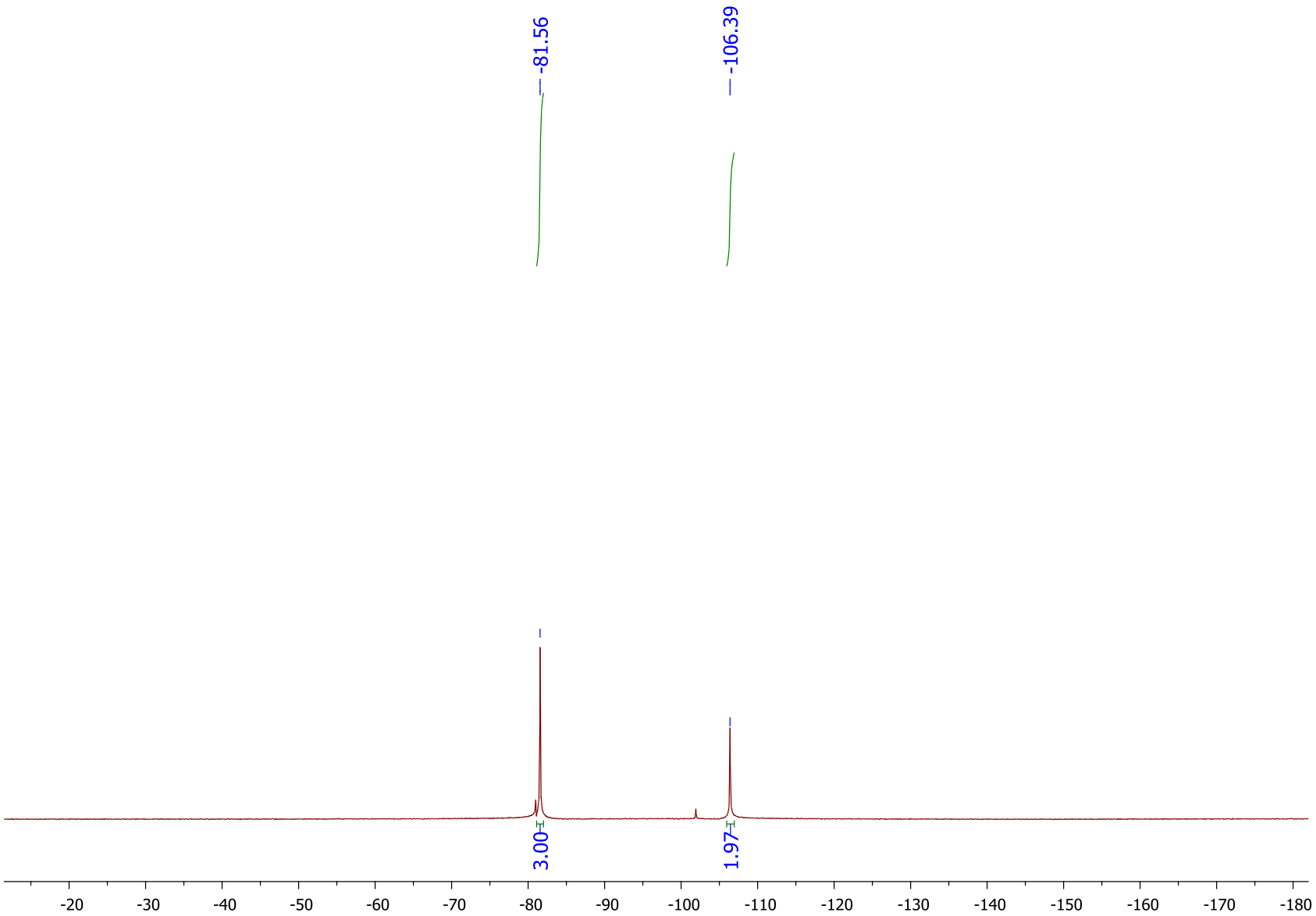

Figure S4. ^{19}F NMR spectrum of **1**·in CD_2Cl_2 at -38 °C.

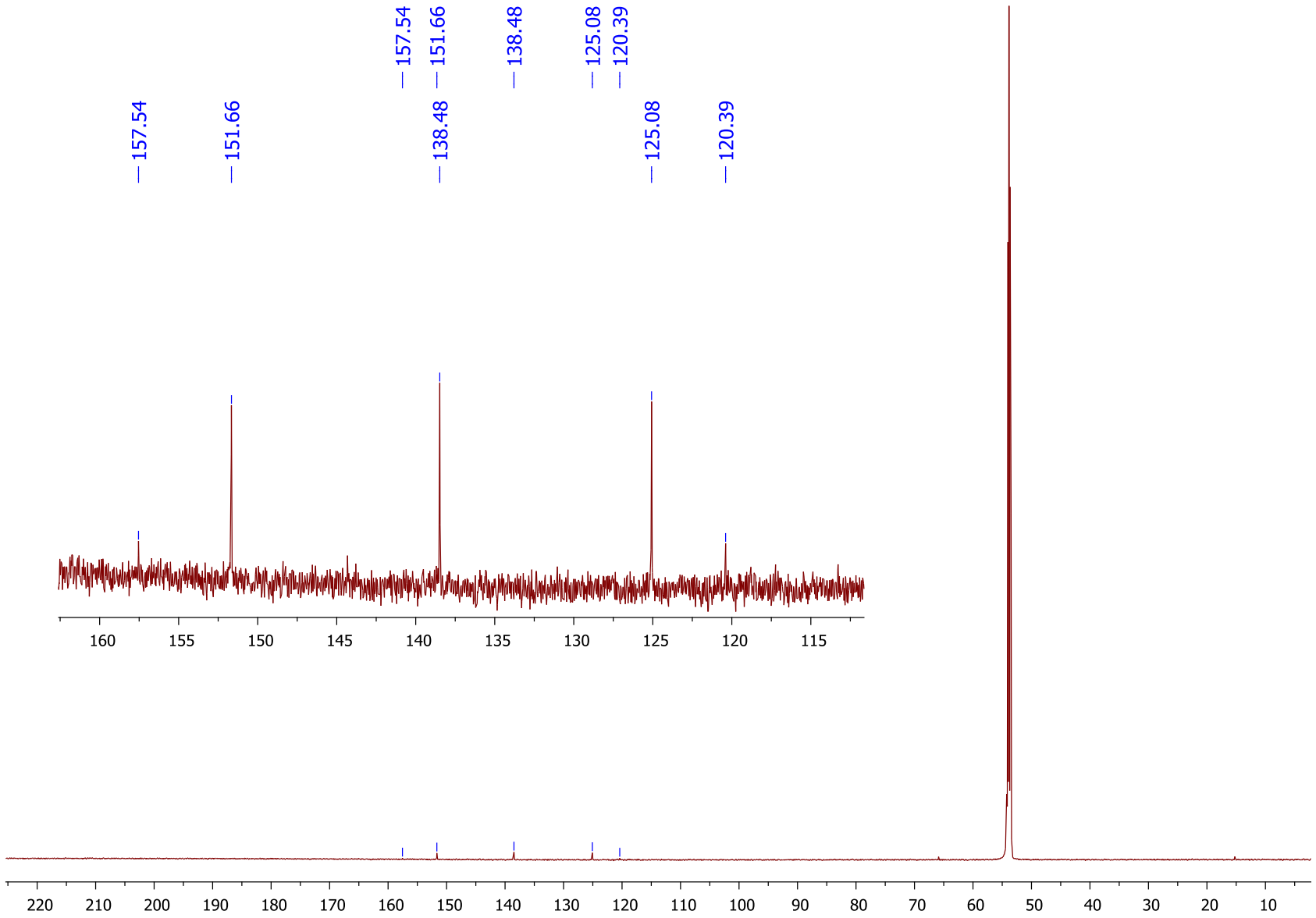

Figure S5. $^{13}C\{^{1}H\}$ NMR spectrum of **1** in CD_2Cl_2 at -38 °C.

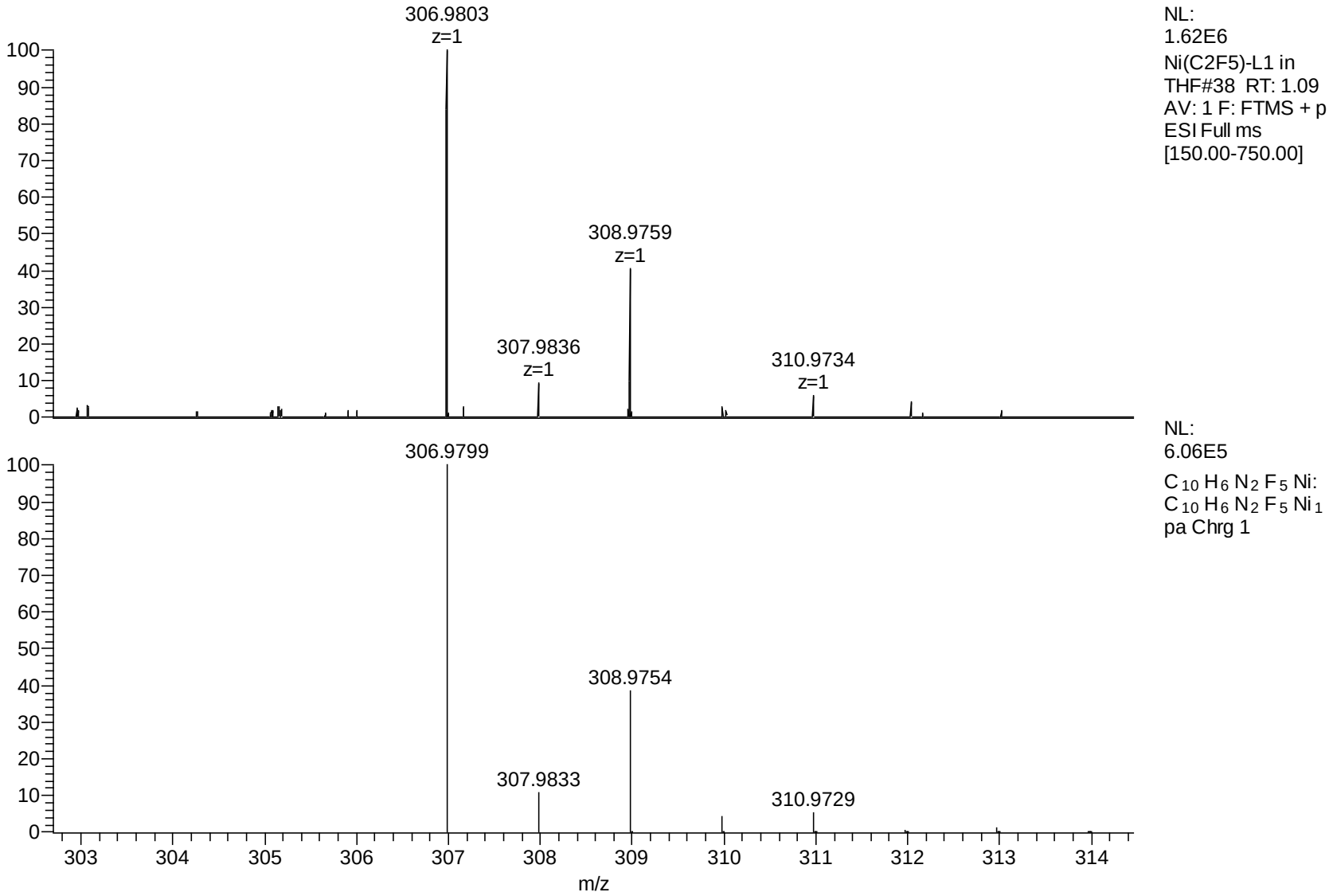

Figure S6. ESI-(HR)MS spectrum of THF solution of **1** (top) and simulated spectrum of $C_{10}H_6N_2F_5Ni$: (bottom).

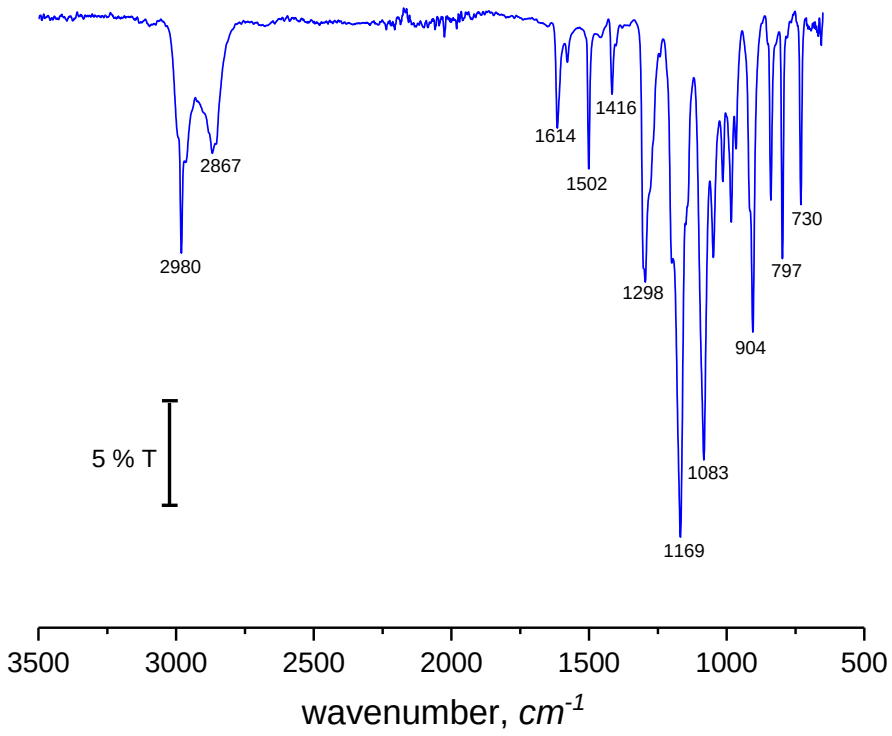

Figure S7. ATR FT-IR transmittance spectrum of **1**.

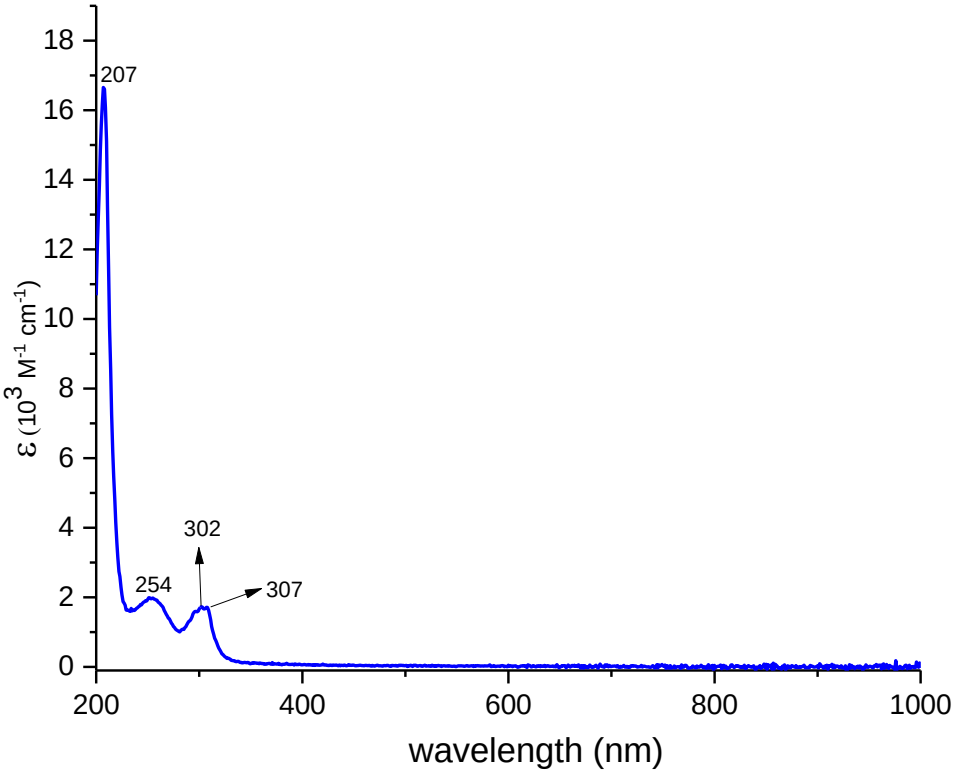

Figure S8. UV-vis absorbance spectrum for **1** in MeCN.

Synthesis of 2

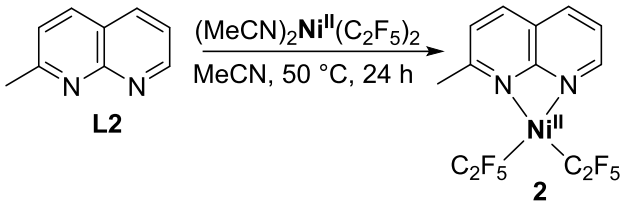

Scheme S2. Synthesis of **2**.

In a nitrogen atmosphere glovebox, to a 100 mL Schlenk flask containing $MeCN)_2Ni(C_2F_5)_2$, (267.4 mg, 0.7060 mmol), **L2** (101.8 mg, 0.7060 mmol), MeCN (5 mL) were added to give a yellow solution. The Schlenk flask was then transferred to an oil bath heated at 50 °C and stirred for 36 hours. The Schlenk flask was transferred back to the glove box then the reaction mixture was passed through a syringe filter to another 20 mL vial and the solvent was removed under vacuum to obtain viscous oil. The yellow oil was dissolved in minimum amount of THF (1 mL) and then precipitated with pentane (10 mL). The remaining liquid was decanted and the remaining solid was dried under vacuum to afford complex **2** as a yellow solid .The powder was dried under vacuum for 12 hours to yield complex **2** (179.4 mg, 0.4068 mmol, 57 % yield) Crystals suitable for X-ray diffraction study were grown by vapor diffusion method in benzene/pentane mixture, where pentane slowly diffused to the benzene solution.

^{1}H NMR (600 MHz, CD_2Cl_2, - 30 °C) δ 8.39 (d , J = 6.8 Hz, 2H, CH_{Naph}), 8.28 (d , J = 8.5 Hz, 1H, CH_{Naph}), 7.60-7.54 (m, 1H, CH_{Naph}), 7.47 (d , J = 8.5 Hz, 1H, CH_{Naph}), 2.51 (s, 3H, CH_{Methyl})

^{13}C{^{1}H} NMR (151 MHz, CD_2Cl_2, - 30 °C) δ 165.97 ($C_{q\ Naph}$), 158.07 ($C_{q\ Naph}$), 150.92 (CH_{Naph}), 138.44 (CH_{Naph}), 137.88 (CH_{Naph}), 127.67 (CH_{Naph}), 126.43-124.31 (m, C_2F_5), 123.76 (CH_{Naph}), 123.27-119.72 (m, C_2F_5), 118.93 ($C_{q\ Naph}$), 118.80-116.88 (m, C_2F_5), 23.16 (CH_{Methyl}).

^{19}F NMR (565 MHz, CD_2Cl_2, - 30 °C) δ -80.46, -81.09, -102.18, 103.43.

HRMS (ESI) calculated for $[M\text{-}C_2F_5]^+$ $C_{11}H_8F_5N_2Ni$: 320.9956; found, 320.9954.

FT-IR (ATR, solid): 1615 (s), 1500 (s), 1292 (br, w), 1162 (br, w), 1088 (br, w), 991 (s), 895 (s), 845 (s), 729 (s) cm^{-1}.

UV-vis (MeCN), λ, nm (ε, $M^{-1}\cdot cm^{-1}$) : 311 (1389), 305 (1498), 248 (3573), 209 (18237).

Elemental Analysis: Expt (Calc): $[C_{13}H_8F_{10}N_2Ni]$: C 35.34 (35.41), H 1.72 (1.83), N 6.47 (6.35).

.

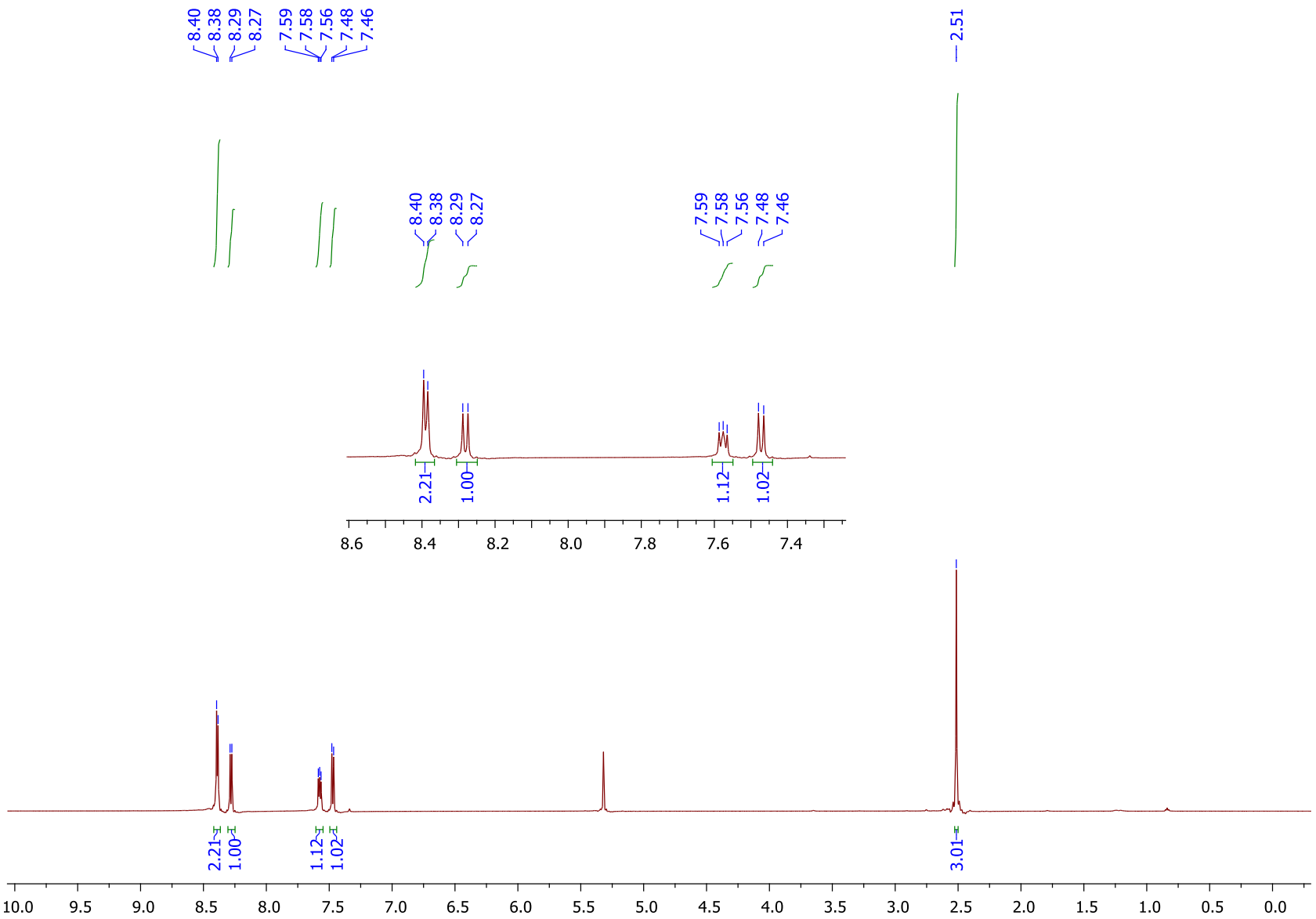

Figure S9. ^{1}H NMR spectrum of **2** in CD_2Cl_2 at -30 °C.

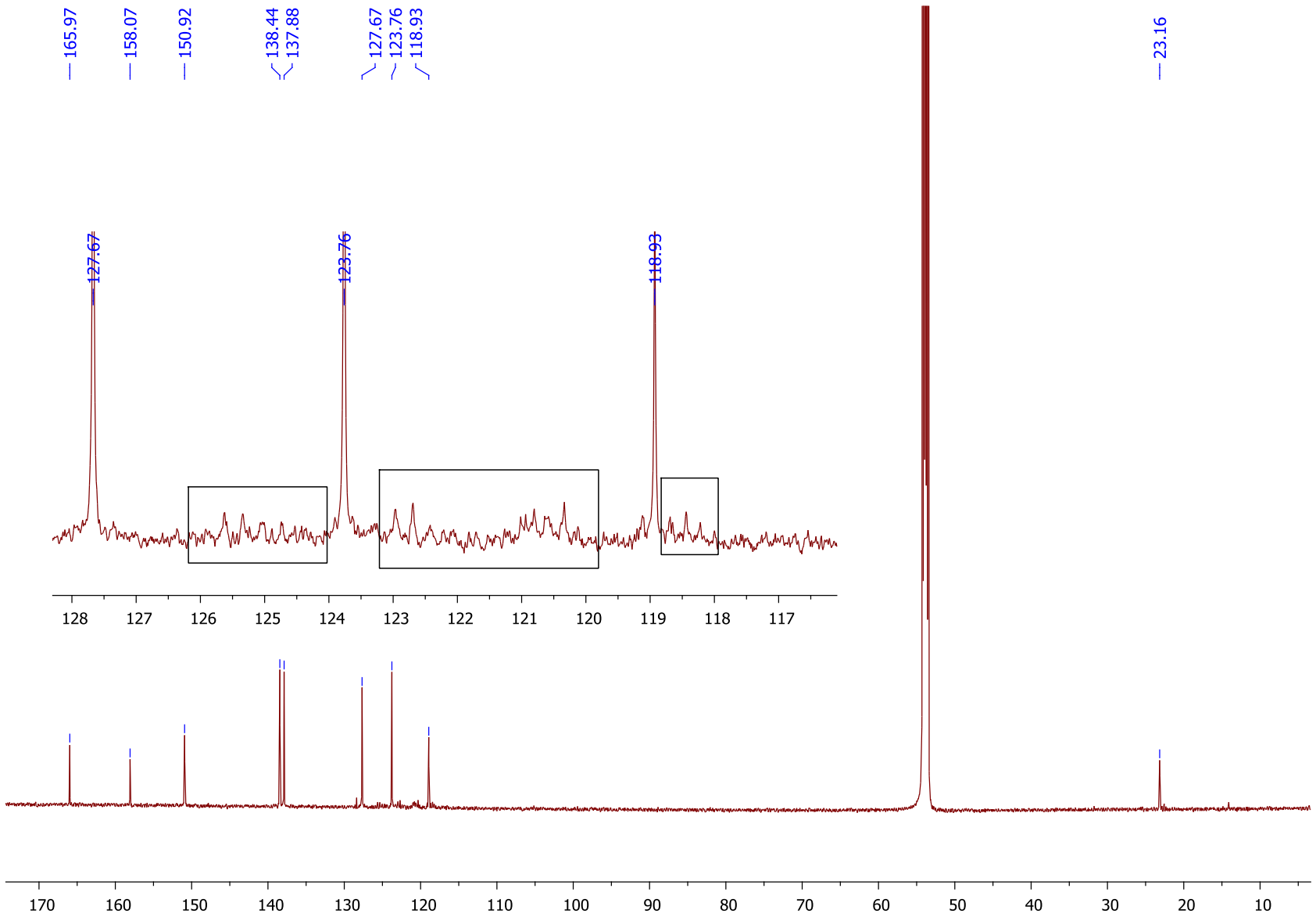

Figure S10. $^{13}C\{^{1}H\}$ NMR spectrum of **2** in CD_2Cl_2 at -30 °C. Boxes represent the regions of C_2F_5 peak multiplets.

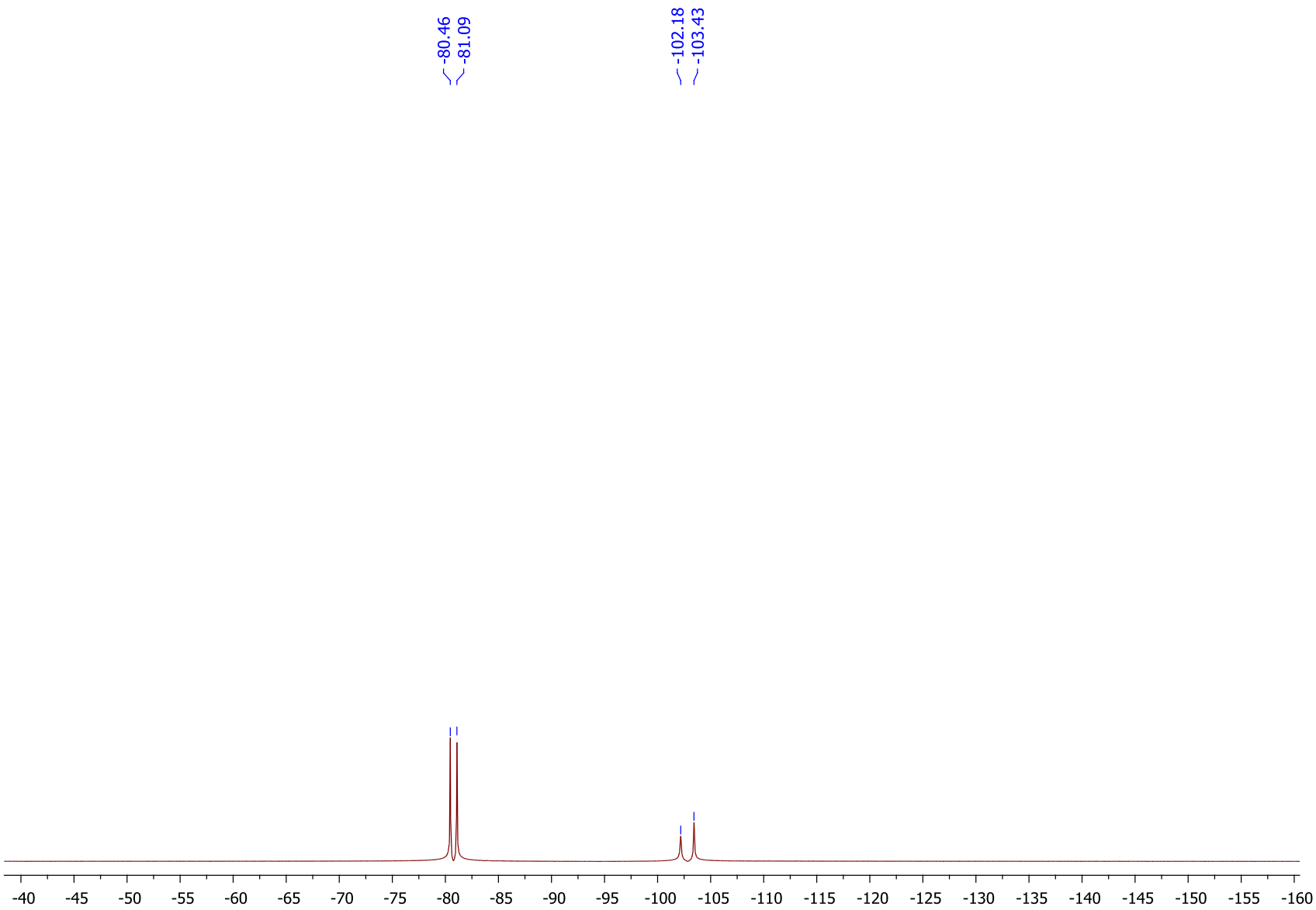

Figure S11. ^{19}F NMR spectrum of **2** in CD_2Cl_2 at -30 °C.

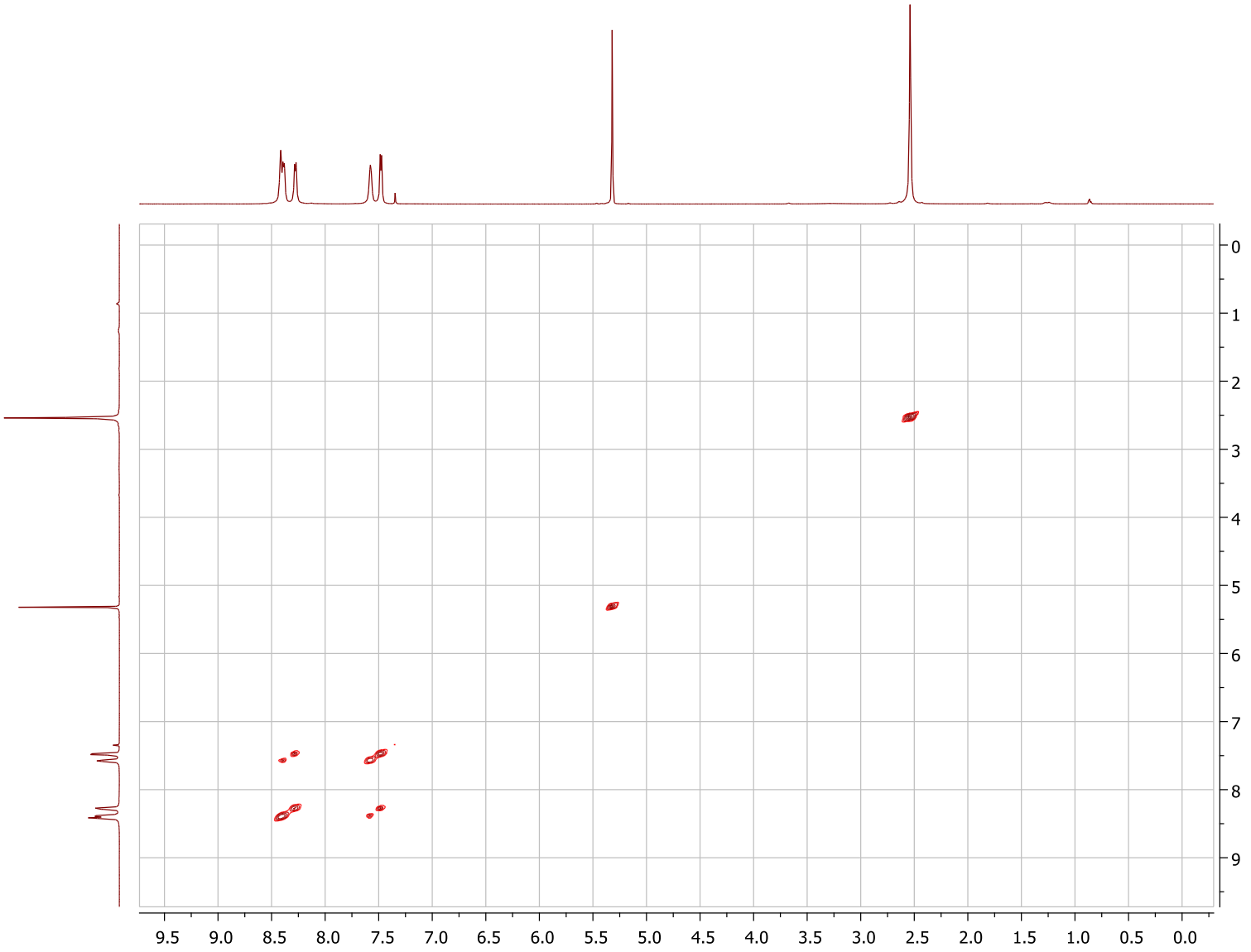

Figure S12. ^{1}H-^{1}H COSY spectrum of **2** in CD_2Cl_2 at 0 °C.

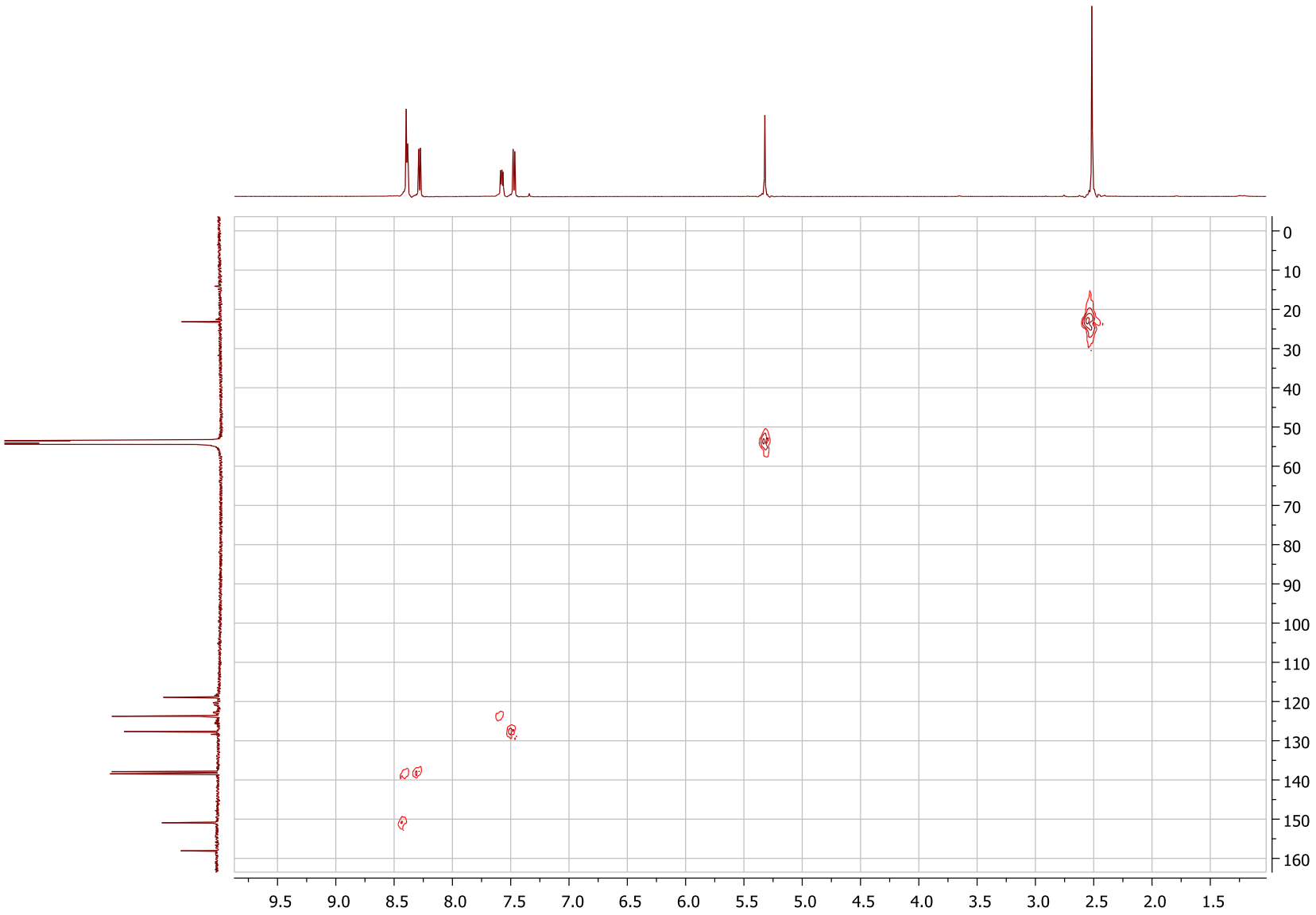

Figure S13. ^{1}H-^{13}C HMQC spectrum of **2** in CD_2Cl_2 at 0 °C.

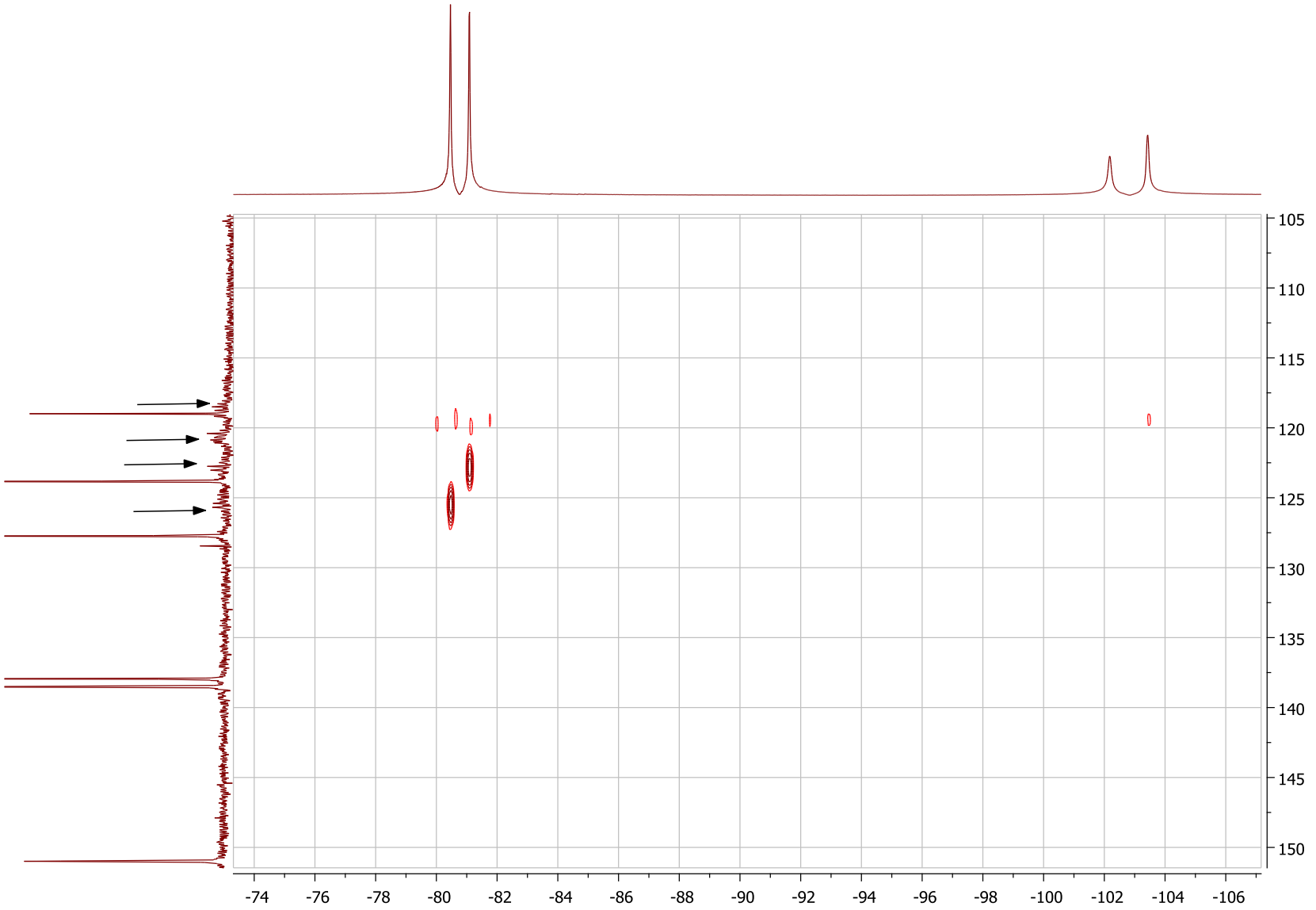

Figure S14. ^{19}F-^{13}C HMQC spectrum of **2** in CD_2Cl_2 at -30 °C. Arrow indicates mutiplets of C_2F_5 peaks.

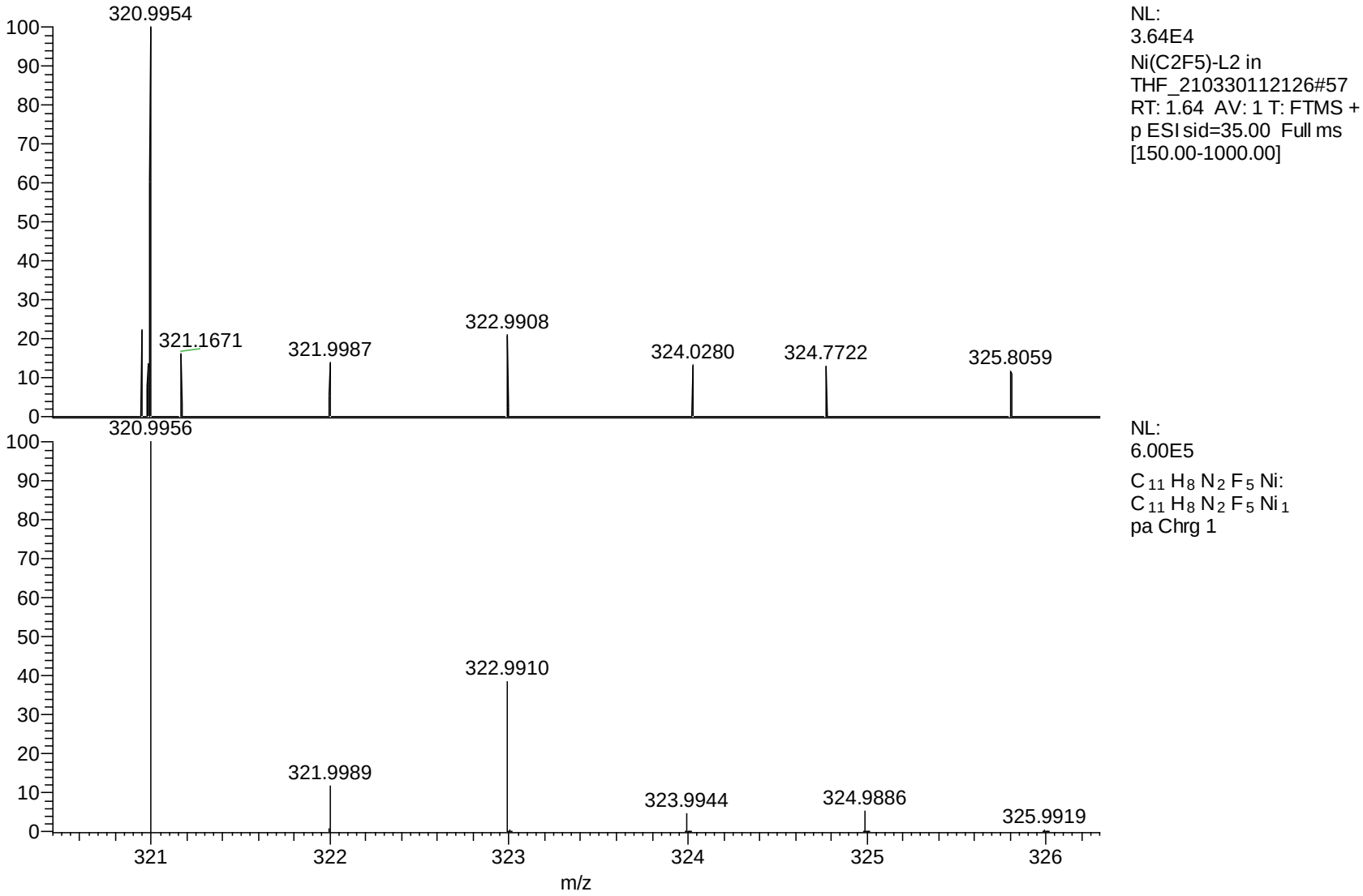

Figure S15. ESI-(HR)MS spectrum of THF solution of **2** (top) and simulated spectrum $C_{11}H_8F_5N_2Ni$: (bottom).

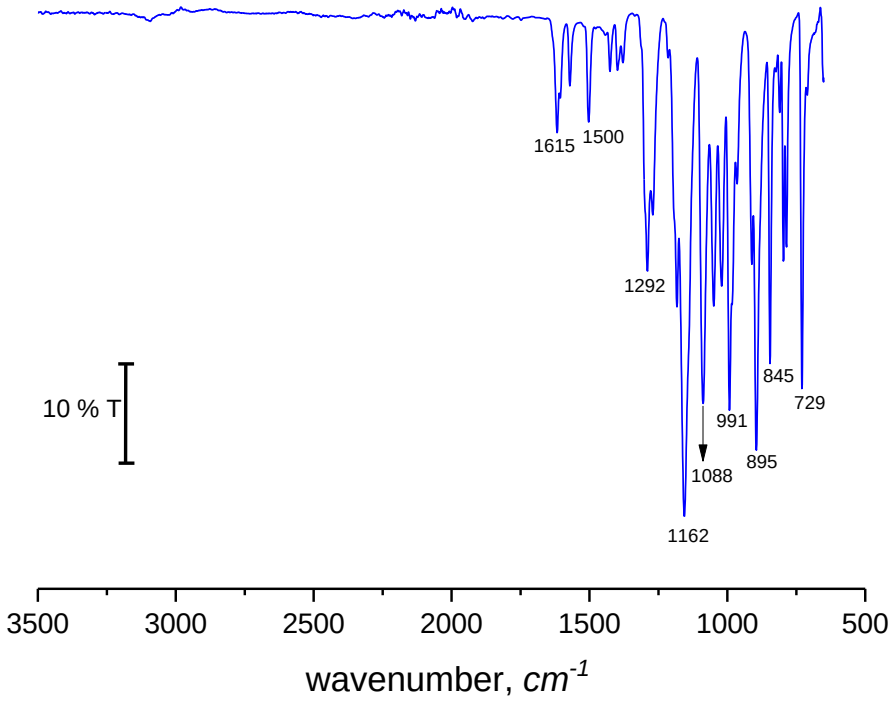

Figure S16. ATR FT-IR transmittance spectrum of **2**.

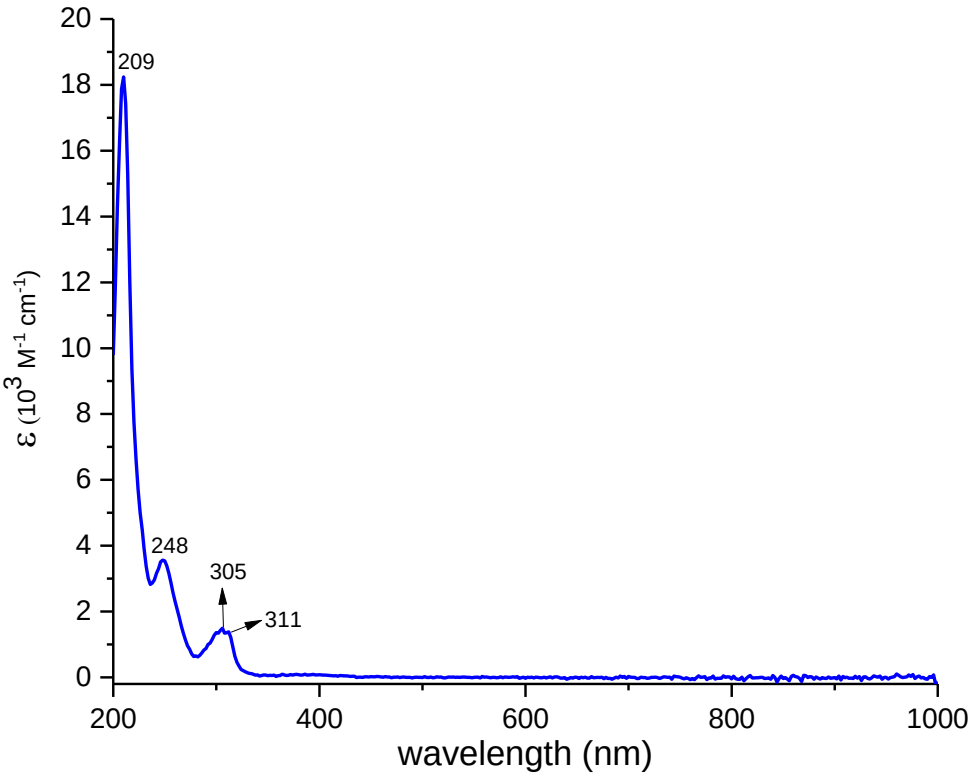

Figure S17. UV-vis absorbance spectrum for **2** in MeCN.

Synthesis of 3

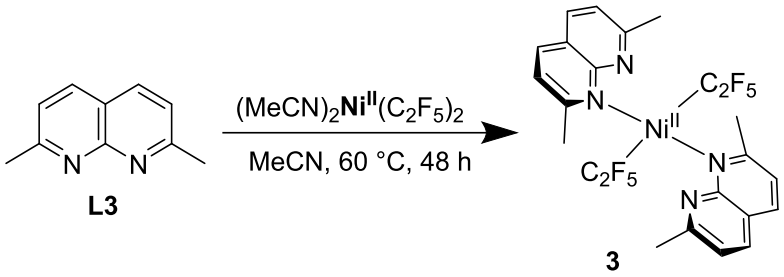

Scheme S3. Synthesis of **3**.

In a nitrogen-filled glovebox, **L3** (201.3 mg, 1.272 mmol), $(MeCN)_2Ni(C_2F_5)_2$, (241 mg, 0.6362 mmol) and MeCN (5 mL) were added to a 50 mL schlenk flask. containing a magnetic stirring bar. The Schlenk flask was then transferred to an oil bath heated at 60 °C and stirred for 48 hours. The Schlenk flask was transferred back to the glove box, and yellow reaction mixture solution was passed through a syringe filter to a 20 mL vial. The remaining powder in the Schlenk flask was dried and the complex was extracted with CH_2Cl_2 (10 mL) and passed through syringe filter to another 20 mL vial. The solvent was removed under vacuum to obtain viscous oil for both 20 mL vial. Further, the oil was washed with cold hexane (20 mL) and the compound was dried under vacuum for 48 hours to obtain complex **3** as yellow solid (434.2 mg, 55% yield). Crystals suitable for X-ray diffraction study were grown by vapor diffusion method in THF/cyclohexane solvents combination, where cyclohexane slowly diffused to the THF solution.

^{1}H NMR (600 MHz, CD_2Cl_2, 23 °C) δ 8.14 (d, J = 8.3 Hz, 2H, CH_{Naph}), 7.42 (d , J = 8.3 Hz, 2H, CH_{Naph}), 2.85 (s, 6H, CH_{Methyl}).

^{13}C NMR (151 MHz, CD_2Cl_2, 23 °C) δ 165.05 ($C_{q\ Naph}$), 157.53 ($C_{q\ Naph}$), 137.91 (CH_{Naph}), 125.85 (CH_{Naph}), 123.97-122.40 (m, C_2F_5), 121.53-120.64 (m, C_2F_5), 119.47-118.87 (m, C_2F_5), 118.31($C_{q\ Naph}$), 24.61 (CH_{Methyl}).

^{19}F NMR (565 MHz, CD_2Cl_2, -25 °C) δ -80.96, -101.84.

HRMS (ESI) calculated for $[M\text{-}C_2F_5]^+$ $C_{22}H_{20}F_5N_4Ni$: 493.0956; found, 493.0956.

FT-IR (ATR, solid): 2981 (br, w), 2328 (br, w), 1609 (br, s), 1511 (br, s), 1288 (s), 1146 (m), 1077 (s), 968 (s), 889 (s), 728 (s) cm^{-1}.

UV-vis (MeCN), λ, nm (ε, $M^{-1}\cdot cm^{-1}$) : 315 (3254), 301 (3490), 259 (3883), 210 (21821).

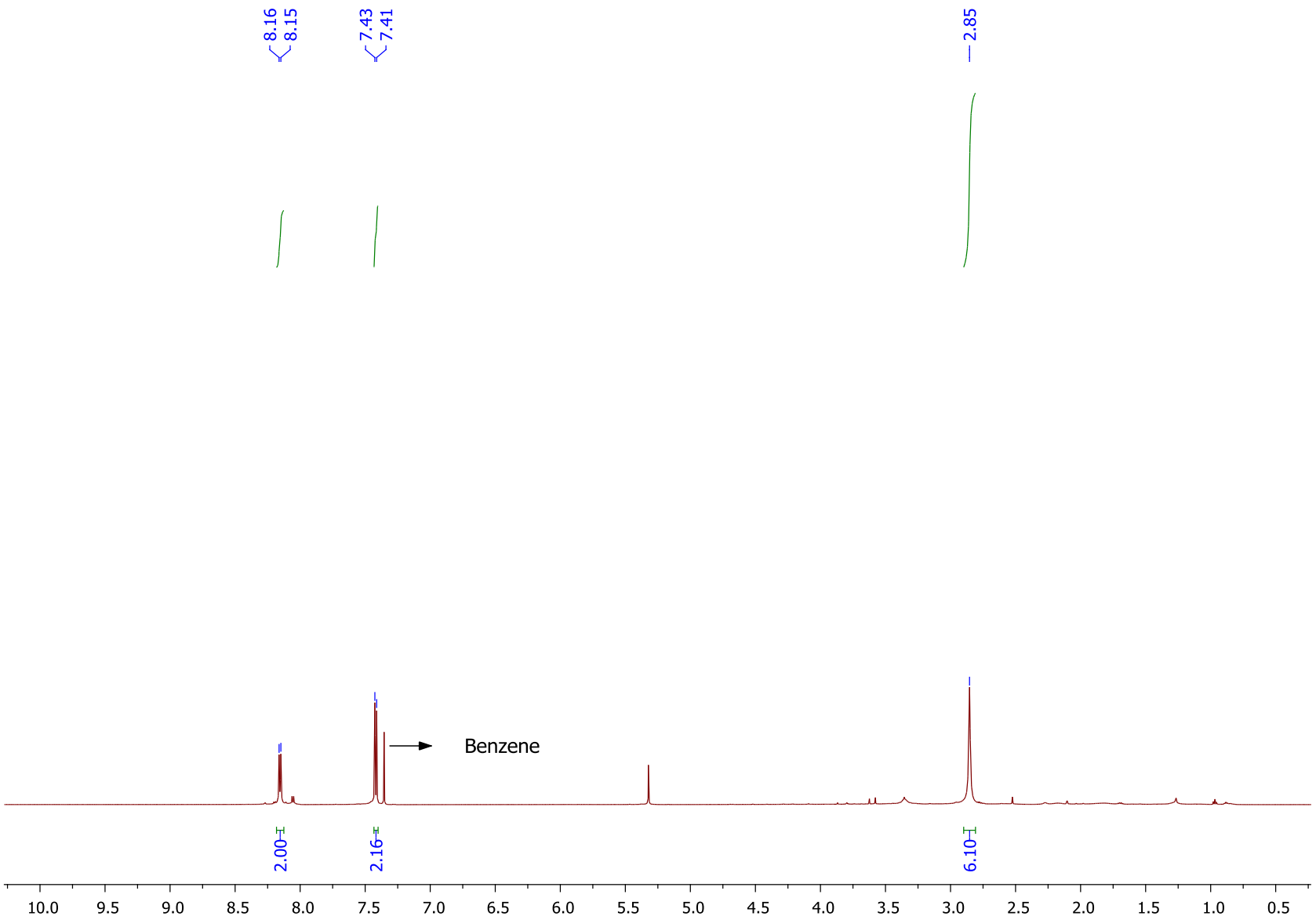

Figure S18. ^{1}H NMR spectrum of **3** in CD_2Cl_2 at 23 °C.

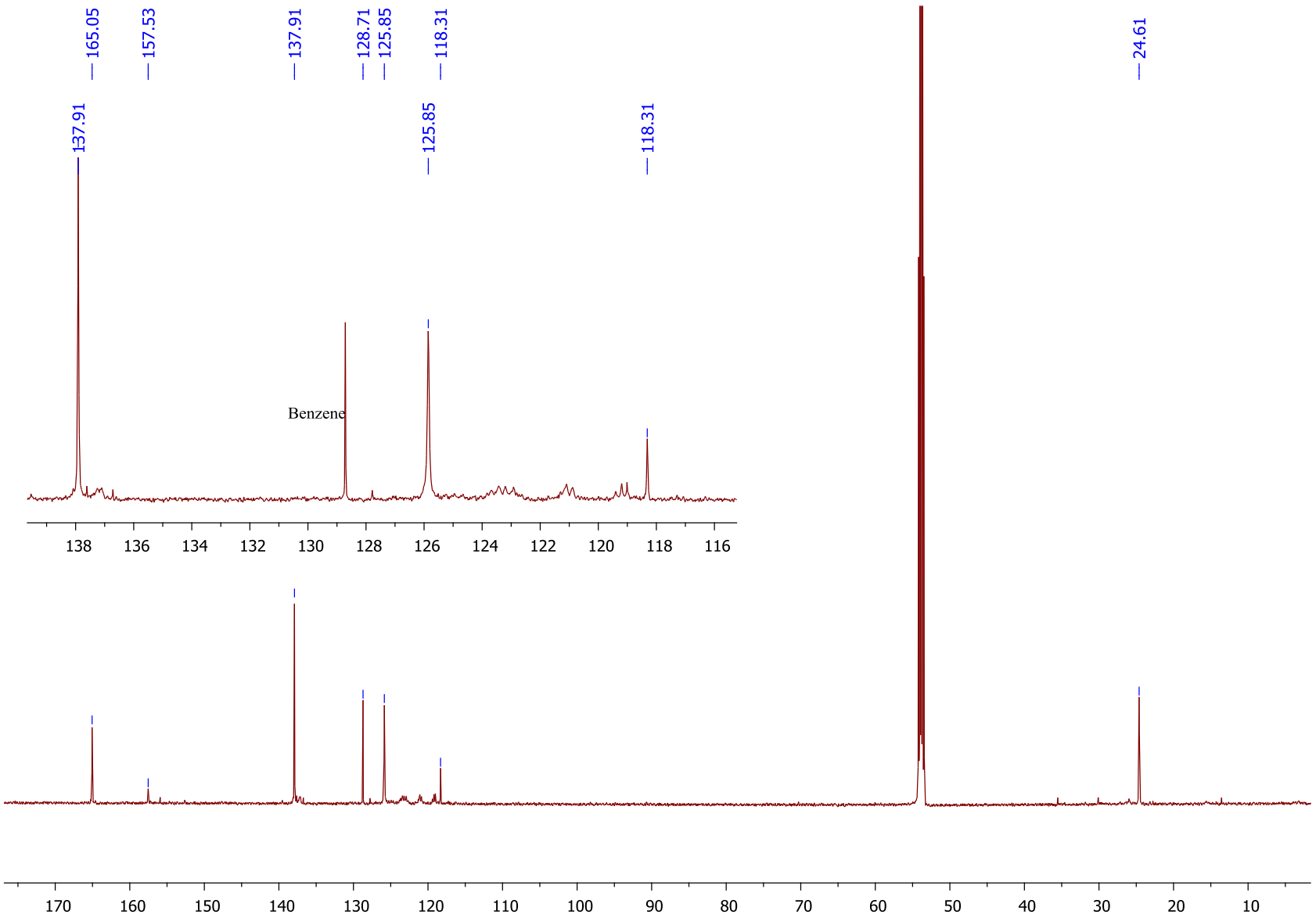

Figure S19. $^{13}C\{^{1}H\}$ NMR spectrum of **3** in CD_2Cl_2 at 23 °C.

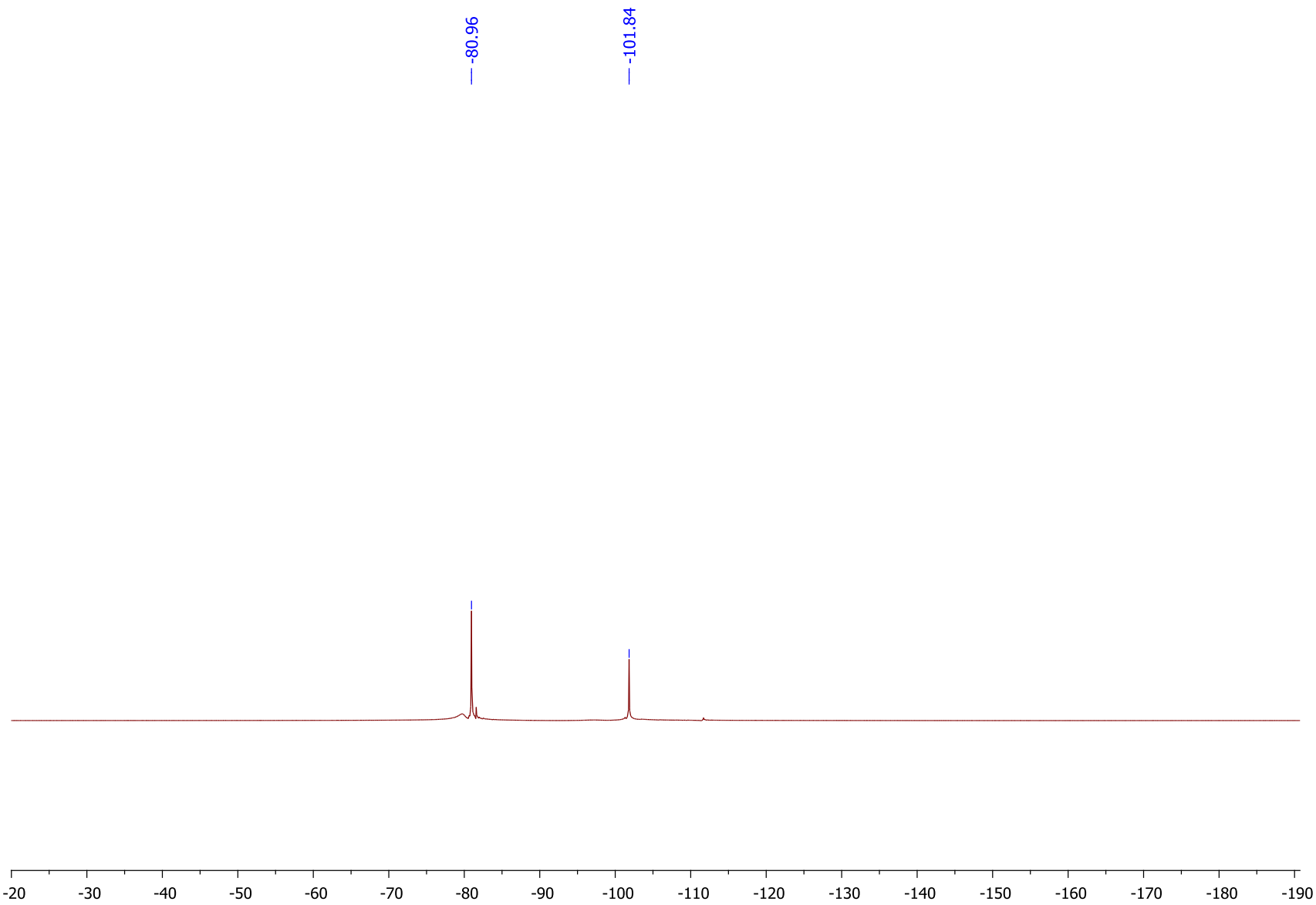

Figure S20. ^{19}F NMR spectrum of **3** in CD_2Cl_2 at -25 °C.

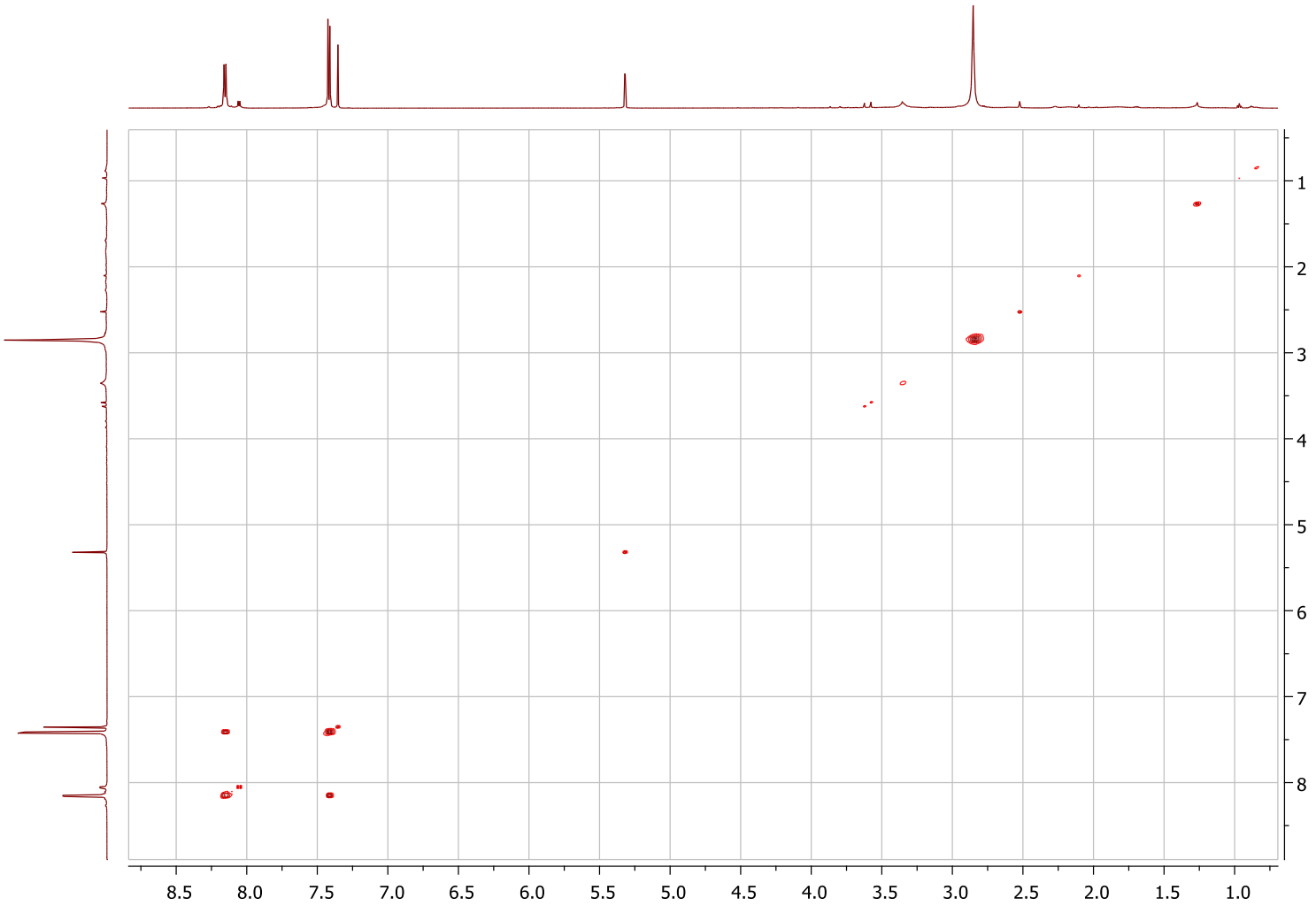

Figure S21. ^{1}H-^{1}H COSY spectrum of **3** in CD_2Cl_2 at 23 °C.

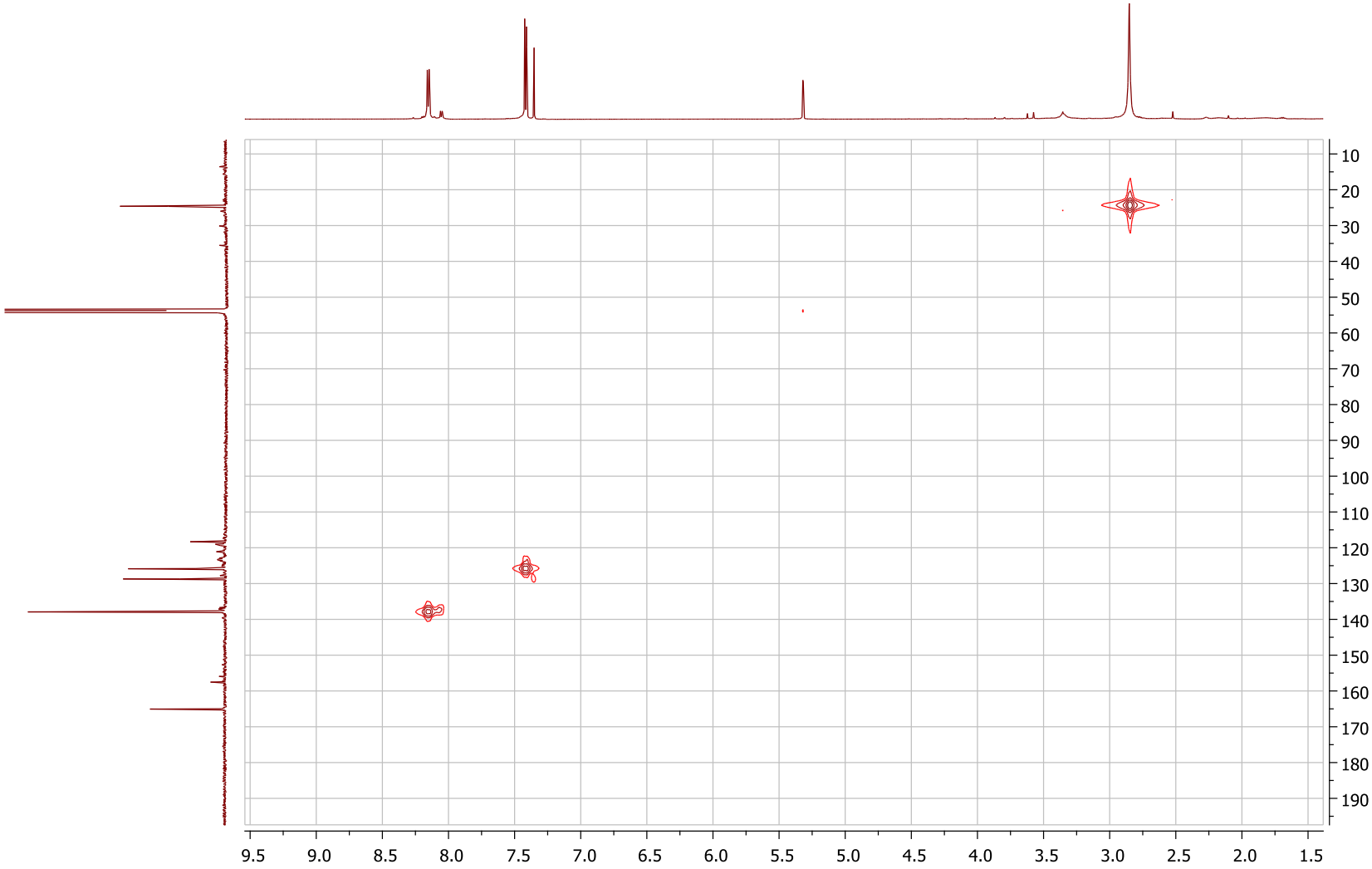

Figure S22. ^{1}H-^{13}C HMQC spectrum of **3** in CD_2Cl_2 at 23 °C.

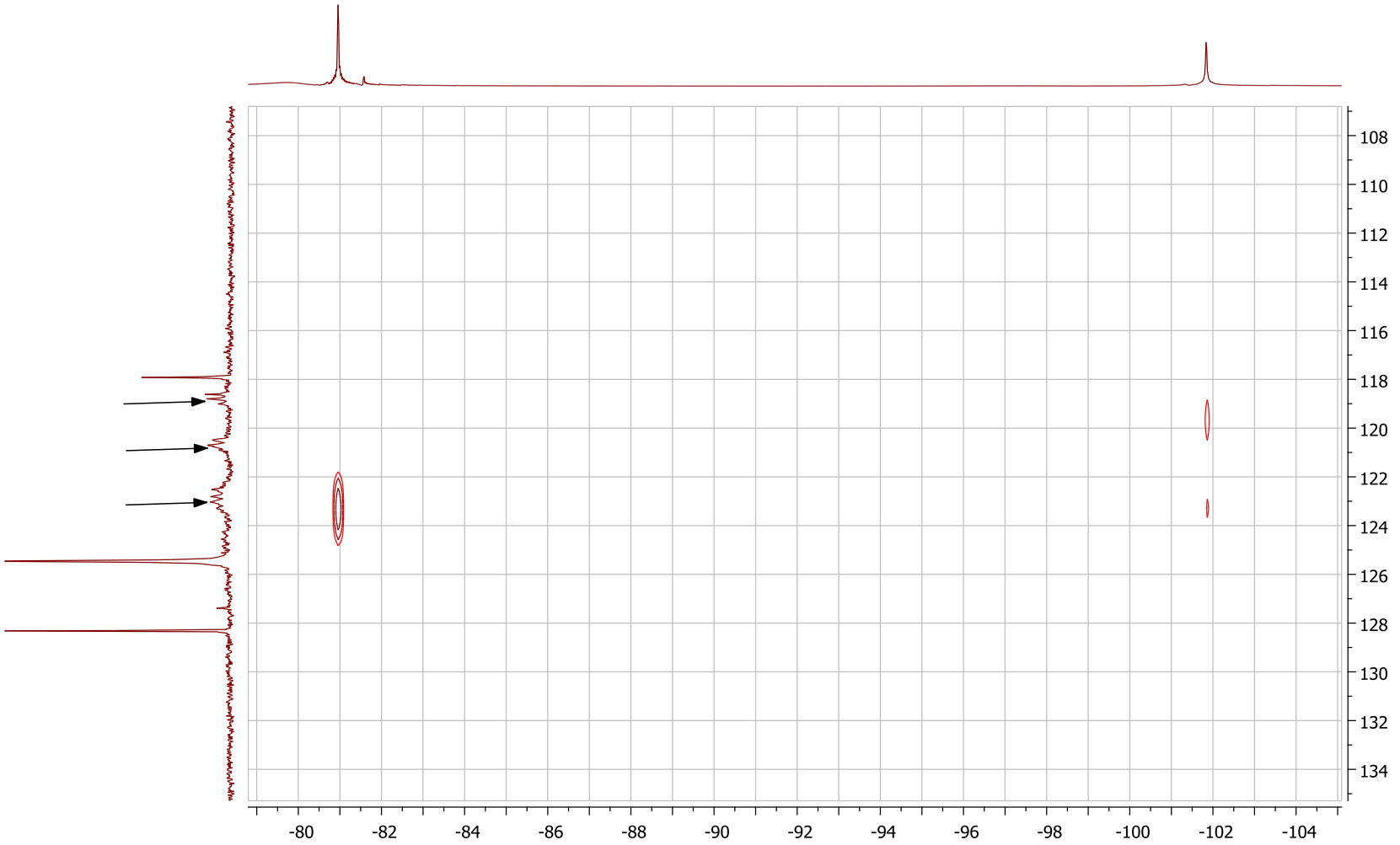

Figure S23. ^{19}F-^{13}C HMQC spectrum of **3** in CD_2Cl_2 at -25 °C. Arrow indicates fluorine region.

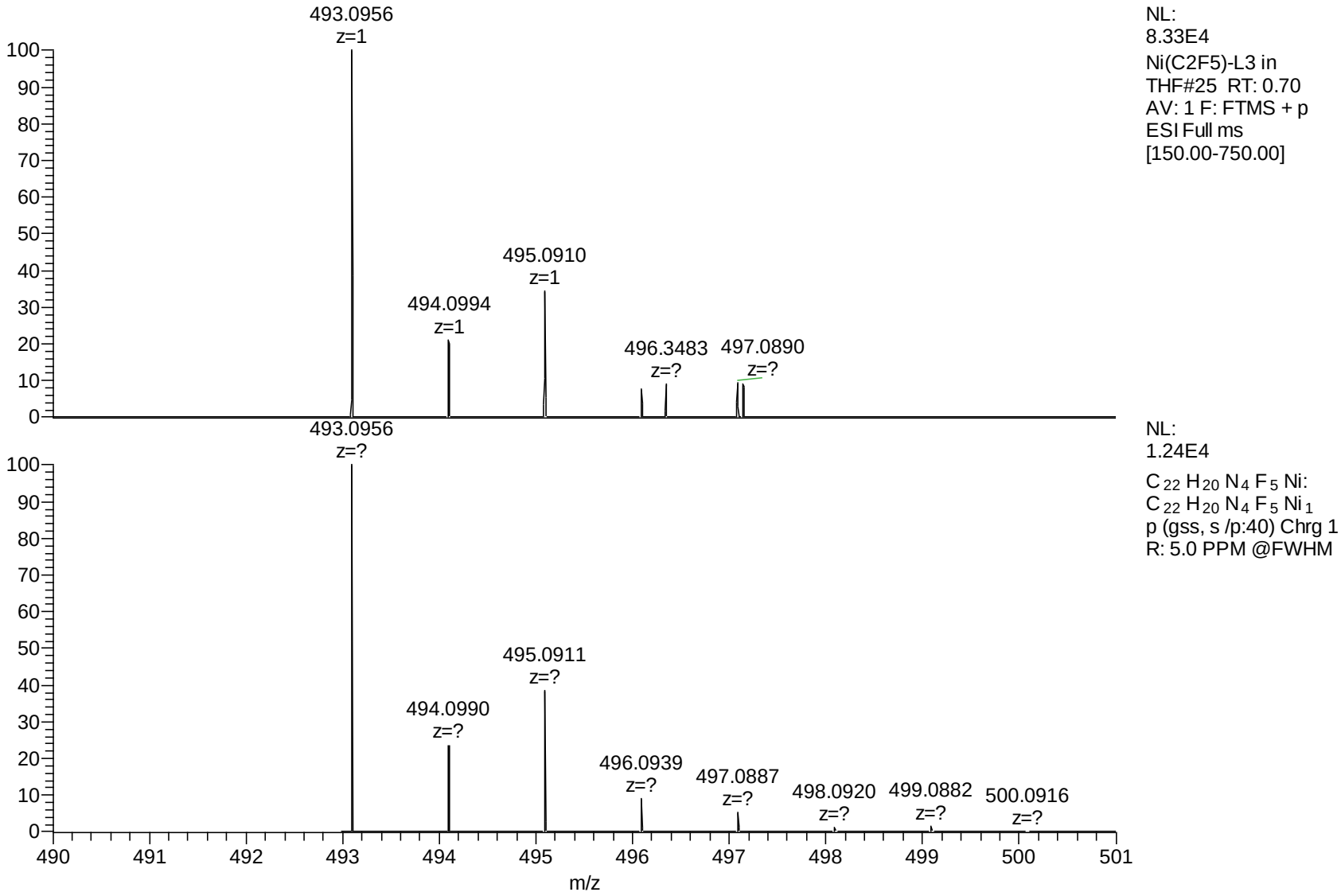

Figure S24. ESI-(HR)MS spectrum of THF solution of **3** (top) and simulated spectrum $C_{22}H_{20}F_5N_4Ni$: (bottom).

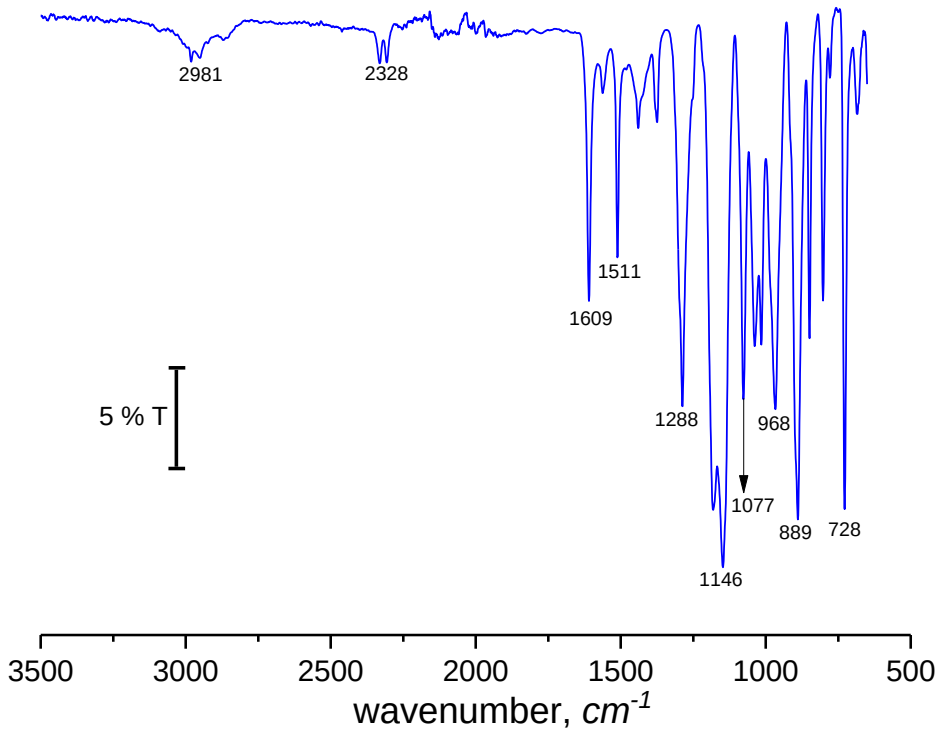

Figure S25. ATR FT-IR transmittance spectrum of **3**.

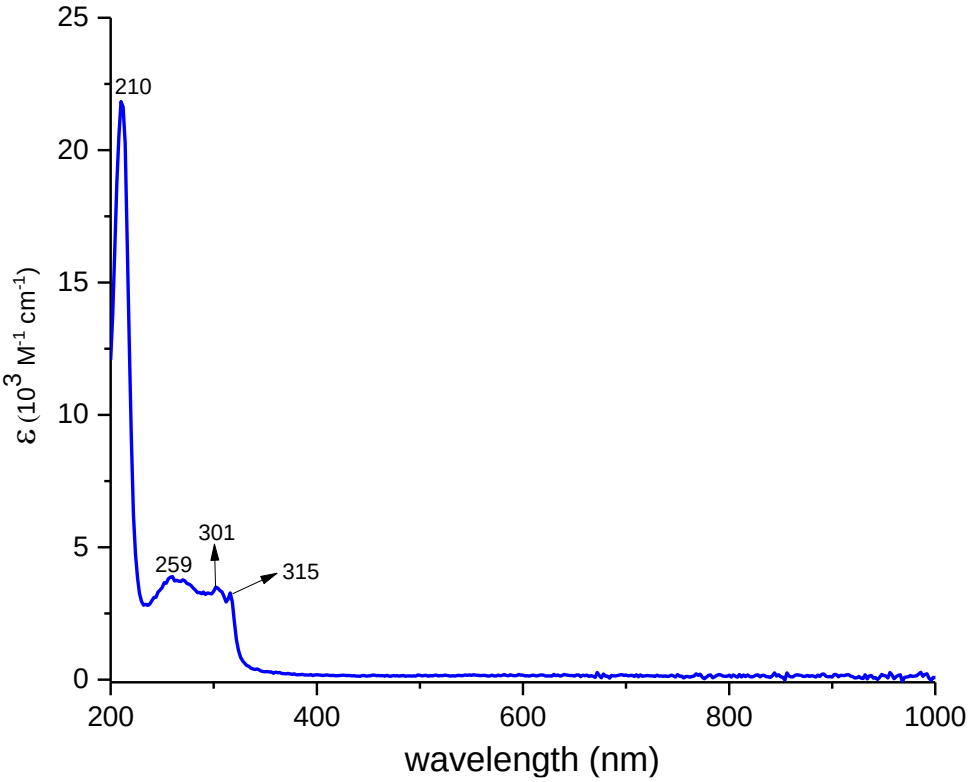

Figure S26. UV-vis absorbance spectrum for **3** in MeCN

Synthesis of 4

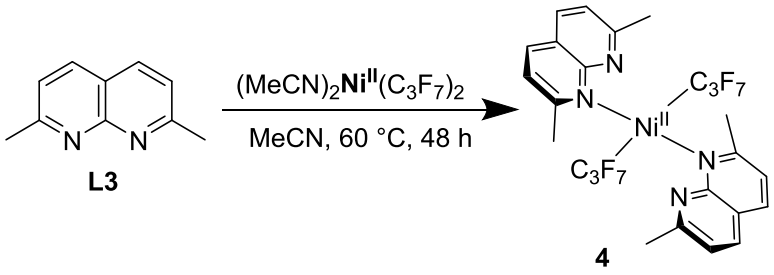

Scheme S4. Synthesis of **4**.

In a nitrogen-filled glovebox, a 100 mL Schlenk flask equipped with a magnetic stir bar was charged with **L3** (100.1 mg, 0.6327 mmol) and $(MeCN)_2Ni(C_3F_7)_2$, (151.4 mg, 0.3163 mmol) dissolved in MeCN (5 mL). The Schlenk flask was t hen transferred to an oil bath heated at 60 °C and stirred for 48 hours to obtain yellow reaction mixture. The Schlenk flask was transferred back to the glove box, then the reaction mixture was passed through a syringe filter to another 20 mL vial and the solvent was removed under vacuum to obtain viscous oil. The desired complex was extracted with diethyl ether (60 mL), transferred to a 100 mL flask; the solvent was removed under vacuum to obtain yellow powder. The solid was washed with cold hexane (15 mL) and the powder was dried under vacuum for 24 hours to obtain complex **4** as yellow solid (258.3 mg, 57% yield). Crystals suitable for X-ray diffraction study were grown by vapor diffusion method in benzene/hexane solvents combination, where hexane slowly diffused to the benzene solution.

^{1}H NMR (400 MHz, CD_2Cl_2, 23 °C) δ 8.12 (d, *J* = 8.2 Hz, 2H, CH_{Naph}), 7.42 (d, *J* = 8.2 Hz, 2H, CH_{Naph}), 3.08 (s, 6H, CH_{Methyl}).

^{13}C{^{1}H} NMR (151 MHz, CD_2Cl_2, 23 °C) δ 164.84 ($C_{q\ Naph}$), 156.49 ($C_{q\ Naph}$),, 137.75 (CH_{Naph}), 126.98-126 (m, C_2F_5), 125 (CH_{Naph}), 123.94-123.23 (m, C_2F_5), 122.14-120.79 (m, C_2F_5), 120.25-119.12 (m, C_2F_5), 118.67($C_{q\ Naph}$), 118.23-117.48 (m, C_2F_5), 111.38-109.93 (m, C_2F_5), 25.03 (CH_{Methyl}).

^{19}F NMR (376 MHz, CD_2Cl_2, 23 °C) δ -79.63, -88.83, -120.63.

HRMS (ESI) calculated for $[M\text{-}C_3F_7]^+$ $C_{23}H_{20}F_7N_4Ni$: 543.0924; found, 543.0878.

FT-IR (ATR, solid): 1608 (s), 1510 (s), 1319 (br s), 1210 (br m), 1176 (br m), 1147 (br m), 1075 (s), 984 (br m), 848 (s), 801 (s), 718 (s), 658 (s) cm^{-1}.

UV-vis (MeCN), λ, nm (ε, $M^{-1}\cdot cm^{-1}$) : 315 (989), 306 (869), 253 (1239), 200 (21970).

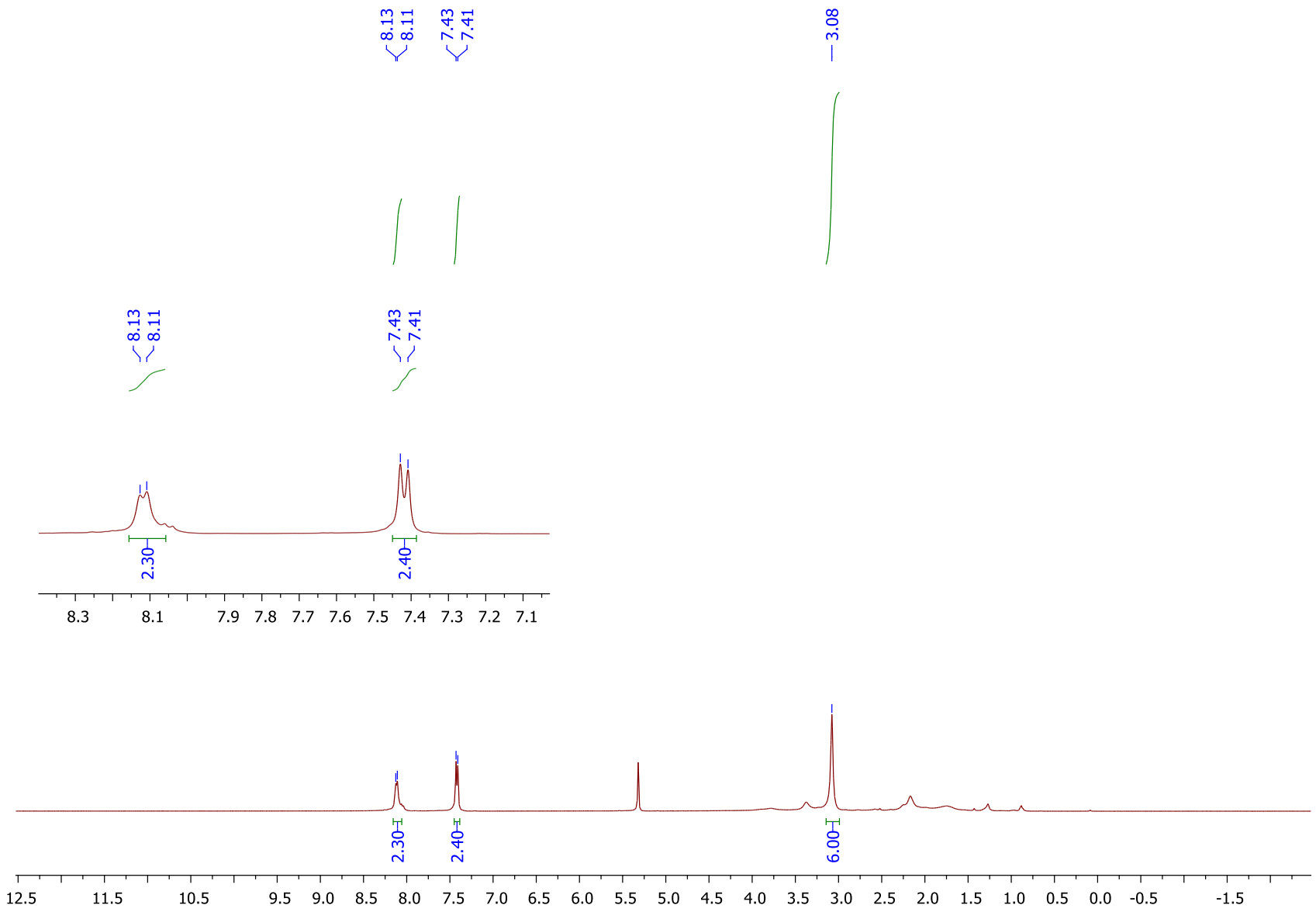

Figure S27. ^{1}H NMR spectrum of **4** in CD_2Cl_2 at 23 °C.

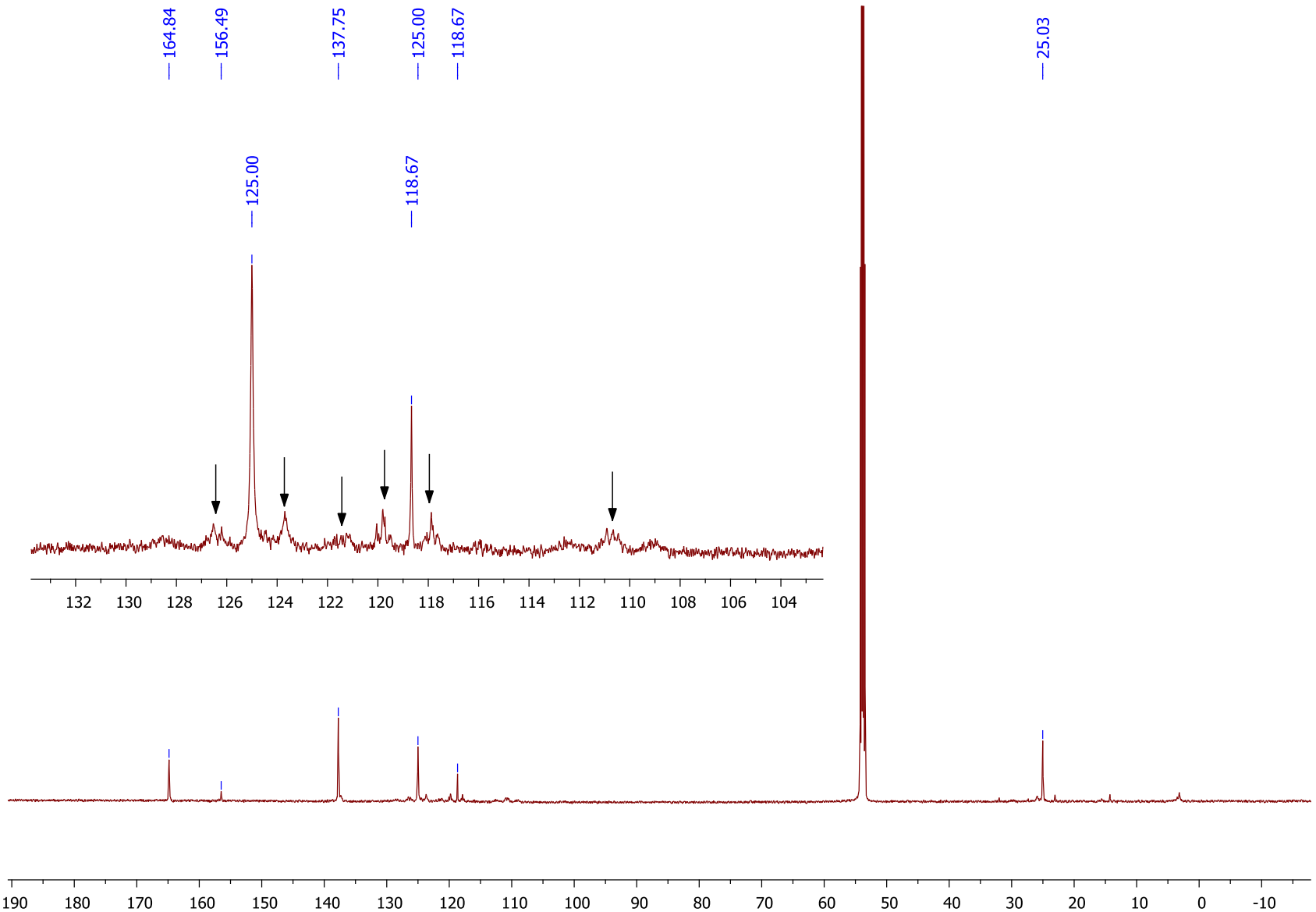

Figure S28. $^{13}C\{^{1}H\}$ NMR spectrum of **4** in CD_2Cl_2 at 23 °C. The arrow point at the multiplet peaks of perfluoroalkyl group.

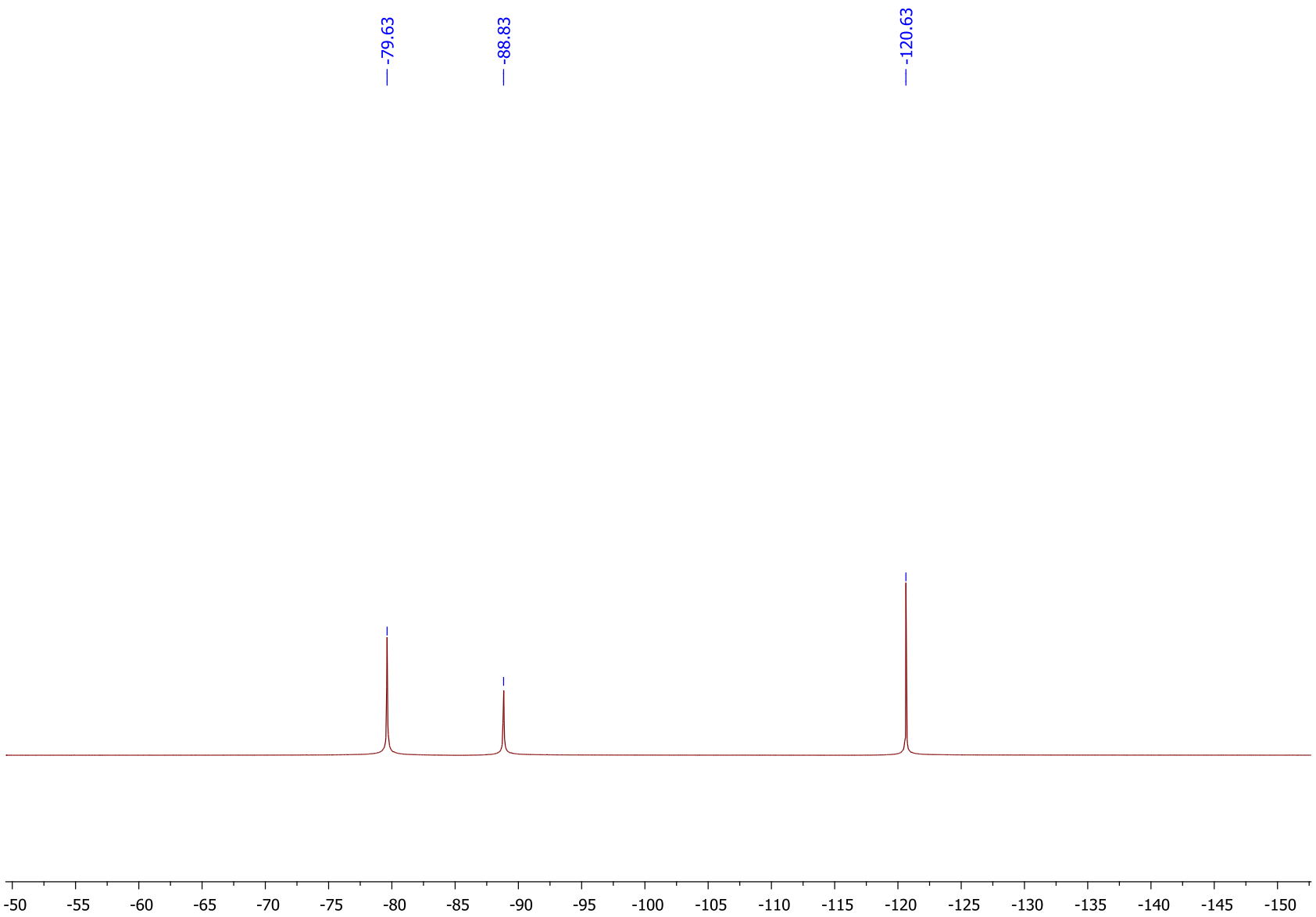

Figure S29. ^{19}F NMR spectrum of **4** in CD_2Cl_2 at 23 °C.

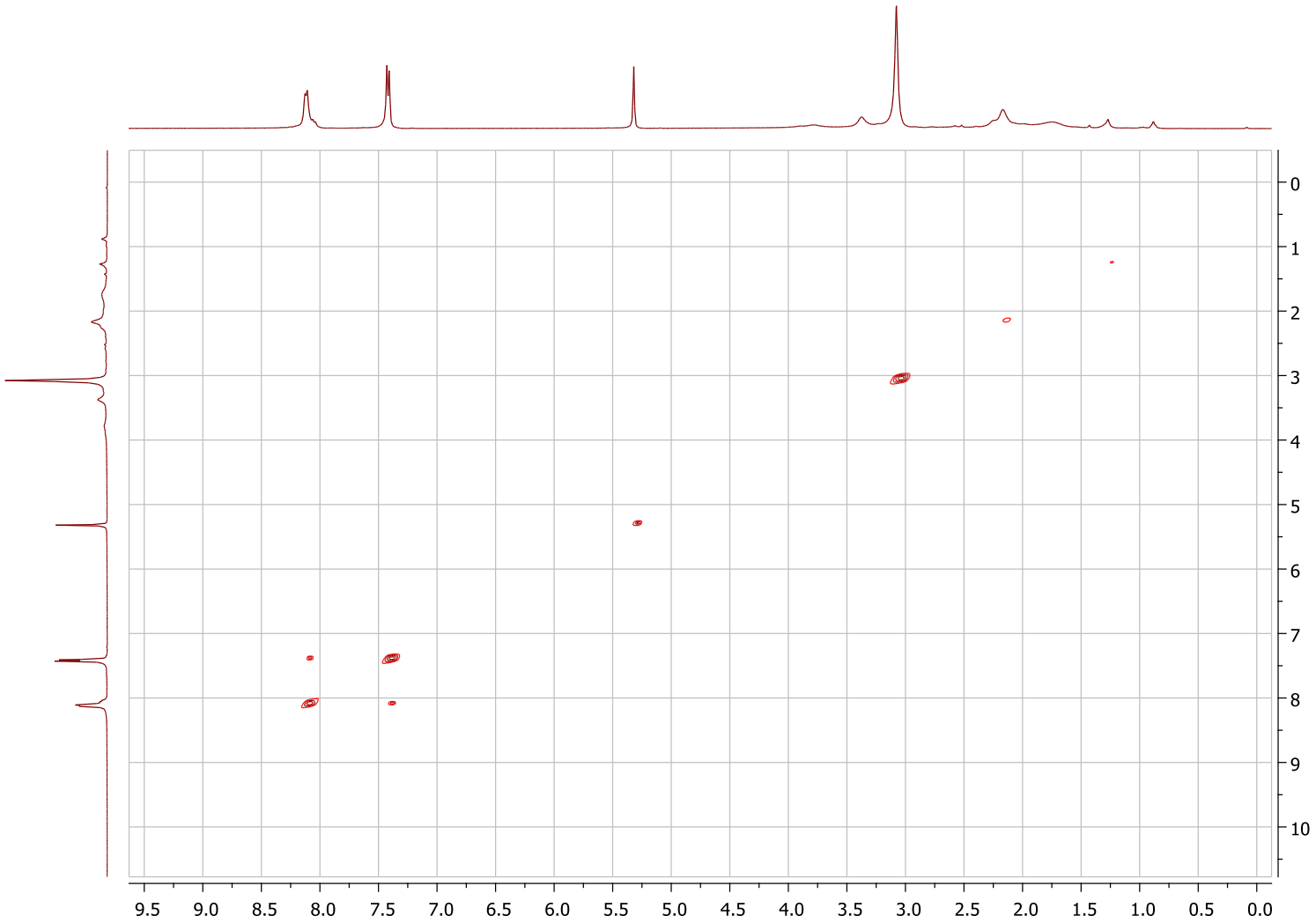

Figure S30. ^{1}H-^{1}H COSY spectrum of **4** in CD_2Cl_2 at 23 °C.

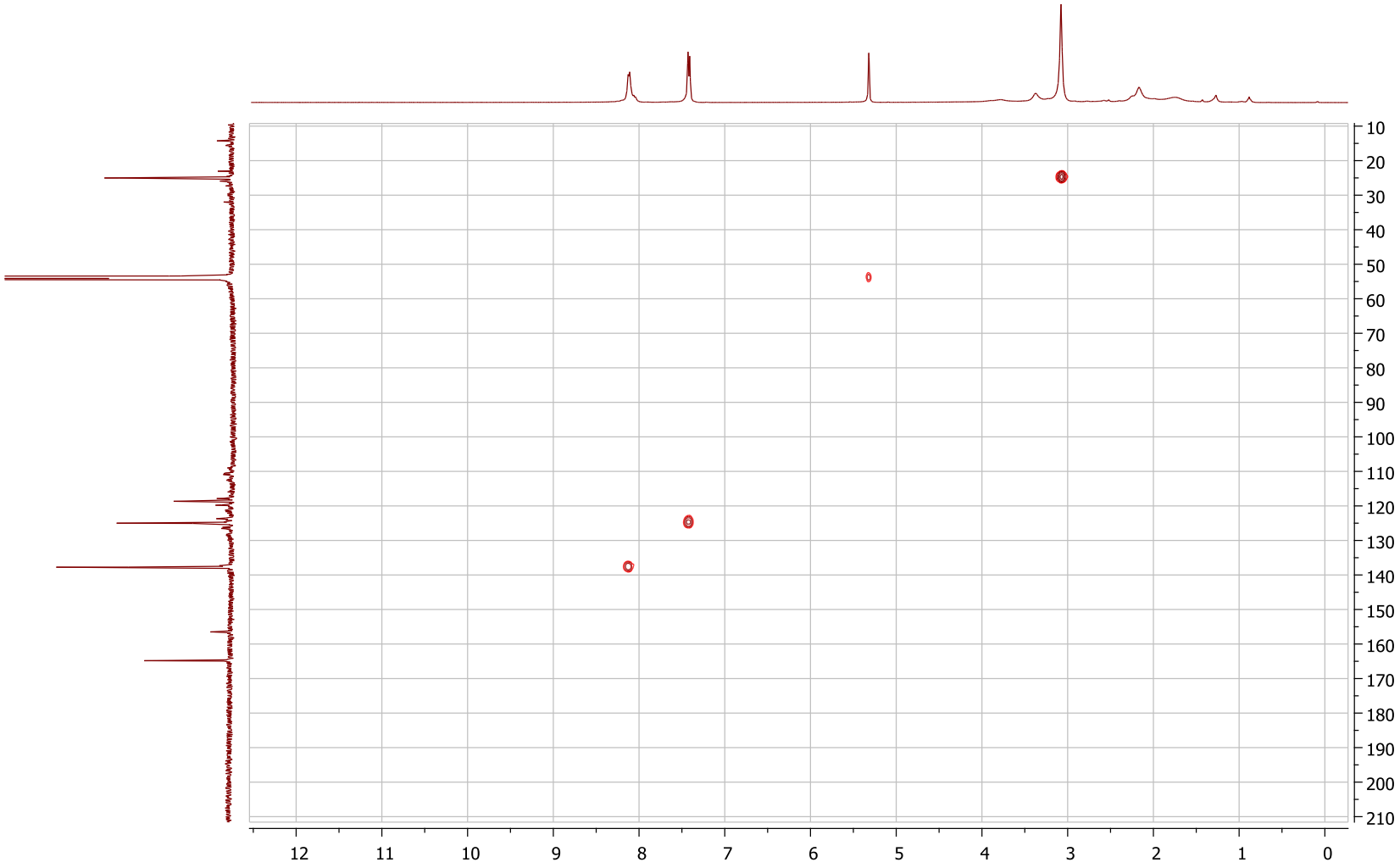

Figure S31. ^{1}H-^{13}C HMQC spectrum of **4** in CD_2Cl_2 at 23 °C.

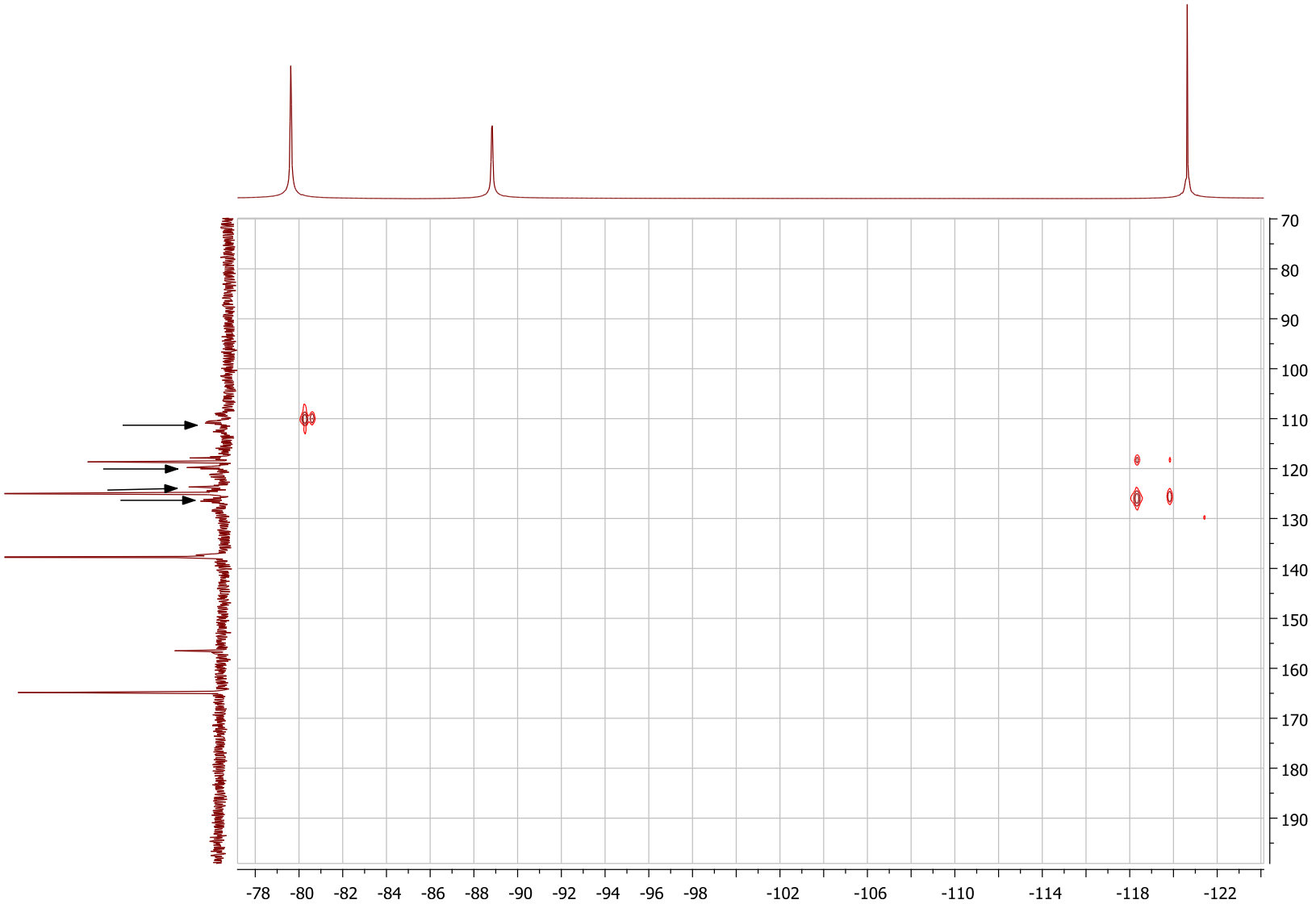

Figure S32. ^{19}F-^{13}C HMQC spectrum of **4** in CD_2Cl_2 at 23 °C. Arrow indicates fluorine region.

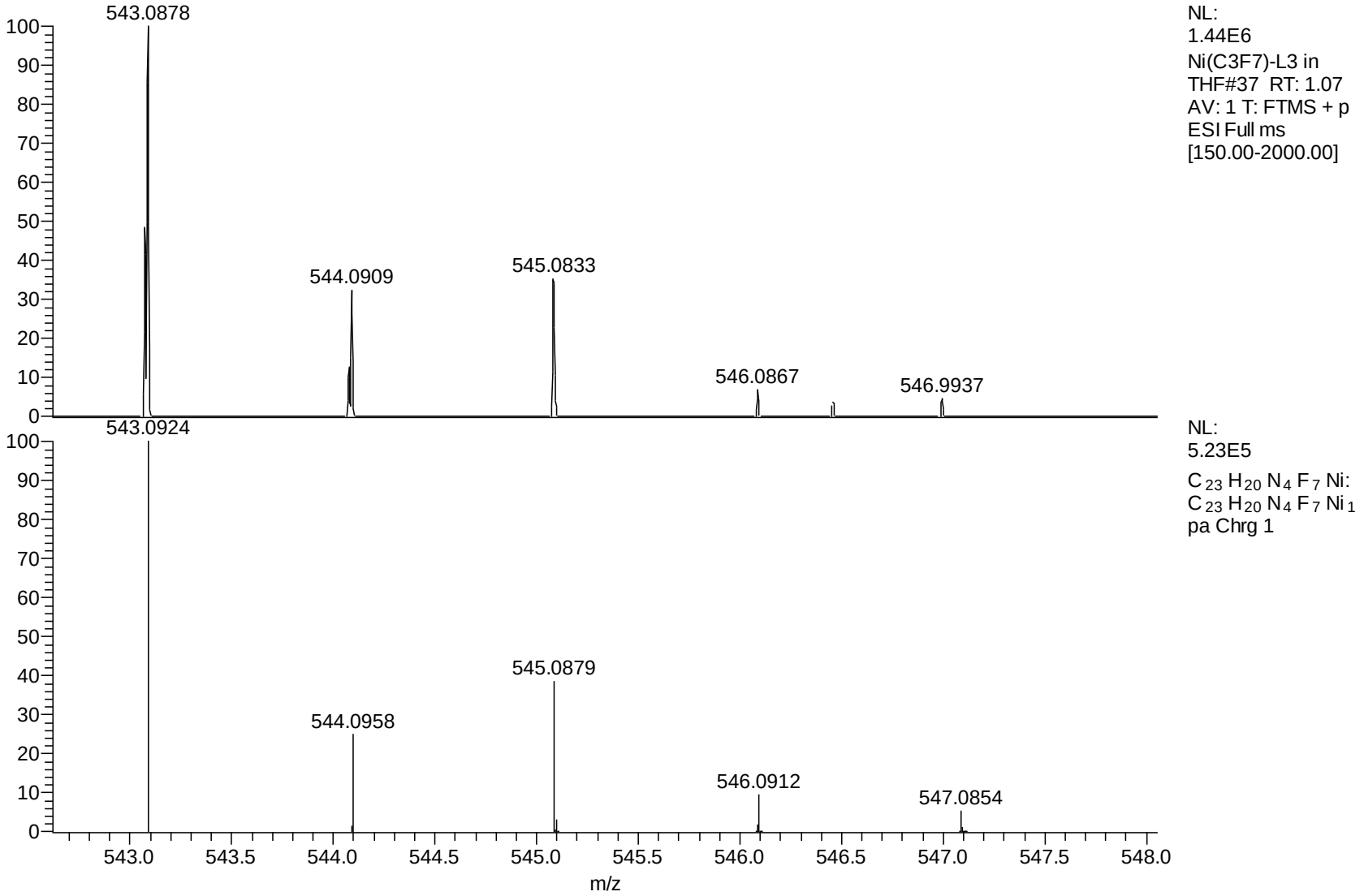

Figure S33. ESI-(HR)MS spectrum of THF solution of **4** (top) and simulated spectrum $C_{23}H_{20}F_7N_4Ni$: (bottom).

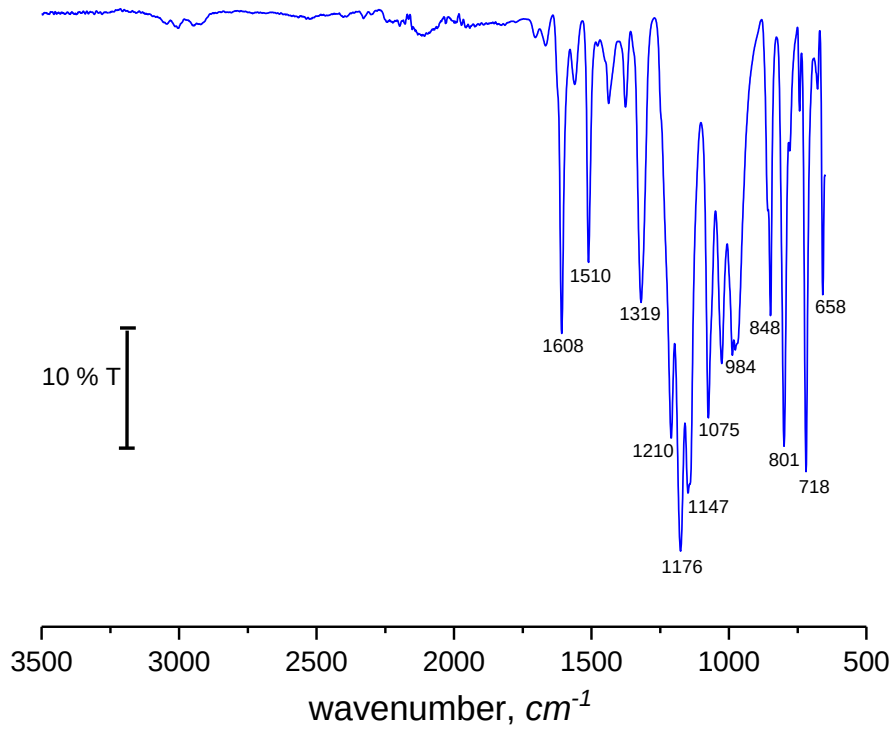

Figure S34. ATR FT-IR transmittance spectrum of **4**.

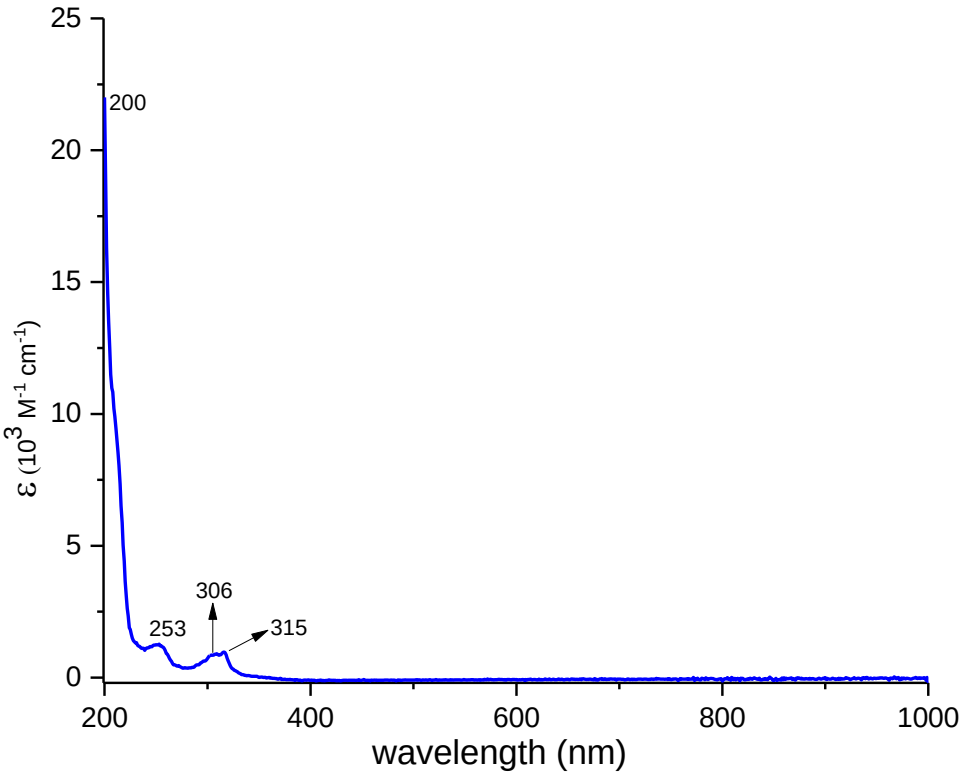

Figure S35. UV-vis absorbance spectrum for **4** in MeCN

Synthesis of 2a

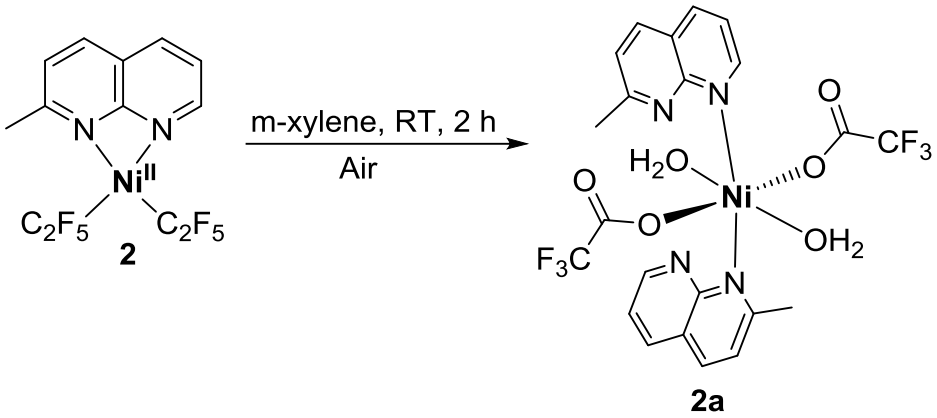

Scheme S5. Synthesis of **2a**.

Complex **2** (50.2 mg, 0.1138 mmol) and water (10.2 μL, 0.5692 mmol) were added in m-xylene (13 mL) in a 50 mL flask equipped with a magnetic stirring bar. The reaction mixture was stirred at room temperature for 2 hours to give a faint yellow solution. The reaction mixture was then passed through syringe filter to a 20 mL vial. The reaction mixture was allowed to evaporate at RT for over a period of one week to yield crystalline complex **2a** (26.5 mg, 38% yield). Crystals suitable for diffraction were grown in benzene solution by slow evaporation method in air.

HRMS (ESI) calculated for $[M\text{-}CF_3CO_2, -2H_2O]^+$ $C_{20}H_{16}O_2N_4F_3Ni$:459.0573; found, 459.0563.

FT-IR (ATR, solid): 3061 (br, w), 2921 (m), 2854 (m), 1688 (s, C=O), 1615 (s), 1499 (s), 1447 (br, s), 1194 (m), 1133 (m), 843 (s), 801 (m), 720 (s) cm^{-1}.

UV-vis (MeCN), λ, nm (ε, $M^{-1}\cdot cm^{-1}$) : 268 (1692), 262 (1887), 255 (1758), 207 (20028).

Elemental Analysis: Expt (Calc): $[C_{22}H_{20}F_6N_4O_6Ni]$: C 42.93 (43.38), H 2.72 (3.31), N 9.19 (9.20).

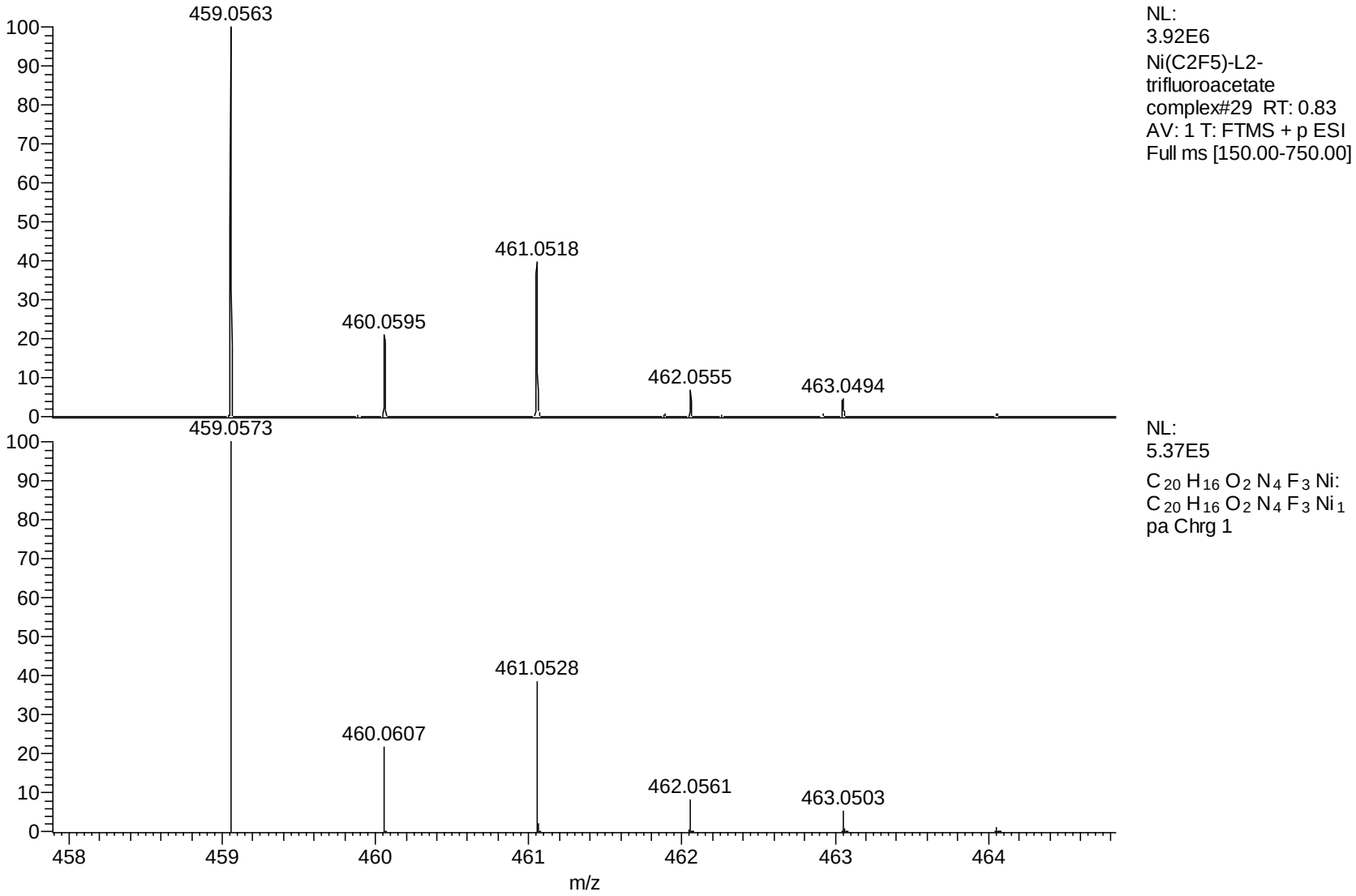

Figure S36. ESI-(HR)MS spectrum of MeOH solution of **2a** (top) and simulated spectrum $C_{20}H_{16}O_2N_4F_3Ni$: (bottom).

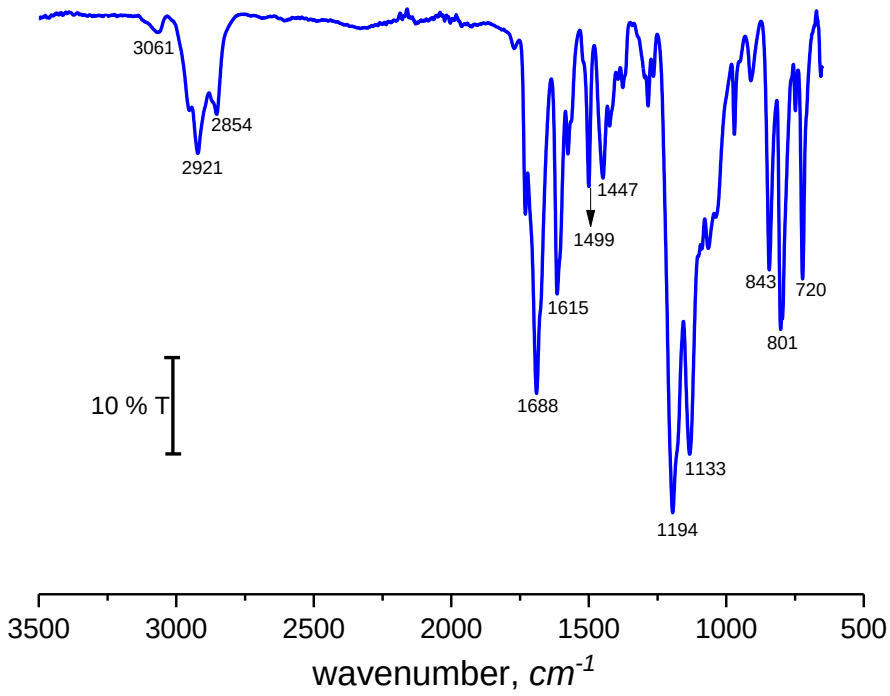

Figure S37. ATR FT-IR transmittance spectrum of **2a**.

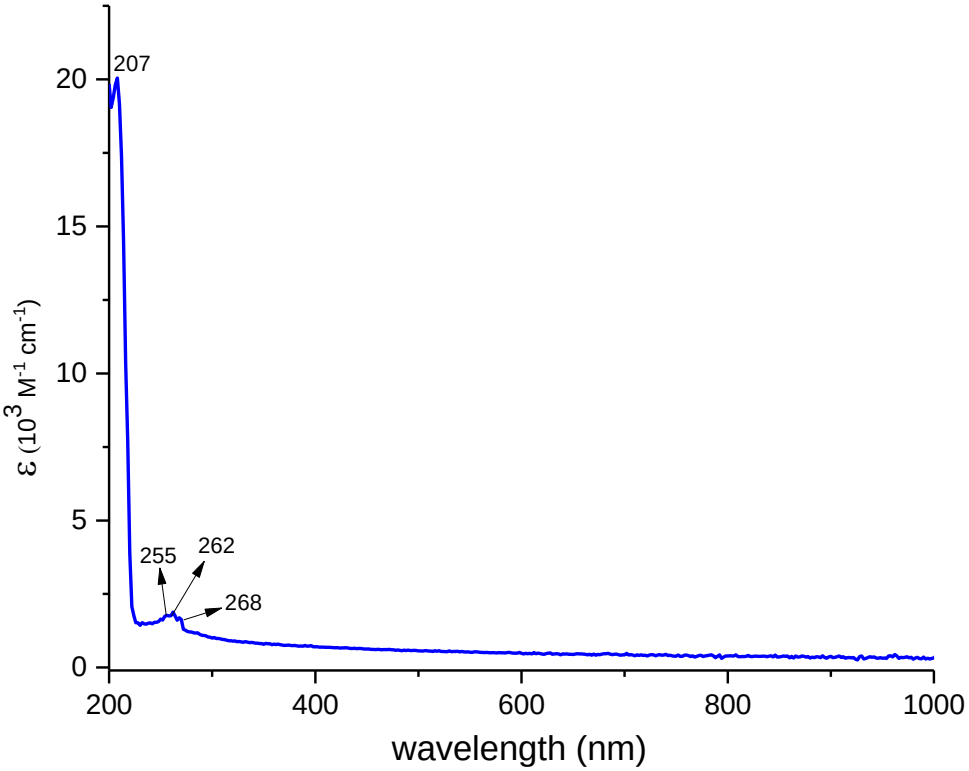

Figure S38. UV-vis absorbance spectrum for **2a** in MeCN

Synthesis of 3a

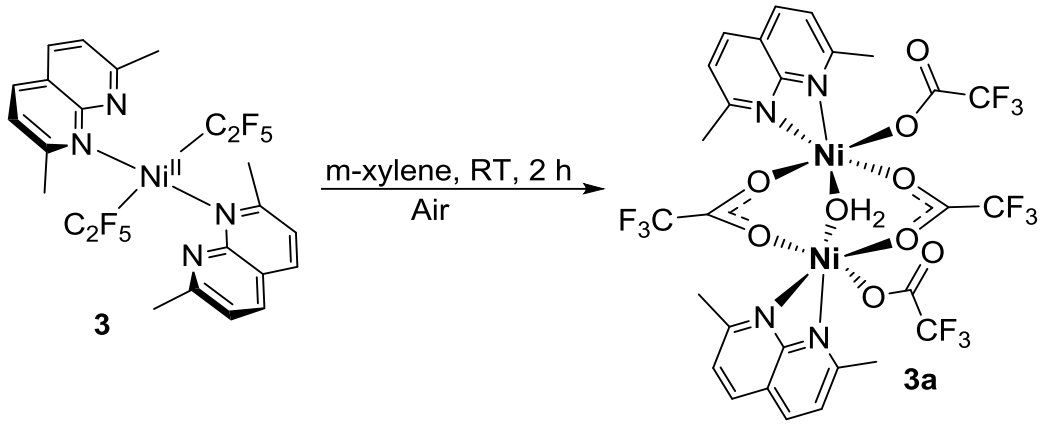

Scheme S6. Synthesis of **3a**.

Complex **3** (60.6 mg, 0.1013 mmol) and water (9.1 μL,0.5066 mmol) were dissolved in m-xylene (15 mL) in a 50 mL flask equipped with a magnetic stirring bar. The reaction mixture was stirred at room temperature for 2 hours to give a pale-yellow color solution. Further the reaction mixture was passed through syringe filter to another 20 mL vial. The reaction mixture was allowed to evaporate at RT for over a period of ten days to yield (43.3 mg, 47% yield) crystals as complex **3a**.

HRMS (ESI) calculated for $[M]^+$ $C_{12}H_{10}O_2N_2F_3Ni$:329.0042; found, 329.0031.

HRMS (ESI) calculated for $[M]^+$ $C_{22}H_{20}O_2N_4F_3Ni$:487.0886; found, 487.0865.

FT-IR (ATR, solid): 3347 (br, w), 3076 (br, w), 2980 (m), 1731 (s, C=O), 1689 (br, m), 1610 (s), 1511 (s), 1199 (br, s), 1141 (br, s), 847 (m), 798 (br, s), 723 (s). cm^{-1}.

UV-vis (MeCN), λ, nm (ε, $M^{-1}\cdot cm^{-1}$) : 272 (545), 266 (581), 212 (1118), 200 (24481).

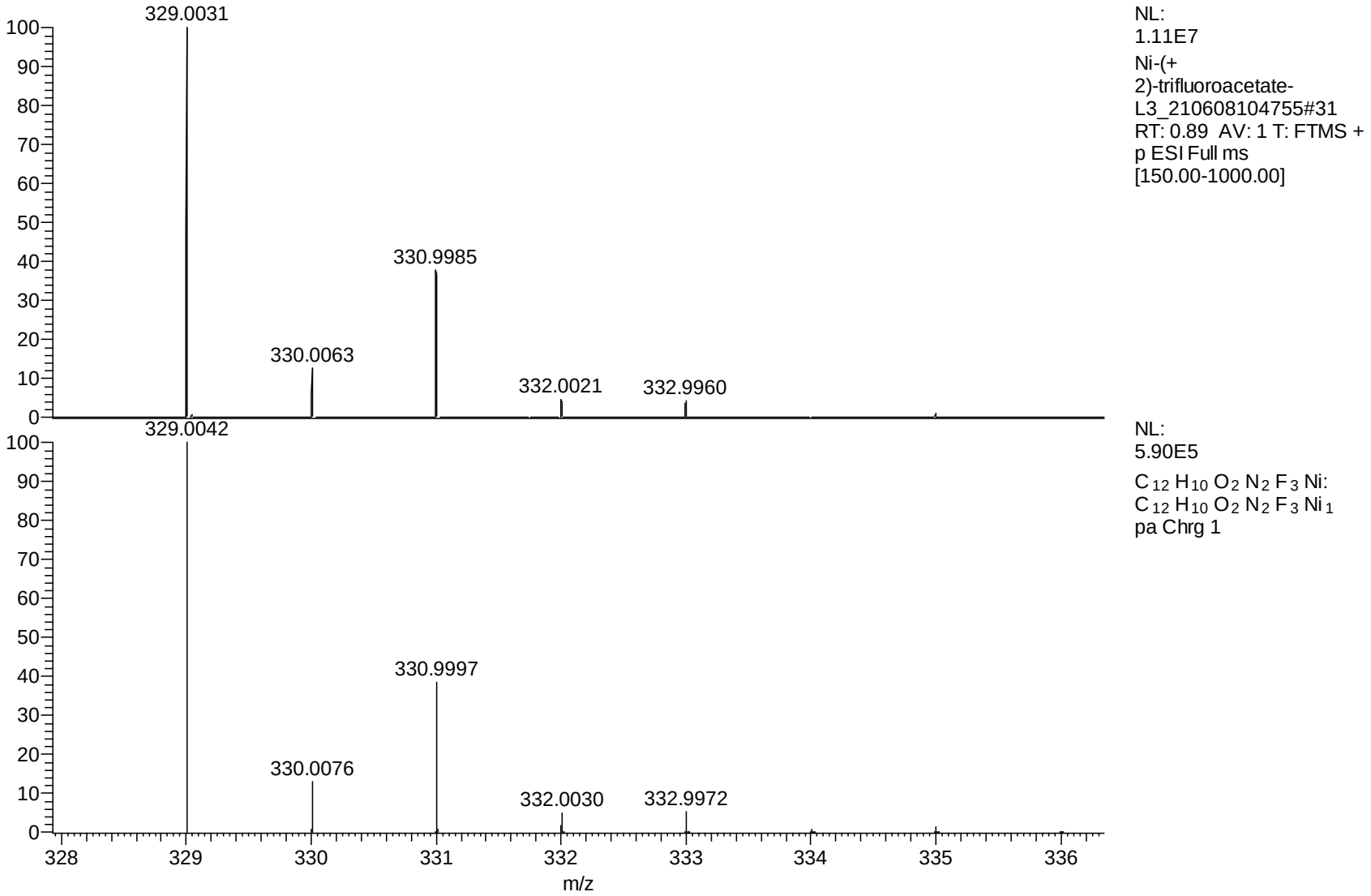

Figure S39. ESI-(HR)MS spectrum of MeOH solution of **3a** (top) and simulated spectrum $C_{12}H_{10}O_2N_2F_3Ni$: (bottom).

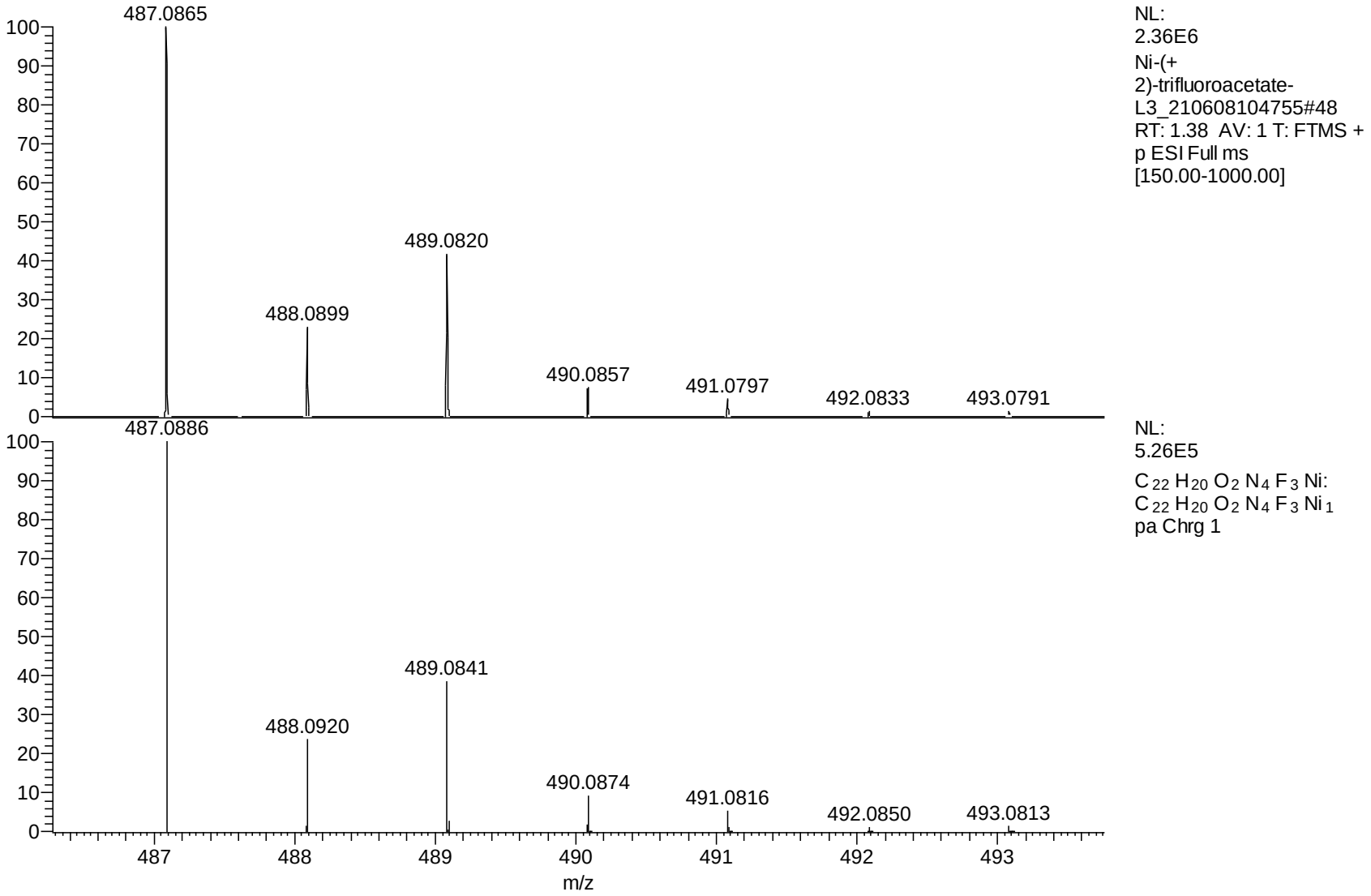

Figure S40. ESI-(HR)MS spectrum of MeOH solution of **3a** (top) and simulated spectrum $C_{22}H_{20}O_2N_4F_3Ni$: (bottom).

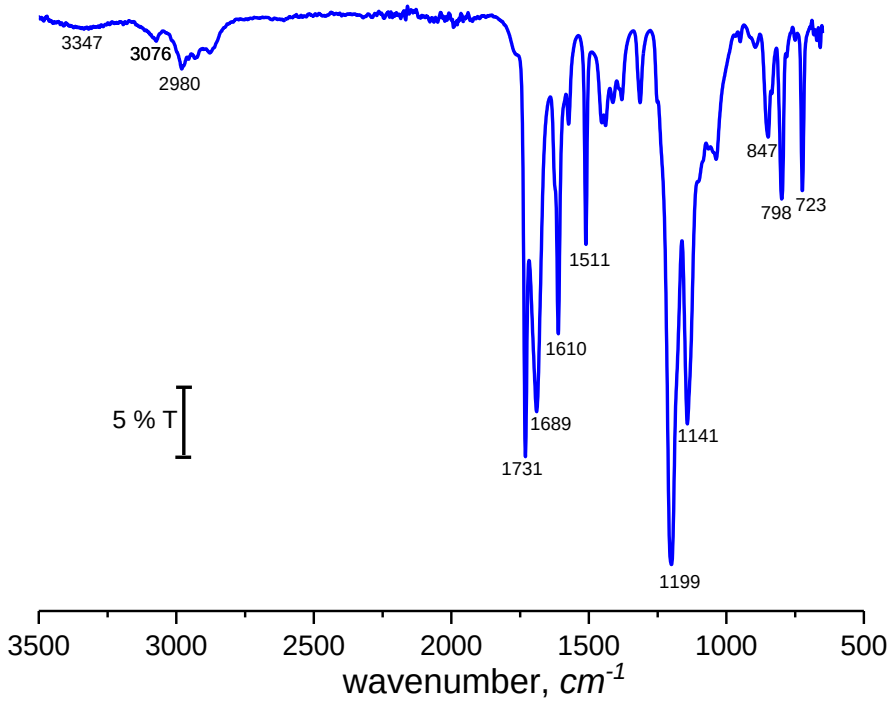

Figure S41. ATR FT-IR transmittance spectrum of **3a**.

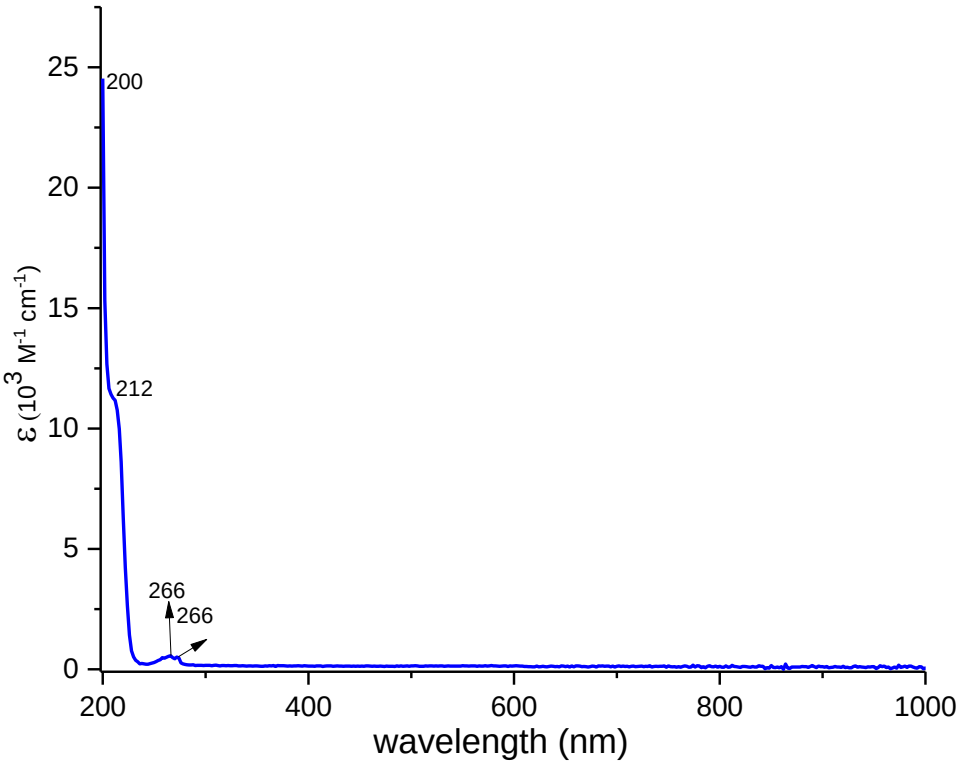

Figure S42. UV-vis absorbance spectrum for **3a** in MeCN

Synthesis of 4a

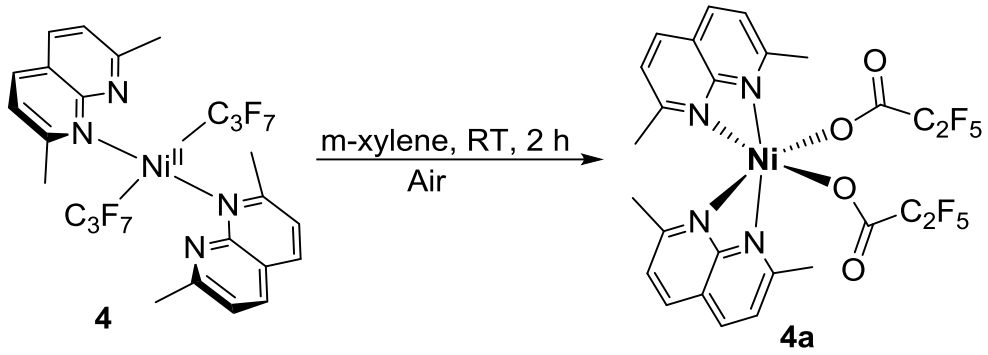

Scheme S7. Synthesis of **4a**.

Complex **3** (56.8 mg, 0.0813 mmol) and water (7.3 μL,0.4068 mmol) were dissolved in m-xylene (15 mL) in a 50 mL flask equipped with a magnetic stirring bar. The reaction mixture was stirred at room temperature for 2 hours to give a pale-yellow color solution. Further the reaction mixture was passed through syringe filter to another 20 mL vial. The reaction mixture was allowed to evaporate at RT for over a period of two weeks to yield (27.8 mg, 48 % yield) pale yellow crystals as complex **4a**.

HRMS (ESI) calculated for $[M\text{-}C_2F_5O_2]^+$ $C_{23}H_{20}O_2N_4F_5Ni$:537.0854; found, 537.0842.

FT-IR (ATR, solid): 3001 (m), 1687 (s, C=O), 1609 (s), 1509 (s), 1313 (br. s), 1206 (br.s), 1158 (m), 1021(s), 851 (s), 800 (s), 727 (s) cm^{-1}.

UV-vis (MeCN), λ, nm (ε, $M^{-1}\cdot cm^{-1}$) : 255 (458), 203 (1913).

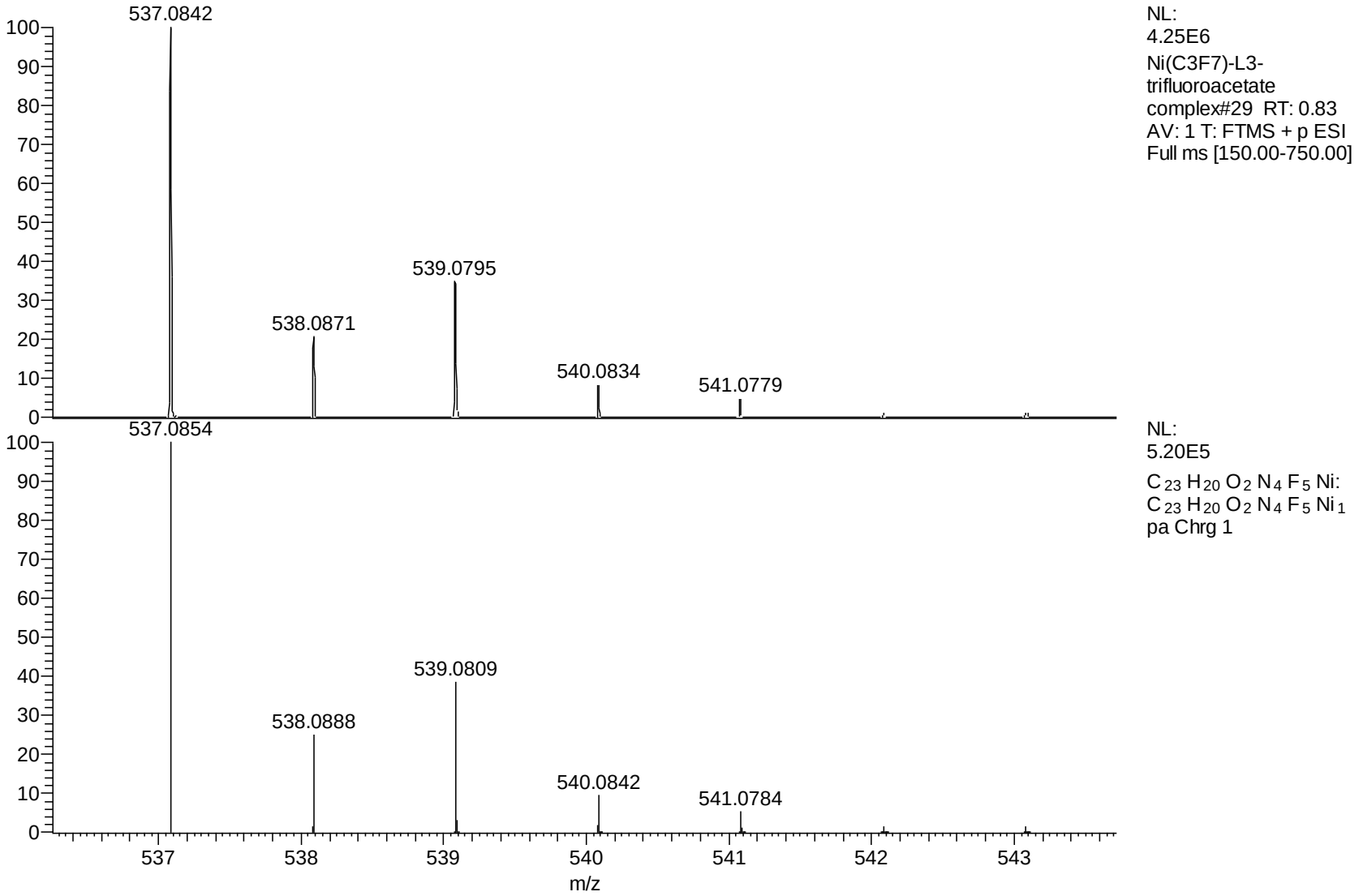

Figure S43. ESI-(HR)MS spectrum of MeOH solution of **4a** (top) and simulated spectrum $C_{23}H_{20}O_2N_4F_5Ni$: (bottom).

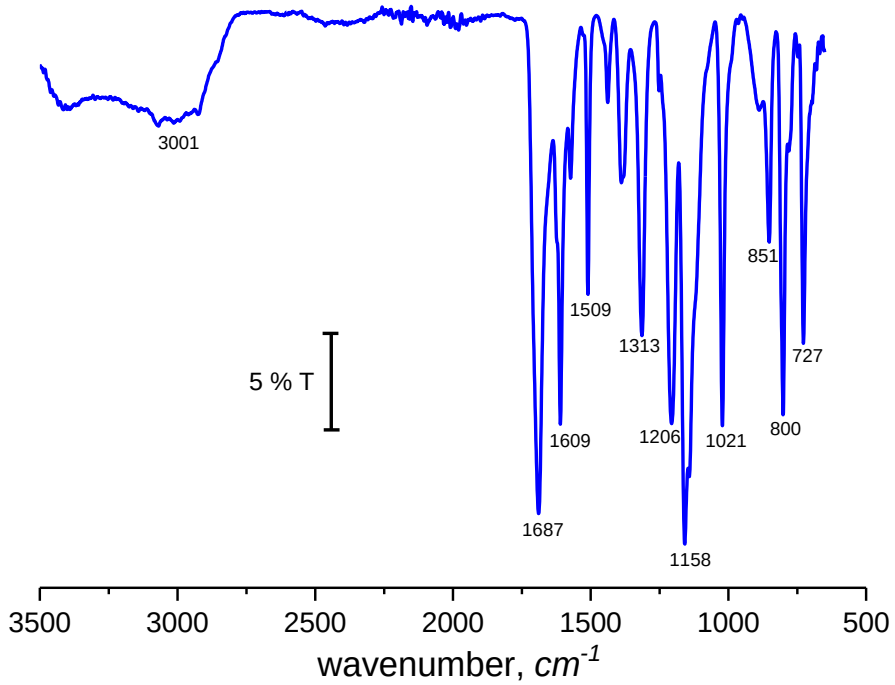

Figure S44. ATR FT-IR transmittance spectrum of **4a**.

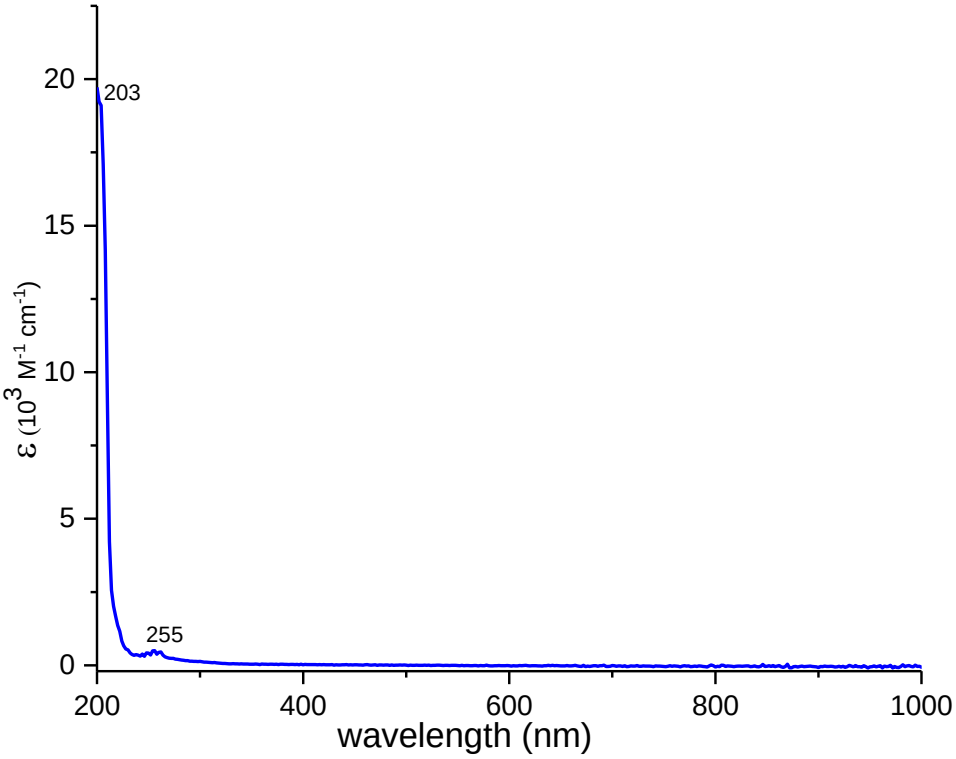

Figure S45. UV-vis absorbance spectrum for **4a** in MeCN.

Cyclic voltammograms

Table S1. Electrochemical properties of complexes **1**, **2, 3** and **4** (V vs Fc).

Complex	E_{pa} vs. Fc/Fc^+, V[a]
1	0.952
2	0.996
3	0.974
4	0.964

[a]In 0.1M ^{n}Bu$_4$NBF$_4$/MeCN at RT, scan rate 100 mV s^{-1}, Pt disk electrode *d* = 1.6 mm.

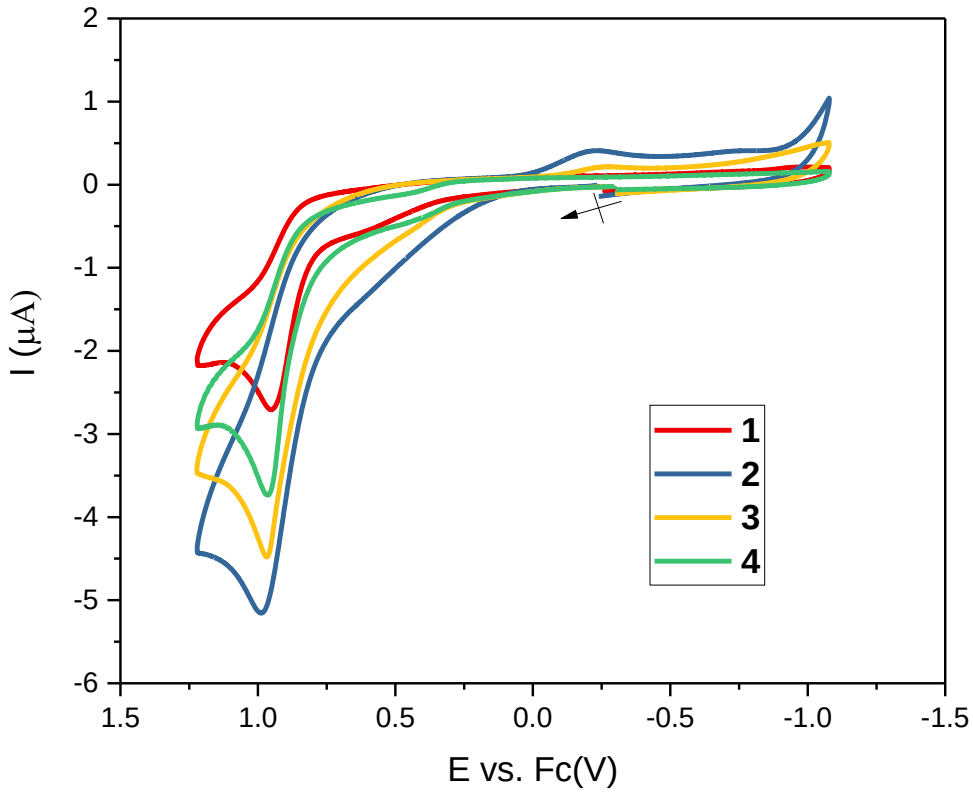

Figure S46. Cyclic voltammograms of complexes **1** (red), **2** (blue), **3** (yellow) and **4** (green). Conditions: 0.1M ^{n}Bu$_4$NBF$_4$/MeCN solutions at RT, scan rate 0.1 V s^{-1}, 1.6 mm Pt disk electrode, the arrow indicates the initial scan direction.

Detection of fluoride during aerobic oxidation of 3

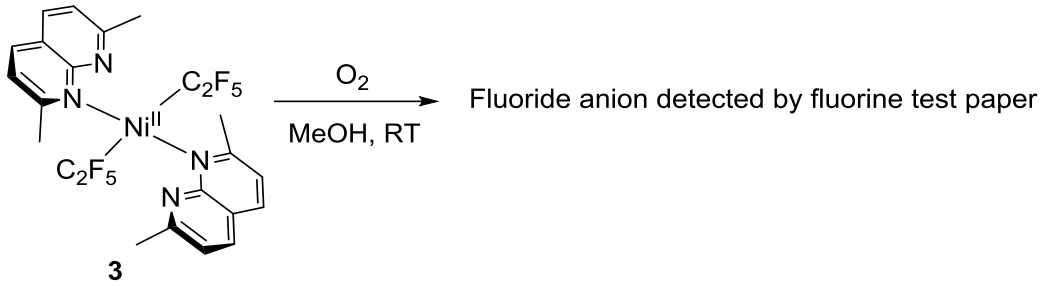

3

Inside the glovebox, solution of complex **3** (4.2 mg, 0.0068 mmol), in MeOH-d_4 (0.4 mL) was placed to a Teflon tube sealed with septum. The tube was removed from glovebox and the reaction mixture was exposed to oxygen gas for four minutes. Next the reaction mixture (0.5 mL) was transferred into another 20 mL vial containing the solvent mixture of MeOH:H_2O (0.5 mL :0.5 mL) with hydrochloric acid (10 µL). The drop of the solution from this mixture was placed on the fluorine paper, which causes color changes from pink to yellow-white indicative of fluoride presence. Three samples were prepared independently to confirm the result.
Control experiments using MeOH:H2O with/without added HCl show no color changes consistent with lack of fluoride at the detectable level. The positive control using Bu4NF solution showed analogous color changes from ping to yellow-white.

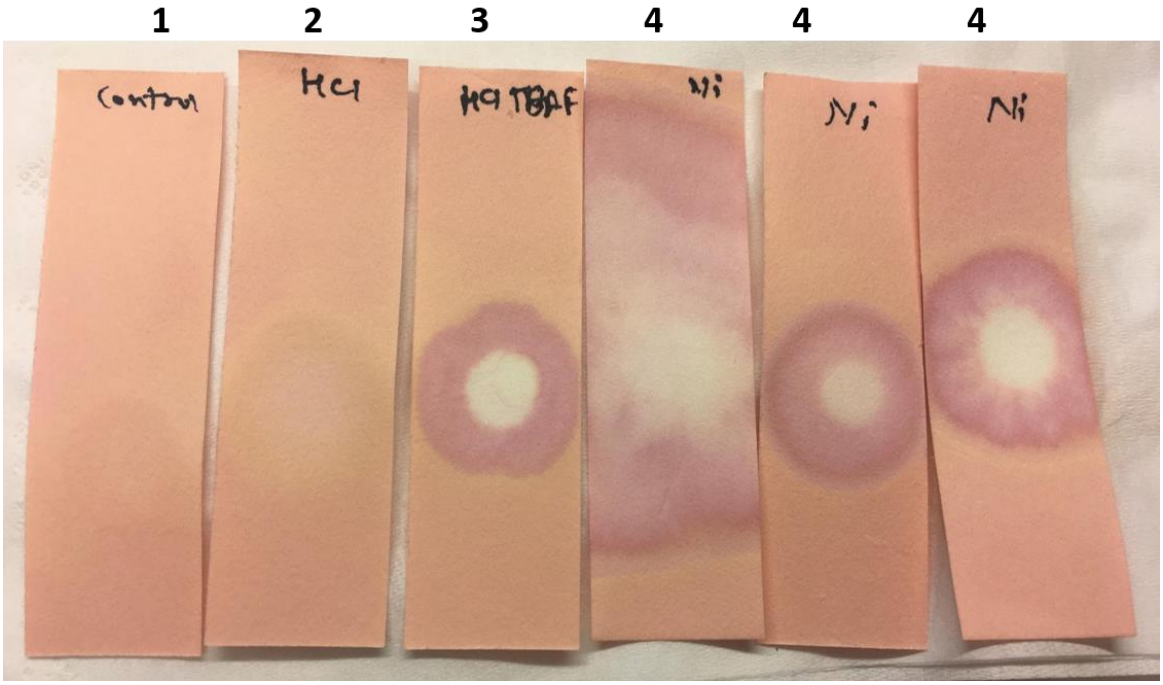

Figure S47. Fluorine paper test results for samples **1-4**. The photographs of fluorine paper strips below correspond to: **1** – negative control solution, MeOH:H_2O (0.5 mL :0.5 mL); **2** – negative control solution, MeOH:H_2O (0.5 mL :0.5 mL) with HCl (10 µL); **3** – positive control solution: MeOH:H_2O (0.5 mL :0.5 mL) with added HCl (10 µL) and tetrabutylammonium fluoride (10 µL); **4-** samples of three reaction mixtures prepared as described above (oxidation of **3** with O_2).

Quantification of perfluorocarboxylate formed by oxidation of 2-4 in MeOH

Aerobic oxidation of 3

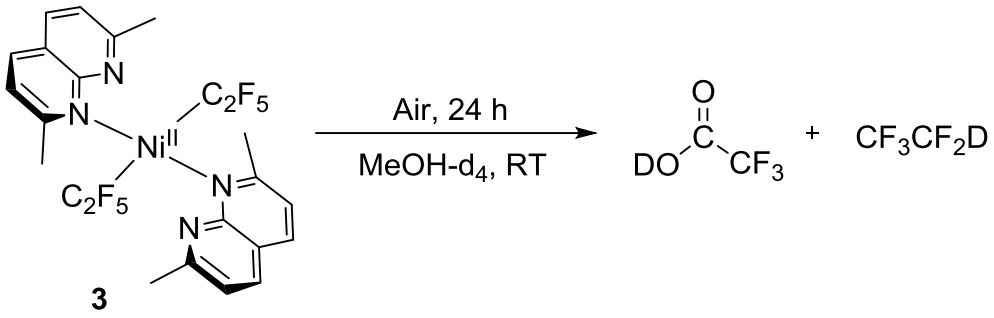

Inside the glovebox, a J. Young NMR tube was charged with complex **3** (11.6 mg, 0.0189 mmol) and α,α,α-trifluorotoluene (2.3 µL, 0.0189 mmol, 1 equiv) dissolved in MeOH-d_4 (0.5 mL). The reaction mixture was exposed to air for two minutes and the tube was sealed with a cap. The NMR tube was then placed in an NMR tube spinner and rotated at RT for 24 hours to ensure good mixing. The reaction mixture was analyzed by ^{19}F NMR showing the peaks of trifluoracetate acid (70% yield) and 1,1,1,2,2-pentafluoroethane (16.5 % yield).

The amount of formed trifluoroacetate (TFA) was determined by ^{19}F NMR integration vs. internal standard, and the reported yield is based on the total number of C_2F_5 groups (two per Ni) as follows: yield of TFA,% = (mol of TFA)*100%/[(mol of Ni complex)*2].

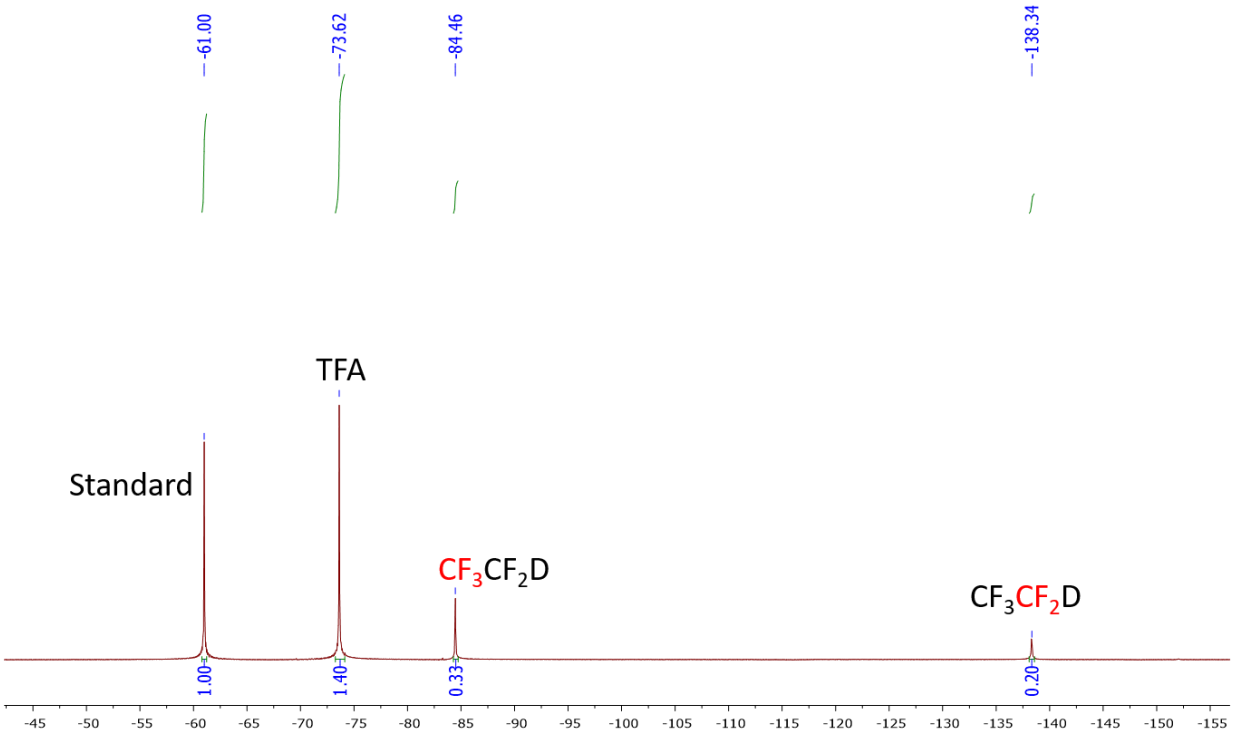

Figure S48. ^{19}F NMR spectrum of the reaction mixture after exposing **3** to air to form trifluoroacetic acid and pentafluoroethane after 24 hours.

Aerobic oxidation of 2

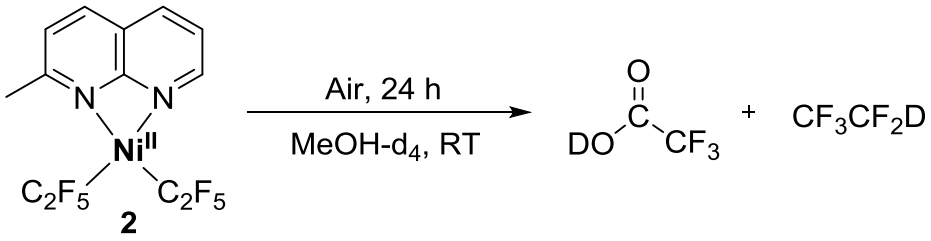

Inside the glovebox, a J. Young NMR tube was charged with complex **2** (14.3 mg, 0.0324 mmol), α,α,α-trifluorotoluene internal standard (4 μL, 0.0324 mmol, 1 equiv) and MeOH-d_4 (0.5 mL). The reaction mixture was exposed to air for two minutes and the NMR tube was sealed with a Teflon cap. The NMR tube was then placed in an NMR tube spinner and rotated RT for 24 h to ensure good mixing. The reaction mixture was then analyzed by ^{19}F NMR showing the peaks of trifluoroacetate (9.5% yield) and 1,1,1,2,2-pentafluoroethane (2% yield).

The amount of formed trifluoroacetate (TFA) was determined by ^{19}F NMR integration vs. internal standard, and the reported yield is based on the total number of C_2F_5 groups (two per Ni) as follows: yield of TFA,% = (mol of TFA)*100%/[(mol of Ni complex)*2].

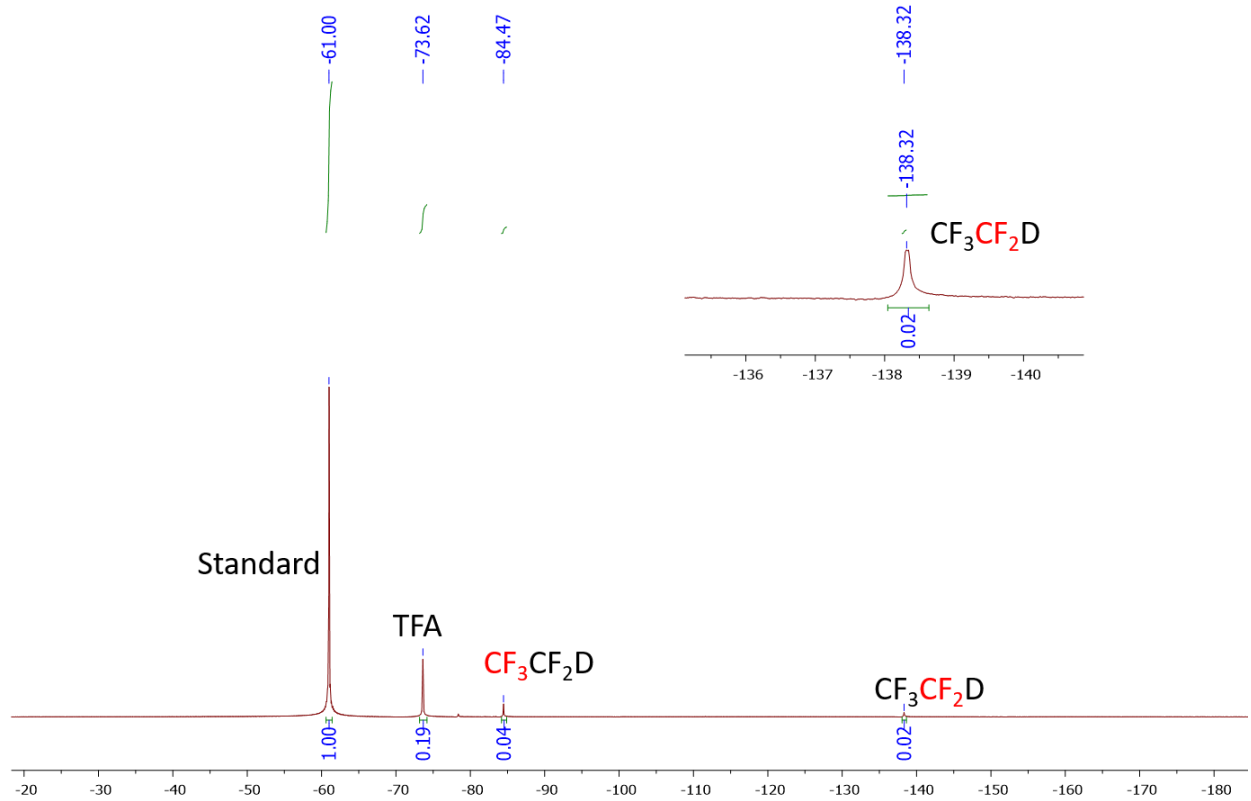

Figure S49. ^{19}F NMR spectrum of the reaction mixture after exposing **2** to air for 24 hours.

Aerobic oxidation of 4

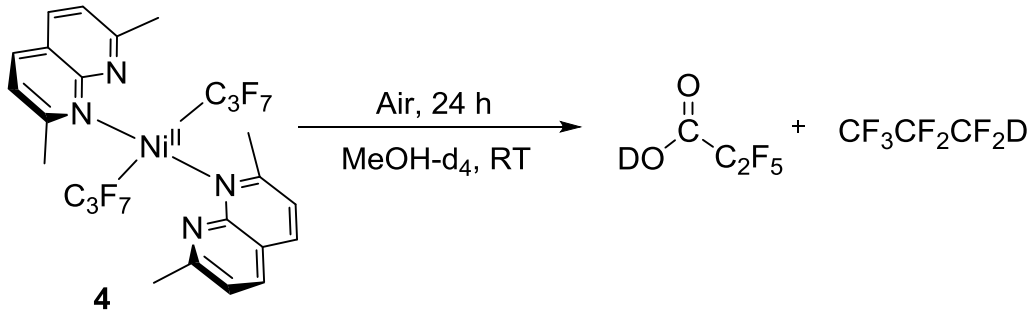

Inside the glovebox, a J. Young NMR tube was charged with complex **4 (**14.8 mg, 0.0207 mmol), α,α,α-trifluorotoluene (2.5 μL, 0.0207 mmol, 1 equiv), and MeOH-d_4 (0.5 mL). The reaction mixture was exposed to air for two minutes and the tube was sealed with a cap. The NMR tube was then placed in an NMR tube spinner and rotated at RT for 24 h to ensure good mixing. The reaction was then analyzed by ^{19}F NMR, showing the peaks of pentafluoropropionate (30.5% yield) and heptafluoropropane (38.5% yield).

The amount of formed pentafluoropropionate was determined by ^{19}F NMR integration vs. internal standard, and the reported yield is based on the total number of C_3F_7 groups (two per Ni) as follows: yield of pentafluoropropionate,% = (mol of pentafluoropropionate)*100%/[(mol of Ni complex)*2].

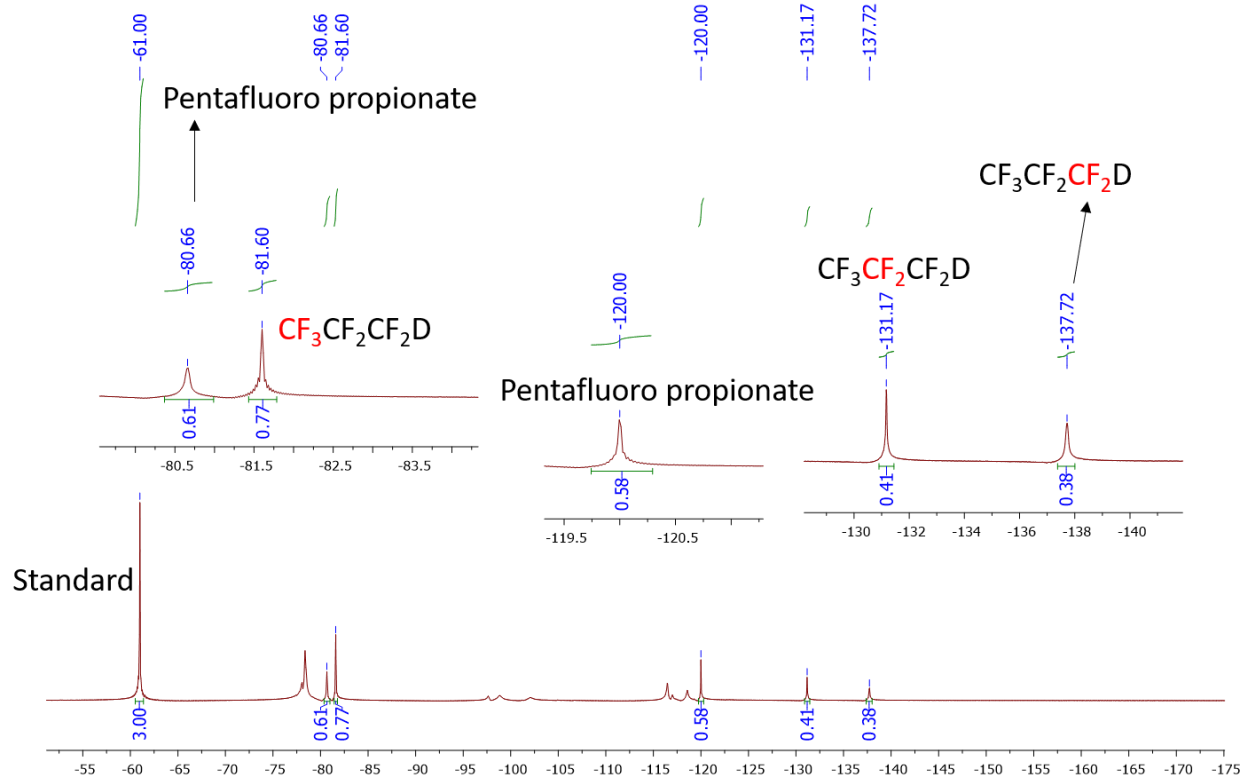

Figure S50. ^{19}F NMR spectrum of the reaction mixture after exposing **4** to air for 24 hours.

Oxidation of 3 with O_2 in MeOH-d_4

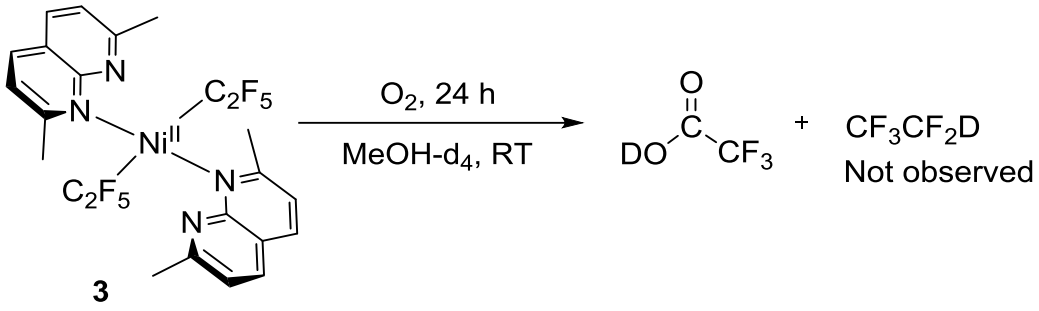

3

Typical procedure. Inside the glovebox, a J. Young NMR tube was charged with complex **3** (12.2 mg, 0.0198 mmol), α,α,α-trifluorotoluene (4.8 μL, 0.0397 mmol, 2 equiv), and MeOH-d_4 (0.5 mL). The reaction mixture was exposed to oxygen gas for three minutes and the tube was sealed with a cap. The reaction mixture was then placed in NMR tube spinner and rotated at RT for 24 h. After completion of the reaction, the reaction was analyzed by ^{19}F NMR showing the peak of trifluoracetate. The amount of formed trifluoroacetate (TFA) was determined by ^{19}F NMR integration vs. internal standard, and the reported yield is based on the total number of C_2F_5 groups (two per Ni) as follows: yield of TFA,% = (mol of TFA)*100%/[(mol of Ni complex)*2].

The experiment was repeated in duplicate under analogous conditions giving 79% yield of TFA in the first run and 74% yield in the second run overall showing consistent results. Average yield is reported in the manuscript. Two NMR spectra are shown below corresponding to duplicate reaction trials.

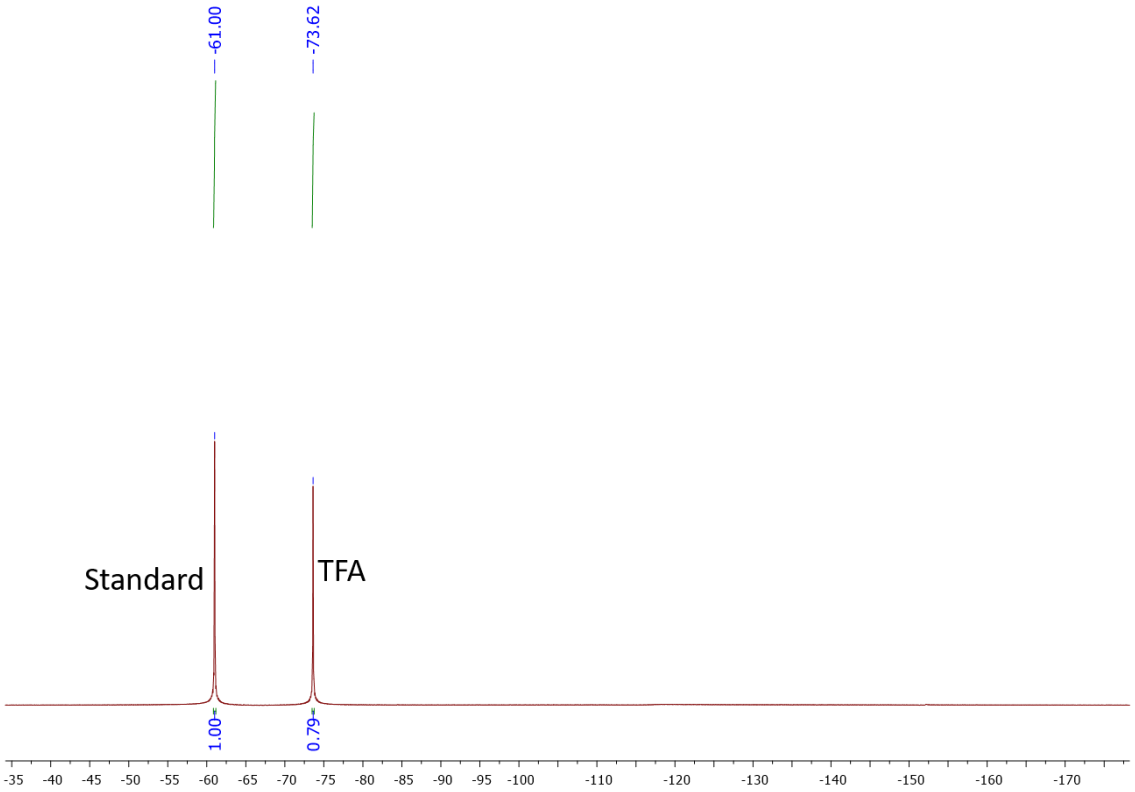

Figure S51. ^{19}F NMR spectrum of the reaction mixture after oxidation of **3** with O_2 in MeOH-d_4 for 24h (trial 1).

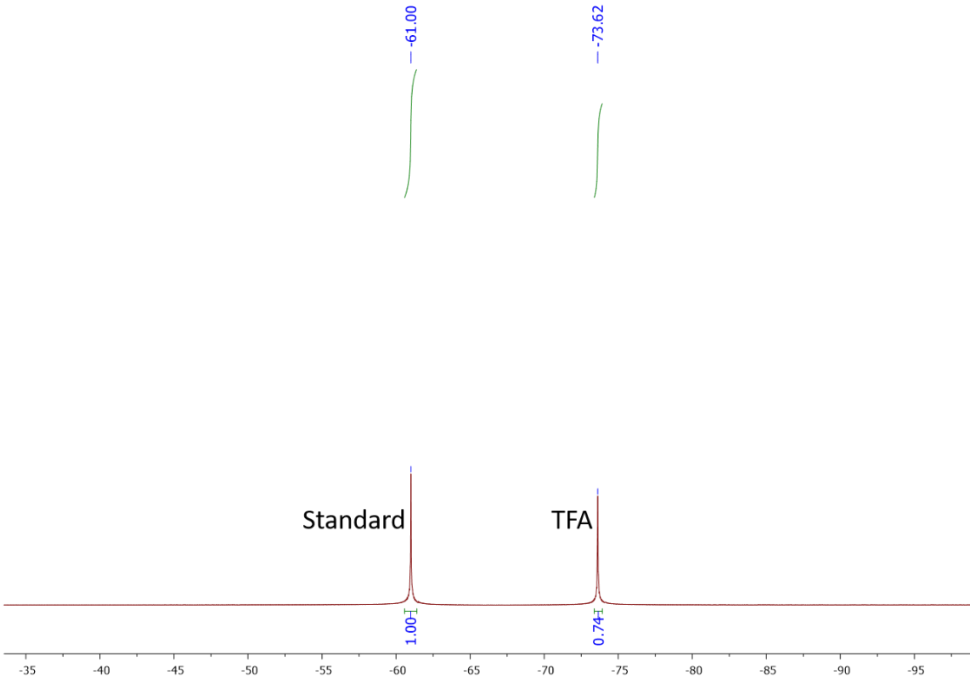

Figure S52. ^{19}F NMR spectrum of the reaction mixture after oxidation of **3** with O_2 in MeOH-d_4 for 24 h (trial 2).

Stability of 3 in methanol followed by NMR spectroscopy

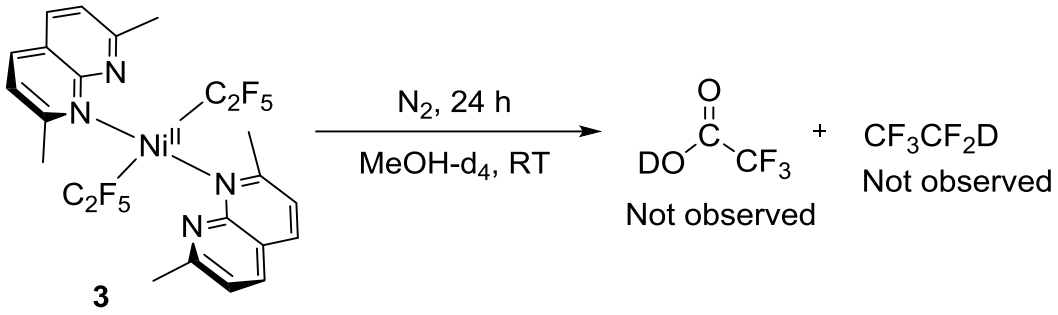

Inside the glovebox, a J. Young NMR tube was charged with complex **3** (6.6 mg, 0.0107 mmol) and MeOH-d_4 (0.5 mL). The reaction mixture was analyzed by NMR spectroscopy showing that the complex remains stable in MeOH solution in the absence of air or oxygen.

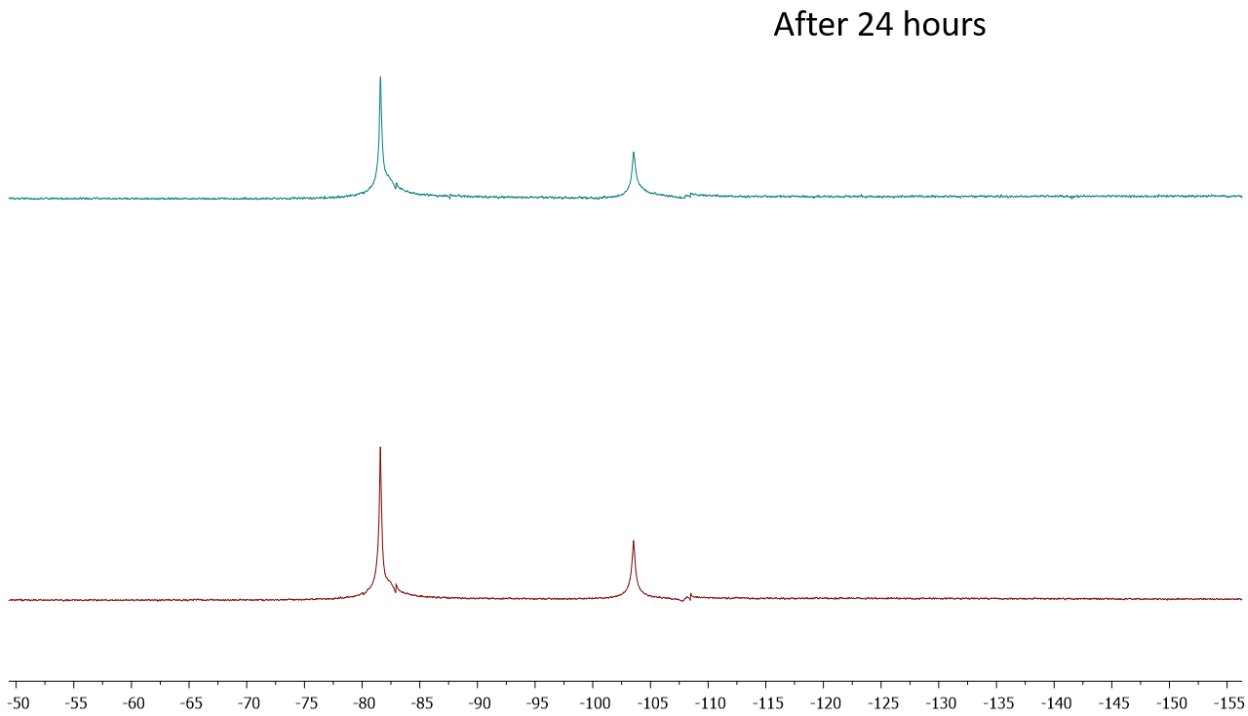

Figure S53. ^{19}F NMR spectrum of the complex **3** in MeOH-d_4, (red) at zero hour (blue) after 24 hours.

Stability of 3 in the presence of 100 equivalents of water under N_2

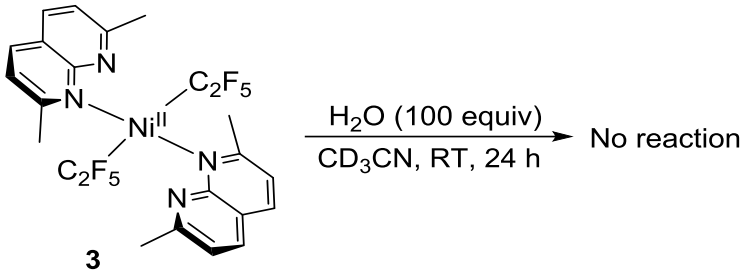

3

To a solution of **3** (4.2 mg, 0.0068 mmol) in MeCN-d_3 in a J. Young NMR tube, water (12.3 µL, 0.6850 mmol) was added and the NMR tube was rotated at RT for 24 hours. The reaction was monitored by NMR spectroscopy. The complex **3** did not show significant decomposition for 24 h at RT; no color changes were observed.

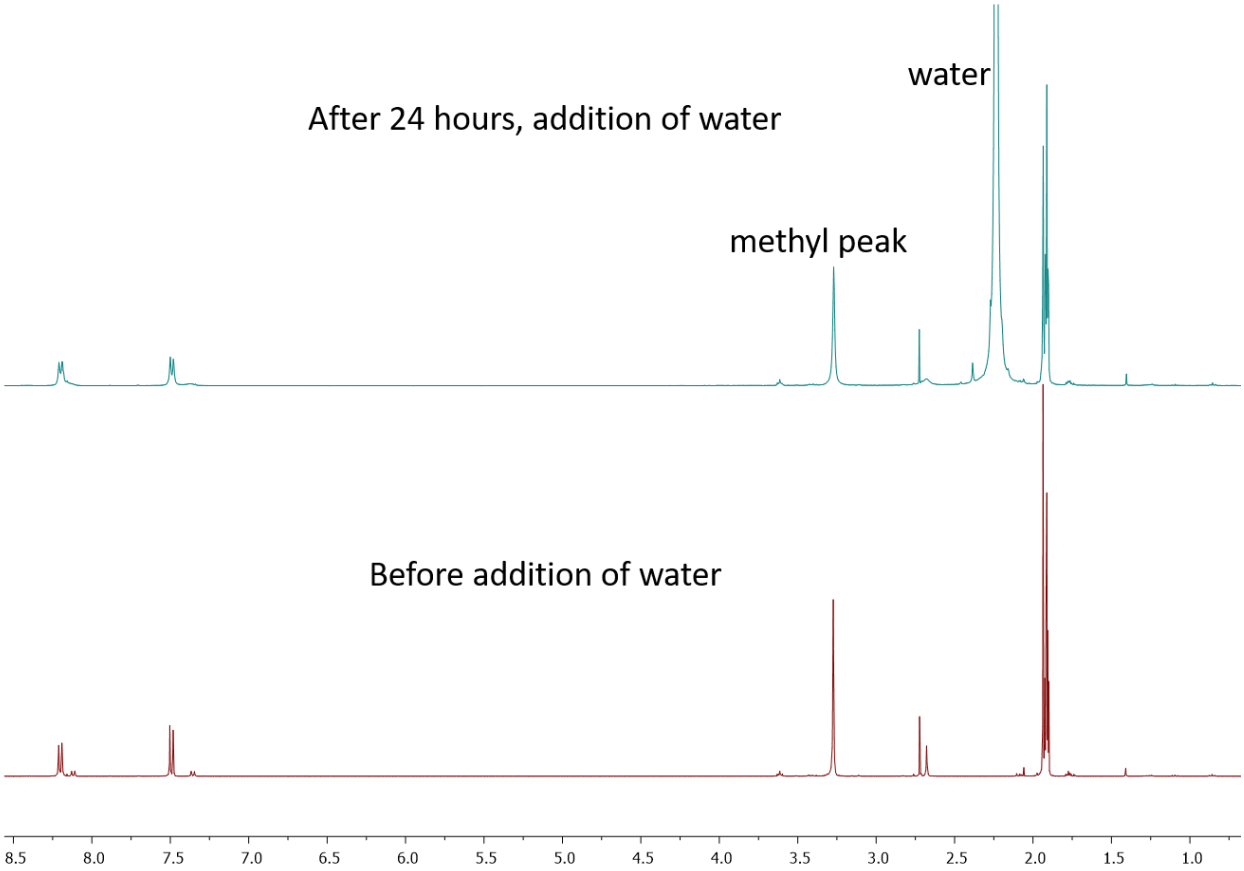

Figure S54. ^{1}H NMR spectrum of **3** in the presence of water at RT in MeCN-d_3 after 24 h. Bottom spectrum is the spectrum of **3** before addition of water.

ESI-MS analysis

Reaction of 3 with O_2 gas

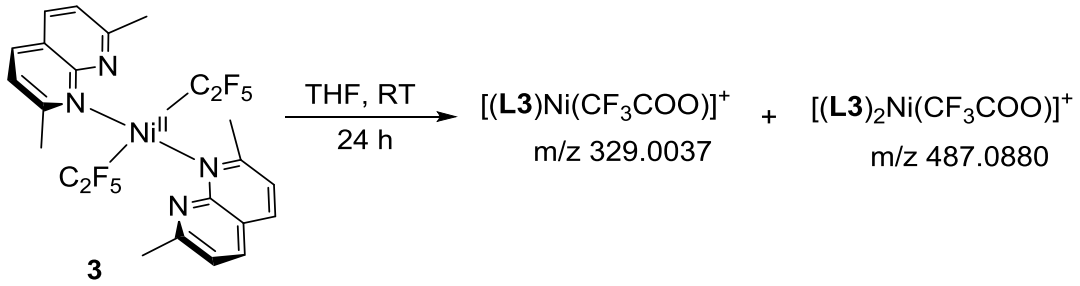

3

Sample preparation - Inside the glovebox, a J. Young NMR tube was charged with complex **3** (6.3 mg, 0.0102 mmol) dissolved in anhydrous THF (0.5 mL). The NMR tube was taken out from the glovebox and connected with oxygen gas cylinder. The reaction mixture was exposed to oxygen gas for three minutes and the tube was sealed with nmr cap. The reaction mixture was then rotated at RT for 24 h. During the course of reaction, the color changes from yellow to purple and then finally to yellow. The reaction was mixture analyzed by direct injection of sample crude using syringe pump to ESI-HRMS, which shows two sets of peaks corresponding to 1:1 and 2:1 **L3** : Ni adducts with trifluoroacetate:

HRMS (ESI) calculated for $[(\mathbf{L3})Ni(CF_3COO)]^+$, $C_{12}H_{10}F_3N_2O_2Ni$: 329.0042; found, 329.0037.

HRMS (ESI) calculated for $[(\mathbf{L3})_2Ni(CF_3COO)]^+$, $C_{22}H_{20}F_3N_4O_2Ni$: 487.0886; found, 487.0880.

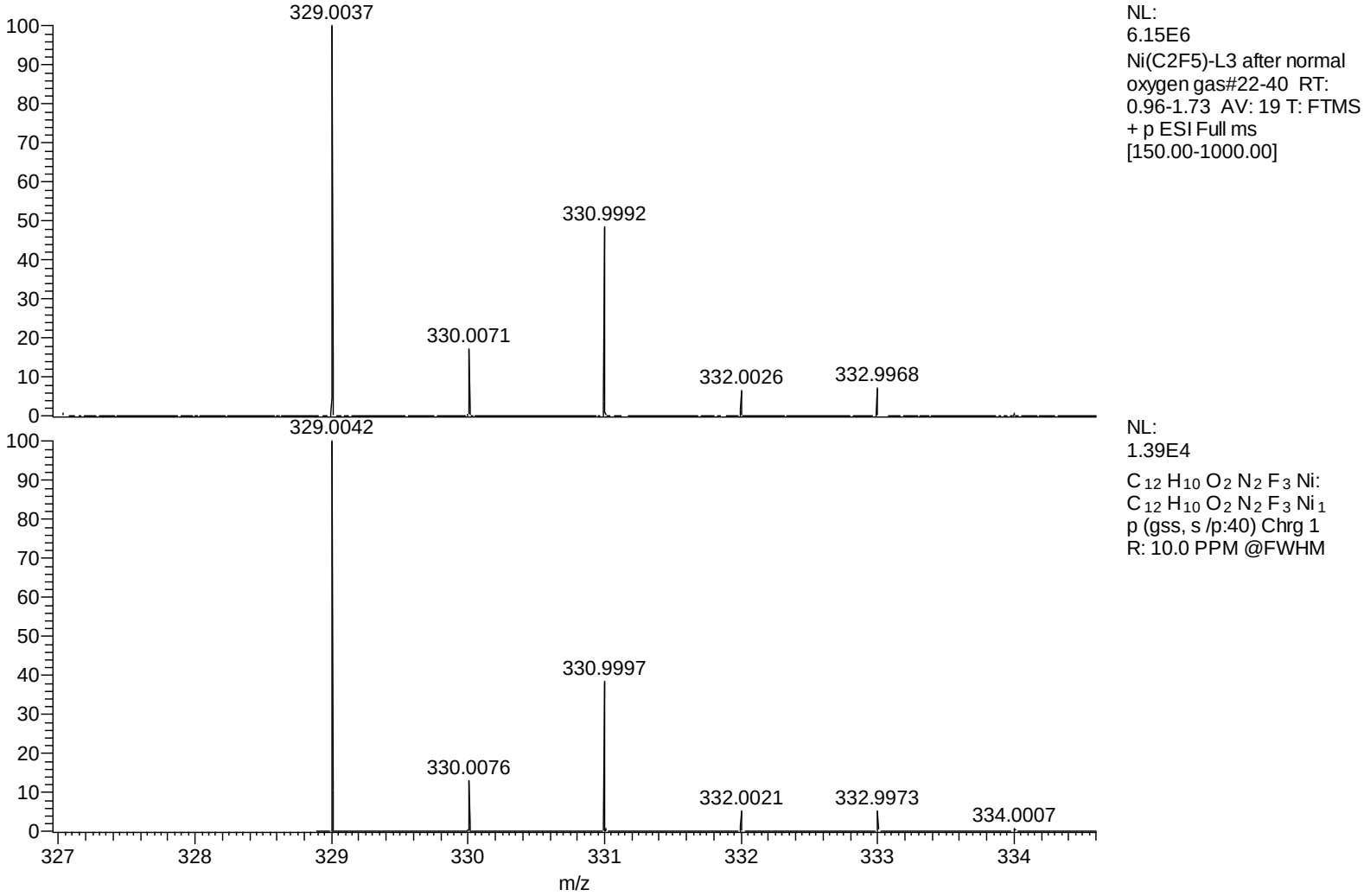

Figure S55. ESI-(HR)MS spectrum of MeOH solution of **3** reacting with oxygen gas (top) and simulated spectrum of [(**L3**)Ni(CF_3COO)]$^+$, $C_{12}H_{10}O_2N_2F_3Ni$ (bottom).

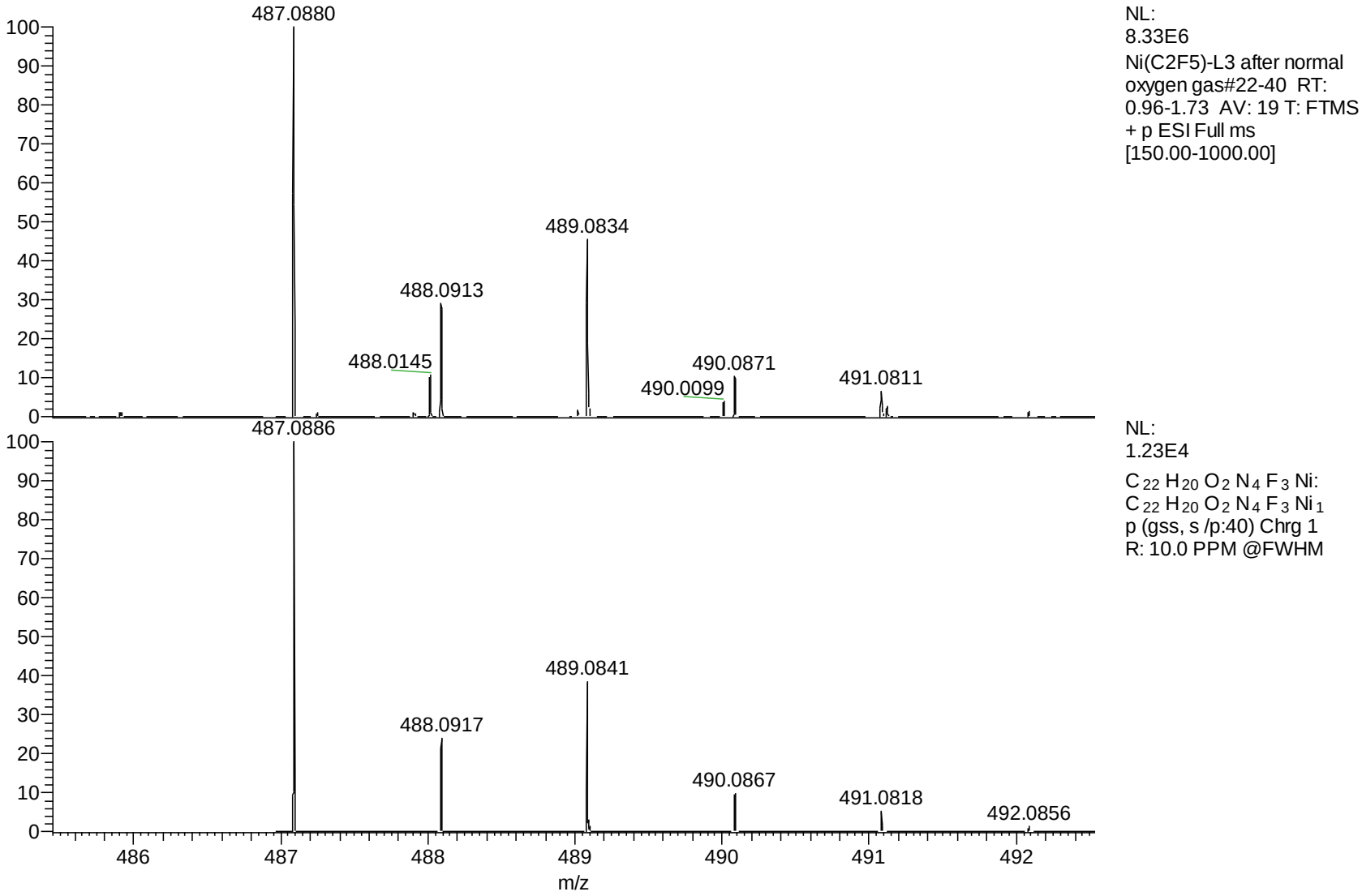

Figure S56. ESI-(HR)MS spectrum of MeOH solution of **3** reacting with oxygen gas (top) and simulated spectrum of $[(\mathbf{L3})_2Ni(CF_3COO)]^+$, $C_{22}H_{20}O_2N_4F_3Ni$: (bottom).

Reaction of 3 with $^{18}O_2$ gas

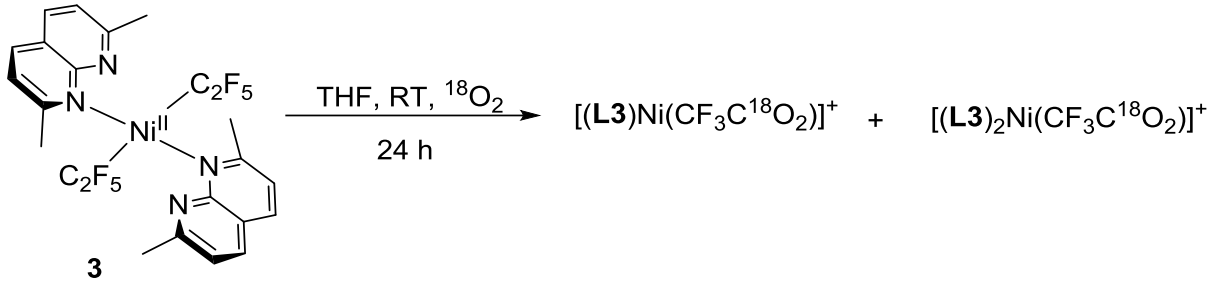

3

Sample preparation - Inside the glovebox, a J. Young NMR tube was charged with complex **3** (4.9 mg, 0.0079 mmol), was dissolved in anhydrous THF (0.5 mL). The NMR tube was taken out from the glovebox and connected with $^{18}O_2$ gas cylinder. The reaction mixture was exposed to labeled oxygen gas for three minutes and the tube was sealed with a cap. The reaction mixture was stirred at RT for 24 hours. During the course of the reaction, the color changed from yellow to purple to again to yellow color The reaction mixture was analyzed by ESI-HRMS showing two sets of peaks corresponding to 1:1 and 2:1 L3:Ni complexes with trifluoroacetate, with main peak corresponding to a doubly-^{18}O-labeled product. The peaks corresponding to the mono-^{18}O-labeled product and non-labeled species were also observed. The ratio reported in the manuscript was calculated from peak intensities corresponding to 1:1 adduct (m/z 333.0121 : m/z 331.0079 : m/z 329.0037), although similar ratio was obtained from comparing intensities of a 2:1 adduct.

HRMS (ESI) calculated for $[(\mathbf{L3})Ni(CF_3C^{18}O_2)]^+$, $C_{12}H_{10}F_3N_2{}^{18}O_2Ni$: 333.0127; found, 333.0121.

HRMS (ESI) calculated for $[(\mathbf{L3})_2Ni(CF_3C^{18}O_2)]^+$, $C_{22}H_{20}F_3N_4{}^{18}O_2Ni$: 491.0971; found, 491.0954.

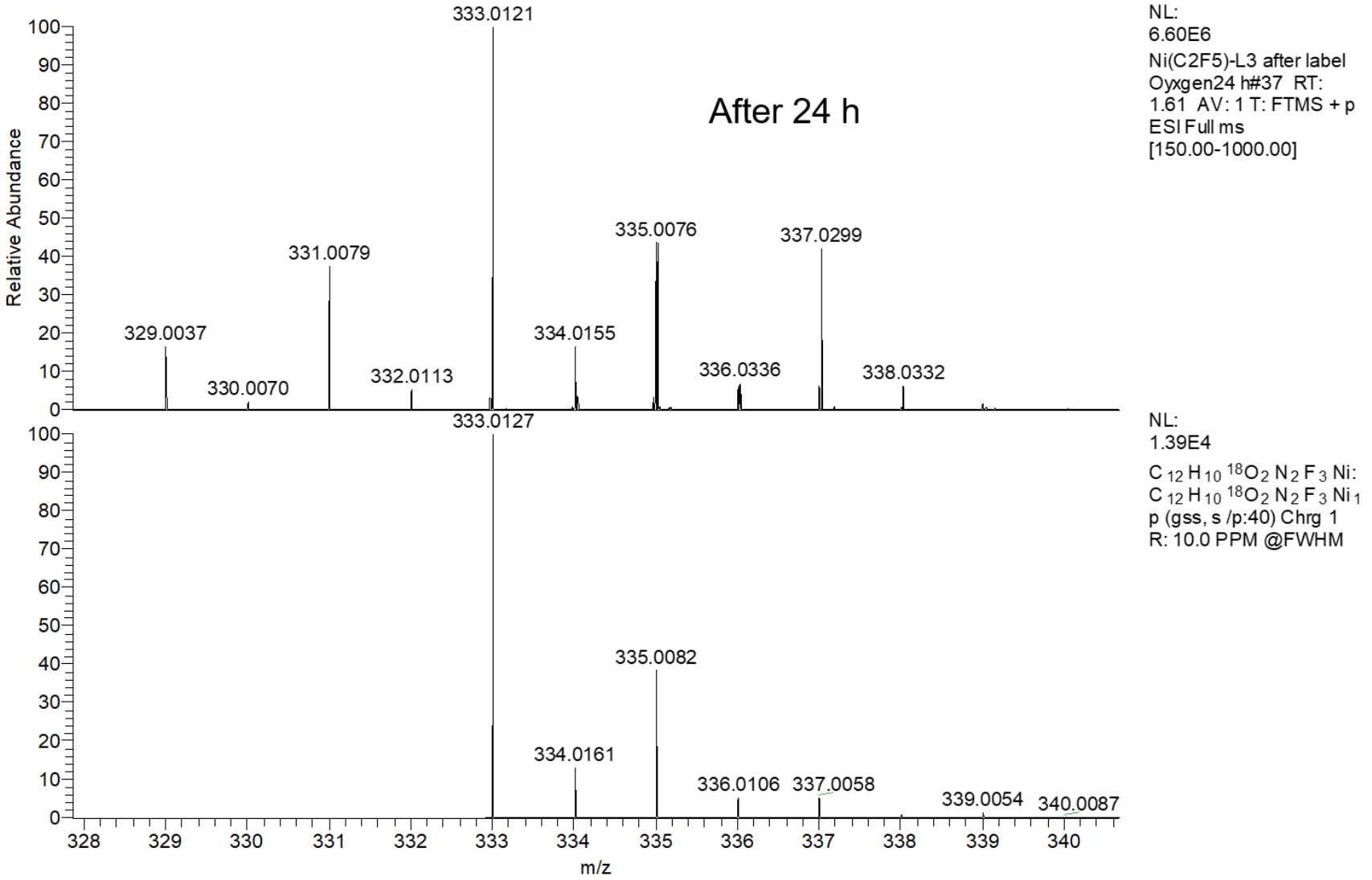

Figure S57.ESI-(HR)MS spectrum of MeOH solution of **3** reacting with $^{18}O_2$ (top) after 24 h and simulated spectrum for [(**L3**)Ni($CF_3C^{18}O_2$)]$^+$, $C_{12}H_{10}{}^{18}O_2N_2F_3Ni$: (bottom).

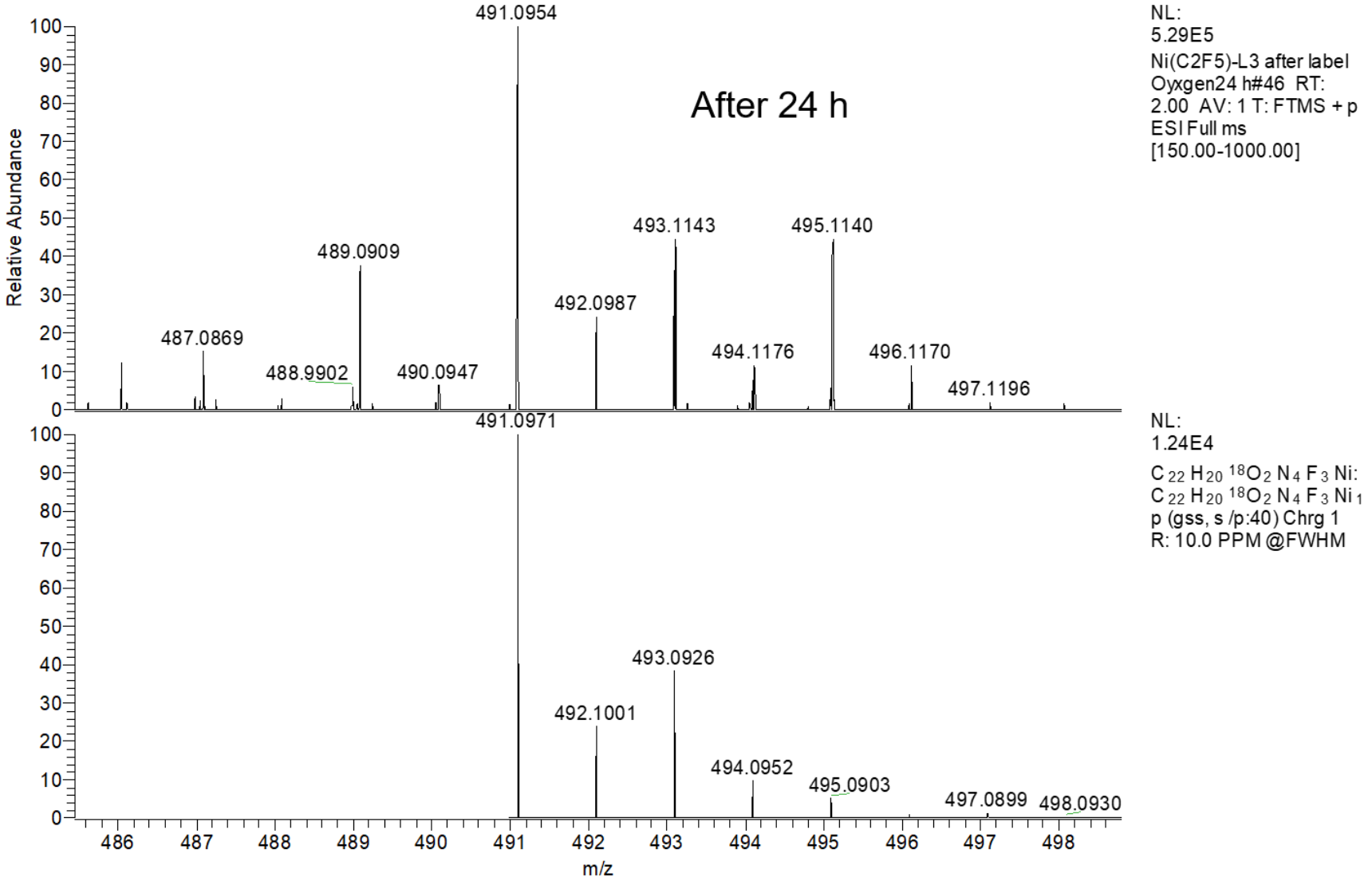

Figure S58. ESI-(HR)MS spectrum of MeOH solution of **3** reacting with $^{18}O_2$ (top) after 24 hour and simulated spectrum $[(\mathbf{L3})_2Ni(CF_3C^{18}O_2)]^+$, $C_{22}H_{20}{}^{18}O_2N_4F_3Ni$: (bottom).

Reaction of 2 with $^{18}O_2$ gas

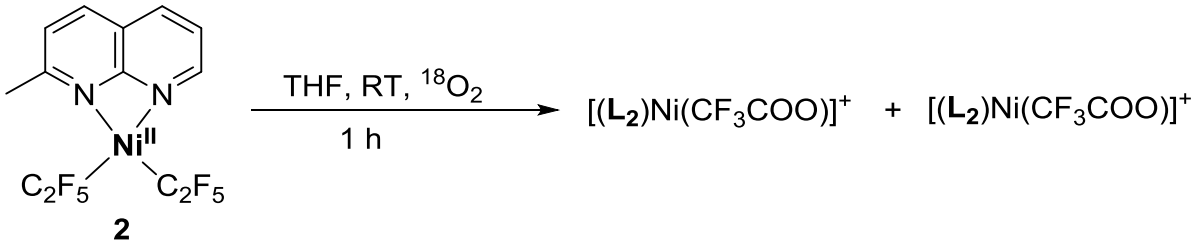

2

Sample preparation - Inside the glovebox, a J. Young NMR tube was charged with complex **2** (5.2 mg, 0.0117 mmol) dissolved in anhydrous THF (0.5 mL). The NMR tube was taken out from the glovebox and connected to labelled $^{18}O_2$ oxygen gas cylinder. The reaction mixture was exposed to labeled oxygen gas for three minutes and the tube was sealed with a cap. The reaction mixture was then rotated at RT for 1 h. After completion of the reaction, the reaction was analyzed by ESI-HRMS, showing two sets of peaks corresponding to complexes with 1:1 and 2:1 ligand to metal ratio.

HRMS (ESI) calculated for [(**L2**)Ni(CF_3COO)]$^+$, $C_{11}H_8F_3N_2{}^{18}O_2Ni$: 318.9971; found, 318.9961.

HRMS (ESI) calculated for [(**L2**)$_2$Ni(CF_3COO)]$^+$, $C_{20}H_{16}F_3N_4{}^{18}O_2Ni$: 463.0658; found, 463.0646.

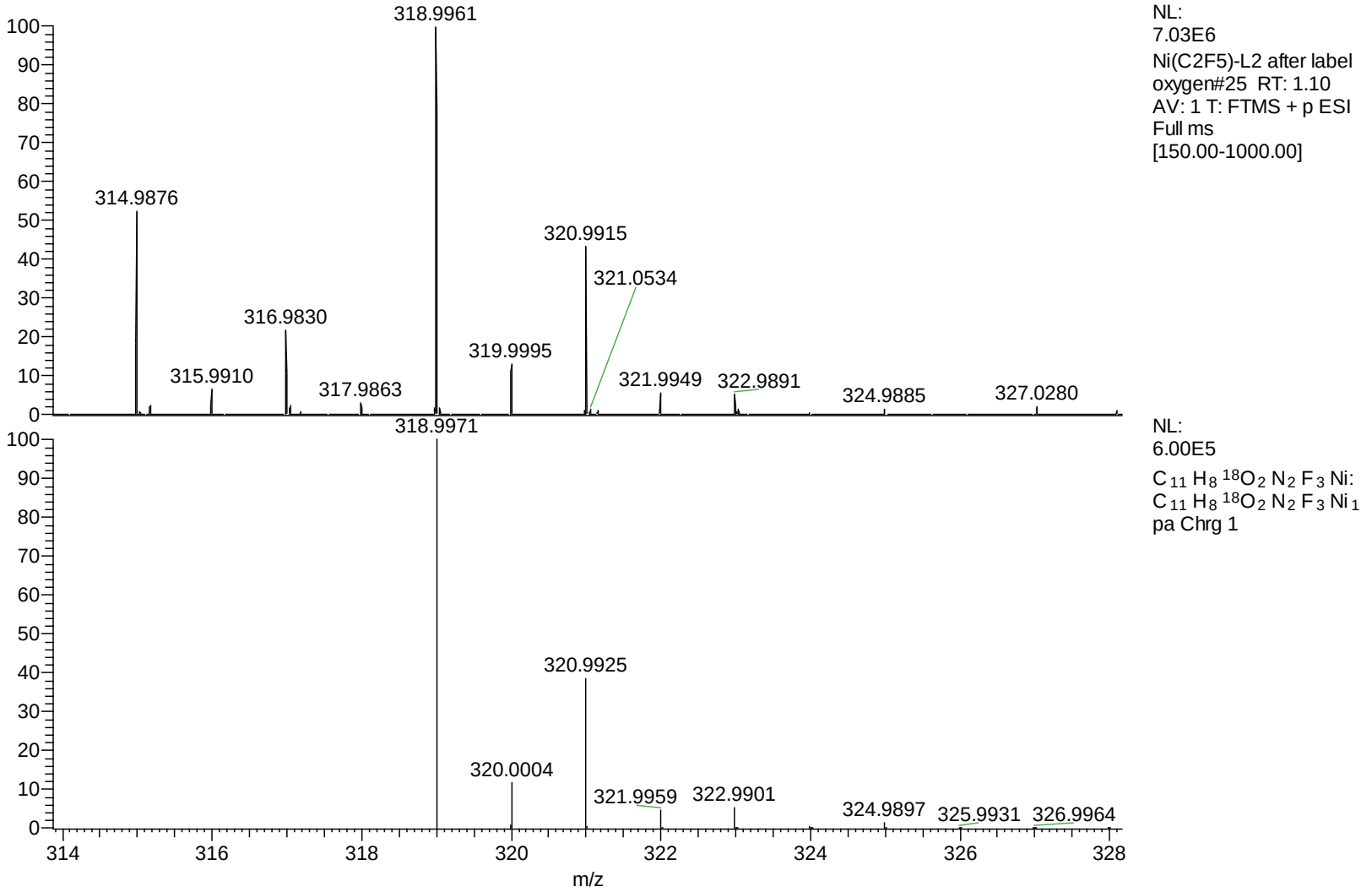

Figure S59. ESI-(HR)MS spectrum of MeOH solution of **2** reacting with $^{18}O_2$ (top) and simulated spectrum [(**L2**)Ni(CF_3COO)]$^+$, $C_{11}H_8{}^{18}O_2N_2F_3Ni$: (bottom)

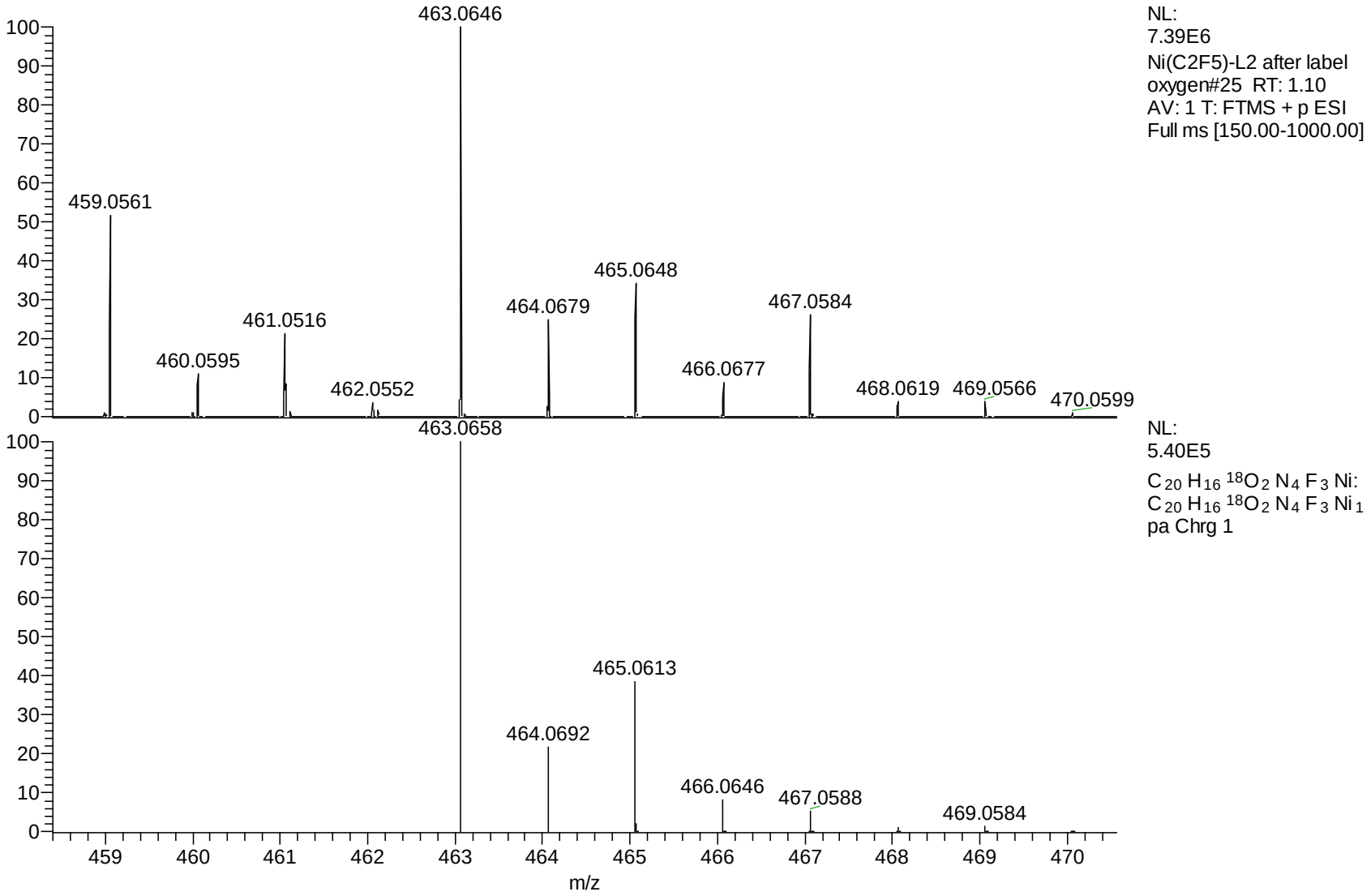

Figure S60. ESI-(HR)MS spectrum of MeOH solution of **2** reacting with $^{18}O_2$ (top) and simulated spectrum[(**L2**)$_2$Ni(CF_3COO)]$^+$, $C_{20}H_{16}{}^{18}O_2N_4F_3Ni$: (bottom)

Reaction of 4 with $^{18}O_2$ gas

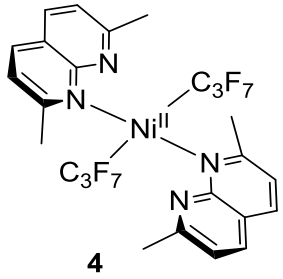

4

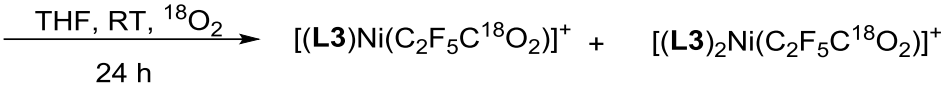

Sample preparation - Inside the glovebox, a J. Young NMR tube was charged with complex **4** (5.1 mg, 0.0071 mmol) dissolved in dry THF (0.5 mL). The NMR tube was taken out from the glovebox and connected with $^{18}O_2$ gas cylinder. The reaction mixture was exposed to labeled oxygen gas for three minutes and the tube was sealed with a cap. The reaction mixture was stirred at RT for 24 h and analyzed by ESI-HRMS, showing two sets of signals corresponding to 1:1 L3:Ni adduct, [(**L3**)Ni(pentrafluoropropionate)]$^+$, and 2:1 complex, [(**L3**)$_2$Ni(pentrafluoropropionate)]$^+$. The main peak corresponds two the product containing two labeled ^{18}O-atoms, with peaks of the mono-labeled and non-labeled pentafluoropropionate at smaller intensities. The ratio reported in the manuscript was calculated from peak intensities corresponding to 1:1 adduct (m/z 383.0086 : m/z 381.0044 : m/z 379.0970), although similar ratio was obtained from comparing intensities of 2:1 adduct.
HRMS (ESI) calculated for [(**L3**)Ni($C_2F_5C^{18}O_2$)]$^+$, $C_{13}H_{10}F_5N_2{}^{18}O_2Ni$: 383.0095; found, 383.0086.

HRMS (ESI) calculated for [(**L3**)$_2$Ni($C_2F_5C^{18}O_2$)]$^+$, $C_{23}H_{20}F_5N_4{}^{18}O_2Ni$: 541.0939; found, 541.0929.

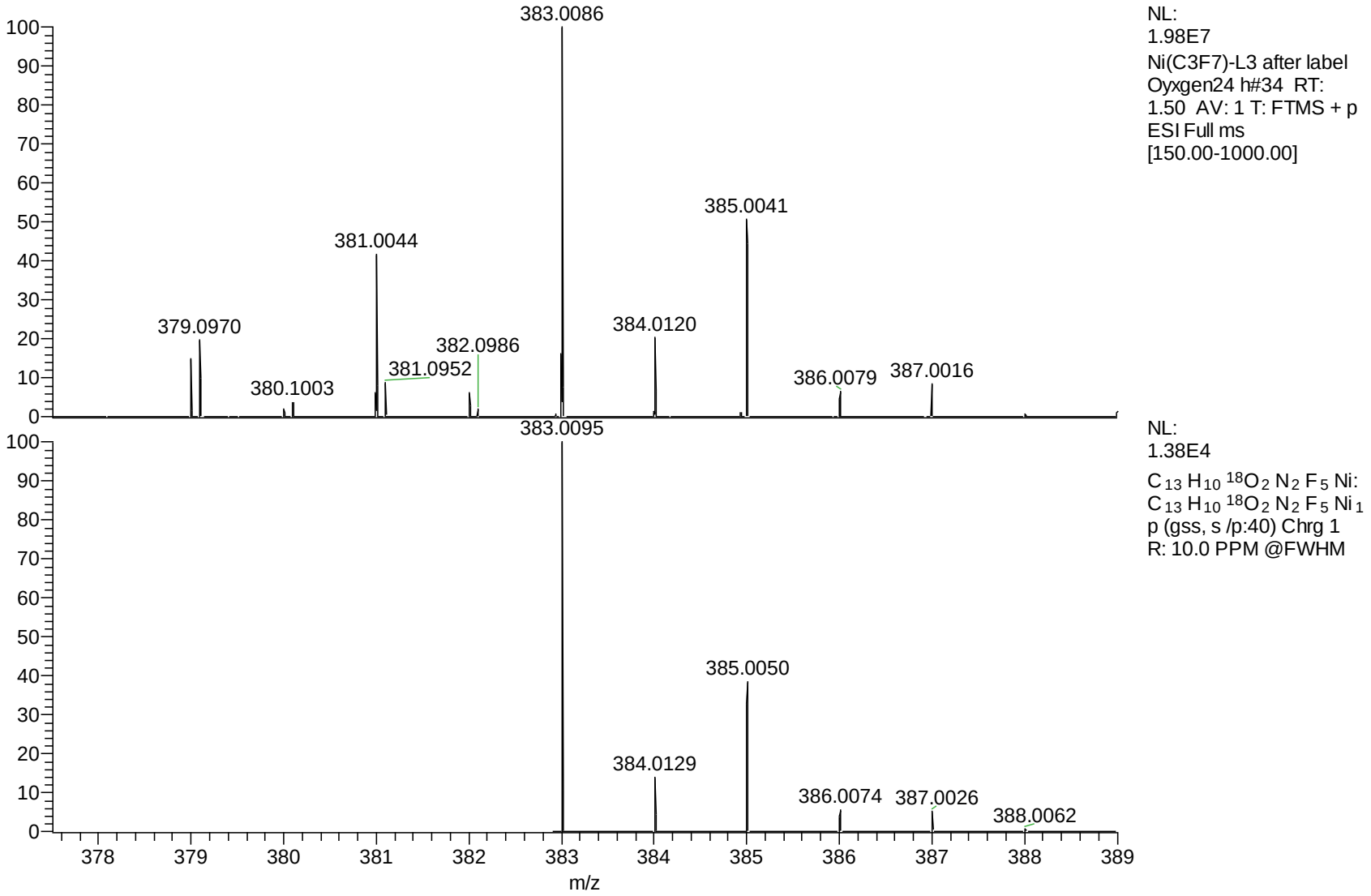

Figure S61. ESI-(HR)MS spectrum of MeOH solution of **4** reacting with label oxygen gas (top) after 24 hour and simulated spectrum [(**L3**)Ni($C_2F_5C^{18}O_2$)]$^+$, $C_{13}H_{10}{}^{18}O_2N_2F_5Ni$: (bottom).

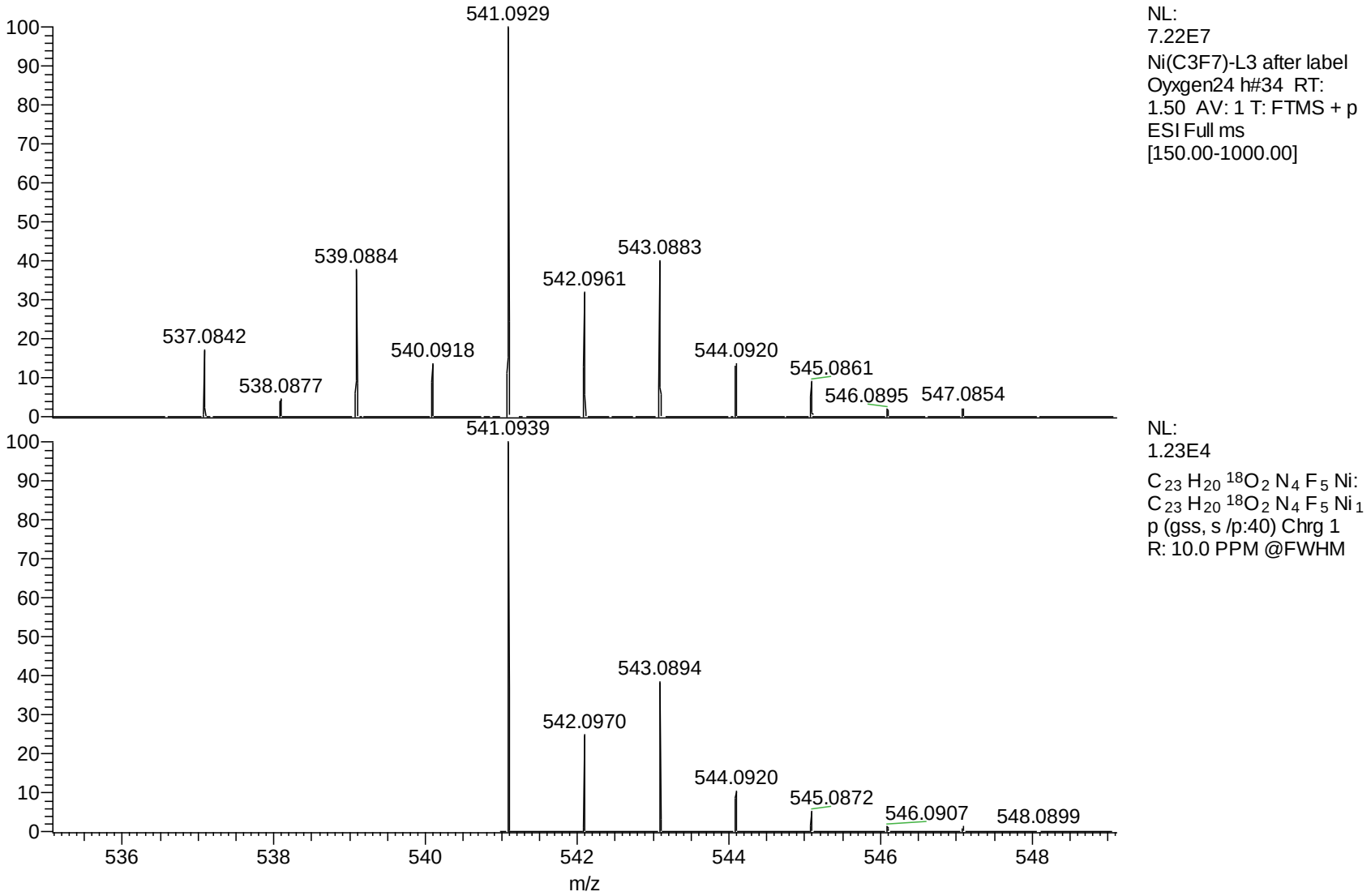

Figure S62. ESI-(HR)MS spectrum of MeOH solution of **4** reacting with label oxygen gas (top) after 24 hour and simulated spectrum $[(\mathbf{L3})_2Ni(C_2F_5C^{18}O_2)]^+$, $C_{23}H_{20}{}^{18}O_2N_4F_5Ni$: (bottom).

Reaction of 3 with O_2 in the presence of $H_2{}^{18}O$

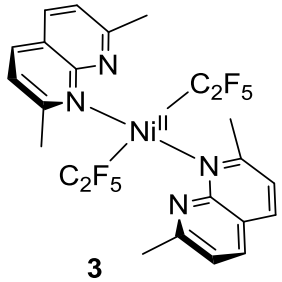

3

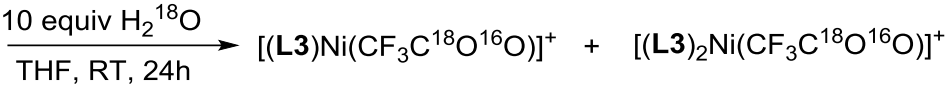

Sample preparation - Inside the glovebox, a J. Young NMR tube was charged with complex **3** (8.2 mg, 0.013 mmol) and $H_2{}^{18}O$ (2.7 μL, 0.13 mmol) were dissolved in dry THF (0.5 mL). The NMR tube was taken out from the glovebox and connected with oxygen gas cylinder. The reaction mixture was exposed to oxygen gas for three minutes and the NMR tube was sealed with a cap. The reaction mixture was stirred at RT for 24 h and analyzed by HRMS showing two sets of signals corresponding to 1:1 **L3**:Ni adduct, [(**L3**)Ni(trifluoroacetate)]$^+$, and 2:1 complex, [(**L3**)$_2$Ni(trifluoroacetate)]$^+$. The main peak corresponds two the product containing one labeled ^{18}O-atom, with peaks of the doubly-labeled and non-labeled trifluoroacetate complexes at smaller intensities. The ratio reported in the manuscript was calculated from peak intensities corresponding to 1:1 adduct, although similar ratio was obtained from comparing intensities of 2:1 adduct.

HRMS (ESI) calculated for [(**L3**)Ni($CF_3C^{18}O^{16}O$)]$^+$,$C_{12}H_{10}F_3N_2{}^{18}O_1{}^{16}O_1Ni$: 331.0085; found, 331.0058.

HRMS (ESI) calculated for [(**L3**)$_2$Ni($CF_3C^{18}O^{16}O$)]$^+$, $C_{22}H_{20}F_3N_4{}^{18}O_1{}^{16}O_1Ni$: 489.0929; found, 489.0897.

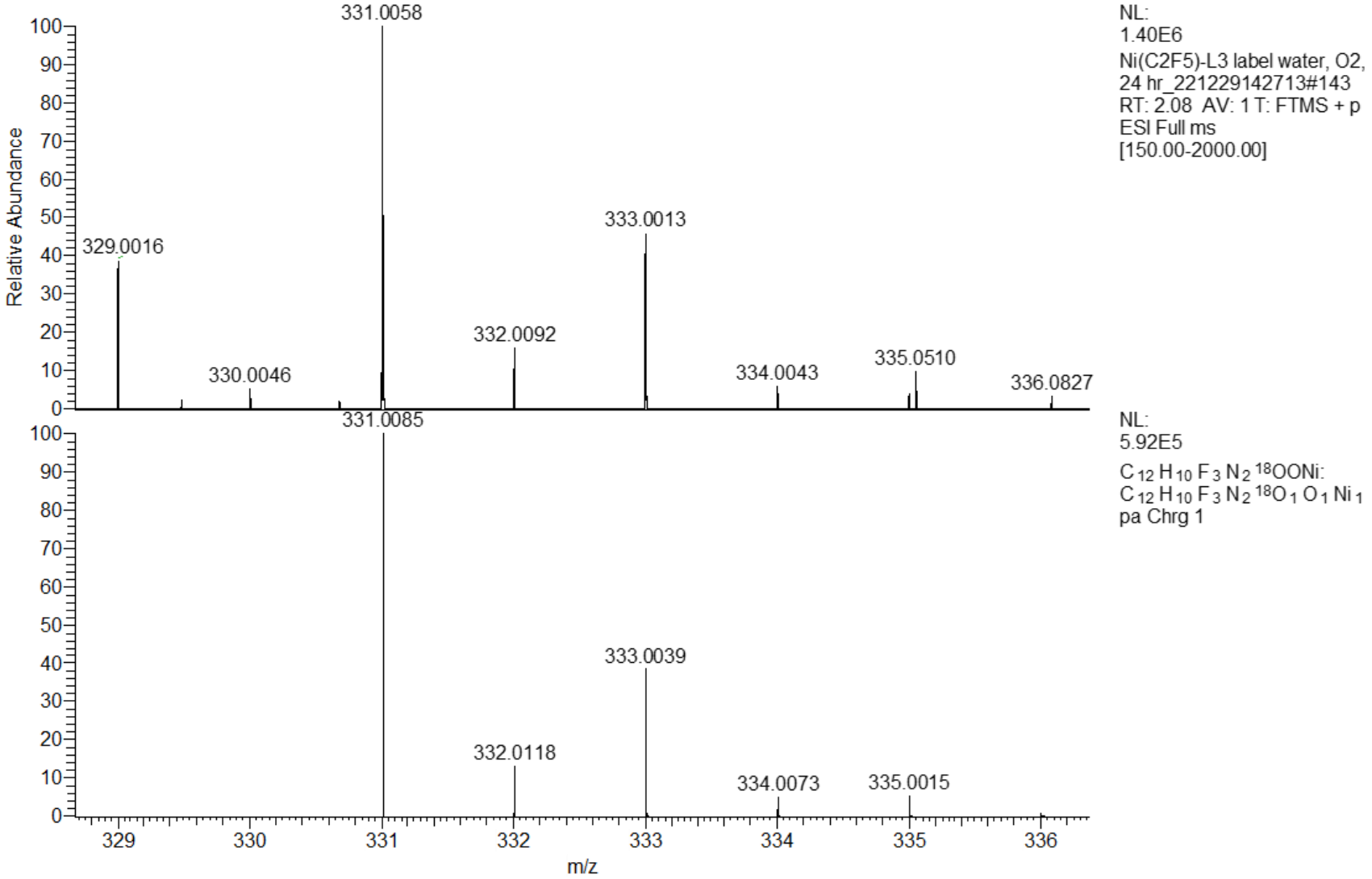

Figure S63. ESI-(HR)MS spectrum of MeOH solution of **3** after reaction with O_2 in the presence of $H_2{}^{18}O$ (top) and simulated spectrum for [(**L3**)Ni($CF_3C^{18}O^{16}O$)]$^+$, $C_{12}H_{10}{}^{18}O^{16}O\ N_2F_3Ni$: (bottom).

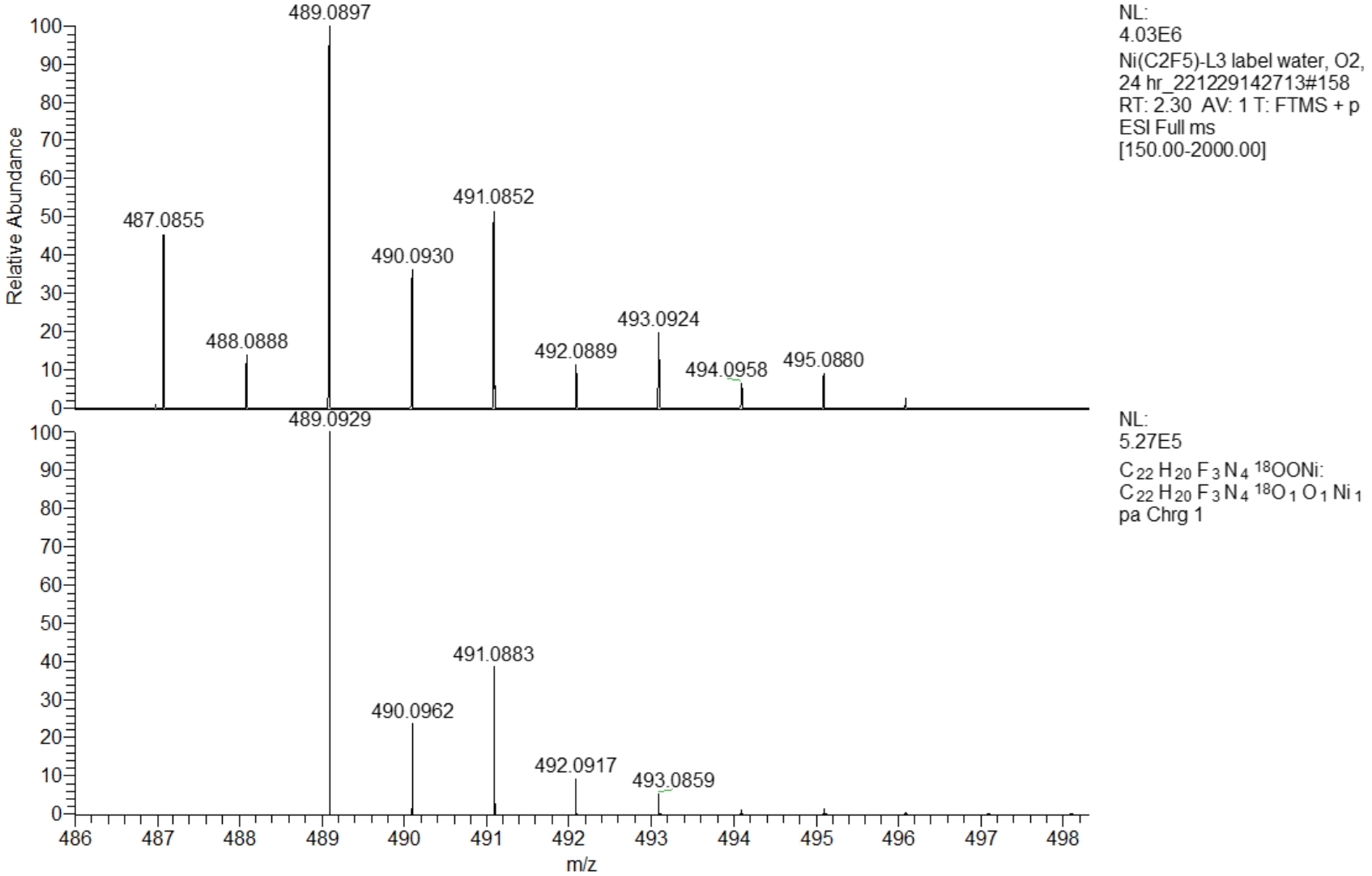

Figure S64. ESI-(HR)MS spectrum of MeOH solution of **3** after reaction with O_2 in the presence of $H_2{}^{18}O$ (top) and simulated spectrum for $[(\mathbf{L3})_2Ni(CF_3C^{18}O^{16}O)]^+$, $C_{22}H_{20}{}^{18}O^{16}ON_4F_5Ni$: (bottom).

Reaction of 3 with $^{18}O_2$ in presence of H_2O

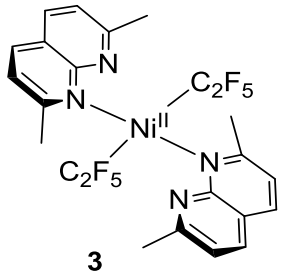

3

$^{18}O_2$, H_2O (10 equiv), THF, RT, 24 hr → [(**L3**)Ni($CF_3C^{18}O^{16}O$)]$^+$ + [(**L3**)$_2$Ni($CF_3C^{18}O^{16}O$)]$^+$

Sample preparation - Inside the glovebox, a J. Young NMR tube was charged with complex **3** (8.3 mg, 0.013 mmol) and water (2.4 μL,0.13 mmol) were dissolved in dry THF (0.5 mL). The NMR tube was taken out from the glovebox and connected with $^{18}O_2$ gas cylinder. The reaction mixture was exposed to oxygen gas for three minutes and the tube was sealed with a cap, stirred at RT for 24 h, and analyzed by ESI-HRMS. ESI-HRMS showed two sets of signals corresponding to 1:1 **L3**:Ni adduct, [(**L3**)Ni(trifluoroacetate)]$^+$, and 2:1 complex, [(**L3**)$_2$Ni(trifluoroacetate)]$^+$. The main peak corresponds two the product containing one labeled ^{18}O-atom, with peaks of the doubly-labeled and non-labeled trifluoroacetate complexes at smaller intensities. The ratio reported in the manuscript was calculated from peak intensities corresponding to 1:1 adduct (m/z 333.1287 : m/z 331.0079 : m/z 329.0035), although similar ratio was obtained from comparing intensities of 2:1 adduct.

HRMS (ESI) calculated for [(**L3**)Ni($CF_3C^{18}O^{16}O$)]$^+$, $C_{12}H_{10}F_3N_2{}^{18}O_1{}^{16}O_1Ni$: 331.0085; found, 331.0079.

HRMS (ESI) calculated for [(**L3**)$_2$Ni($CF_3C^{18}O^{16}O$)]$^+$, $C_{22}H_{20}F_3N_4{}^{18}O_1{}^{16}O_1Ni$: 489.0929; found, 489.0912.

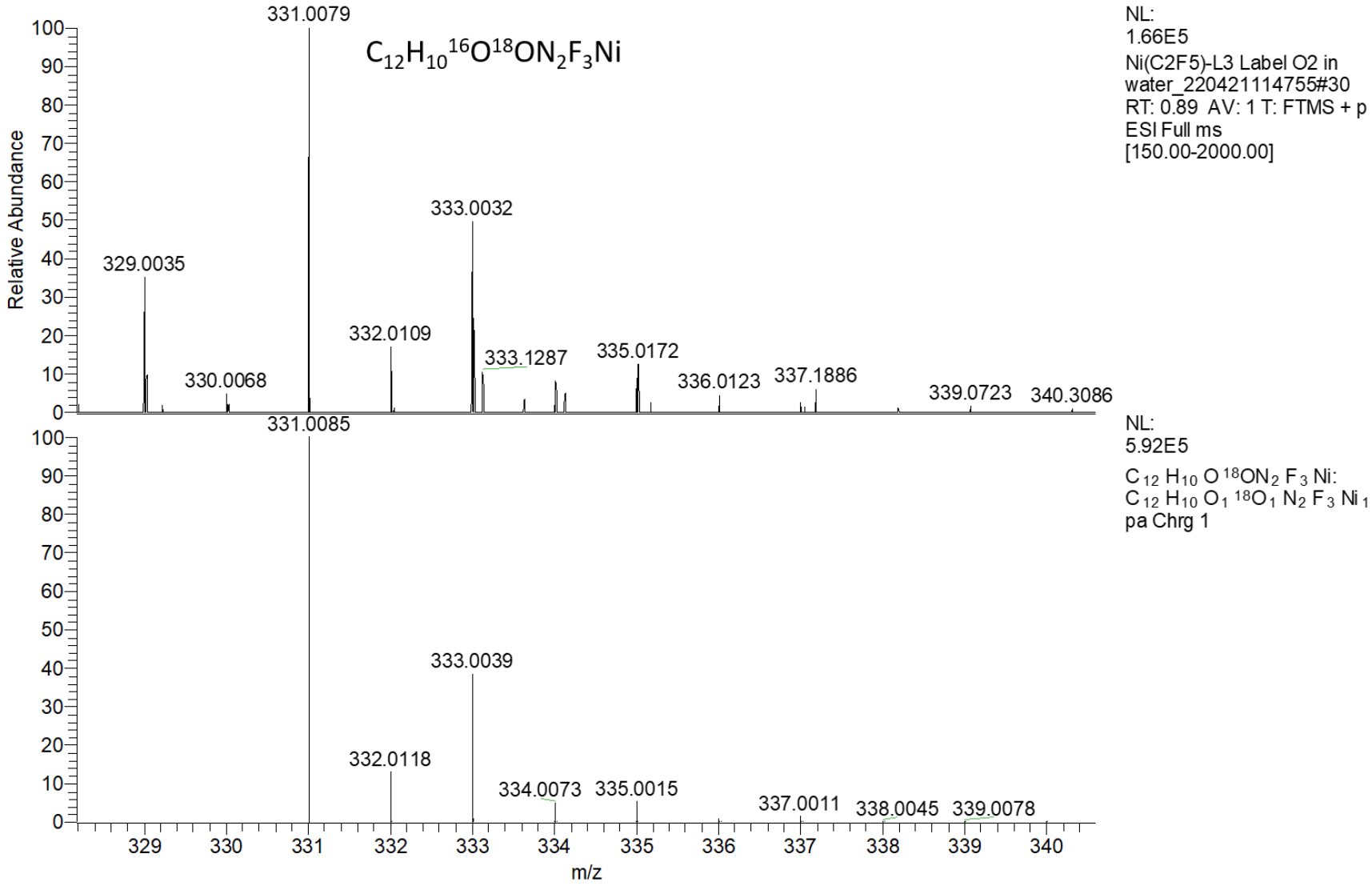

Figure S65. ESI-(HR)MS spectrum of MeOH solution of **3** reacting with $^{18}O_2$ gas in presence of H_2O (top) and simulated spectrum [(**L3**)Ni($CF_3C^{18}O^{16}O$)]$^+$, $C_{12}H_{10}{}^{18}O^{16}O\ N_2F_3Ni$: (bottom).

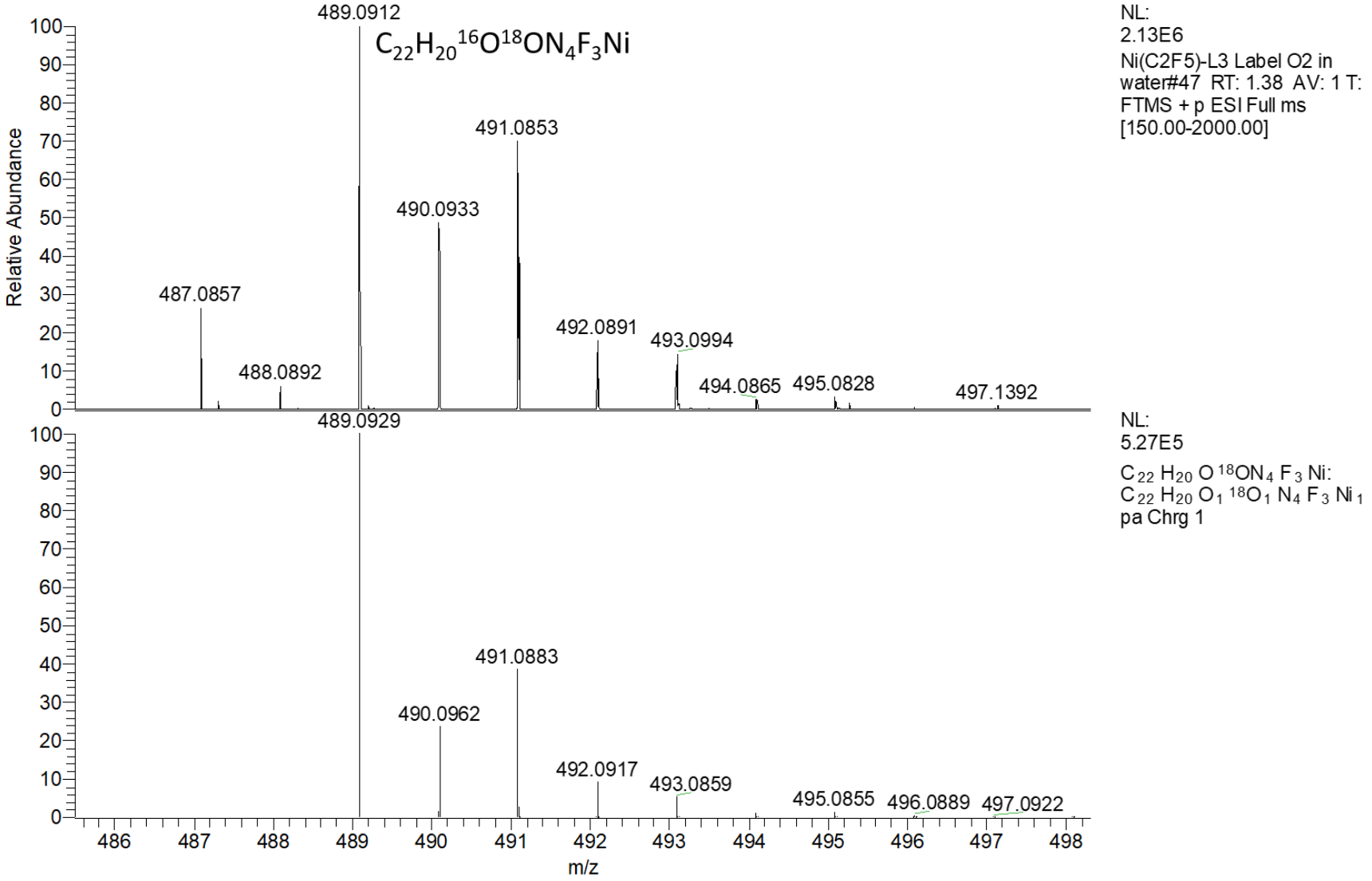

Figure S66. ESI-(HR)MS spectrum of MeOH solution of **3** reacting with $^{18}O_2$ gas in presence of H_2O (top) and simulated spectrum $C_{22}H_{20}{}^{18}O^{16}O\ N_4F_3Ni$: (bottom).

Oxygenation of organic substrates in the presence of O_2 and 3

Oxidation of triphenylphosphine with O_2 in the presence of 3

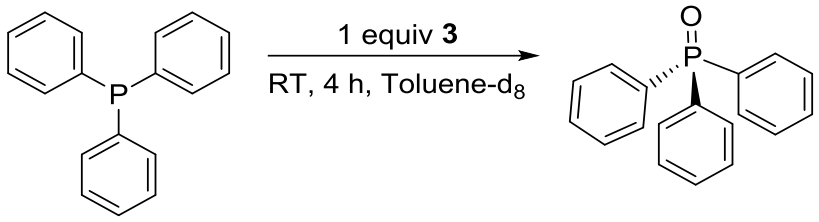

Inside the glovebox, solution of complex **3** (8.3 mg, 0.013 mmol) and triphenylphosphine (3.5 mg, 0.013 mmol) in dry toluene-d_8 (0.5 mL) was placed to a J. Young NMR tube. The NMR tube was removed from glovebox and the reaction mixture was exposed to oxygen gas for four minutes, then stirred at room temperature for 4 h. After completion of the reaction, the reaction mixture was analyzed by $^{31}P\{^1H\}$ NMR spectroscopy, confirms the full consumption of starting material PPh_3 and showing the formation of triphenylphosphine oxide product.

The analogous reaction using 0.5 equiv of **3** relative to PPh_3 resulted in *ca.* 95% clean conversion of PPh_3 to PPh_3O after longer reaction time, 20 h, under otherwise same conditions.

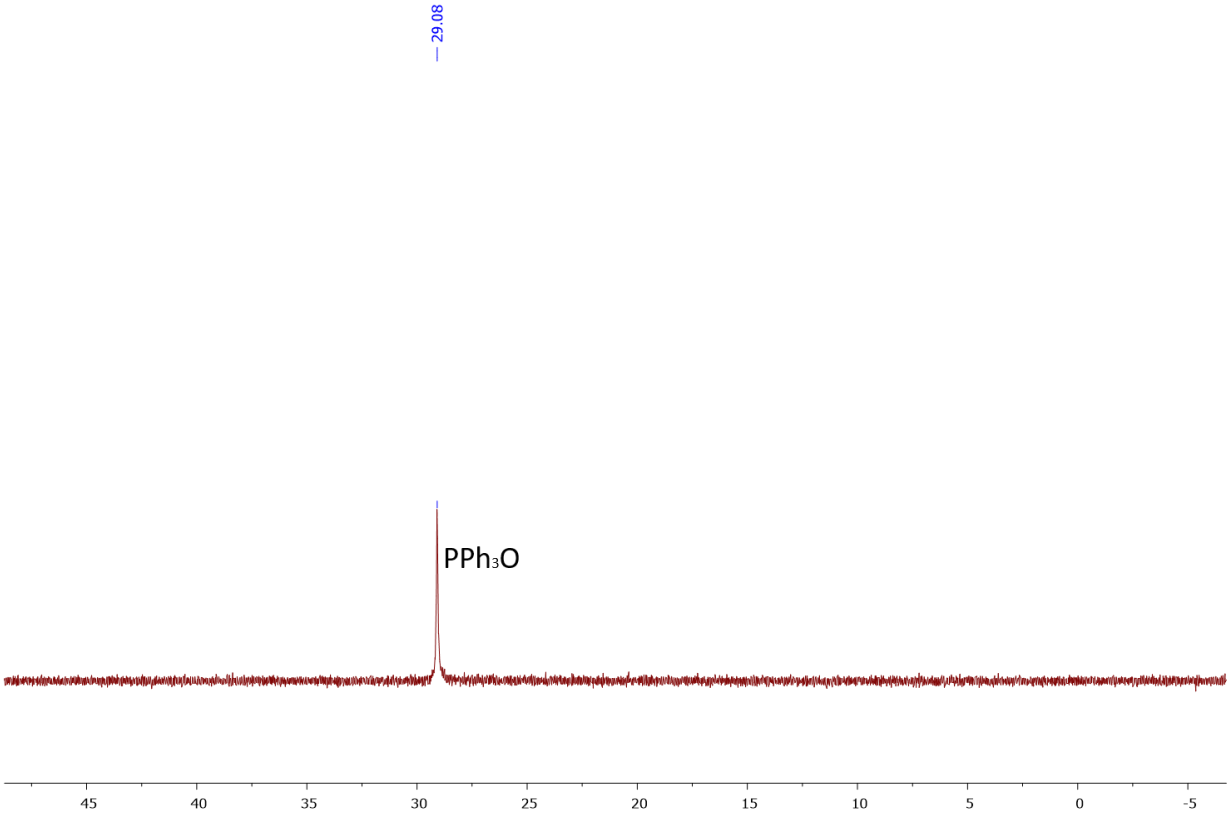

Figure S67. ^{31}P NMR spectrum of **3** reacting with triphenylphosphine in the presence of oxygen at RT in toluene-d_8.

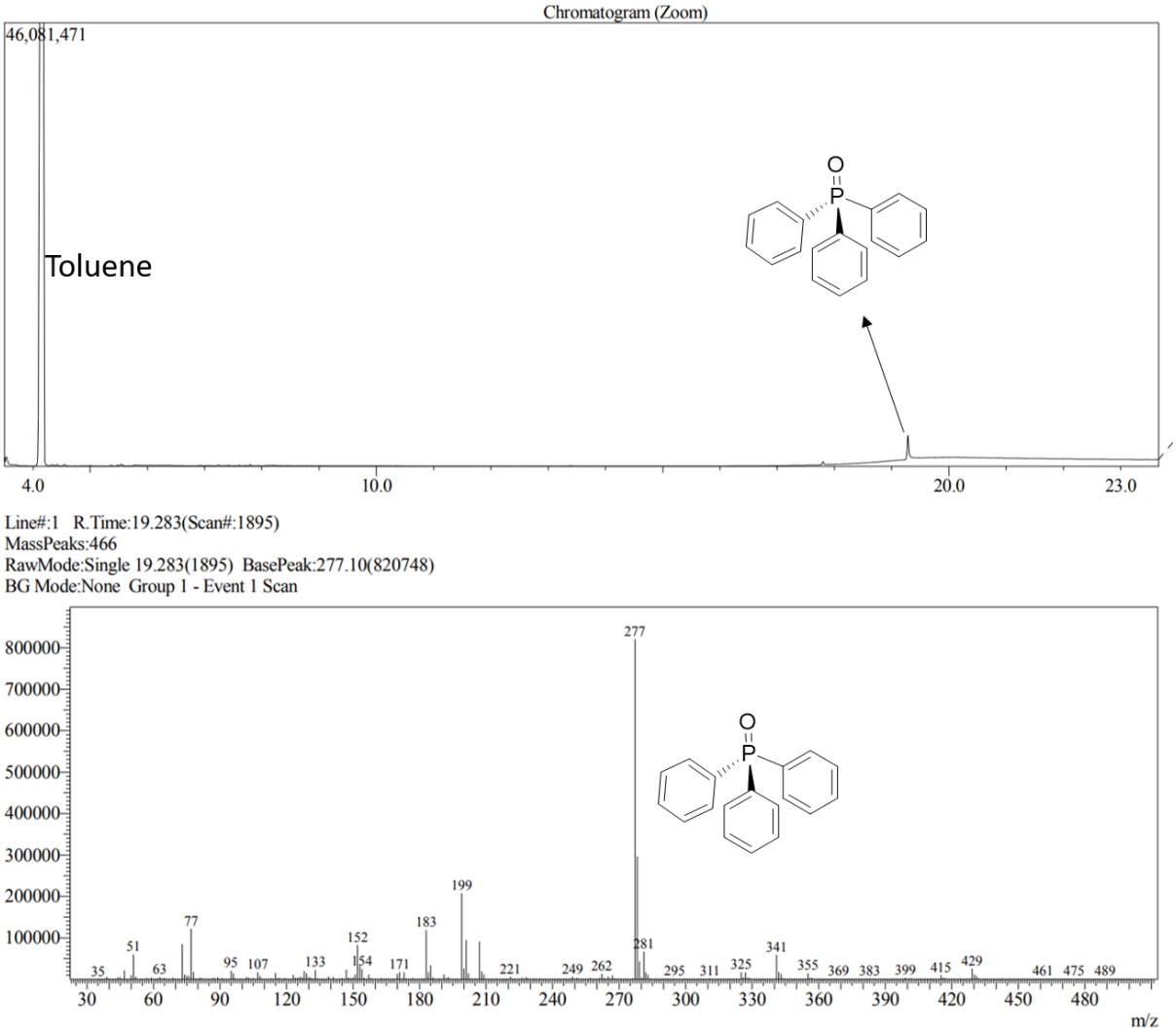

Figure S68. GC-MS spectrum of ethyl acetate solution of the reaction mixture of aerobic oxidation of PPh_3 in the presence of **3**.

Oxidation of PPh_3 with 0.5 equiv O_2 in the presence of 3

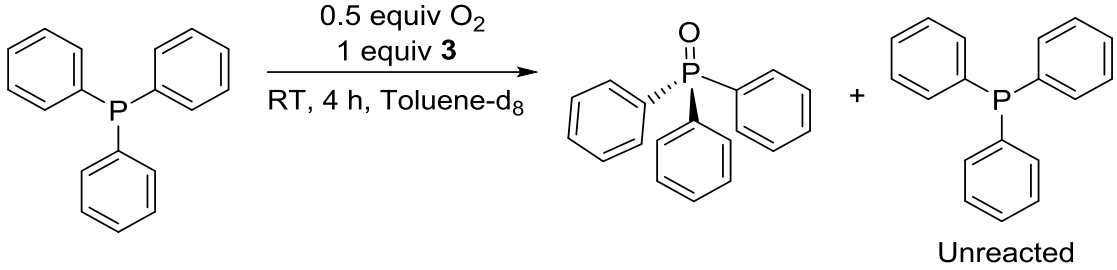

Inside the glovebox, a solution of complex **3** (5.0 mg, 0.0081 mmol), triphenylphosphine (2.1 mg, 0.0081 mmol) in dry toluene-d_8 (0.5 mL) was transferred to an NMR tube equipped with a septum. O_2 gas was injected through the septum using gas-tight syringe (100 µL, 0.004 mmol, 0.5 equiv). The reaction mixture was then stirred at room temperature for 4 h and analyzed by $^{31}P\{^1H\}$ NMR spectroscopy. PPh_3O and PPh_3 were present in ca. 80 : 20 ratio.

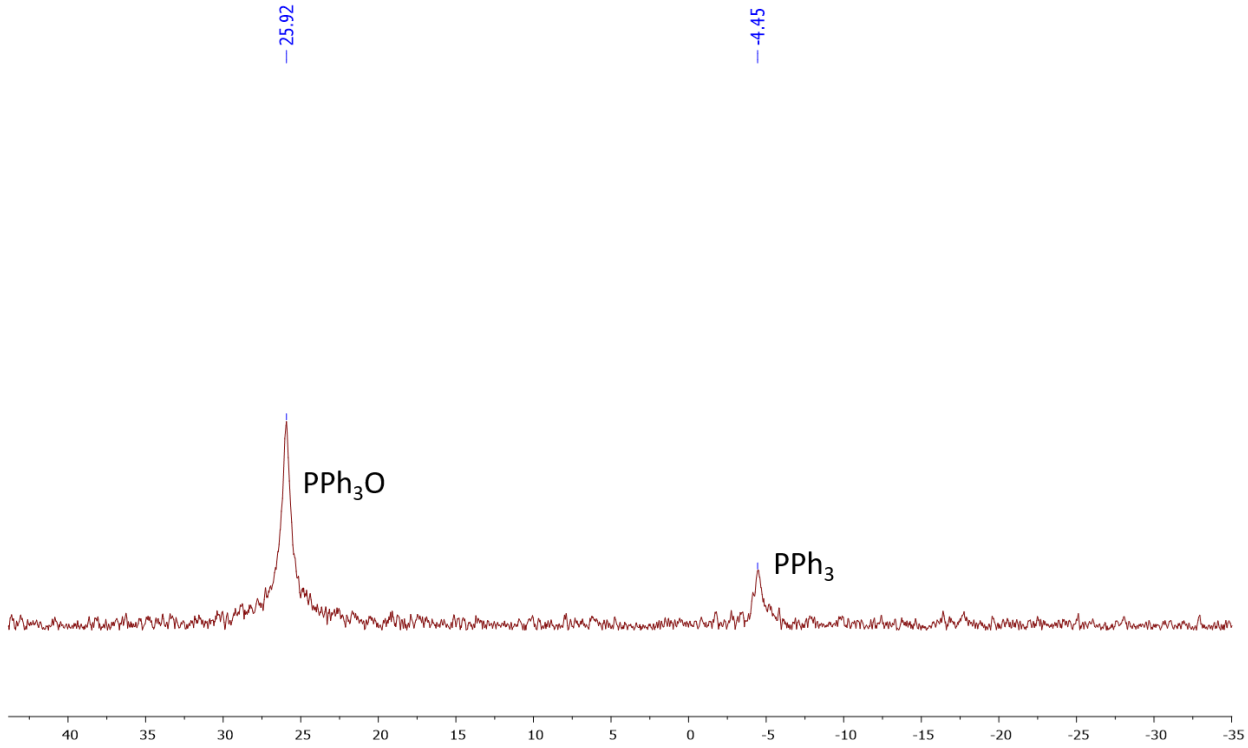

Figure S69 $^{31}P\{^1H\}$ NMR spectrum of half equivalent of oxygen gas reacting with triphenylphosphine in the presence of **3** at RT in toluene-d_8 shows formation of triphenylphosphine oxide product and unreacted starting material.

Oxidation of Triphenylphosphine with $^{18}O_2$ in the presence of 3

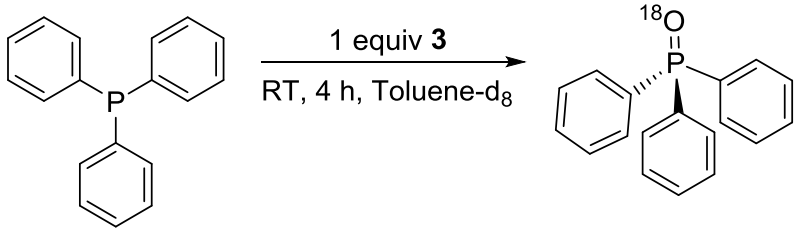

Inside the glovebox, a solution of complex **3** (7.2 mg, 0.012 mmol), triphenylphosphine (3.0 mg, 0.012 mmol) in dry toluene-d_8 (0.5 mL) was placed in a J. Young NMR tube. The NMR tube was removed from glovebox and the reaction mixture was exposed to $^{18}O_2$ gas for four minutes, then sealed with a Teflon cap and stirred at room temperature for 4 hours and analyzed by HRMS and GC-MS analysis, confirming the formation of labeled triphenylphosphine oxide as the main product, with unlabeled PPh_3O^{16} present in small amounts ($PPh_3{}^{18}O$: $PPh_3{}^{16}O$ = 90 :10 based on peak intensities in HRMS and GC-MS spectrum).

HRMS (ESI) calculated for $[M+H]^+$ $C_{18}H_{16}{}^{18}O_1P_1$: 281.0976; found, 281.0941.

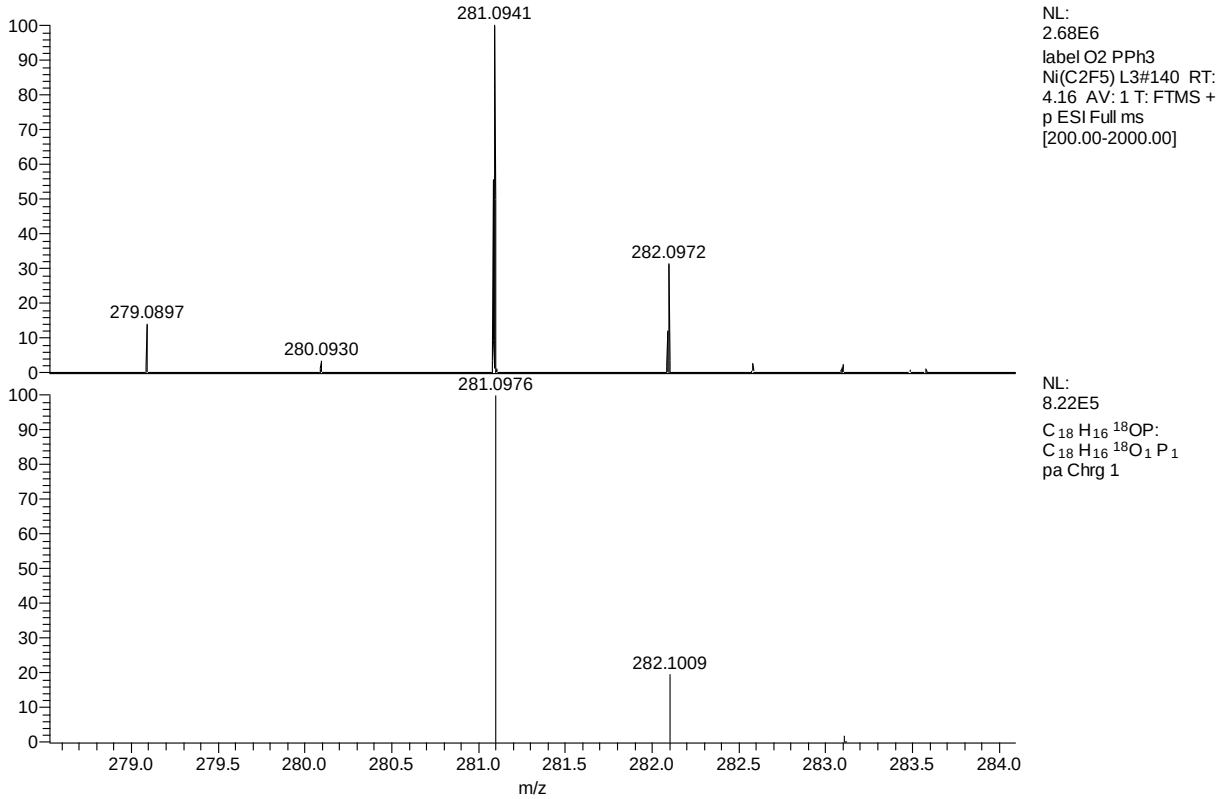

Figure S70. ESI-(HR)MS spectrum of MeOH solution of the product obtained by oxidation of PPh_3 with $^{18}O_2$ in the presence of **3** (top) and simulated spectrum $C_{18}H_{16}P_1{}^{18}O_1$: (bottom).

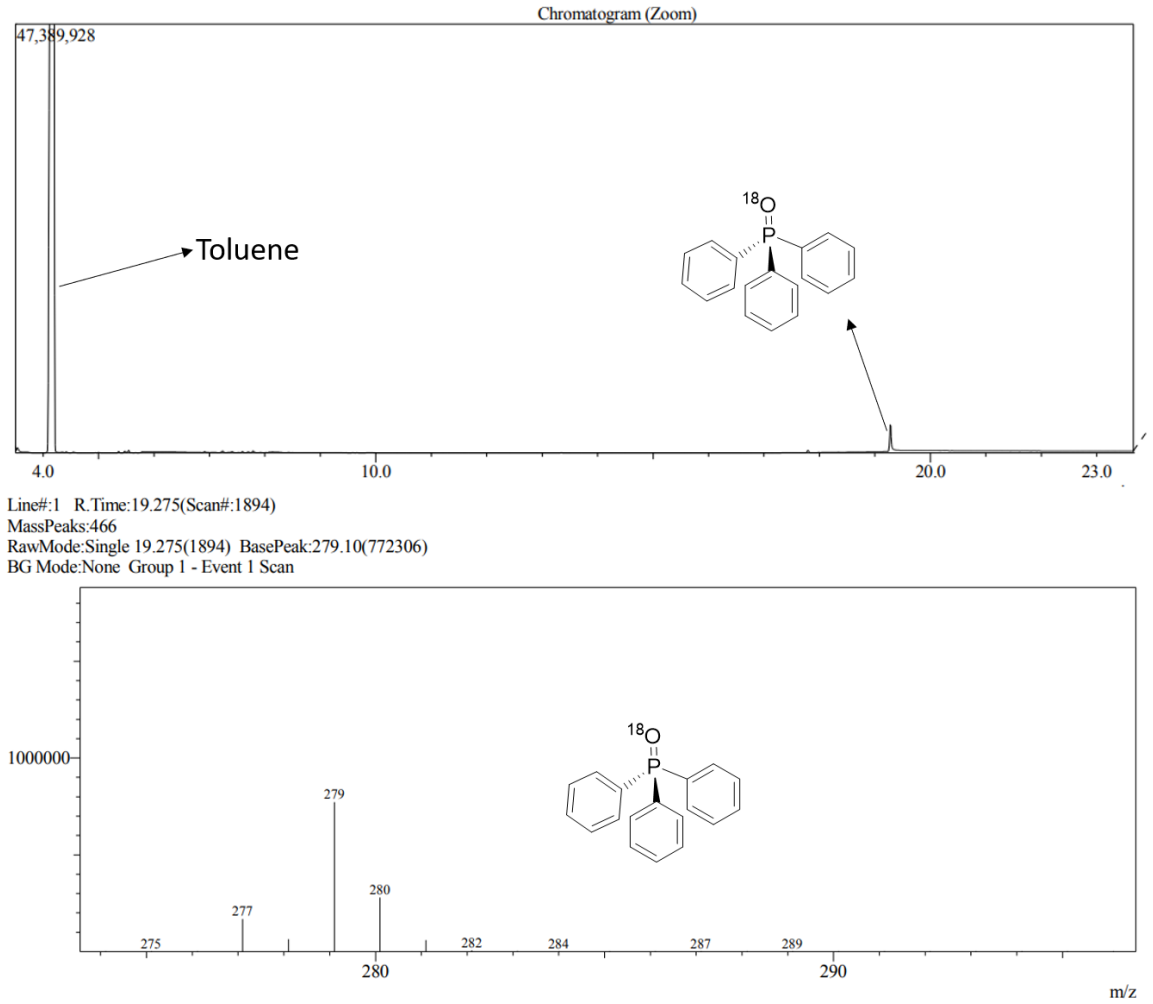

Figure S71. GC-MS spectrum of ethyl acetate solution of reaction mixture of oxidation of PPh_3 with $^{18}O_2$ in the presence of **3**.

Attempted oxidation of PPh_3 with O_2 in the absence of 3

Inside the glovebox, to a 20 mL vial triphenylphosphine (3.5 mg, 0.013 mmol) was dissolved in dry toluene-d_8 (0.5 mL), transferred to a J. Young NMR tube. The NMR tube was then removed from glovebox and the reaction mixture was exposed to oxygen gas for four minutes, Teflon-sealed and stirred at room temperature for 4 hours. The reaction mixture was then analyzed by $^{31}P\{^1H\}$ NMR spectroscopy, showing that starting material remained mostly unreacted along with only trace amount of PPh_3O formed.[10]

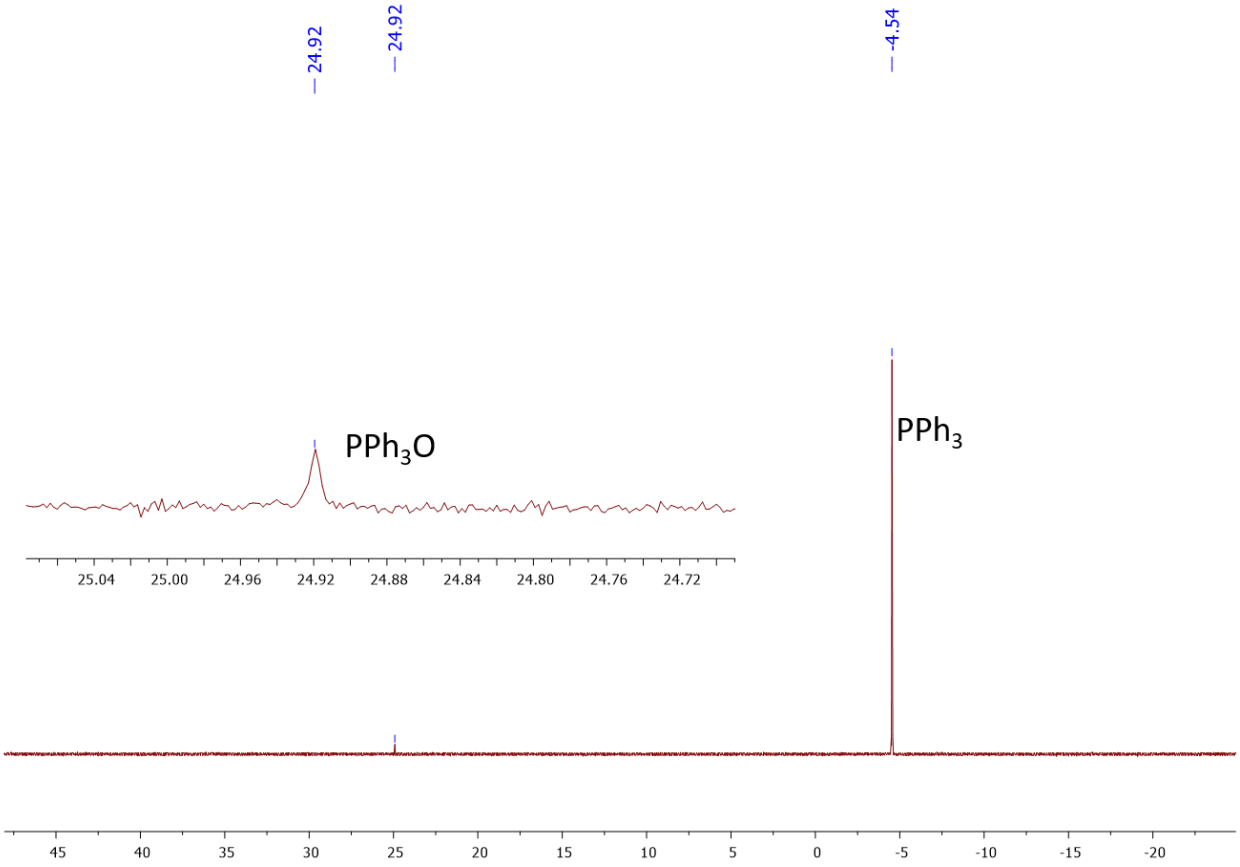

Figure S72. $^{31}P\{^1H\}$ NMR spectrum of attempted PPh_3 oxidation with O_2 in the absence of **3**.

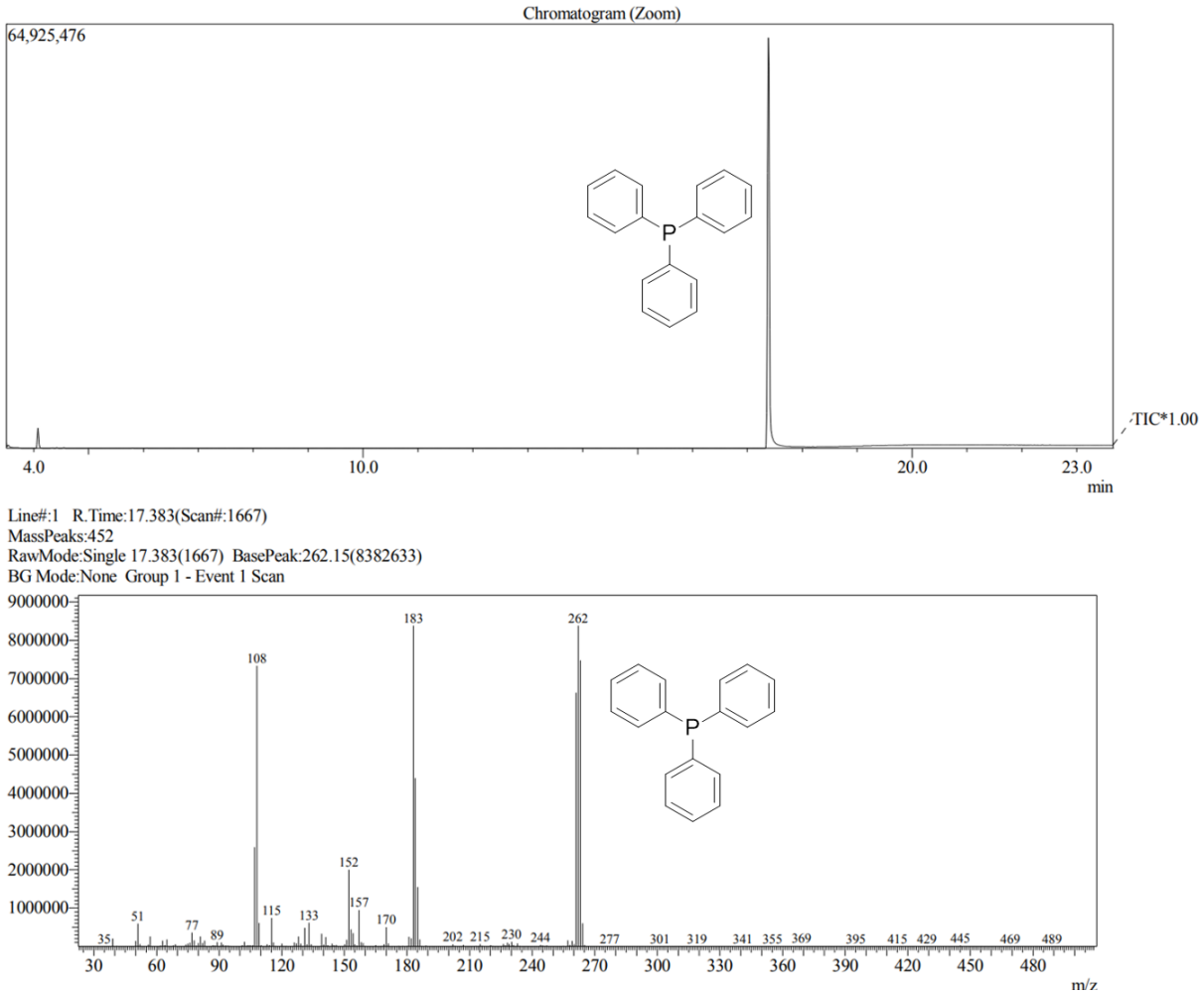

Figure S73. GC-MS spectrum of ethyl acetate solution of the reaction mixture of attempted oxidation of PPh_3 with O_2 in the absence of **3**.

Oxidation of ethyl phenyl sulfide by O_2 in the presence of 3

a) Reaction in the presence of 1 equiv of 3

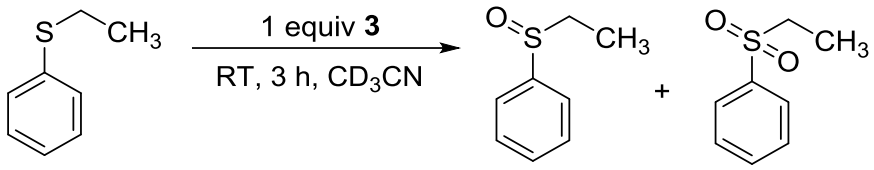

Inside the glovebox, a solution of complex **3** (15.3 mg, 0.0249 mmol), ethyl phenyl sulfide (3.3 µL, 0.0249 mmol) and mesitylene (3.4 µL, 0.0249 mmol) in anhydrous CD_3CN (0.5 mL) was transferred to a J. Young NMR tube. The NMR tube was removed from glovebox and the reaction mixture was exposed to oxygen gas for four minutes, then Teflon-sealed and stirred at room temperature for 3 hours. The reaction mixture was then analyzed by ^{1}H NMR spectroscopy and GC-MS to confirm the formation of ethyl phenyl sulfoxide and ethyl phenyl sulfone in 99% NMR yield by ^{1}H NMR integration of the peak at 1.16-1.15 ppm (CH_3 group ethyl phenyl sulfoxide and ethyl phenyl sulfone overlap) vs. mesitylene as an internal standard. No starting material was present.

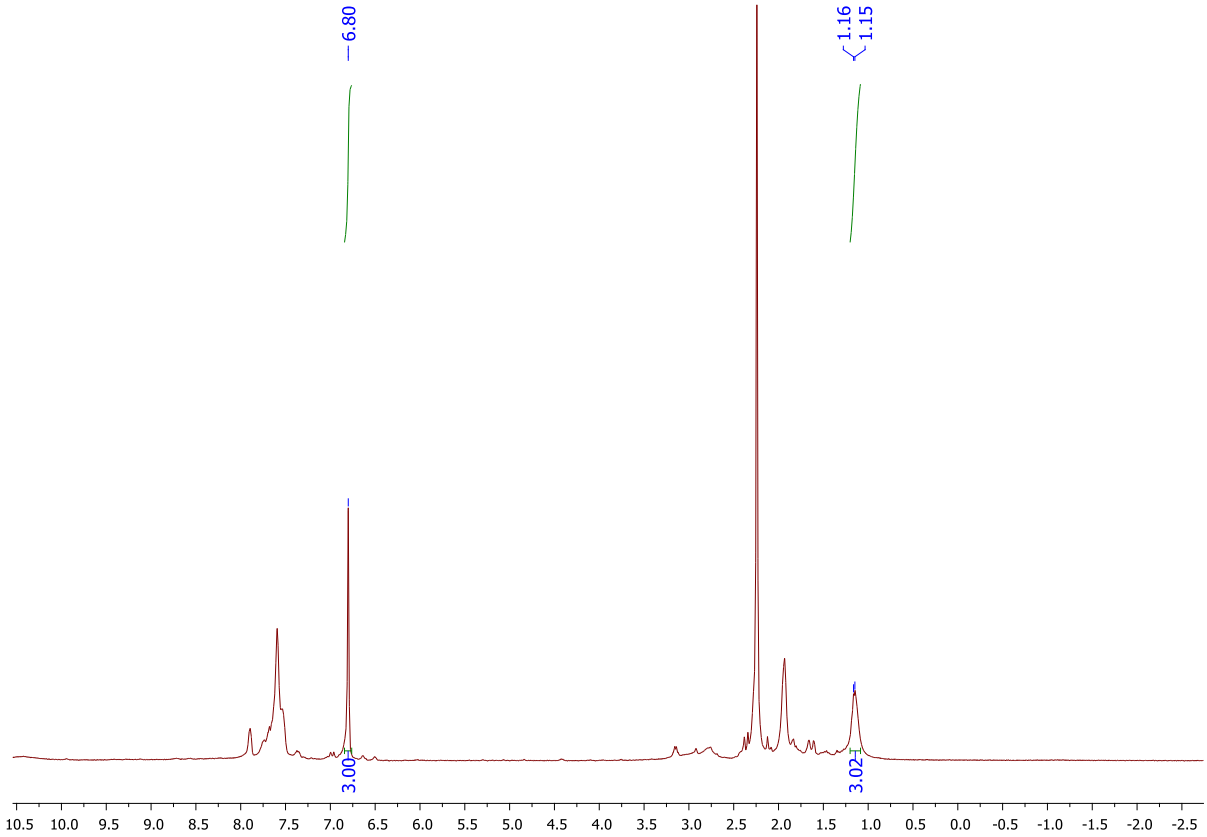

Figure S74. ^{1}H NMR spectrum of the reaction mixture containing 1 equiv ethyl phenyl sulfide and **3** after stirring under O_2 for 3 h.

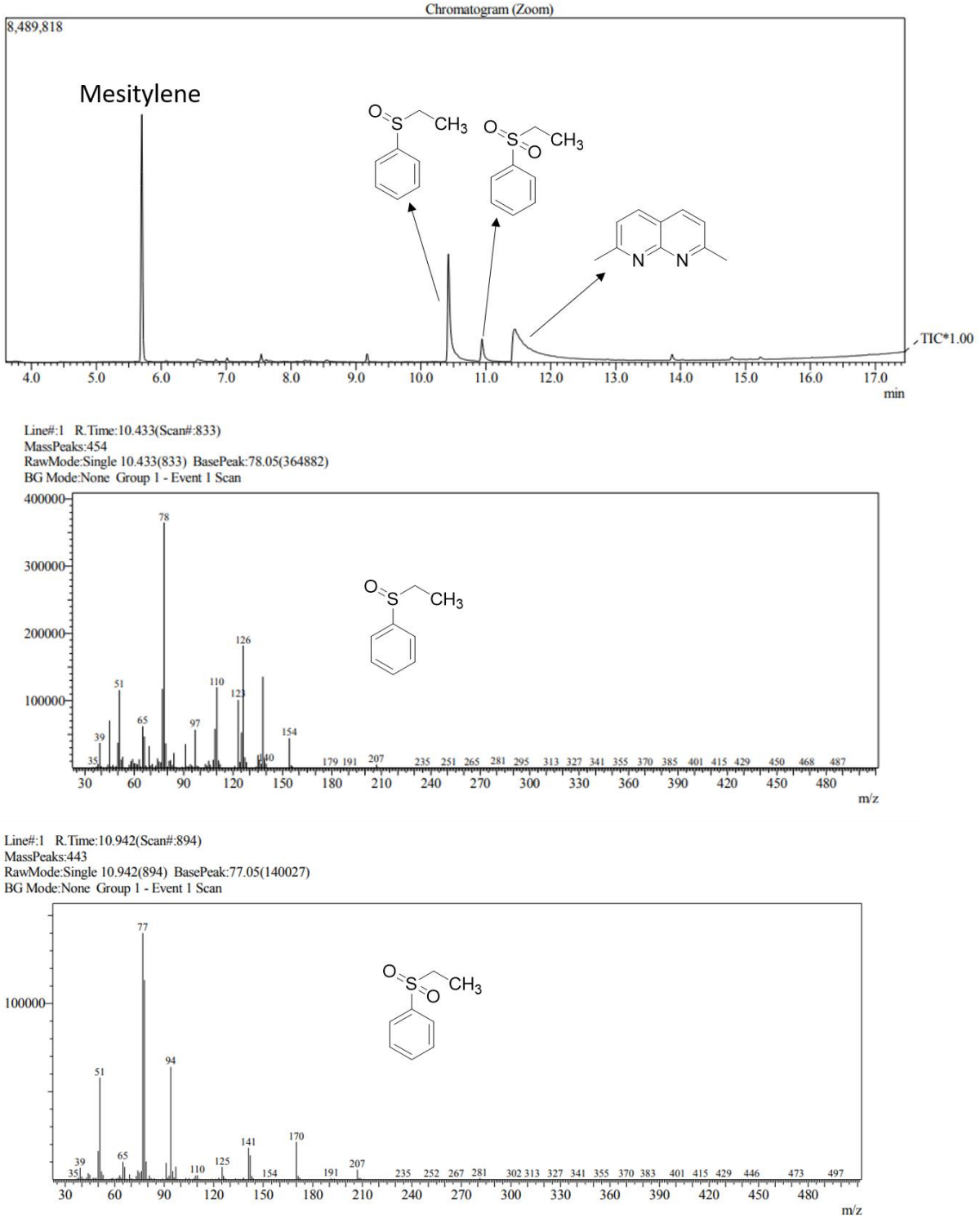

Figure S75. GC-MS spectrum of the reaction mixture containing 1 equiv of ethyl phenyl sulfide and **3** after stirring under O_2 for 3 h; diluted with ethyl acetate.

b) Oxidation of excess ethyl phenyl sulfide (5 equiv relative to 3) by O_2 in the presence of 3

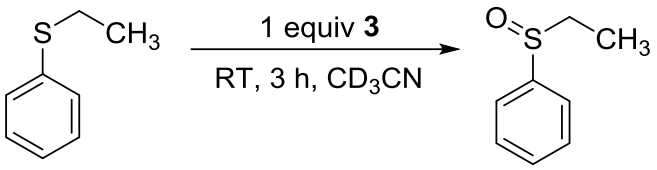

Inside the glovebox, a solution of complex **3** (10.3 mg, 0.0167 mmol), ethyl phenyl sulfide (11.3 µL, 0.0839 mmol; 5 equiv relative to **3**) and mesitylene (2.3 µL, 0.0167 mmol) in anhydrous CD_3CN (0.5 mL) was transferred to a J. Young NMR tube. The NMR tube was removed from glovebox and the reaction mixture was exposed to oxygen gas for four minutes, then Teflon-sealed and stirred at room temperature for 3 hours. The reaction mixture was then analyzed by ^{1}H NMR spectroscopy and GC-MS to confirm the formation of ethyl phenyl sulfoxide in 39% yield based on ethyl phenyl sulfide (1.95 equiv relative to **3**). Yield was determined by ^{1}H NMR integration of the peak at 1.10 ppm (CH_3 group of product) vs. mesitylene as an internal standard. The rest of the material was unreacted sulfide, while no sulfone was detected by GC-MS.

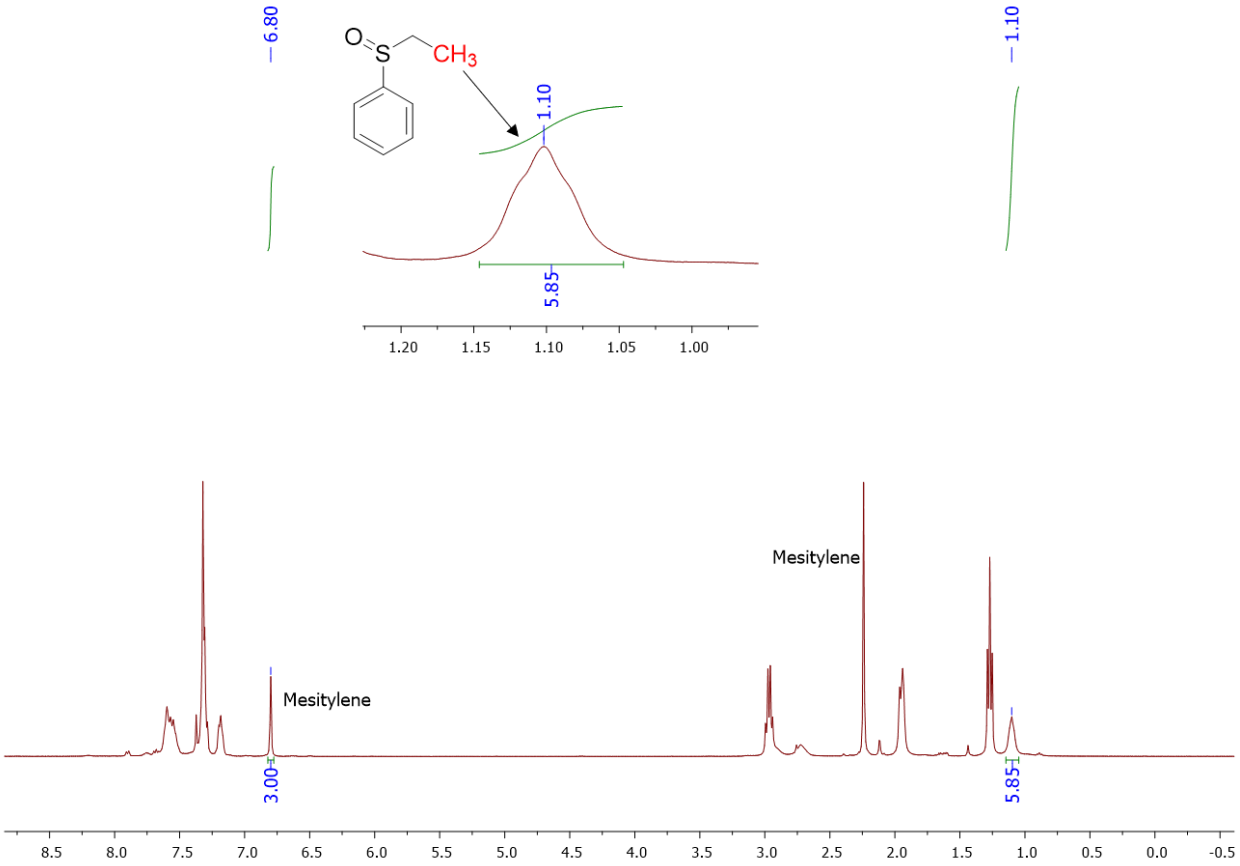

Figure S76. ^{1}H NMR spectrum of the reaction mixture containing 5 equiv of ethyl phenyl sulfide and **3** after stirring under O_2 for 3 h.

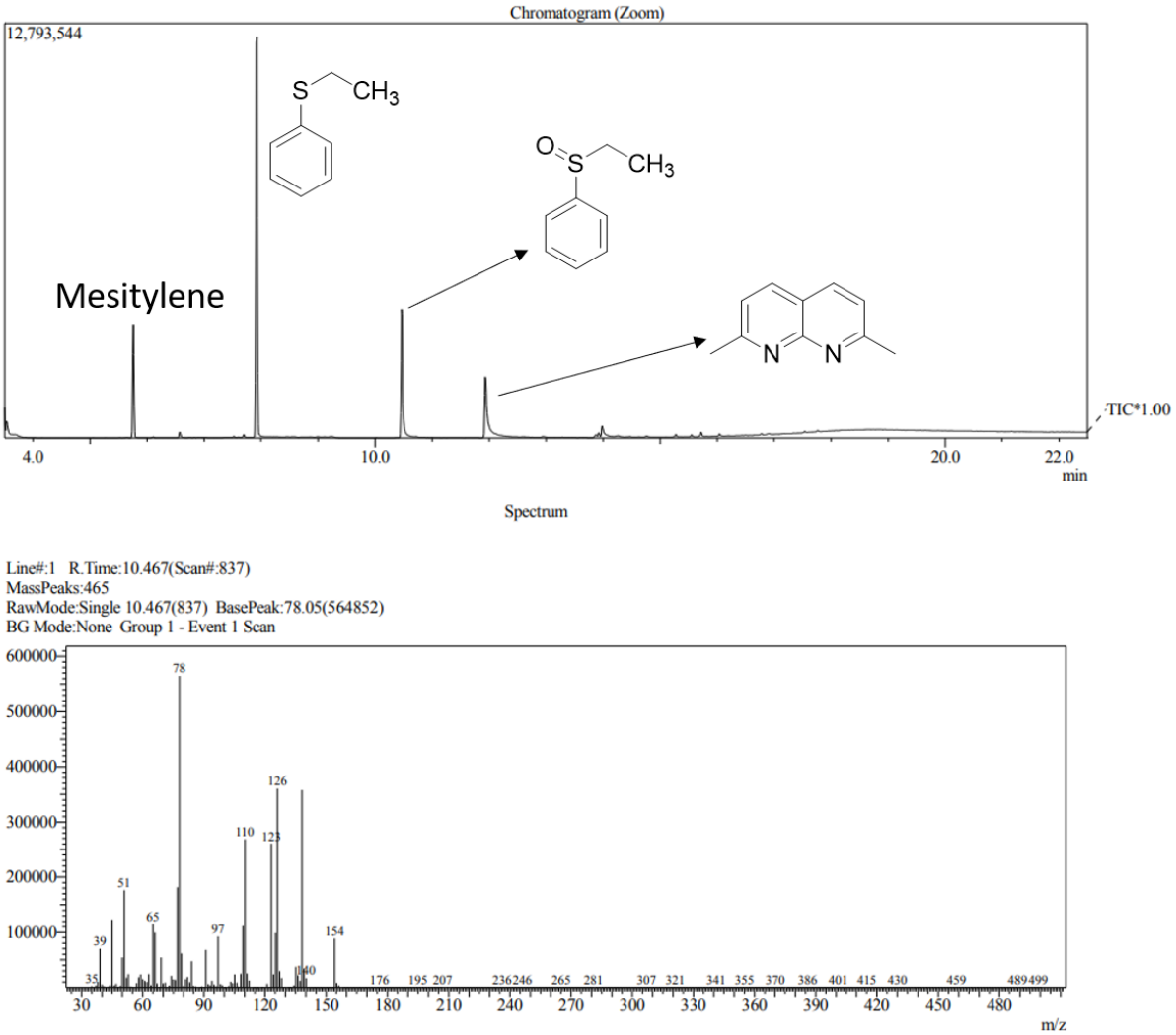

Figure S77. GC-MS spectrum of the reaction mixture containing 5 equiv of ethyl phenyl sulfide and **3** after stirring under O_2 for 3 h; diluted with ethyl acetate.

Attempted oxidation of ethyl phenyl sulfide with O_2 in absence of 3

Inside the glovebox, a solution of ethyl phenyl sulfide (2.2 μL, 0.017 mmol), mesitylene (2.3 μL, 0.017 mmol) in anhydrous CD_3CN (0.5 mL) was transferred to a J. Young NMR tube. The NMR tube was removed from glovebox and the reaction mixture was exposed to oxygen gas for four minutes, then Teflon-sealed and stirred at room temperature for 3 hours. The reaction mixture was then analyzed by ^1H NMR spectroscopy and GC-MS showing that the starting material remains mostly unreacted.

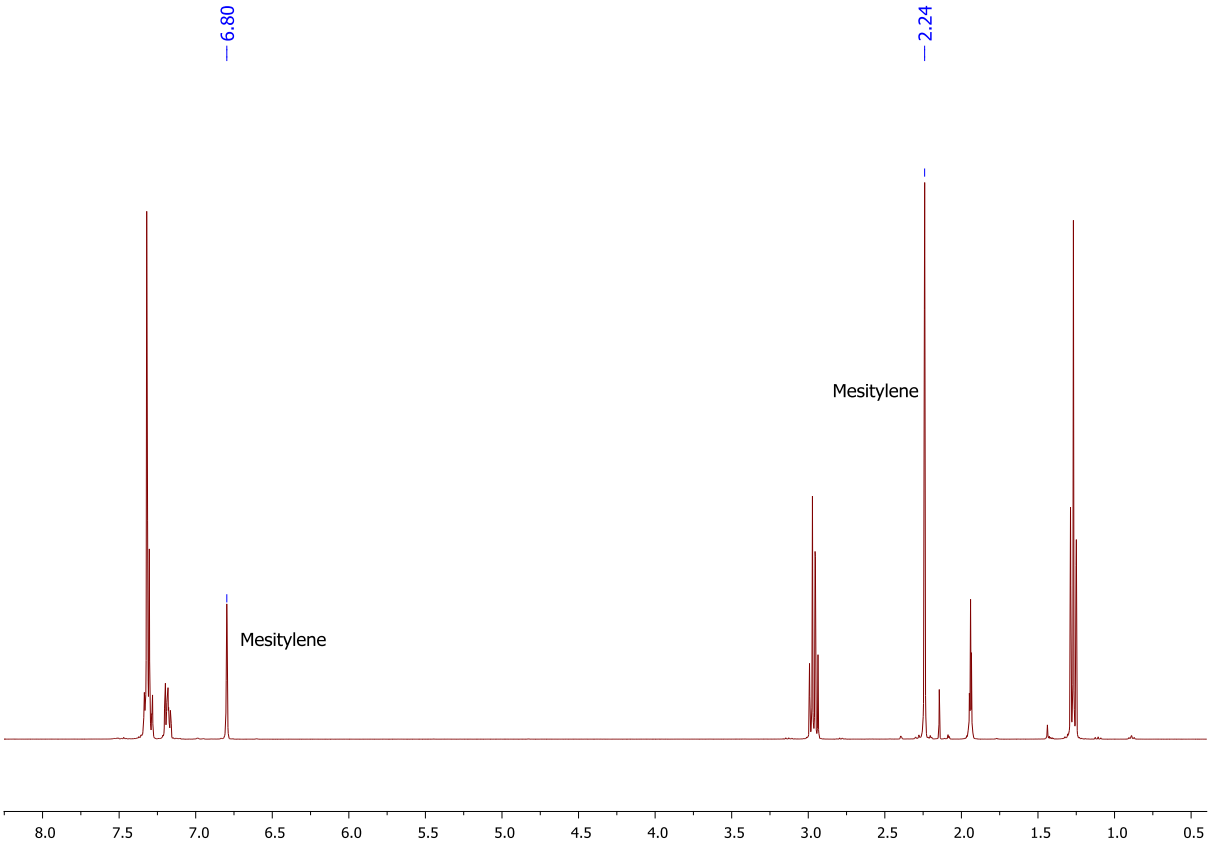

Figure S78. ^1H NMR spectrum of attempted oxidation of ethyl phenyl sulfide in the absence of **3** under O_2.

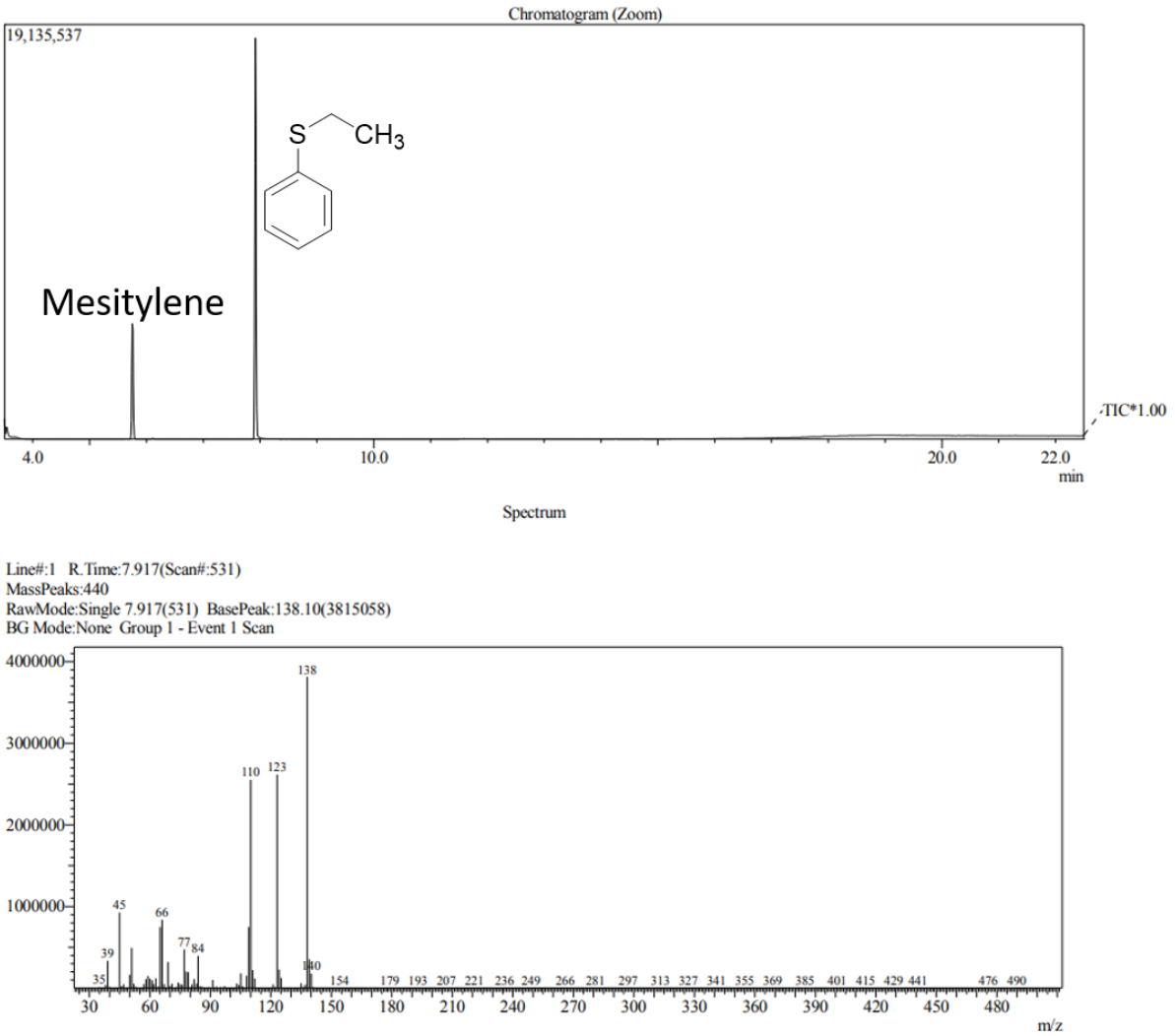

Figure S79. GC-MS spectrum of ethyl acetate solution sample of attempted oxidation of ethyl phenyl sulfide in the absence of **3** under O_2.

Oxidation of *cis*-stilbene with O_2 in the presence of 3

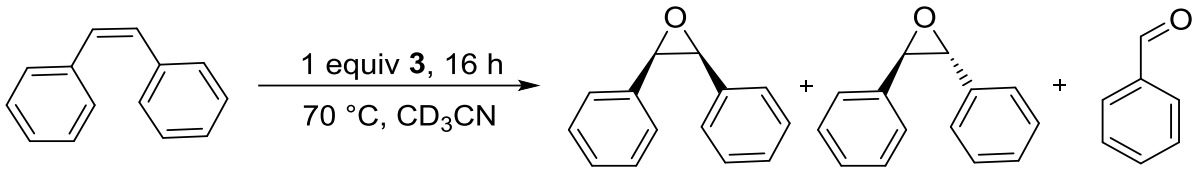

Typical procedure. Inside the glovebox, a solution of complex **3** (33.6 mg, 0.0548 mmol), *cis*-stilbene (9.7 μL, 0.0548 mmol) and mesitylene (7.6 μL,0.0548 mmol) in anhydrous CD_3CN (0.5 mL) was placed to a J. Young NMR tube. The NMR tube was removed from glovebox and the reaction mixture was exposed to oxygen gas for four minutes, then transferred to an oil bath heated at 70 °C for 16 hours. The reaction mixture was analyzed by ^{1}H NMR spectroscopy and GC-MS to confirm identity of products. According to NMR integration, a mixture of *cis*-stilbene oxide (6%), *trans*-stilbene oxide (8%), benzaldehyde (13%) were formed. Unreacted *cis*- and a small amount of *trans*-stilbene were also detected by GC-MS (*trans*-stilbene was present in the commercially available *cis*-stilbene in the amount of ≤1%).

The reaction was repeated in duplicate and consistent yields were obtained in two runs; average yields are reported in the manuscript.

Run	% Yield of *cis*-stilbene oxide	% Yield of *trans*-stilbene oxide	% Yield of benzaldehyde
1	12	16	13
2	15	18	17

The peaks of the following protons were used for ^{1}H NMR integration to determine the yields:

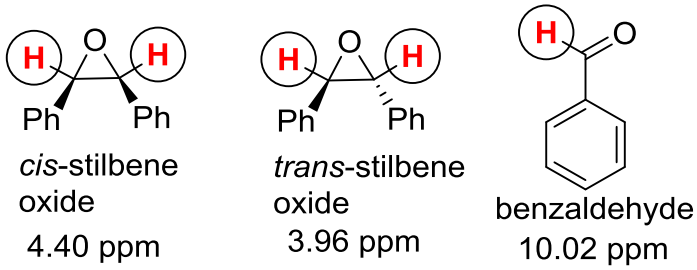

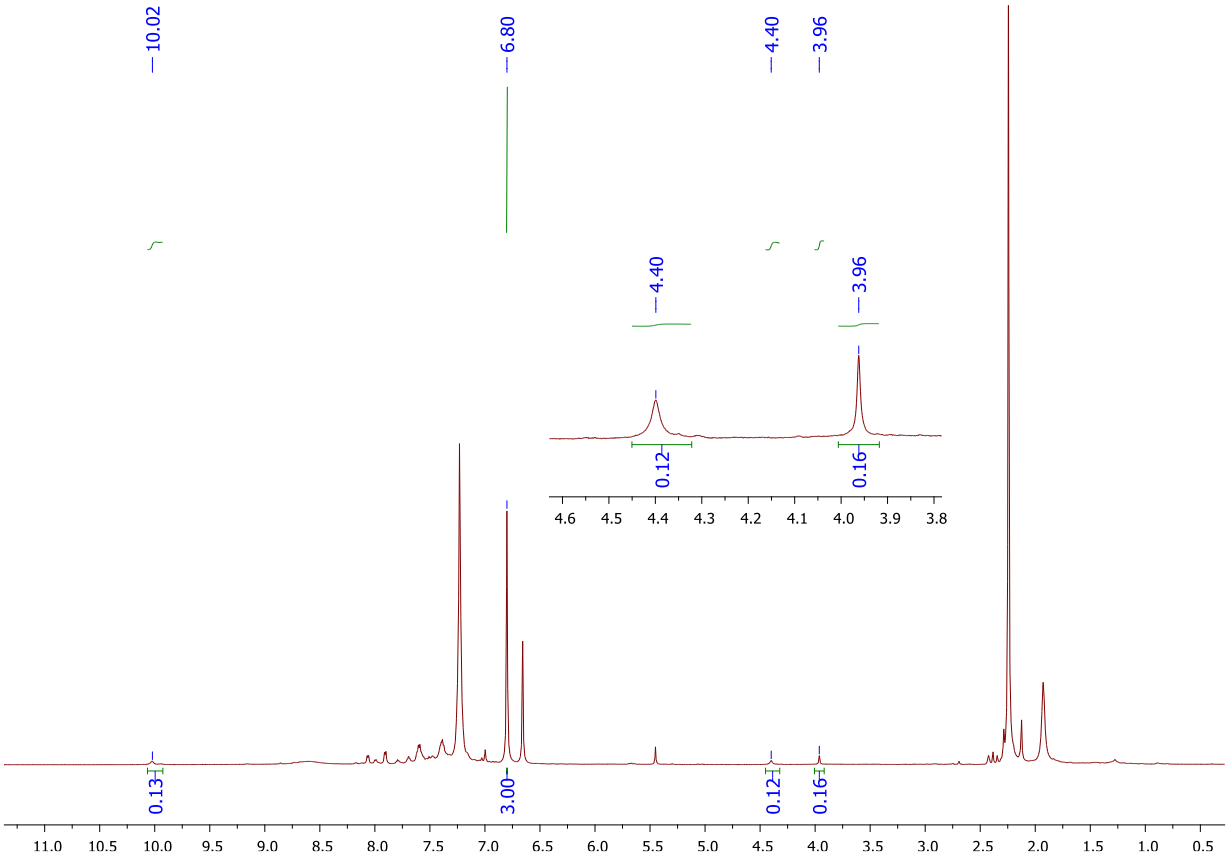

Figure S80. Representative ^{1}H NMR spectrum of the reaction mixture after oxidation of *cis*-stilbene with O_2 in the presence of **3** after 16 h at 70 °C in CD_3CN.

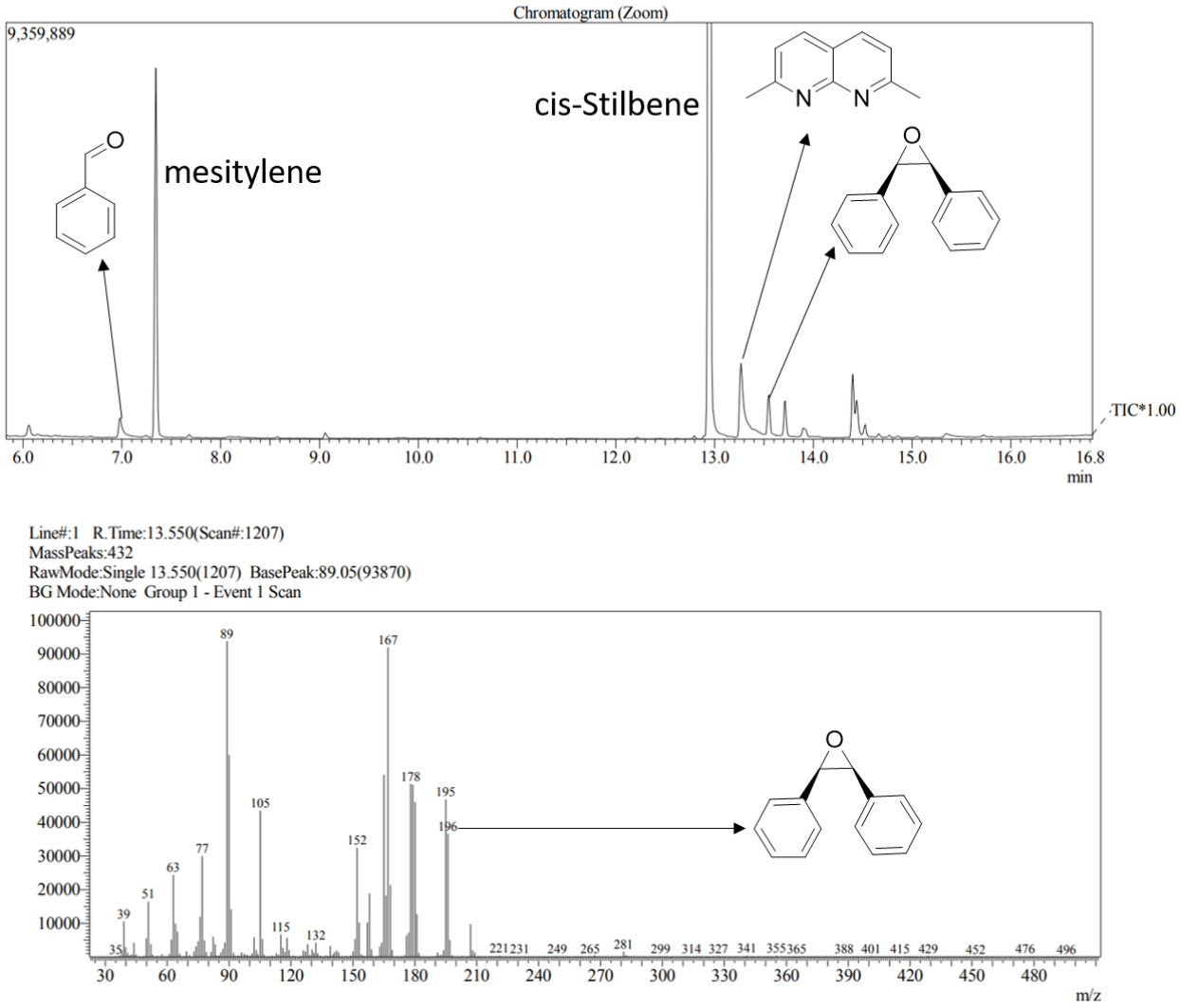

Figure S81. GC-MS spectrum of the reaction mixture after oxidation of *cis*-stilbene with O_2 in the presence of **3** after 16 h at 70 °C in CD_3CN.; diluted with ethyl acetate.

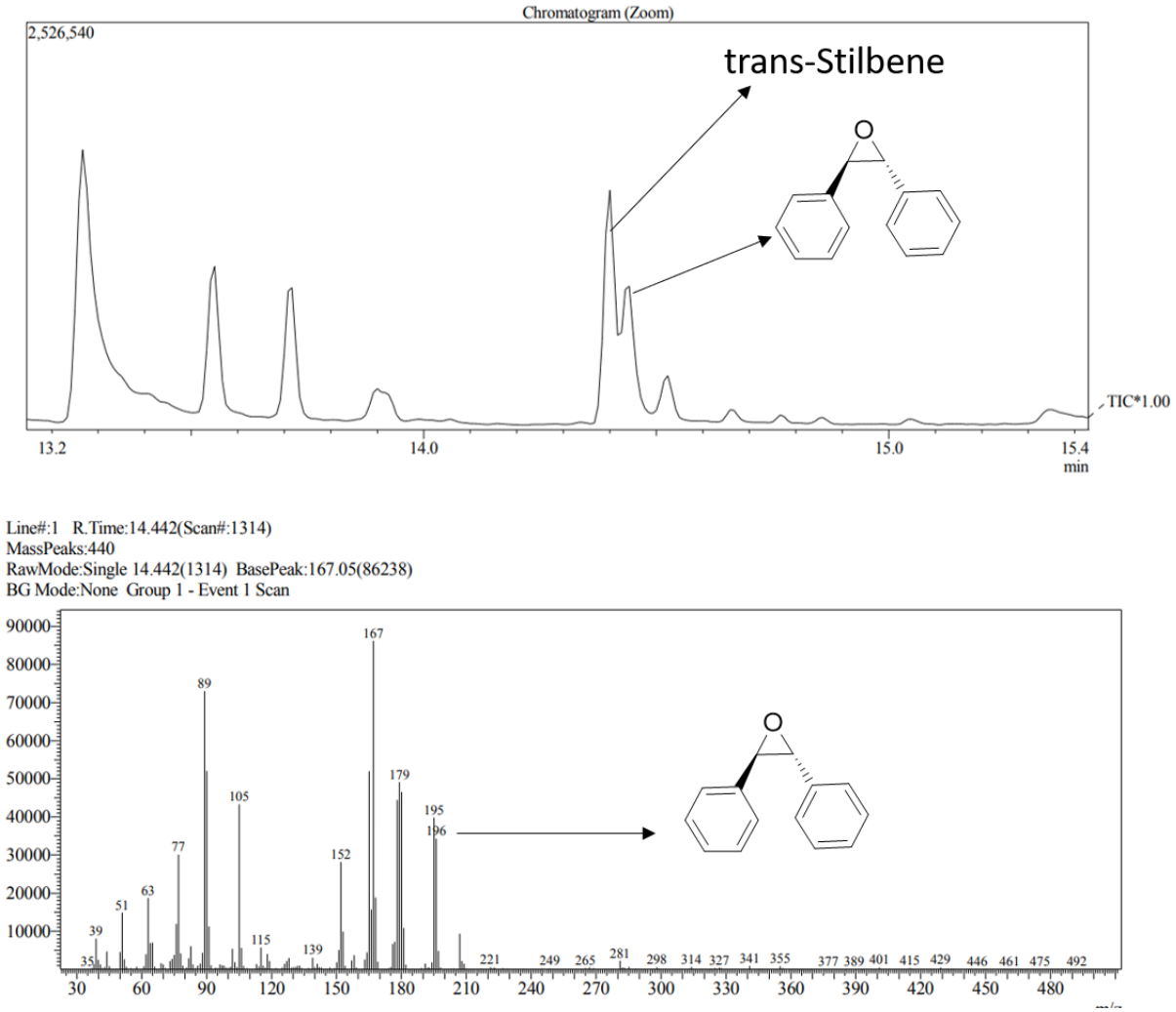

Figure S82. Expanded region of GC-MS spectrum of the reaction mixture after oxidation of *cis*-stilbene with O_2 in the presence of **3** after 16 h at 70 °C in CD_3CN.; diluted with ethyl acetate.

Attempted oxidation of *cis*-stilbene with O_2 in absence of 3

Inside the glovebox, a solution of *cis*-stilbene (8.9 μL, 0.0499 mmol) and mesitylene (6.9 μL,0.0499 mmol) in anhydrous CD_3CN (0.5 mL) was placed to a J. Young NMR tube. The NMR tube was removed from glovebox and the reaction mixture was exposed to oxygen gas for four minutes, then transferred to an oil bath heated at 70 °C for 16 hours. After completion of the reaction, the reaction mixture was analyzed by ^1H NMR spectroscopy showing that no product was formed in absence of complex **3**.

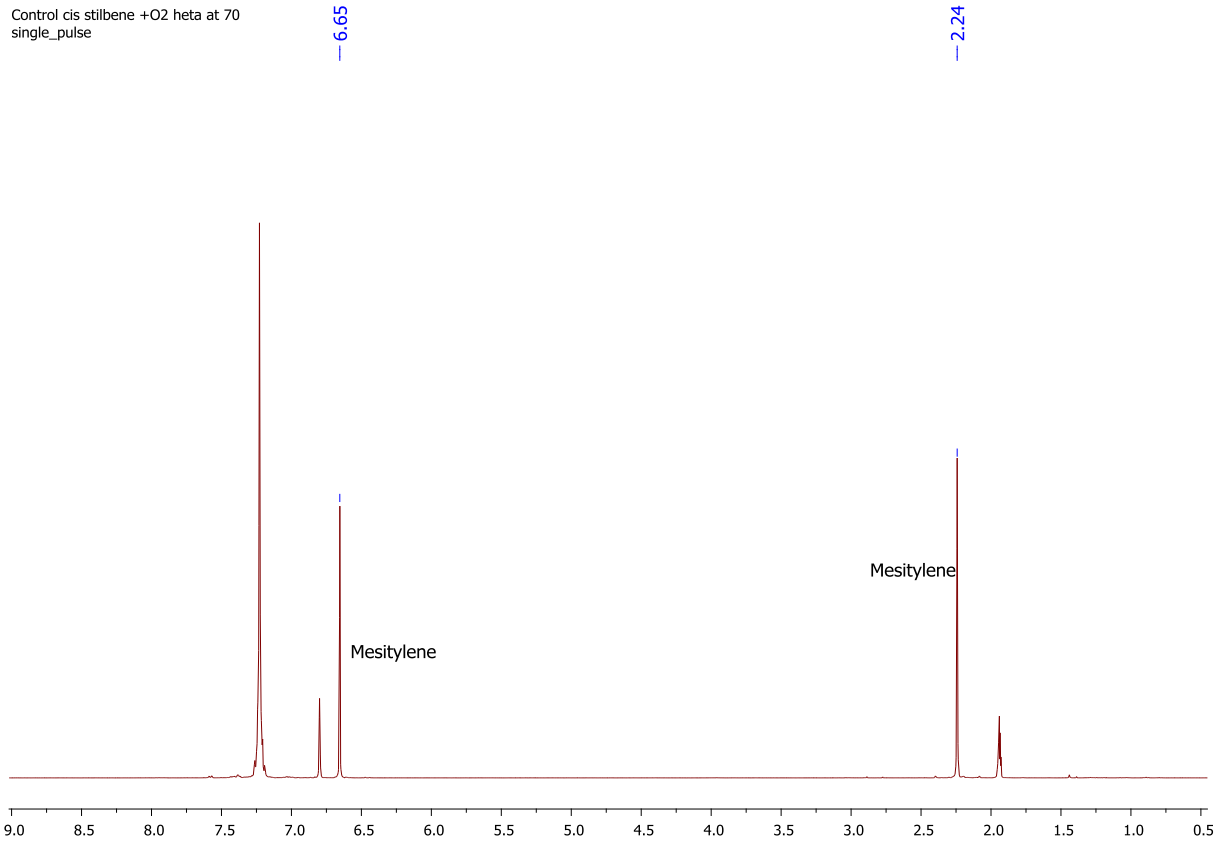

Figure S83. ^1H NMR spectrum of the reaction mixture containing *cis*-stilbene and mesitylene after heating at 70 °C under O_2 for 16 hours in CD_3CN.

Oxidation of *cis*-stilbene with $^{18}O_2$ in the presence of 3

Inside the glovebox, a solution of complex **3** (31.8 mg, 0.0518 mmol), *cis*-stilbene (9.2 μL, 0.0518 mmol) and mesitylene (7.2 μL,0.0518 mmol) in anhydrous CD_3CN (0.5 mL) was placed to a J. Young NMR tube. The NMR tube was removed from glovebox and the reaction mixture was exposed to $^{18}O_2$ gas for four minutes, then transferred to an oil bath heated at 70 °C for 16 hours. After completion of the reaction, the reaction mixture was analyzed by GC-MS to confirms the formation of labeled cis-stilbene oxide and labeled trans-stilbene oxides. The main peak in the mass spectra corresponding to stilbene oxide belong to the ^{18}O-labeled product (see below; M+2 compared to the corresponding mass spectra obtained from the reaction with unlabeled O_2 shown above). The molecular ion peak of benzaldehyde was not sufficiently intense to estimate isotopic composition.

Cis-stilbene oxide: retention time 13.558, m/z 198.

Trans-stilbene oxide: retention time 14.458, m/z 198.

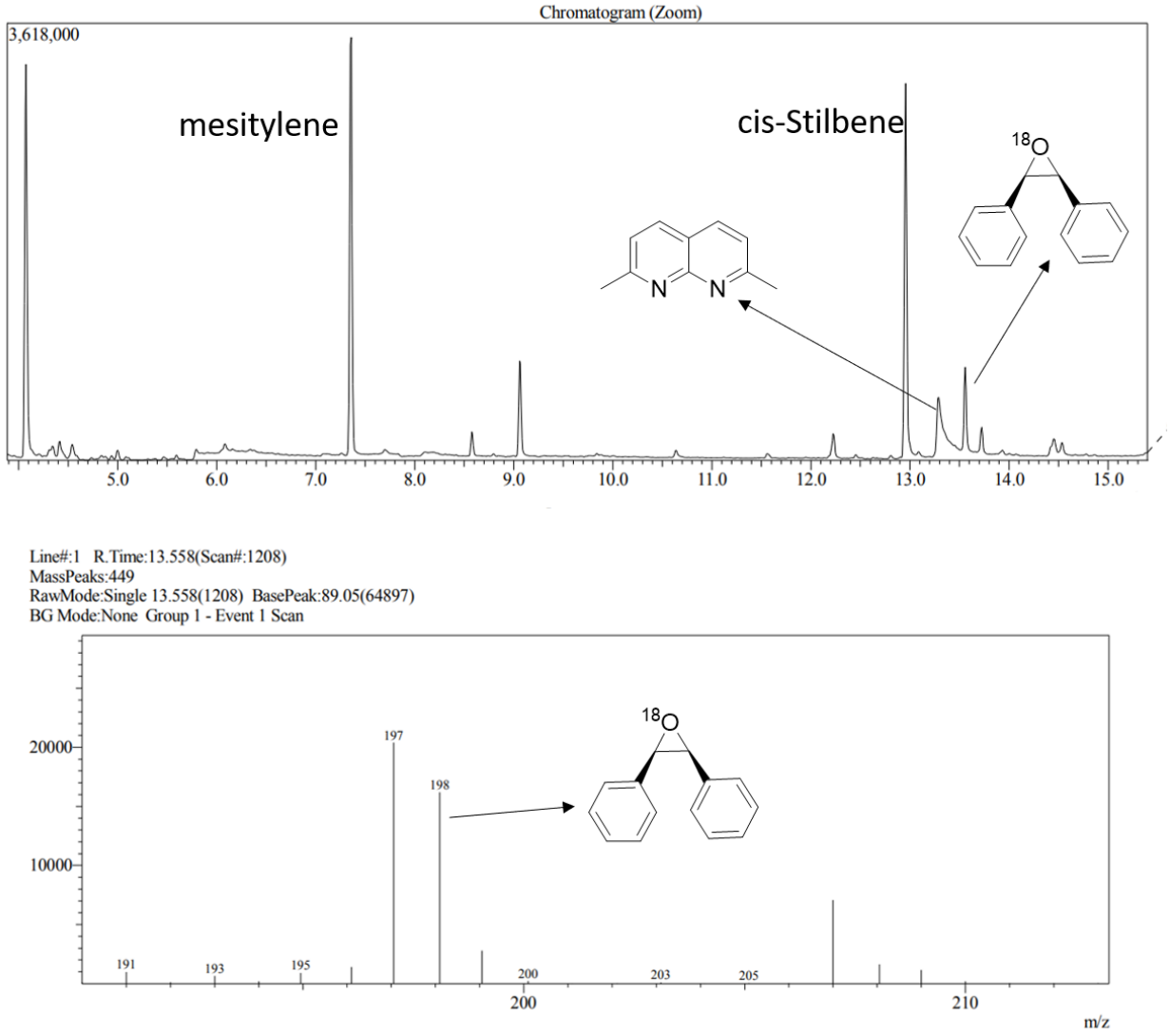

Figure S84. GC-MS spectrum of the reaction mixture after oxidation of *cis*-stilbene with $^{18}O_2$ in the presence of **3** after 16 h at 70 °C in CD_3CN.; diluted with ethyl acetate; diluted with ethyl acetate.

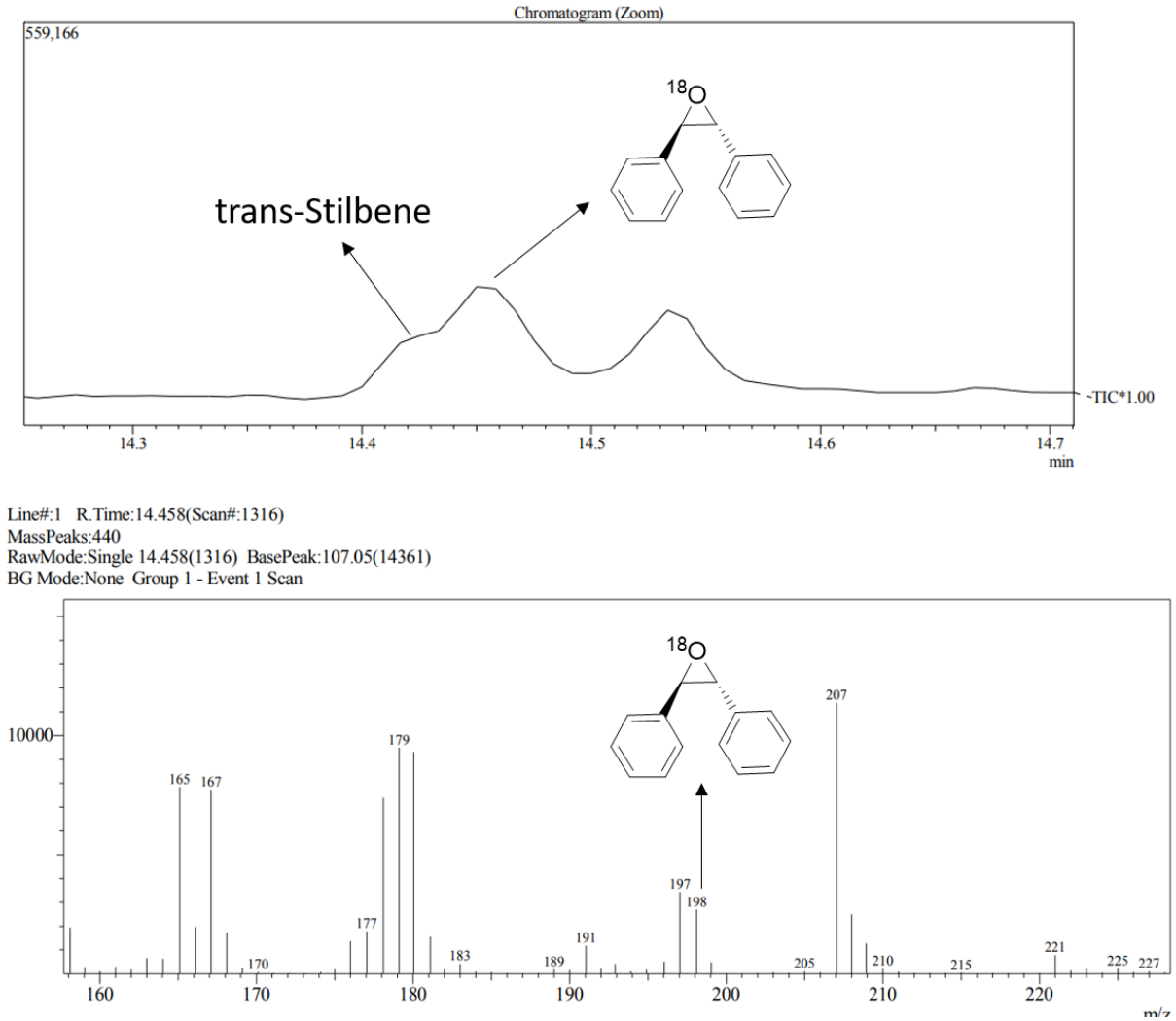

Figure S85. Expanded GC-MS spectrum of the reaction mixture after oxidation of *cis*-stilbene with $^{18}O_2$ in the presence of **3** after 16 h at 70 °C in CD_3CN.; diluted with ethyl acetate.

Oxidation of *trans*-stilbene with O_2 in the presence of 3

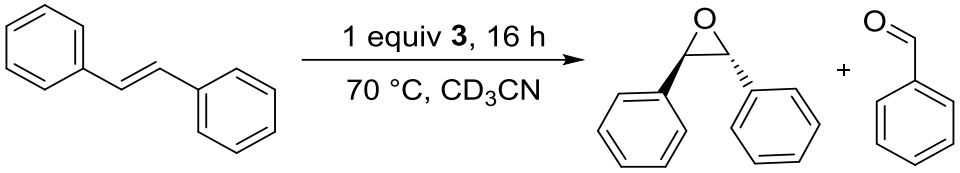

Typical procedure. Inside the glovebox, a solution of complex **3** (34.6 mg, 0.0564 mmol), *trans*-stilbene (10.2 mg, 0.0564 mmol) and mesitylene (7.8 μL, 0.0564 mmol) in anhydrous CD_3CN (0.5 mL) was placed to a J. Young NMR tube. The NMR tube was removed from glovebox and the reaction mixture was exposed to oxygen gas for four minutes, then transferred to an oil bath heated at 70 °C for 16 hours. The reaction mixture was then analyzed by ^1H NMR spectroscopy and GC-MS. The yields were determined by ^1H NMR integration against mesitylene internal standard. The formation of *trans*-stilbene oxide (11%) and benzaldehyde (12%) was confirmed by comparison of ^1H NMR spectra with literature data and by GC-MS. Unreacted *trans*-stilbene was also present (ca. 65%) (see representative NMR spectrum below).

The reaction was repeated four times to give yields consistent within 4-5%. Variations could be due to slight differences in conditions/O_2 mixing and due to volatile nature of benzaldehyde. The yields for four individual trials are given below; the average yields are reported in the manuscript.

Run	%Yield of *trans*-stilbene oxide	% Yield of benzaldehyde
1	9	16
2	10	23
3	11	12
4	17	21

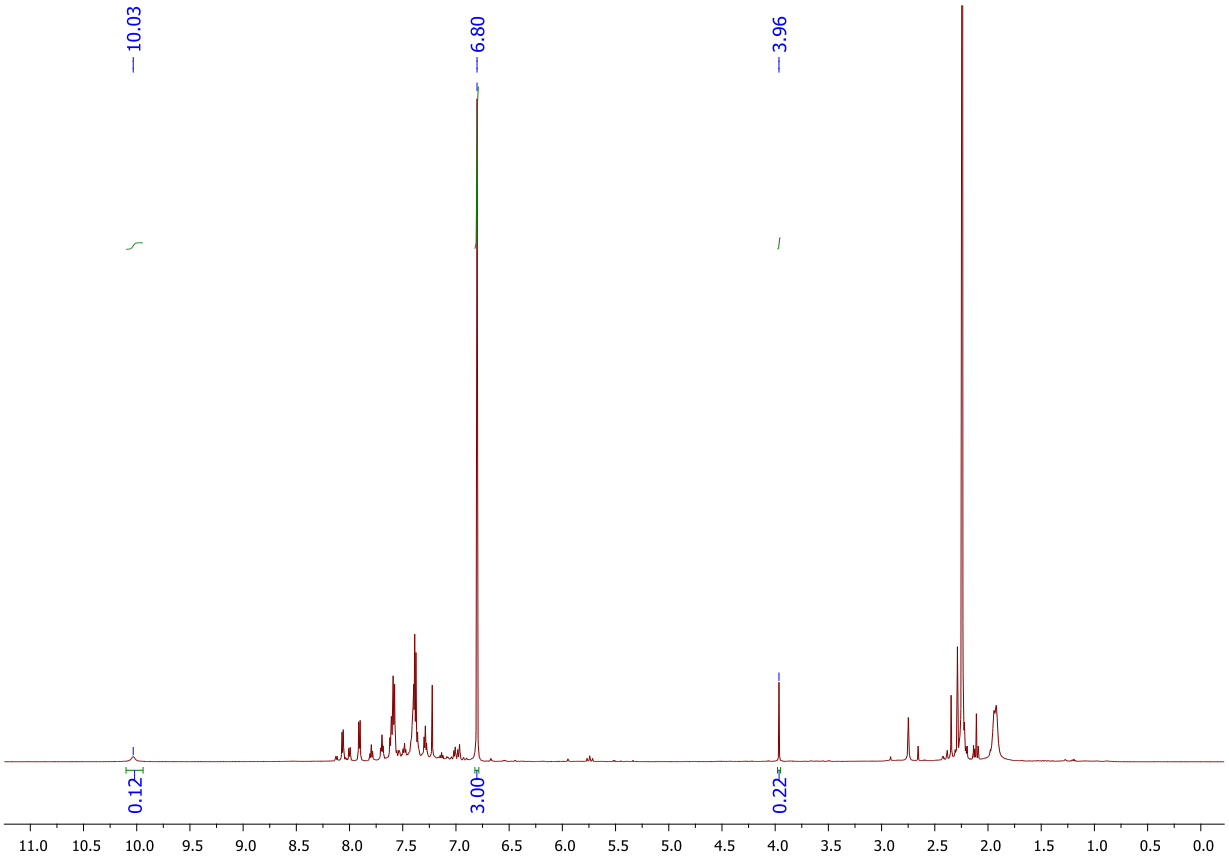

Figure S86. Representative ^{1}H NMR spectrum of the reaction mixture after oxidation of *trans*-stilbene with O_2 in the presence of **3** after 16 h at 70 °C in CD_3CN.

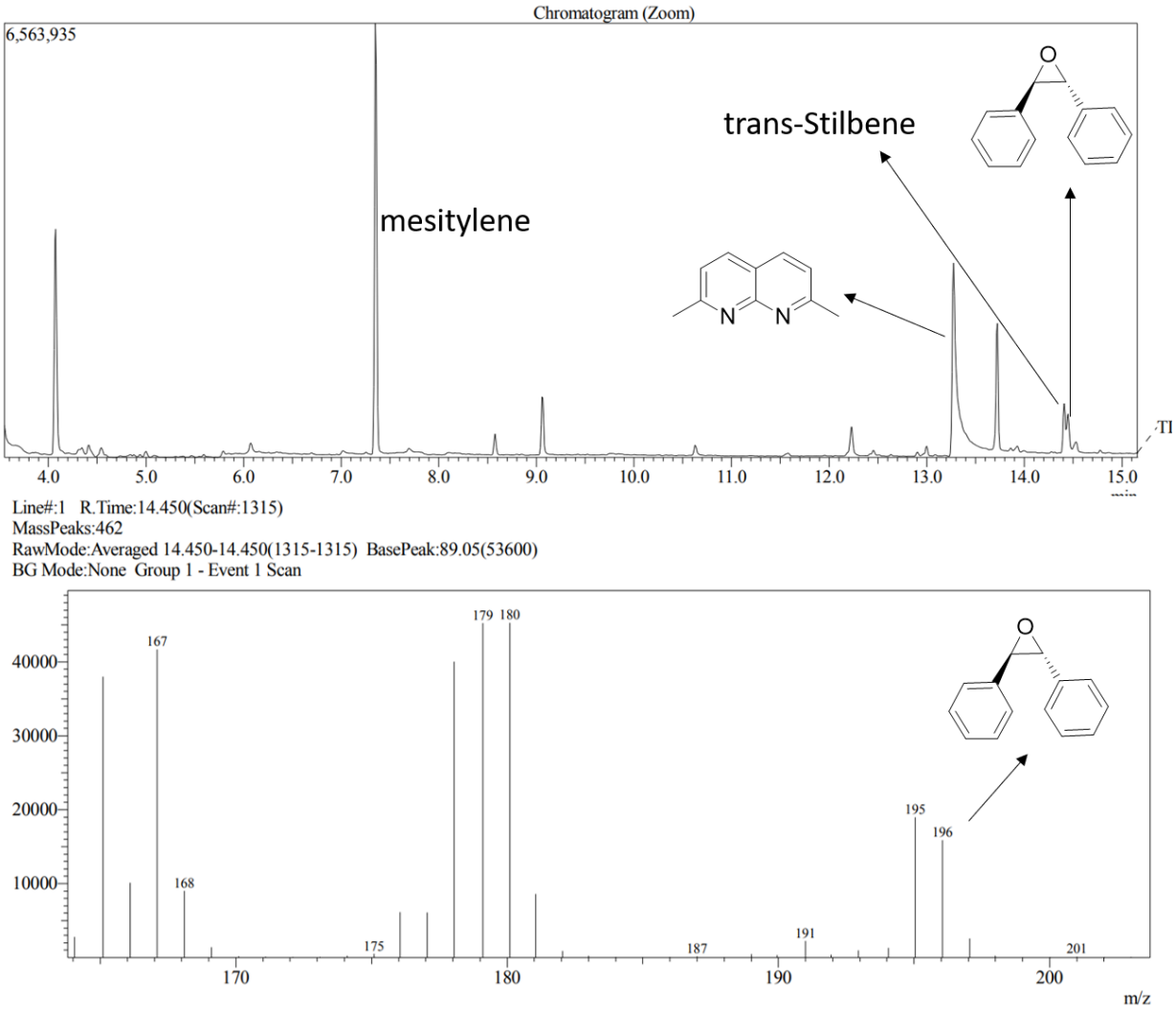

Figure S87. GC-MS spectrum of the reaction mixture sample after oxidation of *trans*-stilbene with O_2 in the presence of **3**; diluted with ethyl acetate.

Attempted oxidation of *trans*-stilbene with O_2 in absence of 3

Inside the glovebox, a solution of *trans*-stilbene (11.2 mg,0.0621 mmol) and mesitylene (8.6 μL, 0.0621 mmol) in anhydrous CD_3CN (0.5 mL) was placed to a J. Young NMR tube. The NMR tube was removed from glovebox and the reaction mixture was exposed to oxygen gas for four minutes, then transferred to an oil bath at 70 °C for 16 hours. The reaction mixture was analyzed by ^1H NMR spectroscopy, showing no product formation in absence of complex **3**.

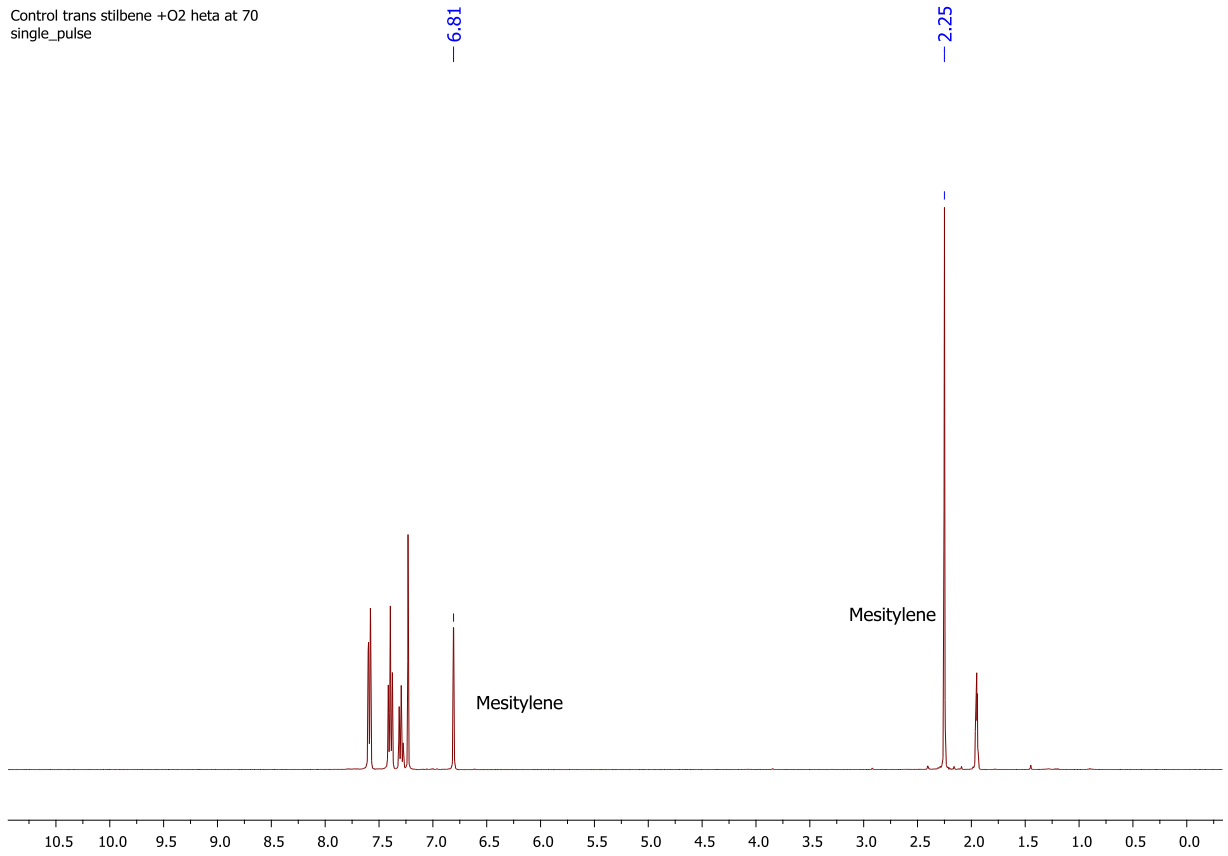

Figure S88. ^1H NMR spectrum of the reaction mixture containing *trans*-stilbene and mesitylene after heating at 70 °C under O_2 for 16 hours in CD_3CN.

Oxidation of benzyl alcohol with O_2 in the presence of 3

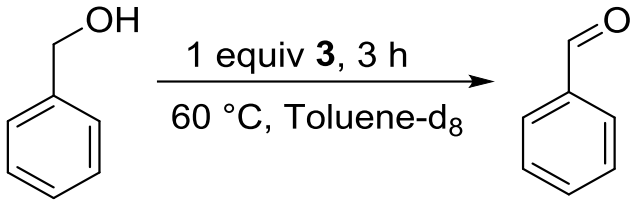

Typical procedure. Inside the glovebox, a solution of complex **3** (38.3 mg, 0.0624 mmol), benzyl alcohol (6.4 μL, 0.0624 mmol) and mesitylene (8.6 μL,0.0624 mmol) in anhydrous toluene-d_8 (0.5 mL) was placed to a J. Young NMR tube. The NMR tube was removed from glovebox and the reaction mixture was exposed to oxygen gas for four minutes, then transferred to an oil bath heated at 60 °C for 3 hours. The reaction mixture was analyzed by ^{1}H NMR spectroscopy and GC-MS; benzaldehyde (39% yield) and unreacted benzyl alcohol were present (26%); GC-MS did now show significant amounts of any other products present in the reaction mixture.

The reaction was repeated in duplicate to give consistent yields of benzaldehyde in two runs: 38% and 39%.

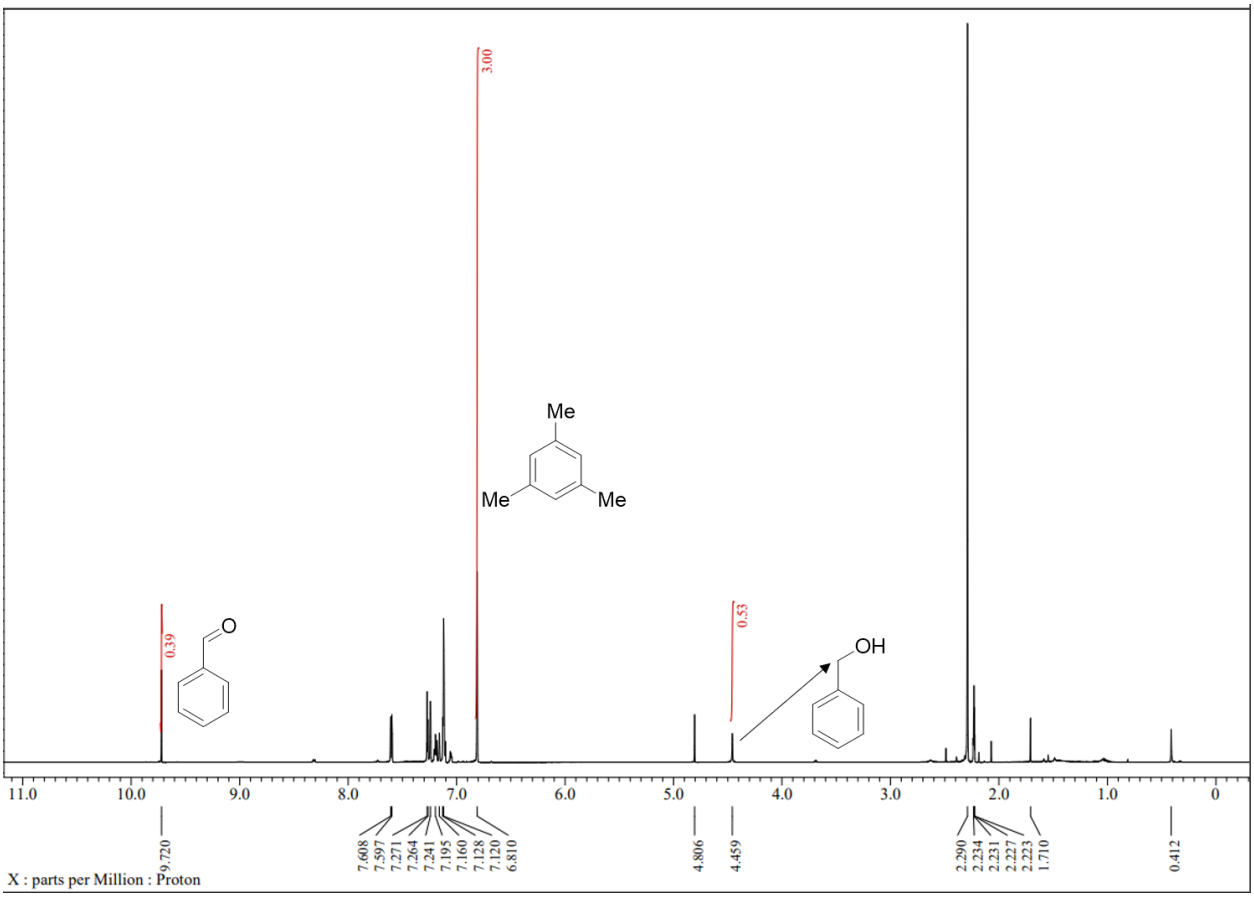

Figure S89. Representative ^{1}H NMR spectrum of the reaction mixture after oxidation of benzyl alcohol with O_2 in the presence of **3** after heating at 60 °C 3 h in toluene-d_8.

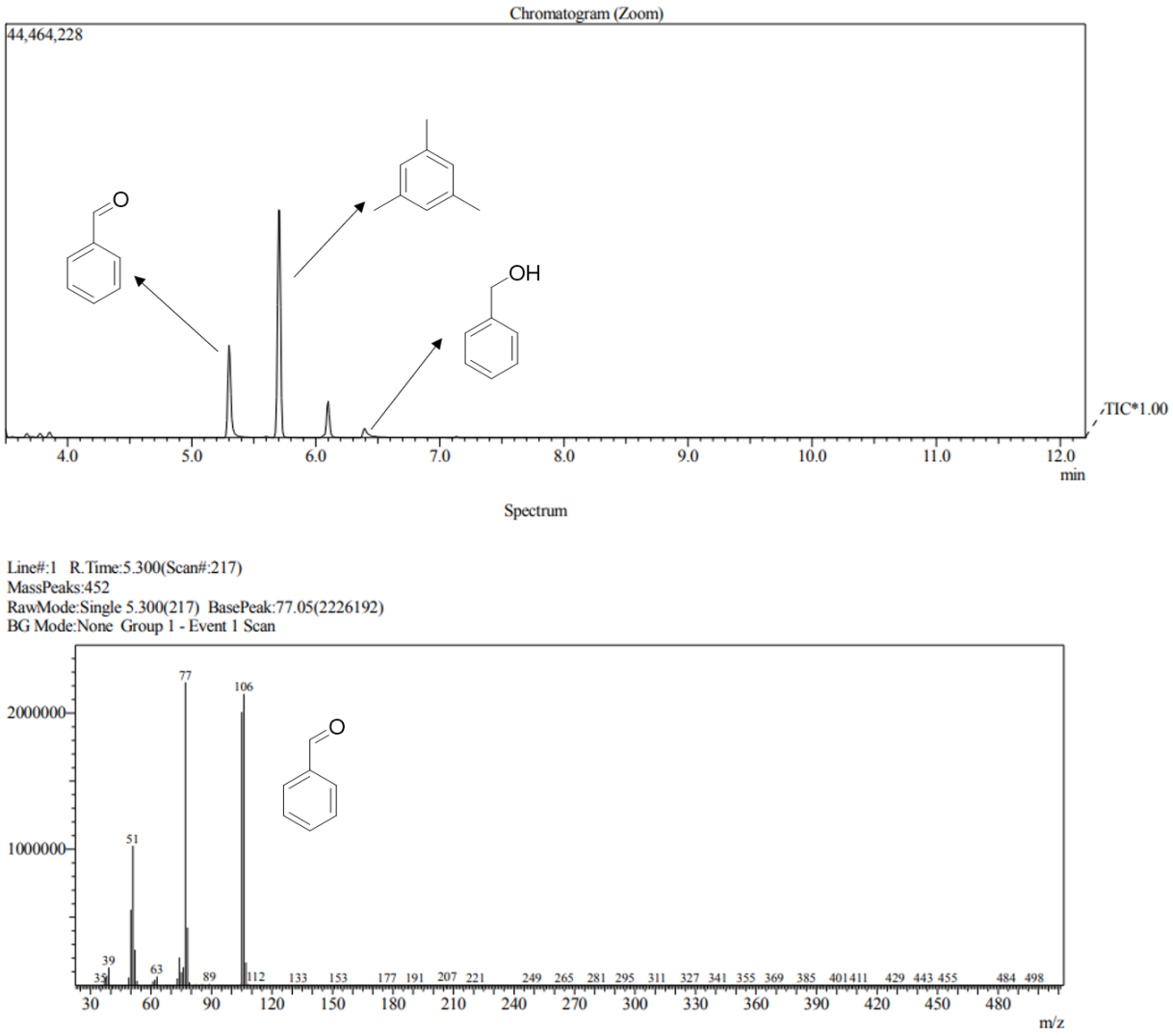

Figure S90. GC-MS spectrum of the reaction mixture after oxidation of benzyl alcohol with O_2 in the presence of **3** after heating at 60 °C 3 h in toluene-d_8; diluted with ethyl acetate.

Attempted oxidation of benzyl alcohol with O_2 in absence of 3

Inside the glovebox, a solution of benzyl alcohol (5.4 μL, 0.0526mmol) and mesitylene (7.3 μL,0.0526 mmol) in anhydrous toluene-d_8 (0.5 mL) was placed to a J. Young NMR tube. The NMR tube was removed from glovebox and the reaction mixture was exposed to oxygen gas for four minutes, then transferred to an oil bath heated at 60 °C for 3 hours. The reaction, the reaction mixture was analyzed by ^{1}H NMR spectroscopy, confirming no product formation in the absence of complex **3**.

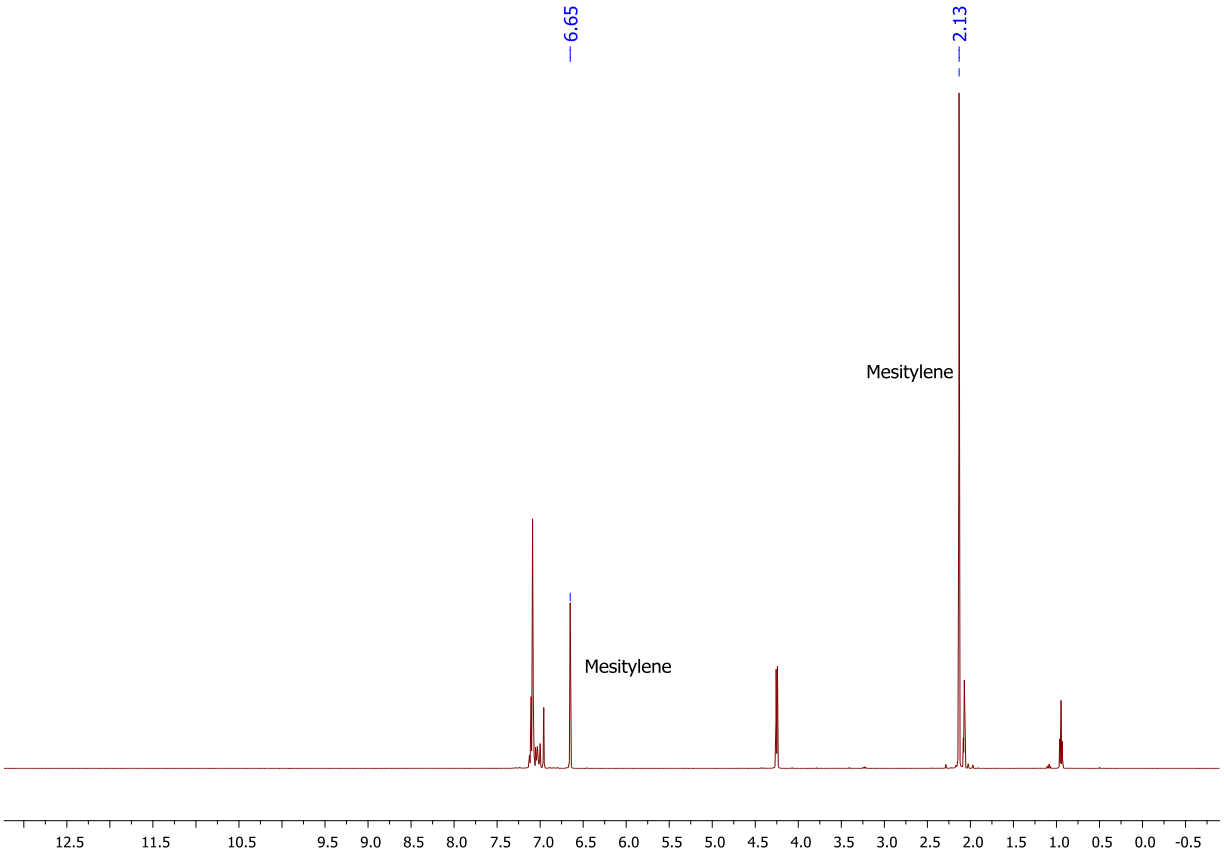

Figure S91. ^{1}H NMR spectrum of the reaction mixture containing benzyl alcohol and mesitylene after heating at 60 °C under oxygen gas for 3 hours in toluene-d_8.

Oxidation of trifluoroethanol with O_2 in the presence of 4

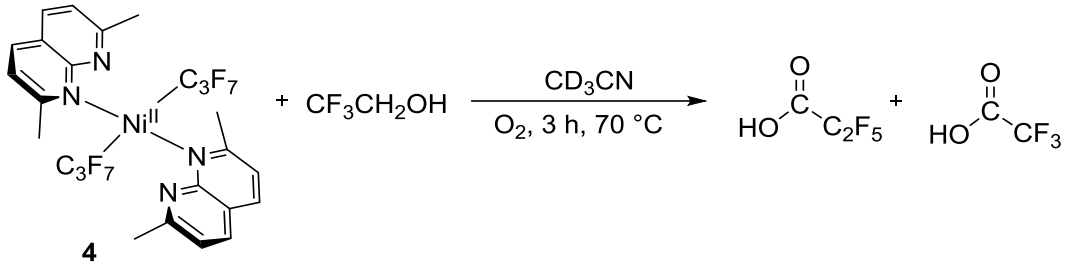

Typical procedure. Inside the glovebox, solution of complex **4** (29.9 mg, 0.0419 mmol), 2,2,2-trifluoroethanol (3 μL, 0.0419 mmol, 1equiv) and α,α,α-trifluorotoluene (5.1 μL, 0.0419 mmol, 1 equiv) in dry CD_3CN (0.5 mL) was placed to a J. Young NMR tube. The NMR tube was removed from glovebox and the reaction mixture was exposed to oxygen gas for four minutes, then transferred to oil bath at 70 °C for 3 hours. The reaction mixture was then analyzed by ^{19}F NMR spectroscopy, confirming the formation of trifluoroacetate formed by oxidation of trifluoroethanol (62% yield based on trifluoroethanol) and pentafluoropropionate formed by competing aerobic oxidation of heptafluoropropyl ligand (34% yield based on total amount of C_3F_7 groups). The yields were determined based on integration against trifluorotoluene internal standard. The reaction was repeated in duplicate to give consistent yields:

Run	% Yield of trifluoroacetate	% Yield of pentrafluoropropionate
1	62	34
2	60	36

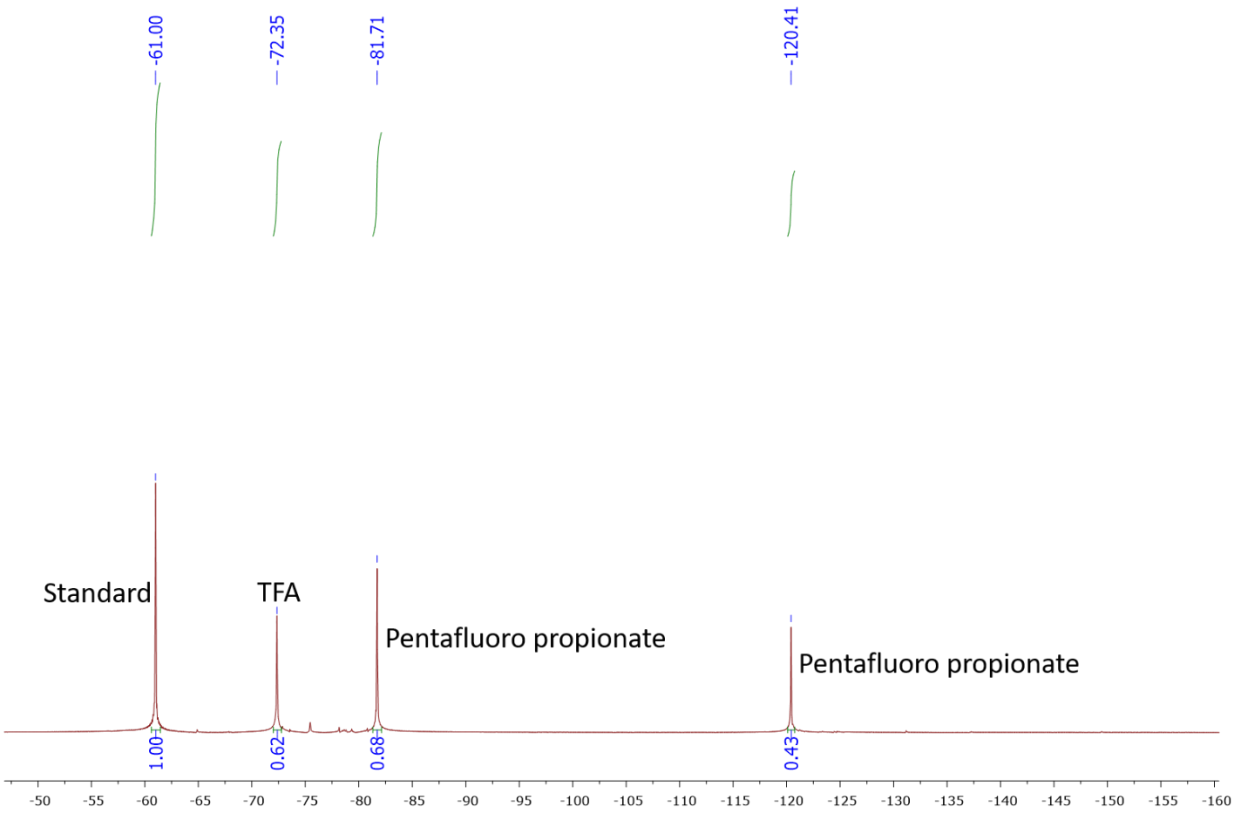

Figure S92. ^{19}F NMR spectrum of the reaction mixture after oxidation of 2,2,2- trifluoroethanol with O_2 in the presence of **4** after heating at 70 °C for 3h in CD_3CN.

Quantification of trifluoroacetate during oxidation of PPh_3 and *trans*-stilbene

To determine to the yield of competitive trifluoroacetate (TFA) formation during oxidation of organic substrates, the amount of TFA was determined during two representative reactions: oxidation of PPh_3 and trans-stilbene as described below. The amount of TFA formed under these conditions was smaller as compared to the amount of TFA formed in the absence of oxygen-accepting substrate. No well-defined stoichiometry was found between the amount of formed TFA and oxidation product(s).

a) TFA formation during PPh_3 oxidation

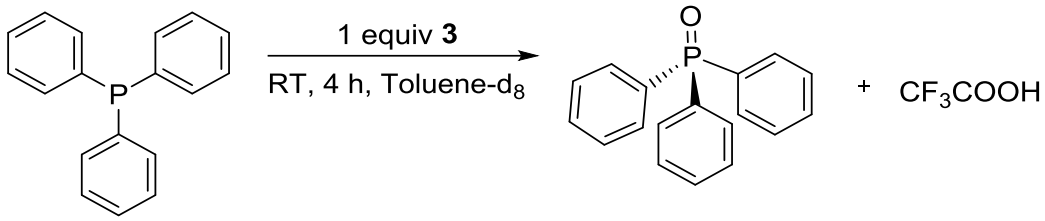

Inside the glovebox, the solution of complex **3** (10.2 mg, 0.0166 mmol), triphenylphosphine (4.3 mg, 0.0166 mmol, 1 equiv) and α,α,α-trifluorotoluene (4 μL, 0.0332 mmol) in anhydrous toluene-d_8 (0.5 mL) was placed to a J. Young NMR tube. The NMR tube was removed from glovebox and the reaction mixture was exposed to oxygen gas for four minutes, then the NMR tube was then placed in an NMR tube spinner and rotated at RT for 4 hours. After completion of the reaction, the reaction mixture was analyzed by $^{31}P\{^1H\}$and ^{19}F NMR spectroscopy, confirming the full consumption of starting material PPh_3 and indicates the formation of trifluoroacetate as a product in (15% yield).

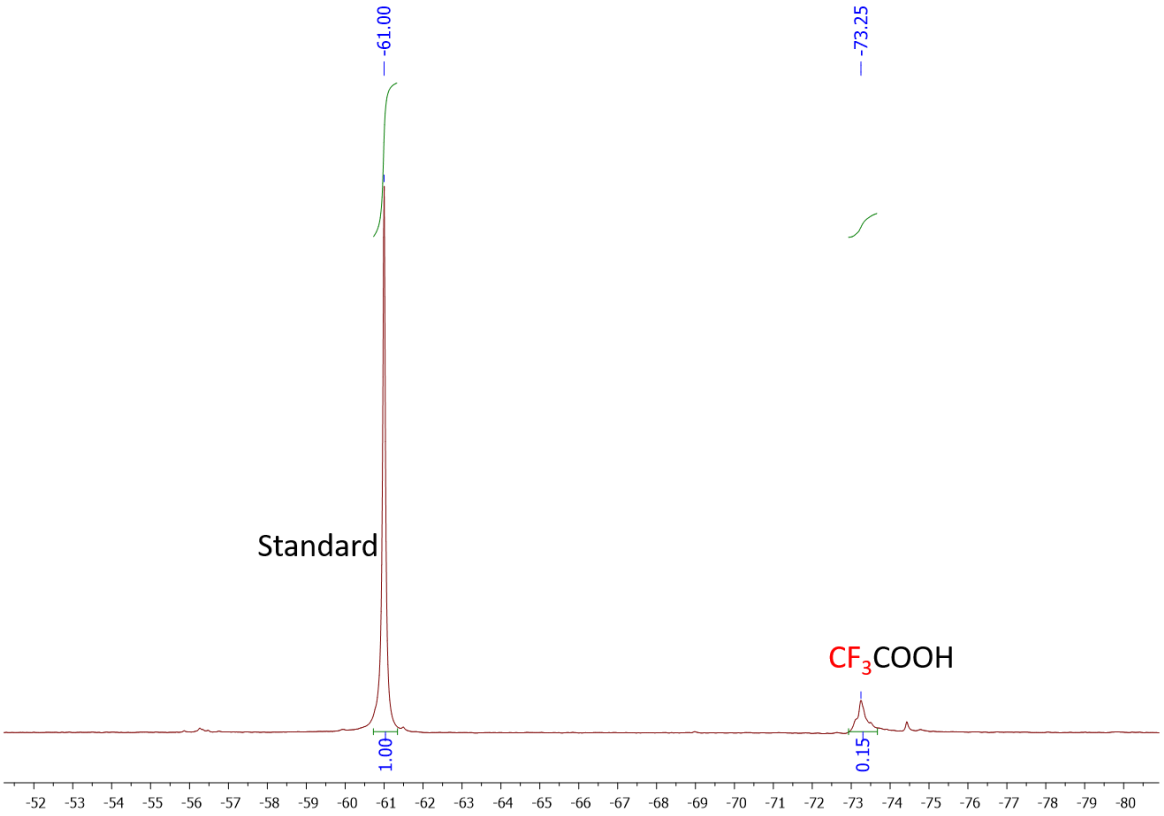

Figure S93. ^{19}F NMR spectrum of the reaction mixture showing TFA formation during oxidation of PPh_3 with O_2/**3**.

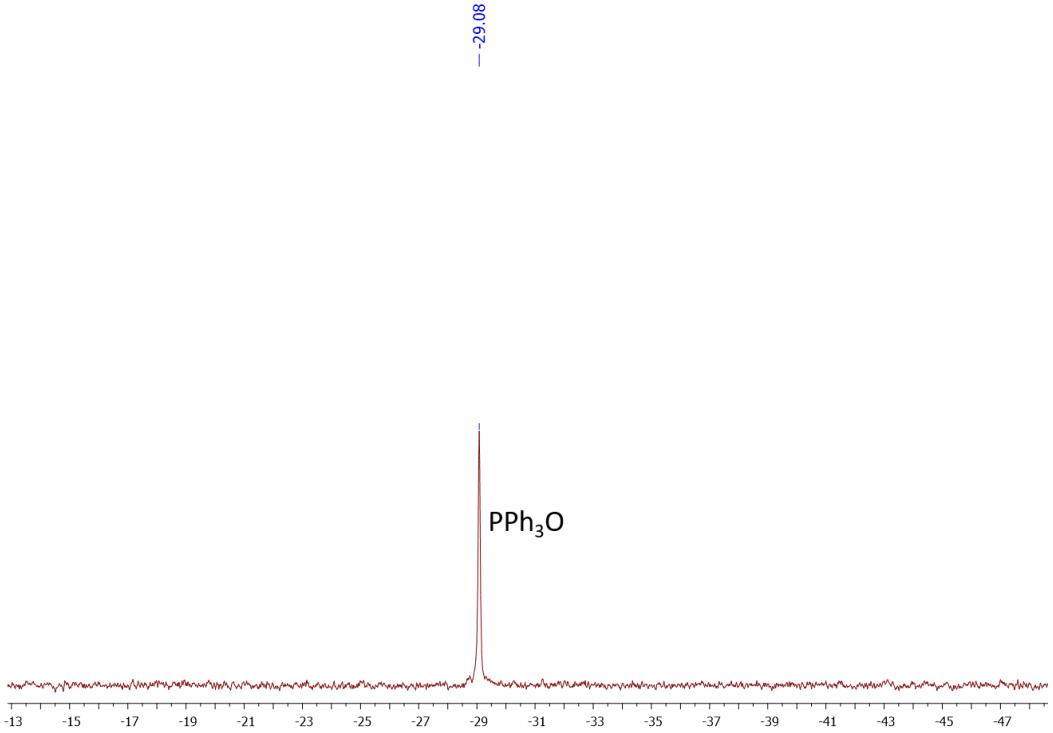

Figure S94. $^{31}P\{^{1}H\}$ NMR spectrum of the reaction mixture showing TFA formation during oxidation of PPh_3 with O_2/**3**.

b) Formation of TFA during oxidation of *trans*-stilbene by O_2 in the presence of 3

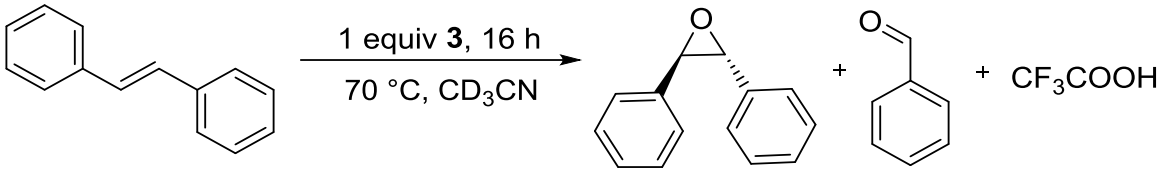

Inside the glovebox, the solution of complex **3** (37.7 mg, 0.0614 mmol), *trans*-stilbene (11 mg, 0.0614 mmol) and α,α,α-trifluorotoluene (15 µL, 0.1229 mmol, 2 equiv) in anhydrous CD_3CN (0.5 mL) was placed to a J. Young NMR tube. The NMR tube was removed from glovebox and the reaction mixture was exposed to oxygen gas for four minutes, then the NMR tube was placed in oil bath and heated at 70 °C for 16 hours. The reaction mixture was analyzed by ^{19}F NMR spectroscopy, confirming the formation of trifluoroacetate as a product in (9% yield). To the same reaction mixture, mesitylene (17.1 µL, 0.1229 mmol, 2equiv) was added and the solution was analyzed by ^{1}H NMR spectroscopy, confirming the formation of *trans*-stilbene oxide (10 % yield) and benzaldehyde (23% yield) as product.

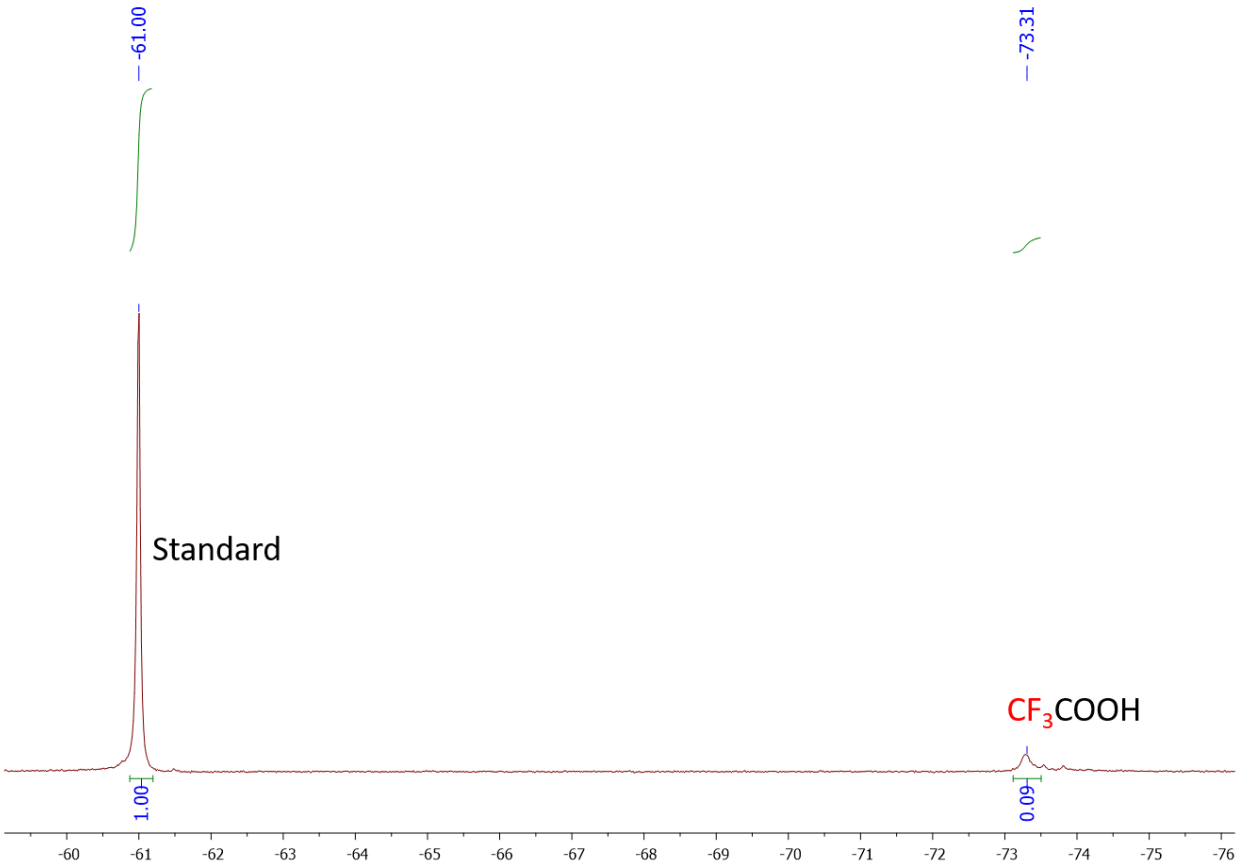

Figure S95. ^{19}F NMR spectrum of the reaction mixture showing TFA formation during oxidation of *trans*-stilbene with O_2/**3**.

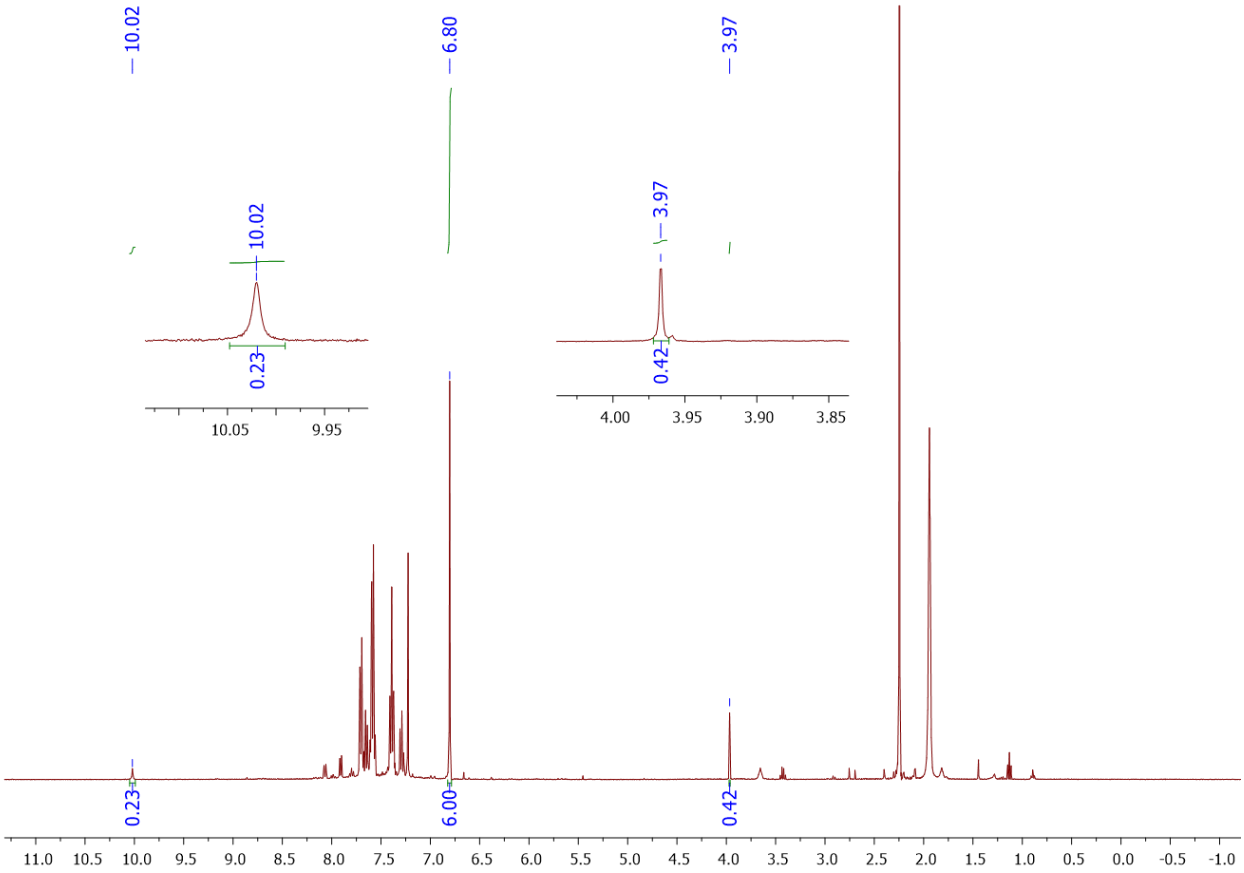

Figure S96. ^{1}H NMR spectrum of t of the reaction mixture showing TFA formation during oxidation of *trans*-stilbene with O_2/**3**.

Radical trap experiments

Reaction of 3 with O_2 in the presence of TEMPO in MeOH-d_4

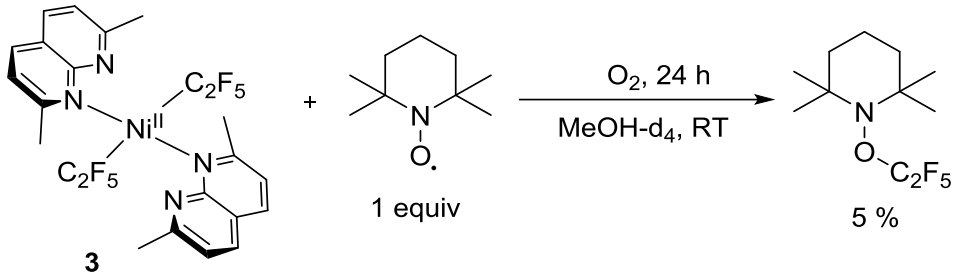

Inside the glovebox, a solution of complex **3** (14.3 mg, 0.0233 mmol), TEMPO (3.6 mg, 0.0233 mmol) and α,α,α-trifluorotoluene (5.7 μL, 0.0466 mmol) in MeOH-d_4 (0.5 mL) was placed to a J. Young NMR tube. The NMR tube was removed from glovebox and the reaction mixture was exposed to oxygen gas for three minutes. The NMR tube was then placed in an NMR tube spinner and rotated at RT for 24 hours to ensure good mixing. The reaction was then analyzed by ^{19}F NMR spectroscopy, confirming the formation of TEMPO-C_2F_5 adduct in 5% yield. The identity of the product was also confirmed by ESI-MS (see experiments below).

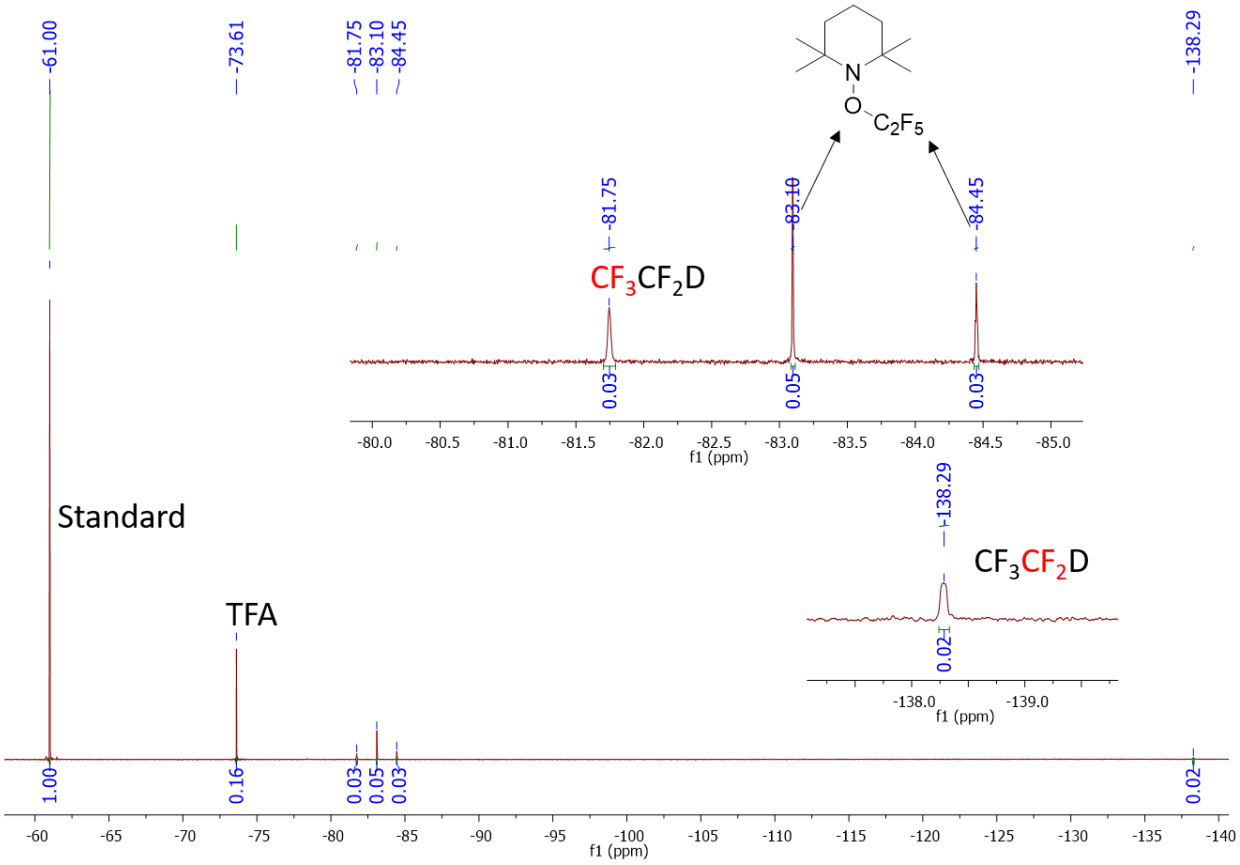

Figure S97. ^{19}F NMR spectrum of the reaction mixture containing TEMPO and **3** at RT under oxygen gas for 24 hours in MeOH-d_4.

Reaction of 3 with O_2 in the presence of TEMPO in C_6D_6

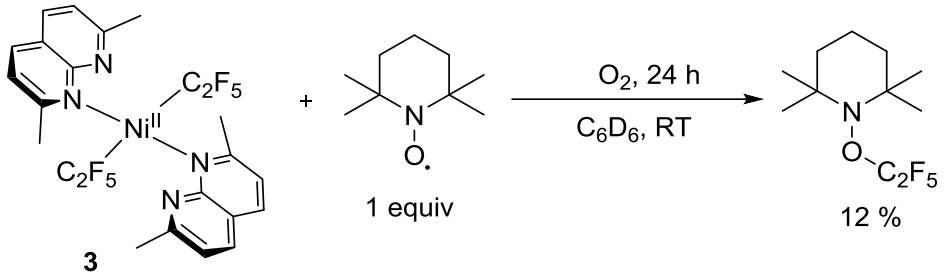

Inside the glovebox, a solution of complex **3** (12.3 mg, 0.0200 mmol), TEMPO (3.1 mg, 0.0200 mmol) and α,α,α-trifluorotoluene (4.9 µL, 0.0401 mmol) in dry C_6D_6 (0.5 mL) was placed to a J. Young NMR tube. The NMR tube was removed from glovebox and the reaction mixture was exposed to oxygen gas for three minutes. The NMR tube was then placed in an NMR tube spinner and rotated at RT for 24 hours to ensure good mixing. The reaction was then analyzed by ^{19}F NMR spectroscopy, confirming the formation of TEMPO-C_2F_5 adduct in 12% yield.

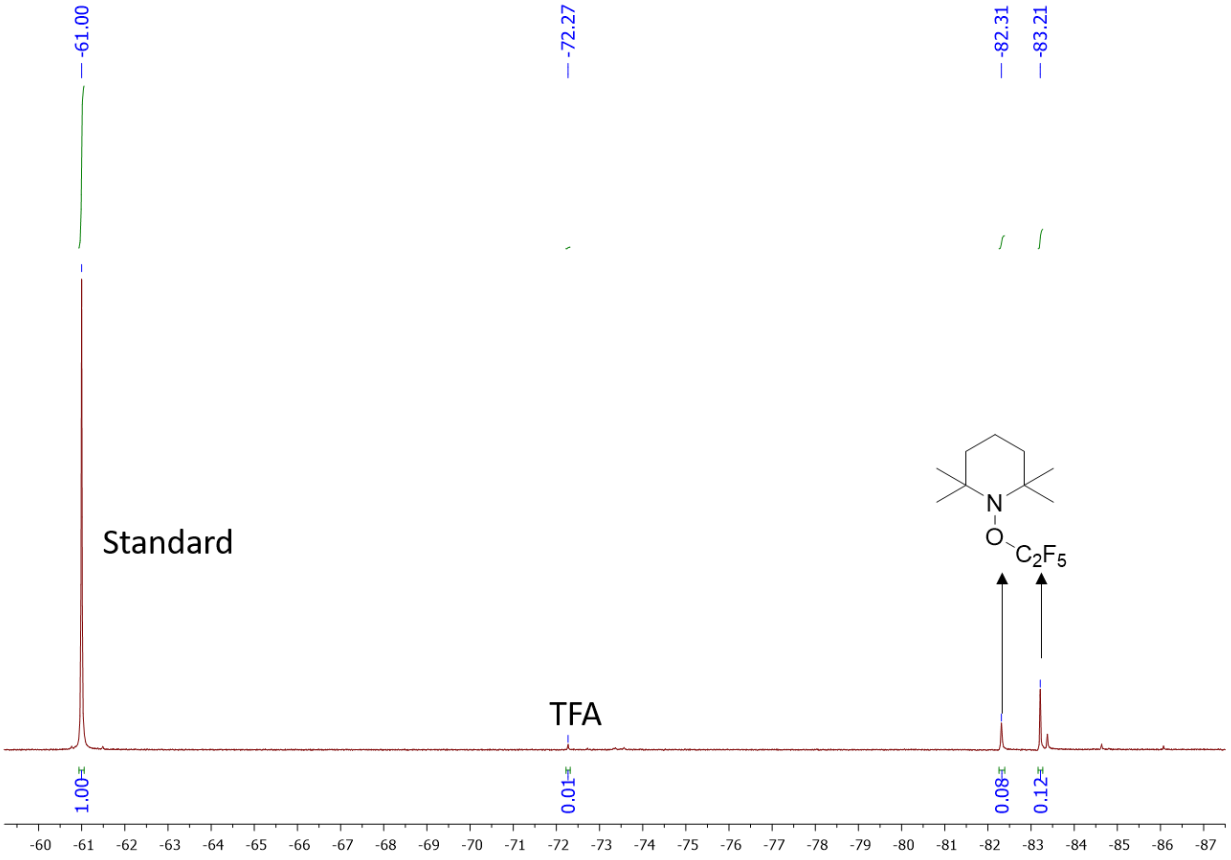

Figure S98. ^{19}F NMR spectrum of the reaction mixture containing TEMPO and **3** at RT under oxygen gas for 24 hours in C_6D_6.

Reaction of 3 with O_2 in the presence of TEMPO in CD_3CN

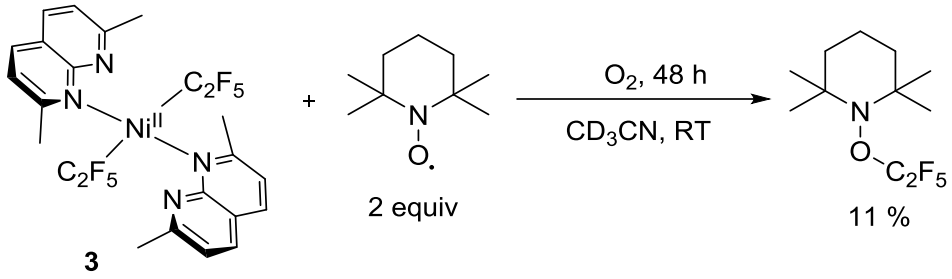

Inside the glovebox, solution of complex **3** (10.3 mg, 0.0167 mmol), TEMPO (5.2 mg, 0.0335 mmol) and α,α,α-trifluorotoluene (4.1 µL, 0.0335 mmol) in dry CD_3CN (0.5 mL) was placed to a J. Young NMR tube. The NMR tube was removed from glovebox and the reaction mixture was exposed to oxygen gas for three minutes. Further the NMR tube was then placed in an NMR tube spinner and rotated at room temperature for 48 hours to ensure good mixing. The reaction was then analyzed by ^{19}F NMR spectroscopy, confirming the formation of TEMPO-C_2F_5 adduct in 11% yield.

HRMS (ESI) calculated for $[M^*H]^+$, $C_{11}H_{18}F_5NO$: m/z 276.1381; found, 276.1287.

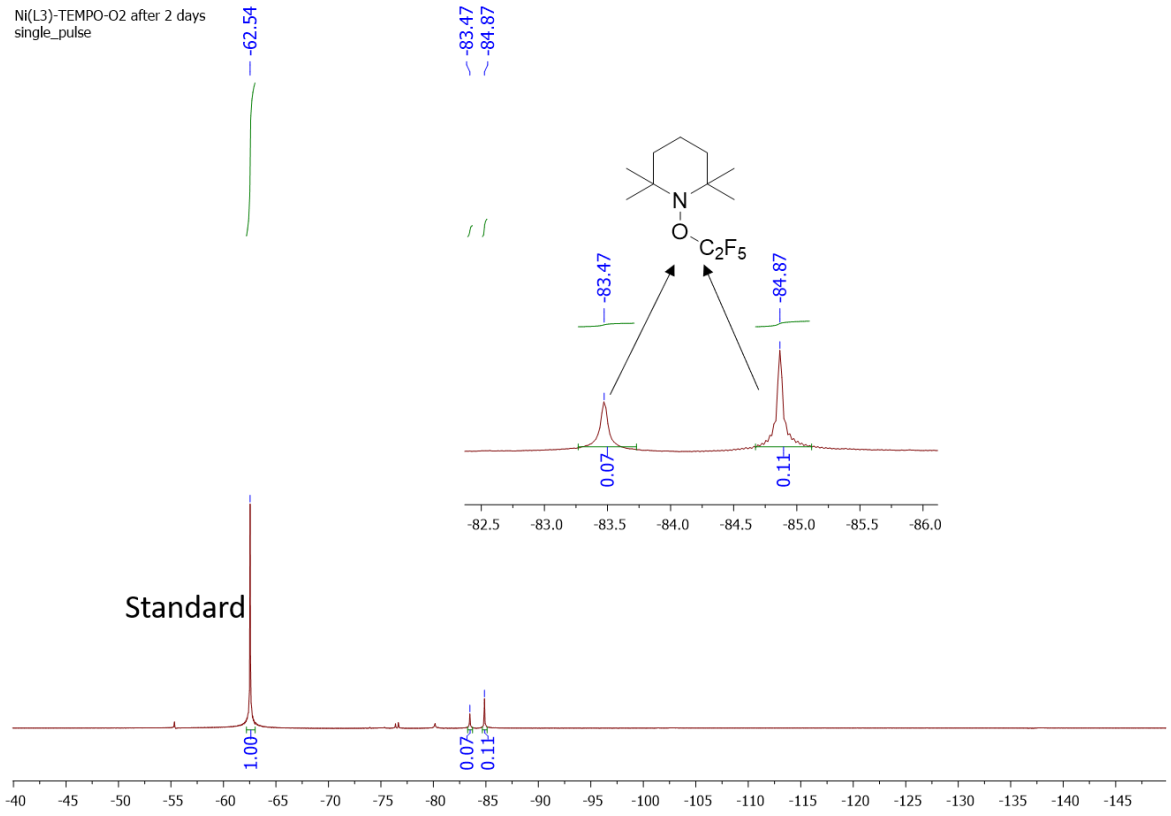

Figure S99. ^{19}F NMR spectrum of the reaction mixture containing TEMPO and **3** at RT under oxygen gas for 48 hours in CD_3CN.

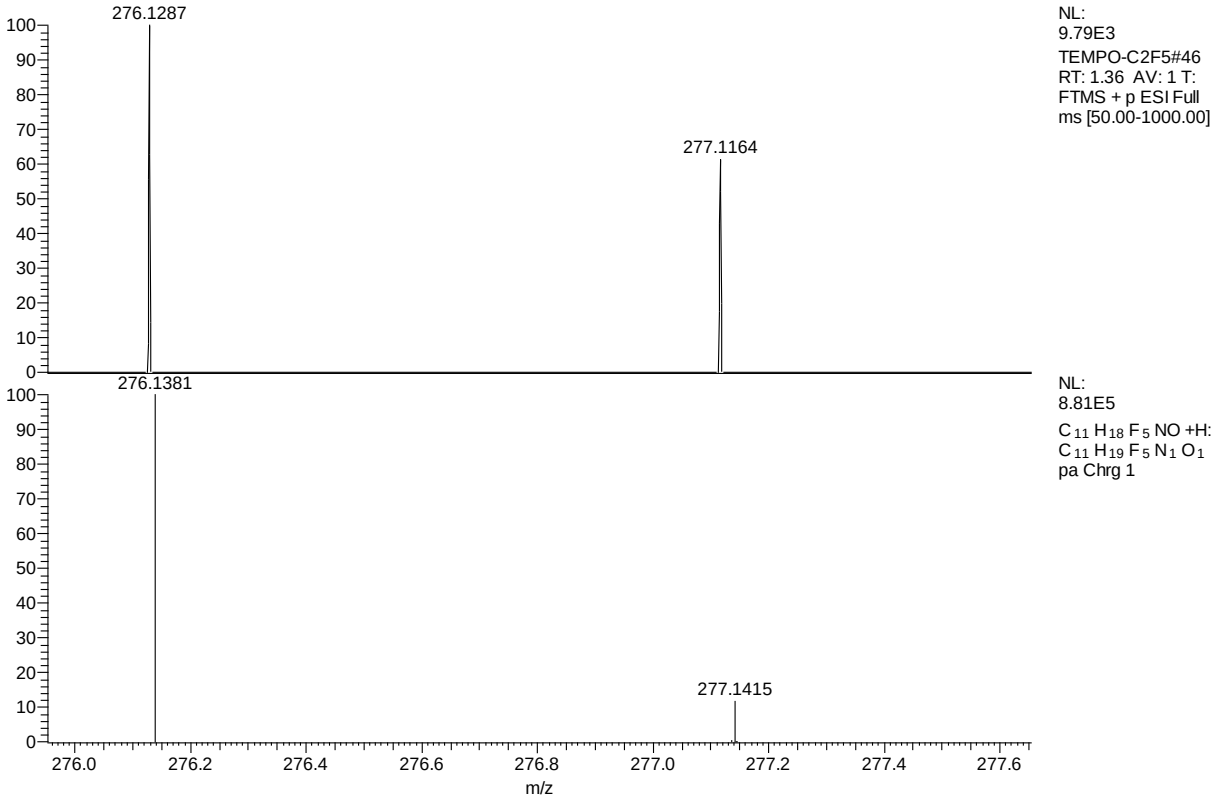

Figure S100. ESI-(HR)MS spectrum of MeCN solution of the reaction mixture (top) and simulated spectrum of $C_{11}H_{18}F_5NO$: (bottom).

Stability of 3 towards TEMPO in the absence of O_2

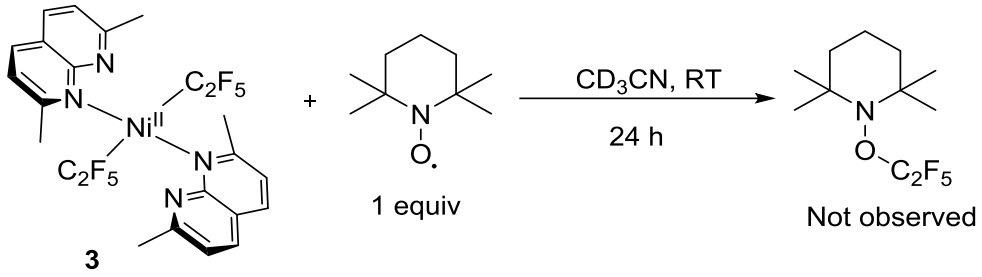

Inside the glovebox, solution of complex **3** (11.3 mg, 0.0184 mmol), TEMPO (2.8 mg, 0.0184 mmol) and α,α,α-trifluorotoluene (11.3 μL, 0.0921 mmol) in anhydrous CD_3CN (0.5 mL) was placed to a J. Young NMR tube. The NMR tube was removed from glovebox and the NMR tube was then placed in an NMR tube spinner and rotated at RT for 24 hours to ensure good mixing. The reaction was then analyzed by ^{19}F NMR spectroscopy, showing the peaks of complex **3**. No TEMPO-C_2F_5 could be detected in the absence of air or oxygen.

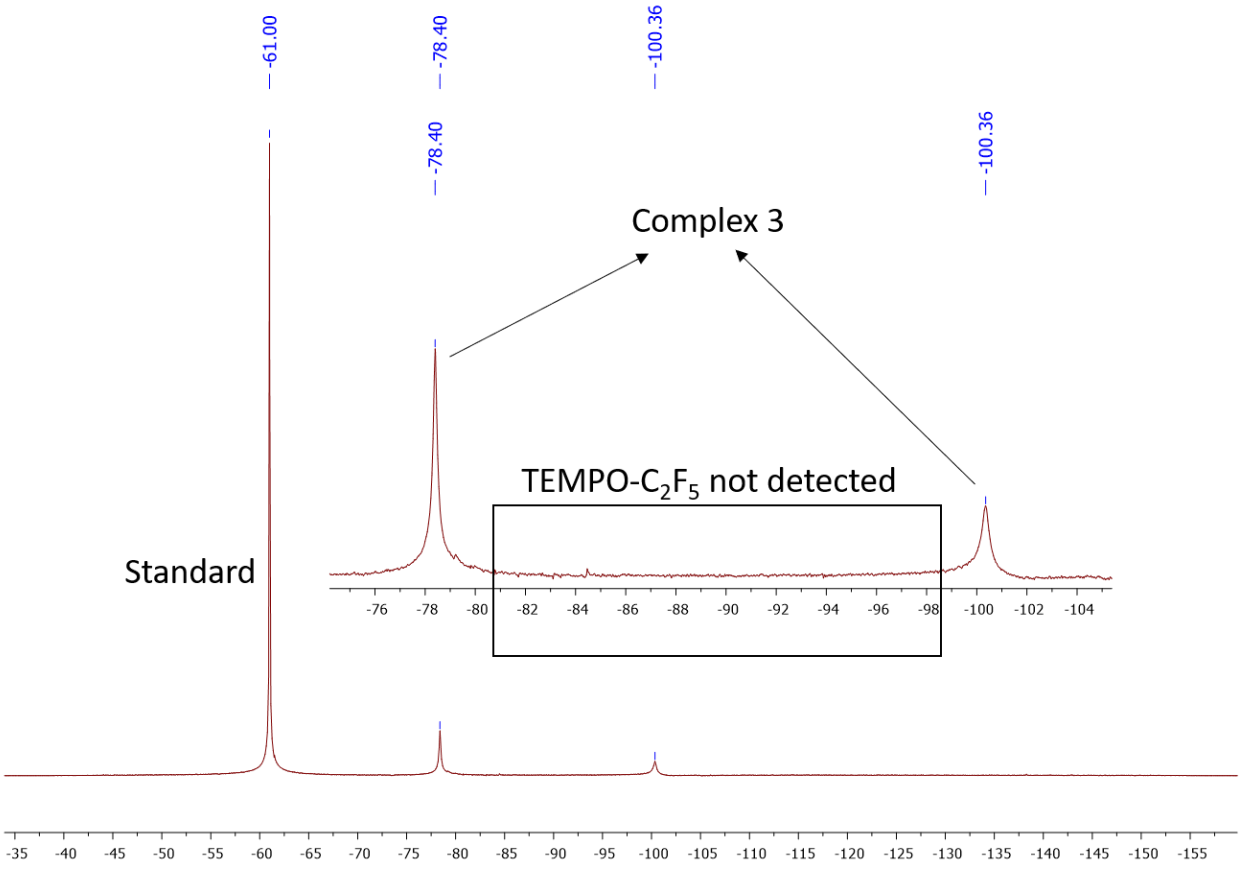

Figure S101. ^{19}F NMR spectrum of the reaction mixture containing TEMPO and **3** at RT for 24 hours in CD_3CN.

EPR spectra

Aerobic oxidation of 3 in the presence of DMPO

To a 20 mL vial, a solution of complex **3** (4.2 mg, 0.0068 mmol), and 5 equivalents of DMPO (3.8 mg, 0.034 mmol) were dissolved in MeOH (0.5 mL). The reaction mixture was exposed to air for five minutes then the sample of the reaction mixture was transferred to a quartz capillary tube and analyzed by EPR at RT. Experimental and simulated spectra are given below.

DMPO (5,5-dimethyl-1-pyrroline N-oxide) is a common trap for oxygen-derived radicals. The observed signal allows to conclude that the formation of OH radical and Fenton-type chemistry does not occur to a significant extent under these conditions (e.g. via Ni-mediated formation of H_2O_2 from O_2 and its decomposition to OH radical and OH^-) as a as stable DMPO-OH adduct is characterized by significantly different set of superhyperfine splitting parameters.[11-13] No signal was observed in the absence of O_2, confirming that background reactivity between DMPO and the Ni^{II} starting material does not occur.

The splitting constants of the observed DMPO adduct (A_N = 13.7, A_H = 8.0, g = 2.007) resemble the DMPO adduct observed during aerobic oxidation of trifluoromethyl analog **A** (Scheme 1, a), (**L3**)$Ni^{II}(CF_3)_2$ in the presence of 1 equiv of **L3**,[14] and they are similar to those reported for superoxide adducts of first-row transition metals such as Cu,[15] Co,[16] or Ni.[17]

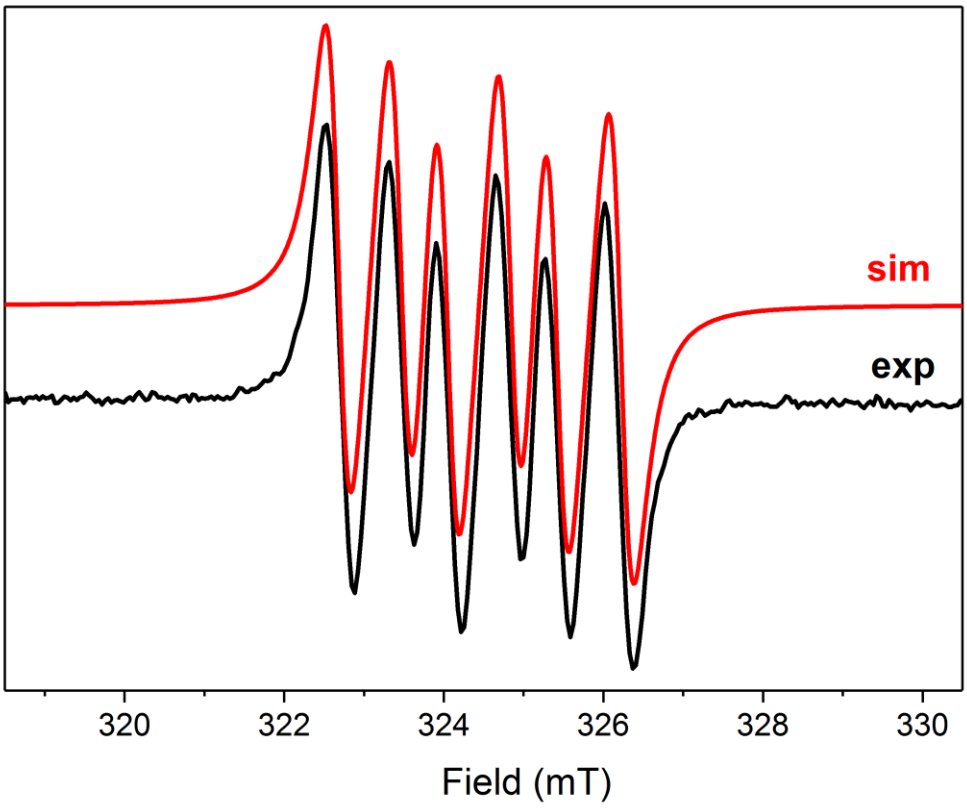

Figure S102. Experimental (black line) and simulated (red line) EPR spectra of the solution of **3** exposed to air for 5 min at RT in MeOH in the presence of DMPO spin trap. Simulation parameters: A_N=13.7 G; A_H=8.0 G, g=2.007.

Detection of Ni^{III} species during oxidation of 3

To a J. Young NMR tube complex **3** (4.8 mg, 0.0078 mmol) was dissolved in 0.5 mL of degassed 2-methyltetrahydrofuran in the glovebox, then the solution was exposed to oxygen gas for 1.5 min to give purple solution, which was frozen and analyzed by EPR spectroscopy at 91 K. Then the same solution was unfrozen, continued to be gently agitated under O_2 atmosphere for 20 min at RT, quickly flushed with N_2 to remove excess O_2, frozen and analyzed by EPR spectroscopy at 91 K. Essentially the same signal was observed after 1.5 min and after 20 min, with higher intensity signal after 20 min; the initially observed broad feature at g ~ 2.27 disappeared in a spectrum after 20 min. Upon further reaction, the signal shows diminished intensity and eventually disappears. The spectrum obtained after 20 min was used for EPR simulation using EasySpin.

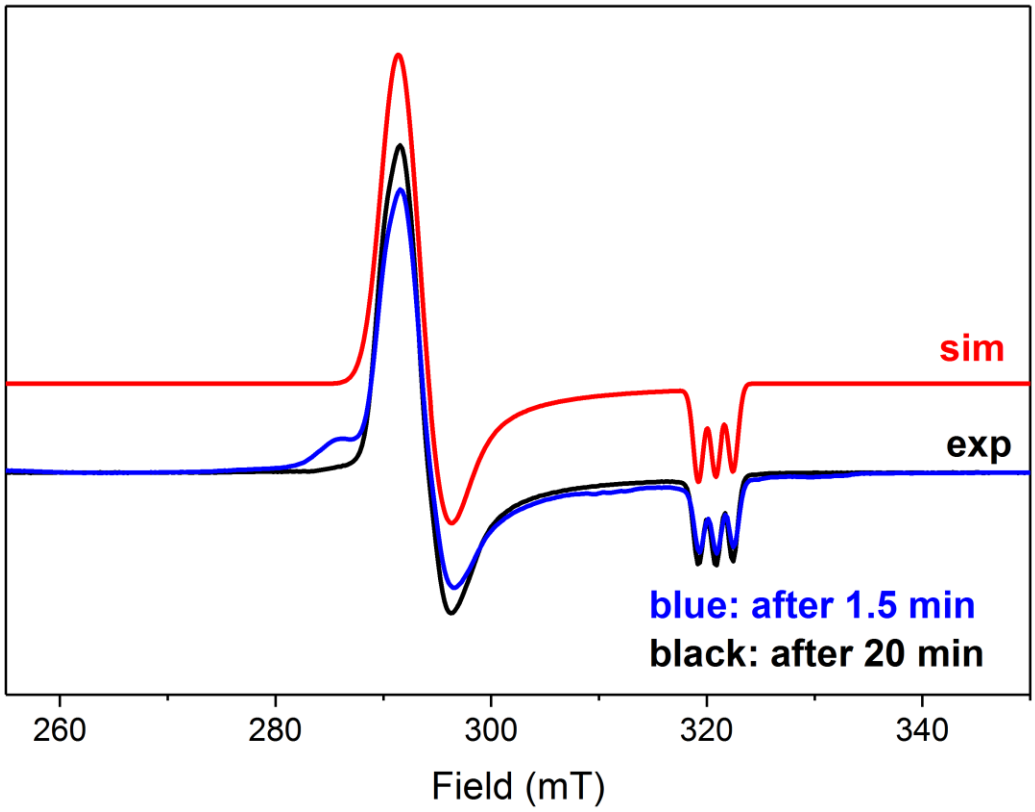

Figure S103. Experimental X-band EPR spectra of the product of oxidation of **3** with O_2 (blue line: after 1.5 min upon exposure to O_2; black line: after 20 min upon exposure to O2; MeTHF glass, 91 K) and simulated EPR spectrum (red line). Simulation parameters: g_x = 2.228, g_y = 2.206, g_z =2.023 (A_N = 16.3 G) (Hstrain = 113.0; 133.6; 30.07).

EPR signal observed during aerobic oxidation of **3** could be simulated both as a rhombic or axial signal, however, RMSD (root-mean-square deviation) compared to experimental EPR spectrum was smaller for rhombic signal simulations giving consistently better fit to experimental data, even when different initial guesses were used; the results reported in the main text correspond to simulation as a rhombic signal and the comparison is shown below.

Table S2. The comparison between rhombic and axial signal simulation for complex 3.

Signal	Optimized parameters used in EasySpin simulation	RSMD
Rhombic	$g_x = 2.228$ $g_y = 2.206$ $g_z = 2.023$ ($A_N = 16.3$ G)	0.00719113
Axial	$g_\perp = 2.218$ $g_\parallel = 2.023$ ($A_N = 16.0$ G)	0.012473

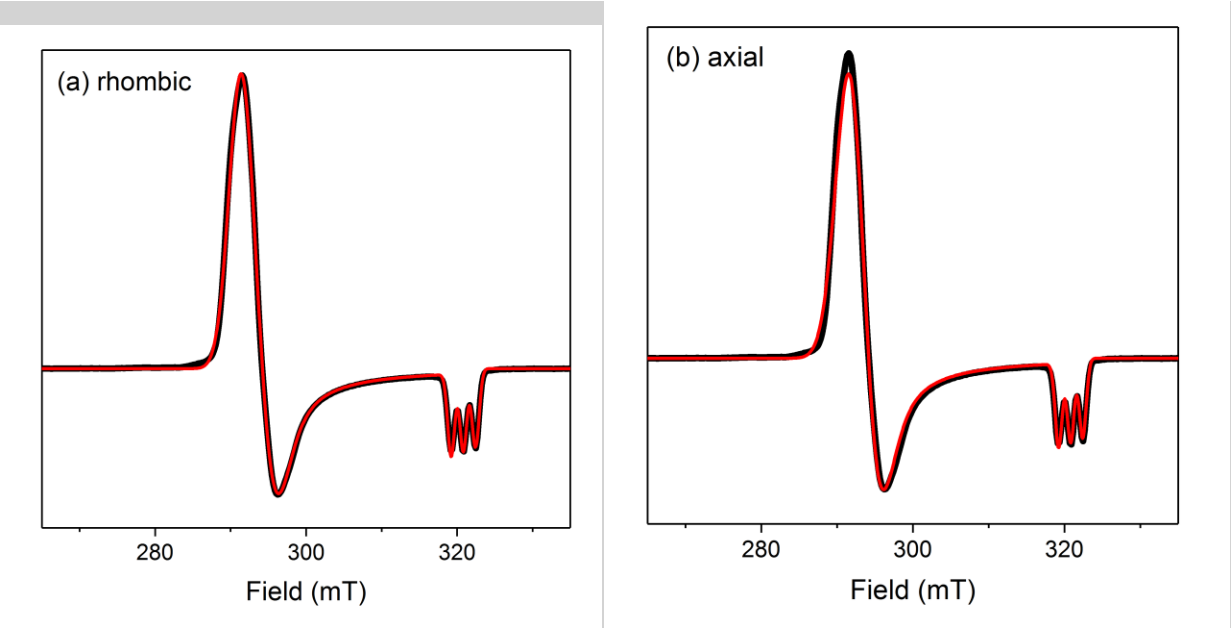

Figure S104. (a) Comparison of the experimental EPR spectra of the product of oxidation of **3** with O_2 (black line; microwave frequency 9.082 GHz, MeTHF glass, 91 K) and a simulated rhombic signal. Simulation parameters: $g_x = 2.2199$, $g_y = 2.1835$, $g_z = 2.0202$ ($A_{N,zz} = 16.8$ G) (Hstrain = 113.0; 133.6; 30.07). (b) Comparison of the experimental EPR spectra of the product of oxidation of **3** with O_2 (black line; microwave frequency 9.082 GHz, MeTHF glass, 91 K) and a simulated axial signal. Simulation parameters: $g_{perp} = 2.218$, $g_{per} = 2.023$ ($A_{N,zz} = 16.0$ G) (Hstrain = 147.3; 29.63).

Detection of Ni^{III} species during oxidation of 4

To a J. Young NMR tube complex **4** (6.2 mg, 0.0086 mmol) was dissolved in 0.5 mL of degassed THF in the glovebox, then the solution was exposed to oxygen gas for three minutes to give purple solution, which was frozen at – 78 °C. Then the reaction mixture was diluted with 2-MeTHF at -78 °C and the spectrum was measured at 94 K.

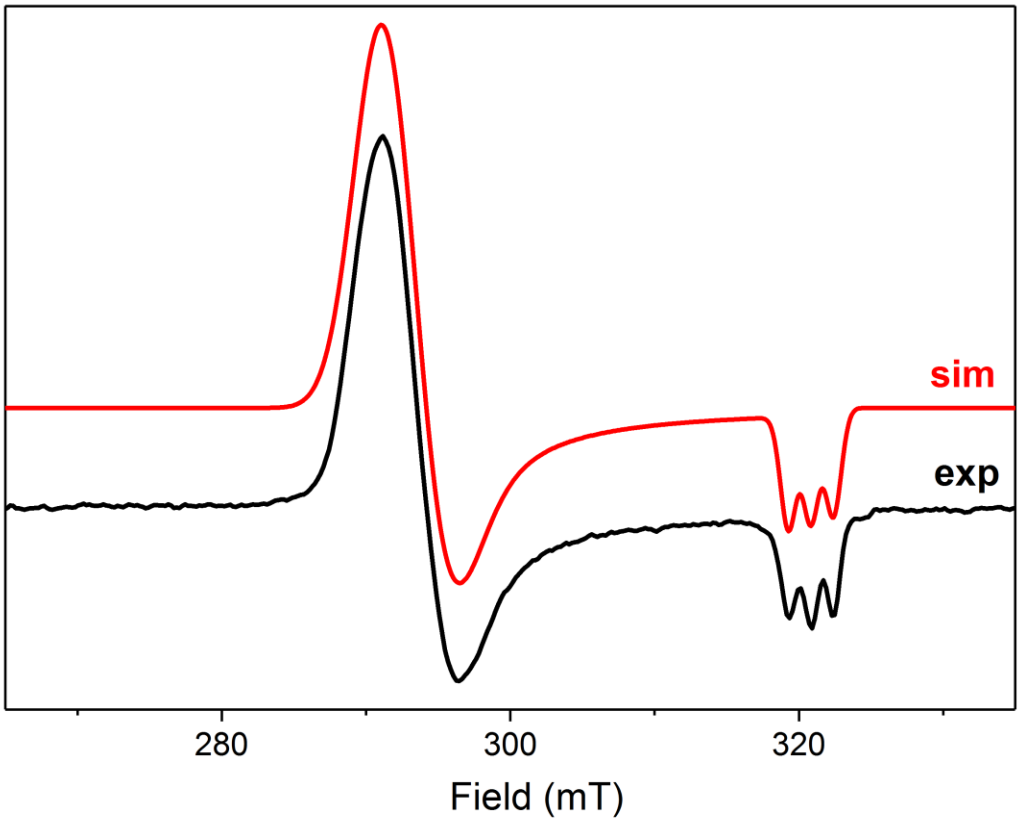

Figure S105. Experimental (black line) EPR spectrum of the product of oxidation of **4** with O_2 (THF/MeTHF glass, 94 K, 9.074 GHz) and simulated EPR spectrum (red line). Simulation parameters: g_x = 2.229, g_y = 2.205, g_z =2.021 (A_N = 15.7 G) (HStrain = 138.5; 146.4; 35.28).

Detection of Ni^{III} species during oxidation of 3 with O_2 at low temperature

To a J. Young NMR tube complex **3** (5.2 mg, 0.0084 mmol) was dissolved in 0.5 mL of degassed CH_2Cl_2 in the glovebox, then the solution was exposed to oxygen gas for three minutes to give purple solution, which was frozen at – 78 °C. Then the reaction mixture was diluted with 2-MeTHF at -78 °C and the spectrum was measured at 91 K.

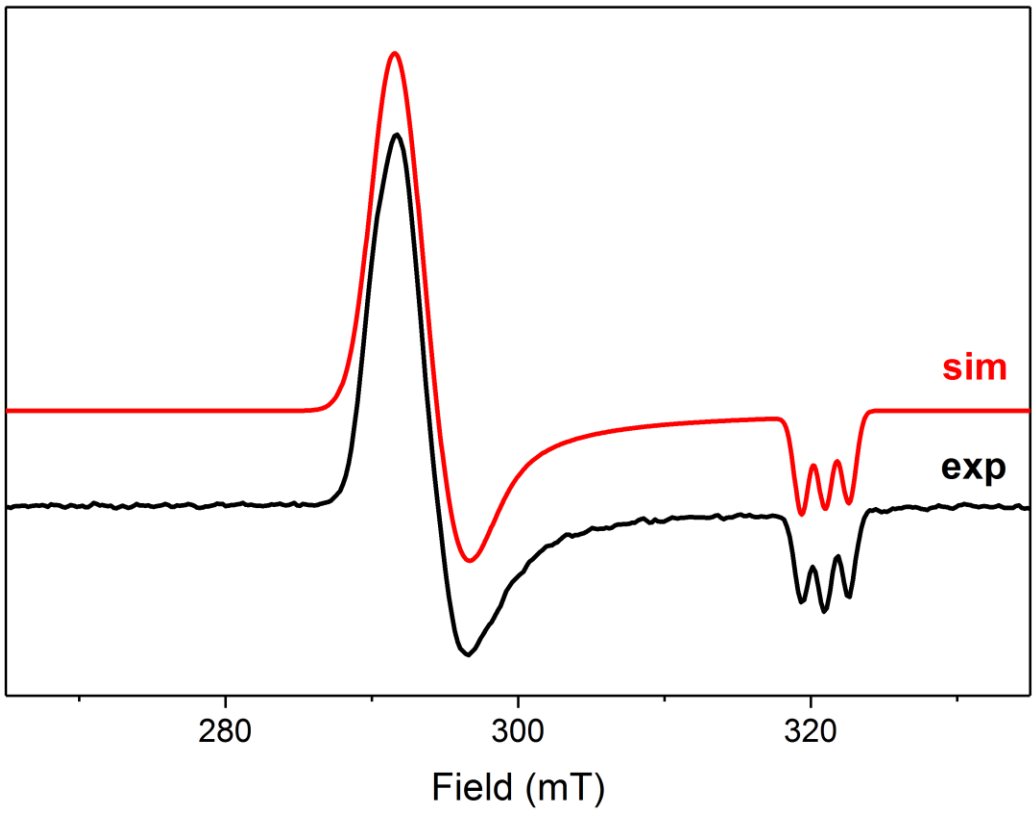

Figure S106. Experimental (black line) EPR spectrum of the product of oxidation of **3** with O_2 (CH_2Cl_2/MeTHF 1/10 glass, 91 K, 9.080 GHz) and simulated EPR spectrum (red line). Simulation parameters: g_x = 2.226, g_y = 2.203, g_z =2.021 (A_N = 16.3 G) (HStrain = 110.6; 133.7; 31.94).

Methyl acrylate polymerization initiated by 3/O_2

In addition to TEMPO trapping experiments, the ability of complex **3** to generate free radicals induced by its aerobic oxidation was tested in the experiment using large excess methyl acrylate as a substrate prone to free radical polymerization. In the presence of **3** mixed with O_2 (1 equiv to **3**) and large excess of methyl acrylate, formation of polymethyl acrylate was observed, which required mild heating. At the same time, complex **3** itself in the absence of O_2 did not initiate any appreciate reactivity as well as O_2 in the absence of **3** under analogous conditions.

a) Reaction in the presence of 3 and O_2:

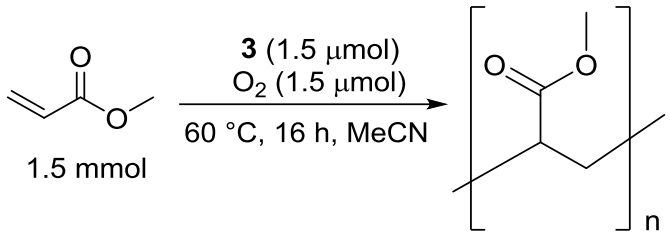

Inside the glovebox, solution of methyl acrylate (136 μL, 1.5 mmol), complex **3** (0.0015 mmol, added from prepared stock solution; methylacrylate : **3** = 1000 : 1 mol:mol) in anhydrous acetonitrile (0.4 mL) was placed to a septum vial. The tube was insulated with Teflon tape and further covered with electric tape and the vial was removed from glovebox. Oxygen gas was injected using gas-tight microsyringe (39 μL, 0.0015 mmol, 1 equiv relative to **3**) and the reaction tube was transferred to an oil bath and heated at 60 °C for 16 hours. The volatiles were removed under vacuum and the residue was vacuum-dried for 48 hours. The obtained amorphous solid material was analyzed by ^{1}H NMR spectroscopy and FT-IR confirming the formation of polymethyl acrylate polymer in 74% yield.

The obtained ^{1}H and 2D NMR spectra match those previously reported for polymethyl acrylate.[18-19]

FT-IR (ATR, solid): 2953 (br. s), 1726 (s), 1435 (s), 1151 (m), 825 (br. s) cm^{-1}.

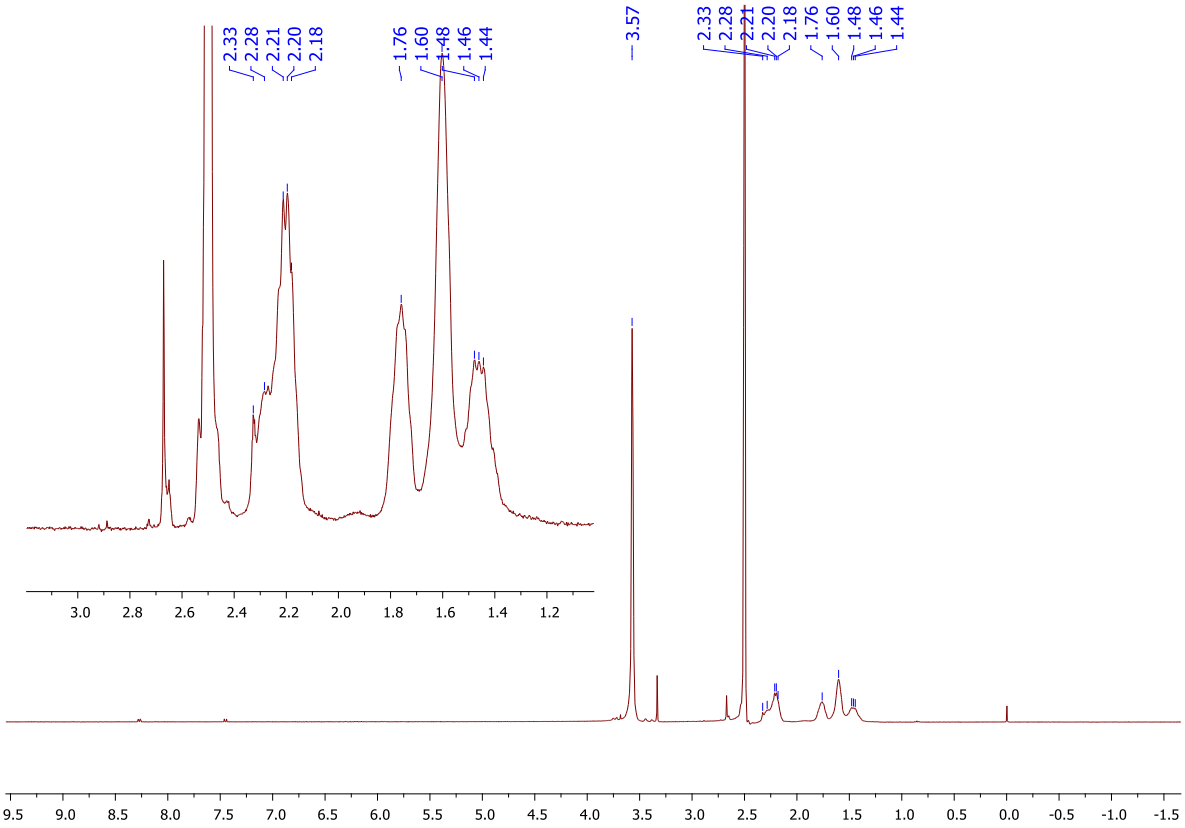

Figure S107. ^{1}H NMR spectrum of poly(methyl acrylate) in DMSO-d_6 obtained by the reaction in the presence of **3**/O_2.

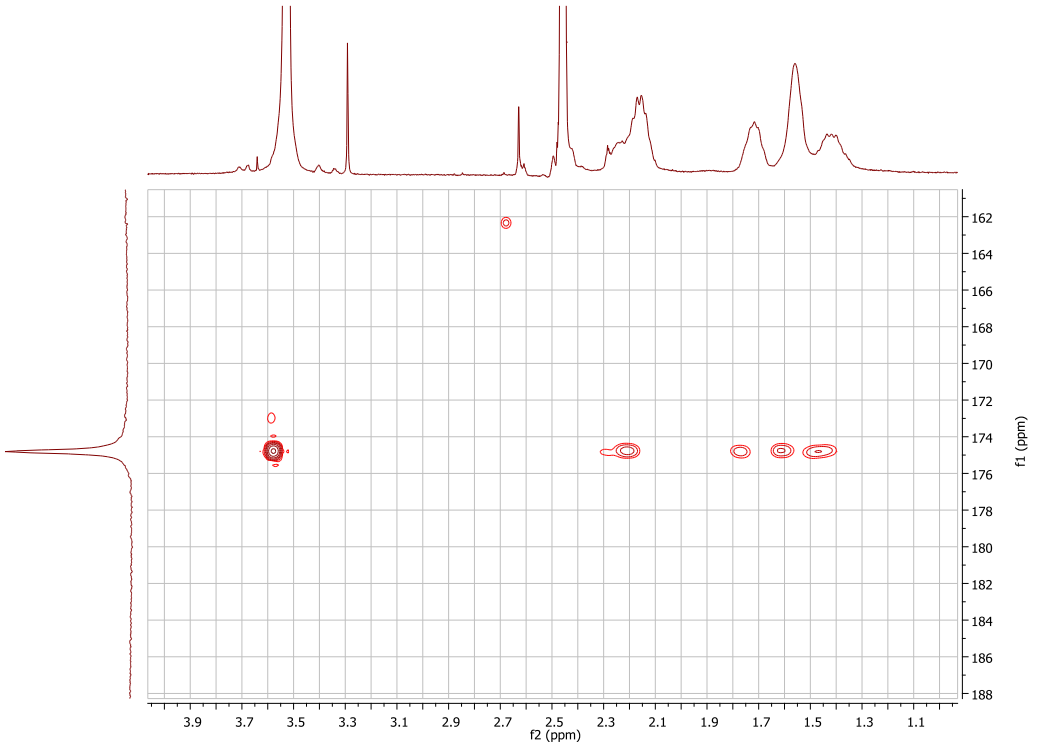

Figure S108. 2D ^{1}H-^{13}C HMBC NMR spectrum of poly(methyl acrylate) in DMSO-d_6 obtained by the reaction in the presence of **3**/O_2.

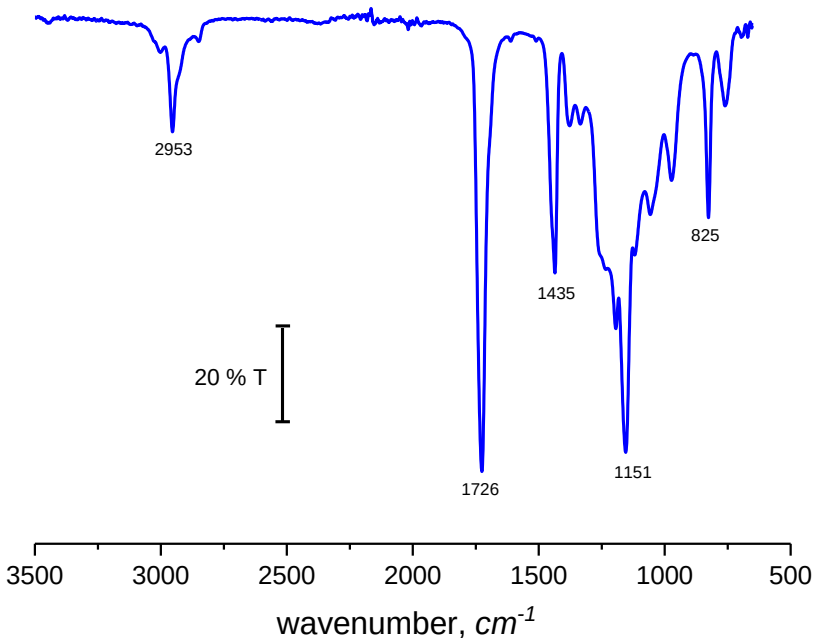

Figure S109. FT-IR spectrum of poly(methyl acrylate) in DMSO-d_6 obtained by the reaction in the presence of **3**/O_2.

b) Attempted polymerization of methyl acrylate in the absence of 3

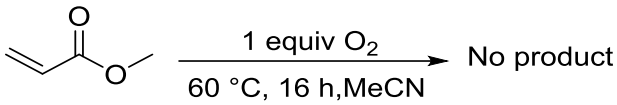

Inside the glovebox, a solution of methyl acrylate (136 μL, 1.5 mmol) in anhydrous acetonitrile (0.4 mL) was placed to a septum vial. The tube was insulated with Teflon tape and further covered with electric tape and the vial was removed from glovebox. Oxygen gas was injected using gas-tight microsyringe (39 μL, 0.0015 mmol) and the reaction tube was transferred to an oil bath and heated at 60 °C for 16 hours. The volatiles were removed under vacuum and the residue was vacuum-dried for 24 hours; no solid residues were obtained. The reaction mixture was analyzed by ^{1}H NMR spectroscopy confirms no formation of polymethyl acrylate.

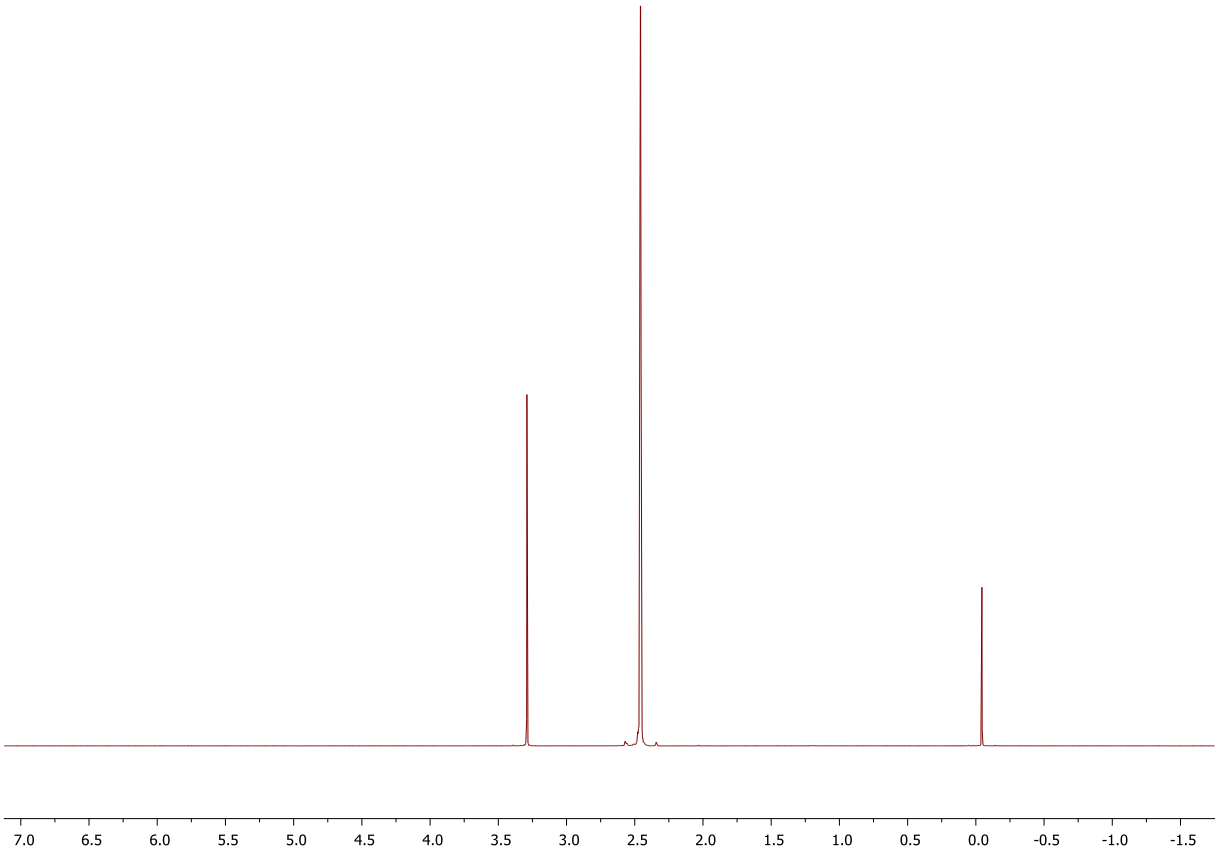

Figure S110. ^{1}H NMR spectrum of the reaction mixture containing methyl acrylate after heating at 60 °C under O_2 for 16 hours in DMSO-d_6 after evaporation of volatiles. Only solvent peaks were observed.

c) Attempted polymerization of methyl acrylate in the presence of 3 with exclusion of O_2

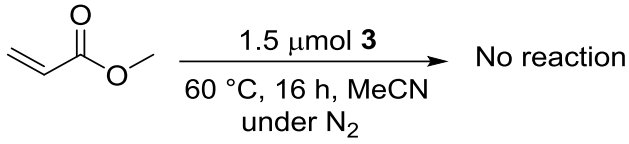

Inside the glovebox, solution of methyl acrylate (136 μL, 1.5 mmol), complex **3** (0.0015 mmol, added from prepared stock solution) in anhydrous acetonitrile (0.4 mL) was placed to a 50 mL schlenk flask. Next, the schlenk flask was removed from glovebox and transferred to an oil bath and heated at 60 °C for 16 hours. The volatiles were removed under vacuum and no solid residue was obtained.

d) Polymerization of methyl acrylate in the presence of thermally activated AIBN as a radical initiator

Inside the glovebox, the solution of methyl acrylate (136 μL, 1.5 mmol), AIBN (0.0015 mmol, added from prepared stock solution) in anhydrous acetonitrile (0.4 mL) was placed to a 50 mL Schlenk flask. The Schlenk flask was heated in an oil bath at 60 °C for 16 hours. The volatiles were removed under vacuum and a solid residue was obtained in 84 % yield.

GPC analysis of poly(methyl acrylate) samples obtained by the reaction in the presence of 3 and O2 (entry (a) above) and in the presence of AIBN (entry (d) above).

Conditions:	M_w	M_n	PDI
(a) Methyl acrylate (1.5 mmol), **3** (0.0015 mmol), O_2 (0.0015 mmol), 60 °C, MeCN, 16 h	120,000	47,000	2.5
(d) Methyl acrylate (1.5 mmol), AIBN (0.0015 mmol), 60 °C, MeCN, 16 h	120,000	53,000	2.2

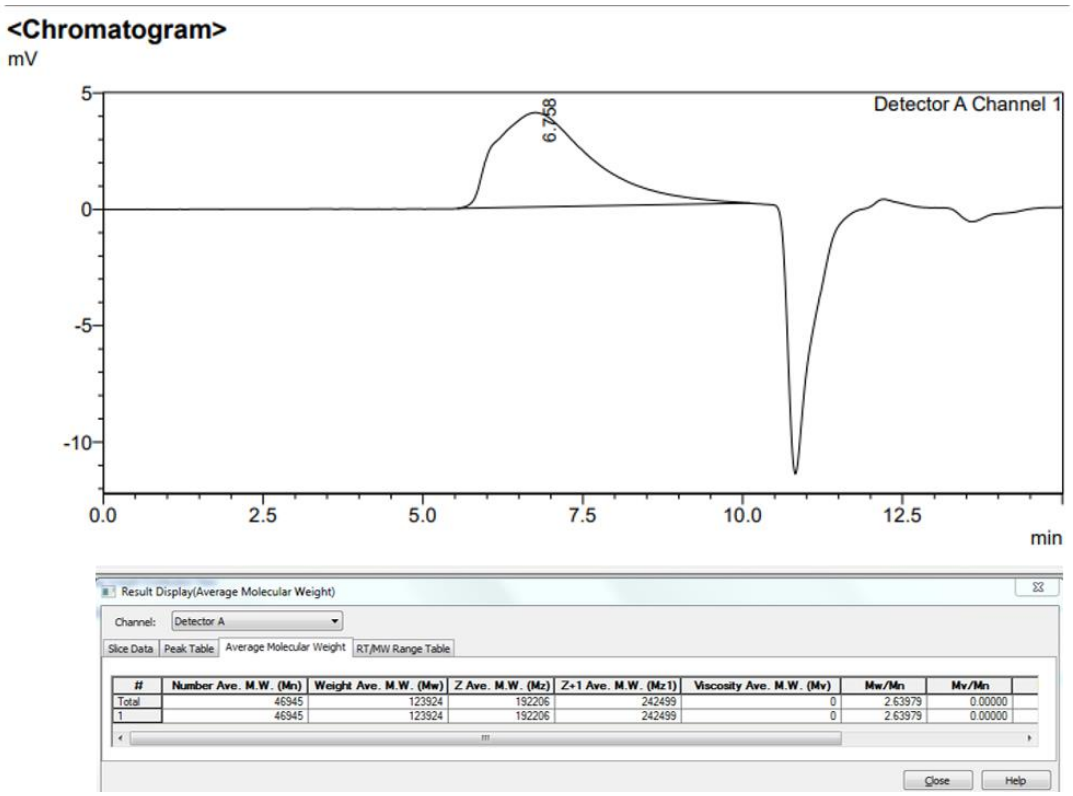

Figure S111. GPC trace of poly(methyl acrylate) sample obtained in the presence of **3** and O_2 (entry (a) above).

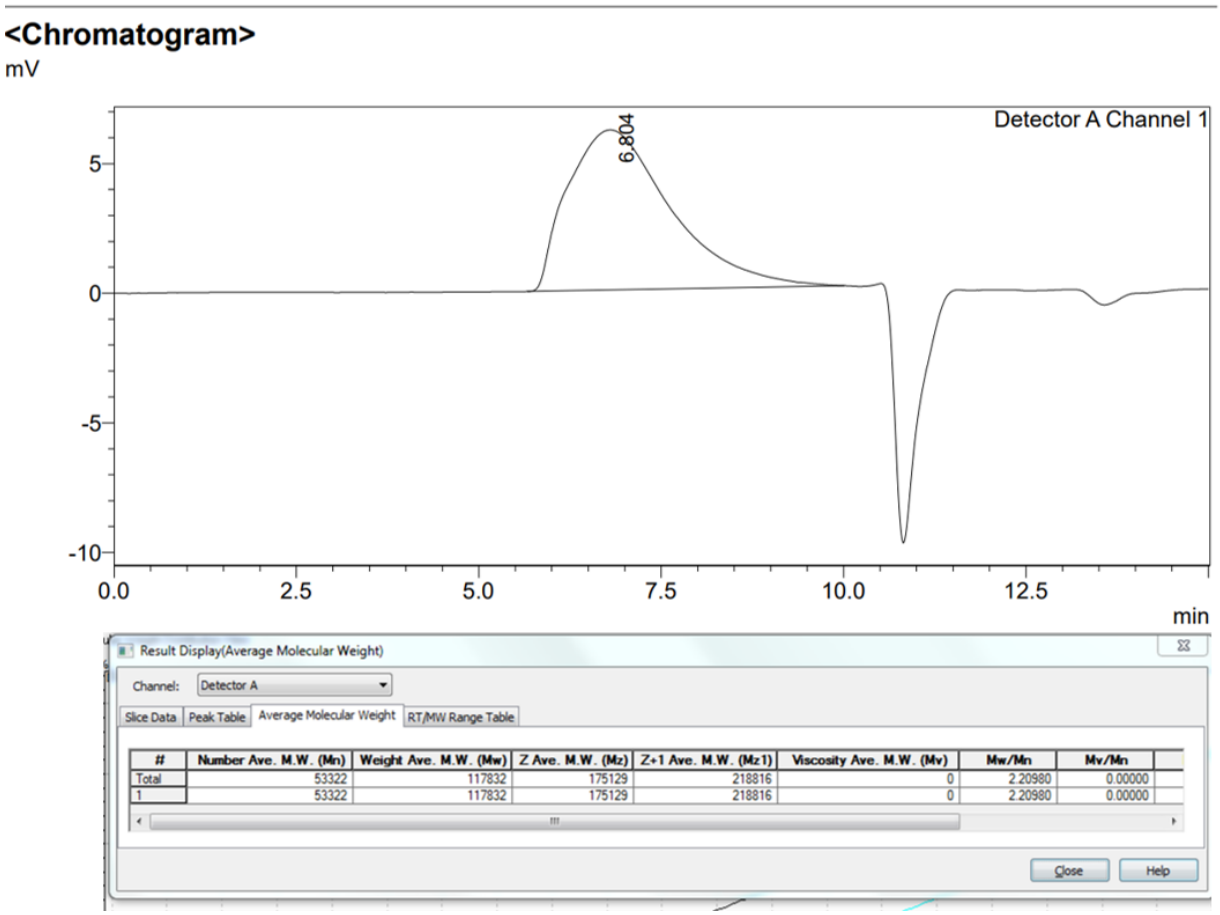

Figure S112. GPC trace of poly(methyl acrylate) sample obtained in the presence of AIBN (entry (d) above).

Decomposition of cumene hydroperoxide catalyzed by 3

Considering that Path (ii) in Scheme 5 involves proposed Ni-catalyzed decomposition of pefluoroalkylhydroperoxide, we have tested the ability of **3** to catalyze decomposition of cumene hydroperoxide as a model substrate using 20 mol% of complex **3**. Decomposition into a mixture of 2-phenyl-2-propanol and acetophenone is observed catalytic on Ni.

Previous studies indicate that 2-phenyl-2-propanol is indicative of a heterolytic O-O cleavage pathway, while acetophenone indicates contribution of homolytic O-O cleavage pathway via formation of cumyloxy radical, which then undergoes defragmentation to form acetophenone via methyl radical loss. Based on observation of a mixture of two products, both pathways are likely to contribute in case of complex **3**.[20-23]

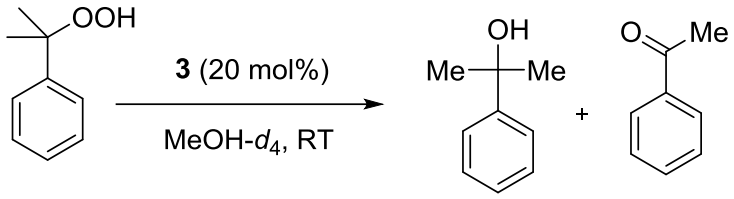

Inside the glovebox, solution of complex **3** (4.2 mg, 0.0068 mmol), cumene hydroperoxide (80 wt%, technical grade) (6.3 μL, 0.034 mmol, 5 equiv) and mesitylene (4.7 μL, 0.034 mmol) in MeOH-d_4 (0.5 mL) was placed to a J. Young NMR tube. The NMR tube was removed from glovebox and the NMR tube was then placed in an NMR tube spinner and rotated to ensure good mixing. The reaction was monitored periodically by ^{1}H NMR spectroscopy (see below) for 20 hours, confirming the formation of 2-phenyl-2-propanol and acetophenone.

The commercially available sample of cumene hydroperoxide contained trace amount of acetophenone (< 2%) and 2-phenyl-2-propanol (9-10%).

Reaction time	Yield of acetophenone, %	Yield of 2-phenyl-2-propanol
5 min	21 %	41%
3 hours	24 %	57%
20 hours	35 %	59%

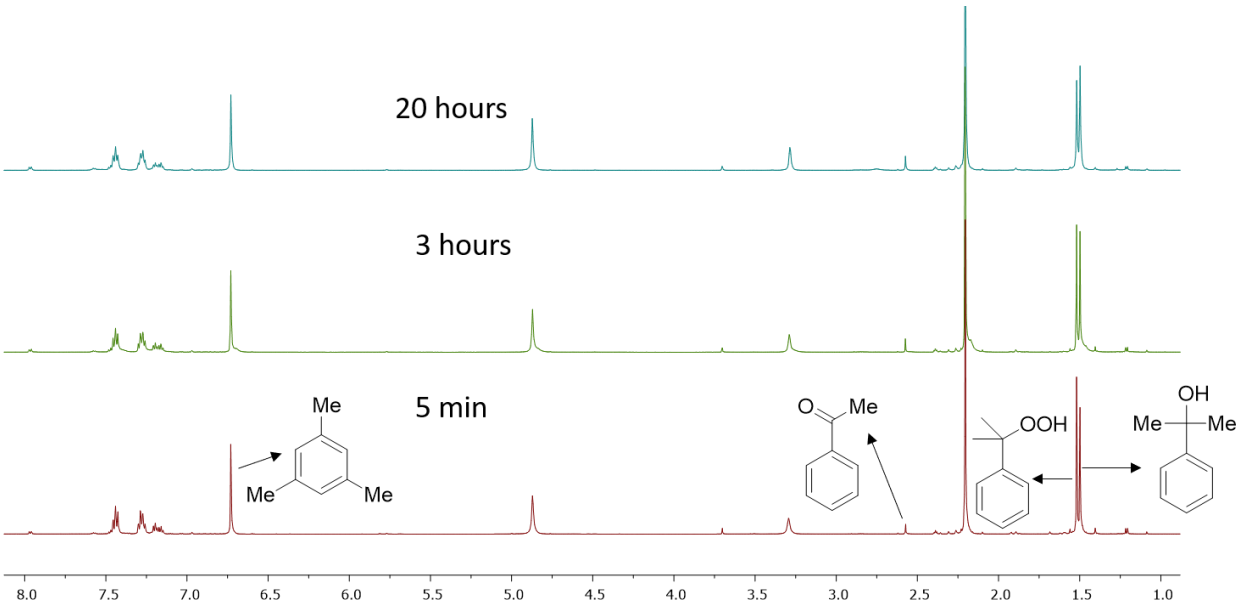

Figure S113. ^{1}H NMR spectrum of decomposition of cumene hydroperoxide in the presence of **3** (20 mol%) at RT in MeOH-d_4.

Explanation for the formation of doubly labeled trifluoroacetate

The formation of a doubly labeled TFA under $^{18}O_2$ in an anhydrous solvent implies that labeled water could result from Ni-mediated reduction of O_2 or from O_2-derived H_2O_2. Such reactivity is known for Pt methyl complexes and was proposed for O_2-activation by Fe complexes to form hydrogen peroxide, while sequential O_2 reduction of O_2 to peroxide and then hydroxide has also been reported for tetramethylcyclam Ni^I complex. If H_2O_2 is indeed formed, Ni salts are also known to exhibit catalase-like reactivity promoting H_2O_2 disproportionation to water and oxygen.[24-25] To detect H_2O_2, we then performed the reaction in the presence of 1,3-diphenylisobenzofuran (DPBF), which is known to react specifically with H_2O_2 to form 9-hydroxyanthracen-10(9H)-one, while the reaction with other reactive oxygen species (ROS) such as superoxide, alkylperoxy or alkoxy radicals results in the formation of 1,2-dibenzoylbenzene.[26-27] The aerobic oxidation of **3** in the presence of DPBF resulted in the formation of a mixture of 9-hydroxyanthracen-10(9H)-one and 1,2-dibenzoylbenzene, consistent with the presence of H_2O_2 along with other ROS. The formation of trifluoroacetate in 46% yield was also observed when **3** was oxidized with 1.1 equiv of H_2O_2 under inert atmosphere. See the experimental details below.

Detection of hydrogen peroxide and other reactive oxygen species using DPBF

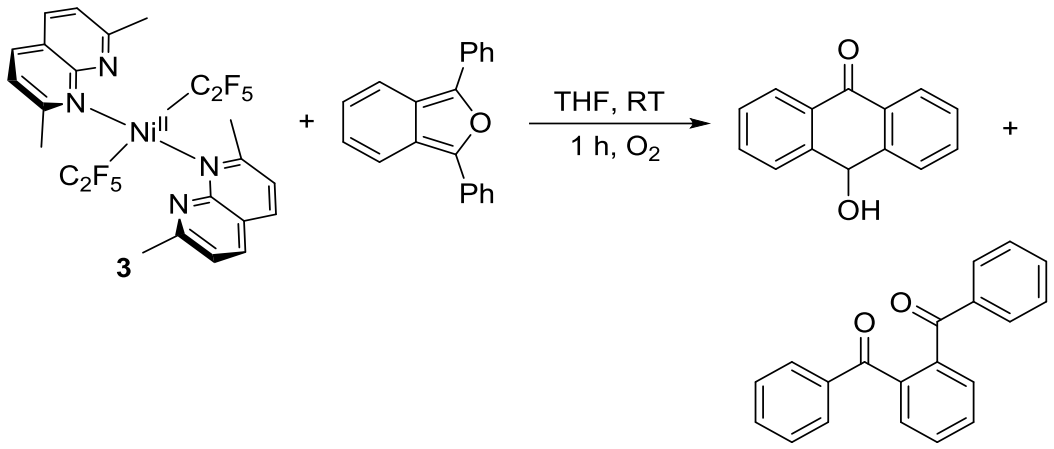

Inside the glovebox, solution of complex **3** (8.3 mg, 0.0135 mmol), 1,3-Diphenylisobenzofuran (3.6 mg, 0.0135 mmol) in dry THF (0.5 mL) was placed to a J. Young NMR tube. The NMR tube was removed from glovebox and the reaction mixture was exposed to oxygen gas for three minutes, then sealed with a Teflon cap and stirred at room temperature for 1 hour. After completion of the reaction, the reaction mixture was analyzed GC-MS analysis, confirming the formation of 1,2-dibenzoylbenzene and 9-hydroxyanthracene-10(9H)-one along with 1,2-dibenzoylbenzene.

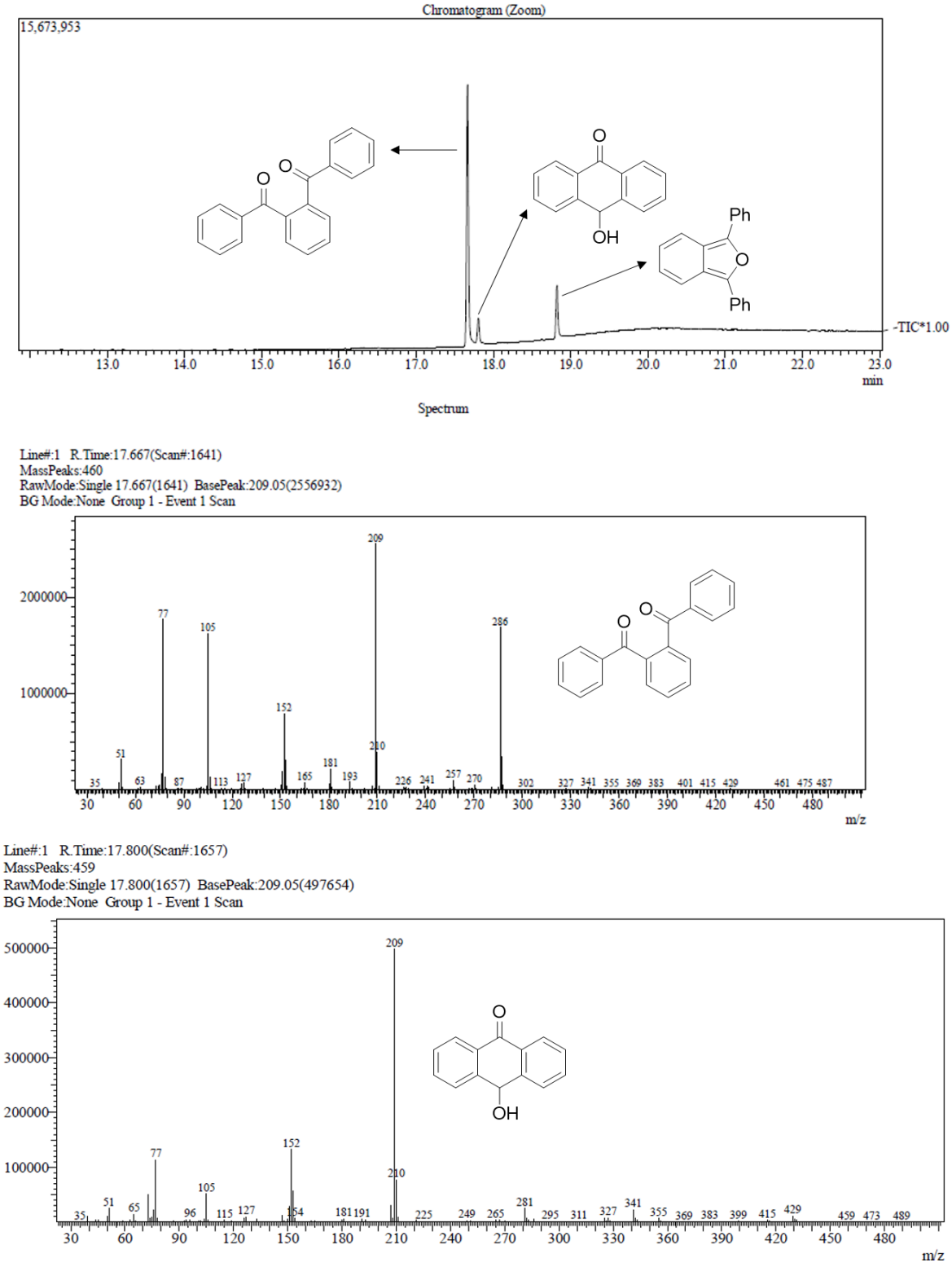

Figure S114. GC-MS spectrum of ethyl acetate solution of the reaction mixture of 1,3-diphenylisobenzofuran with O_2 in the presence of **3**.

Oxidation of 3 with H_2O_2

Inside the glovebox, a solution of complex **3** (20.1 mg, 0.0327 mmol), hydrogen peroxide (30%) (2.6 μL, 0.0365 mmol) and α,α,α-trifluorotoluene (8 μL, 0.0655 mmol) in MeOH-d_4 (0.5 mL) was placed to a J. Young NMR tube. The NMR tube was removed from glovebox and the NMR tube was then placed in an NMR tube spinner and rotated at RT for 24 hours to ensure good mixing. The reaction mixture was then analyzed by ^{19}F NMR spectroscopy, showing the peaks of trifluoroacetate acid (46% yield) and 1,1,1,2,2-pentafluoroethane (7% yield). The same reaction mixture was analyzed by HRMS (see below) to give results similar to aerobic oxidation reaction mixtures.

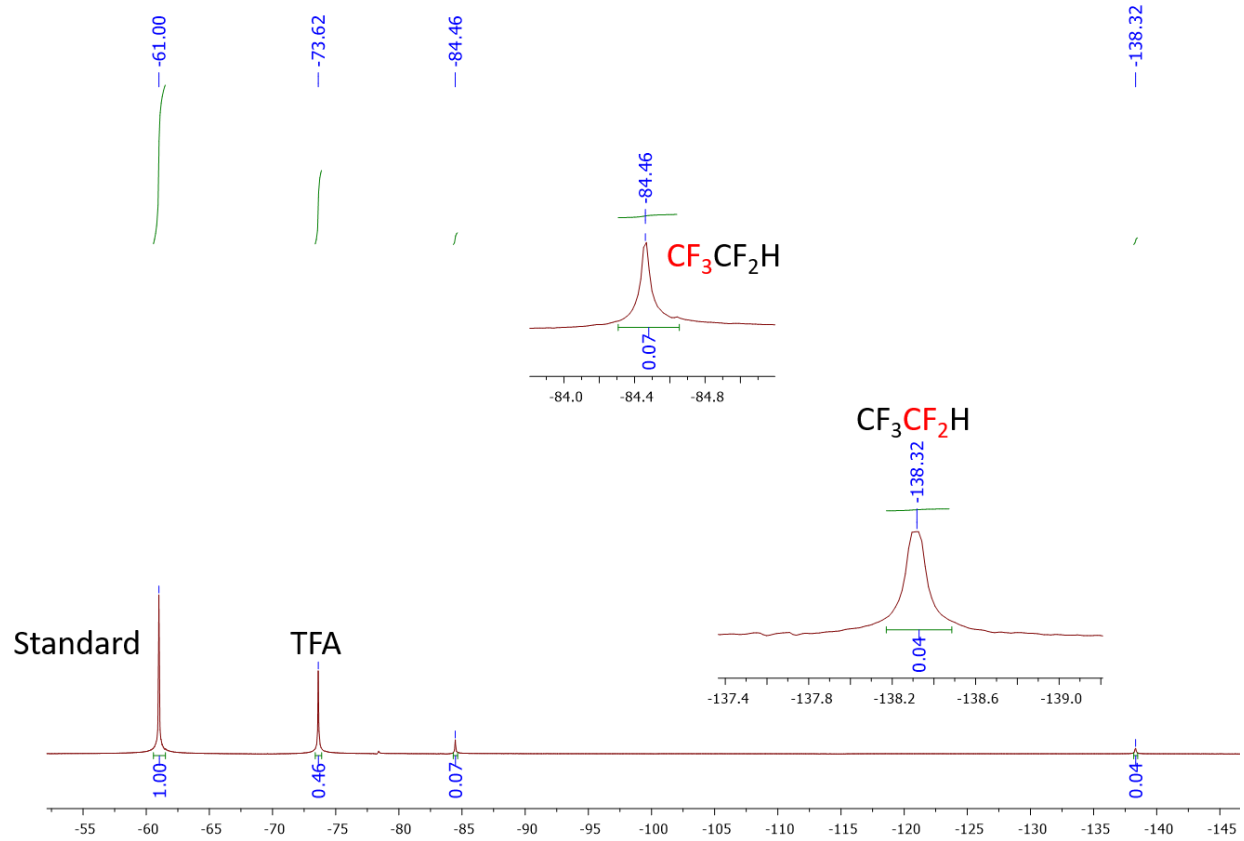

Figure S115. ^{19}F NMR spectrum of the reaction mixture containing hydrogen peroxide and **3** after stirring under oxygen gas at RT for 24 hours.

HRMS (ESI) calculated for $[(\mathbf{L3})Ni(CF_3COO)]^+$ $C_{12}H_{10}F_3N_2O_2Ni$: 329.0042; found, 329.0046.

HRMS (ESI) calculated for $[(\mathbf{L3})_2Ni(CF_3COO)]^+$ $C_{22}H_{20}F_3N_4O_2Ni$: 487.0886; found, 487.0886.

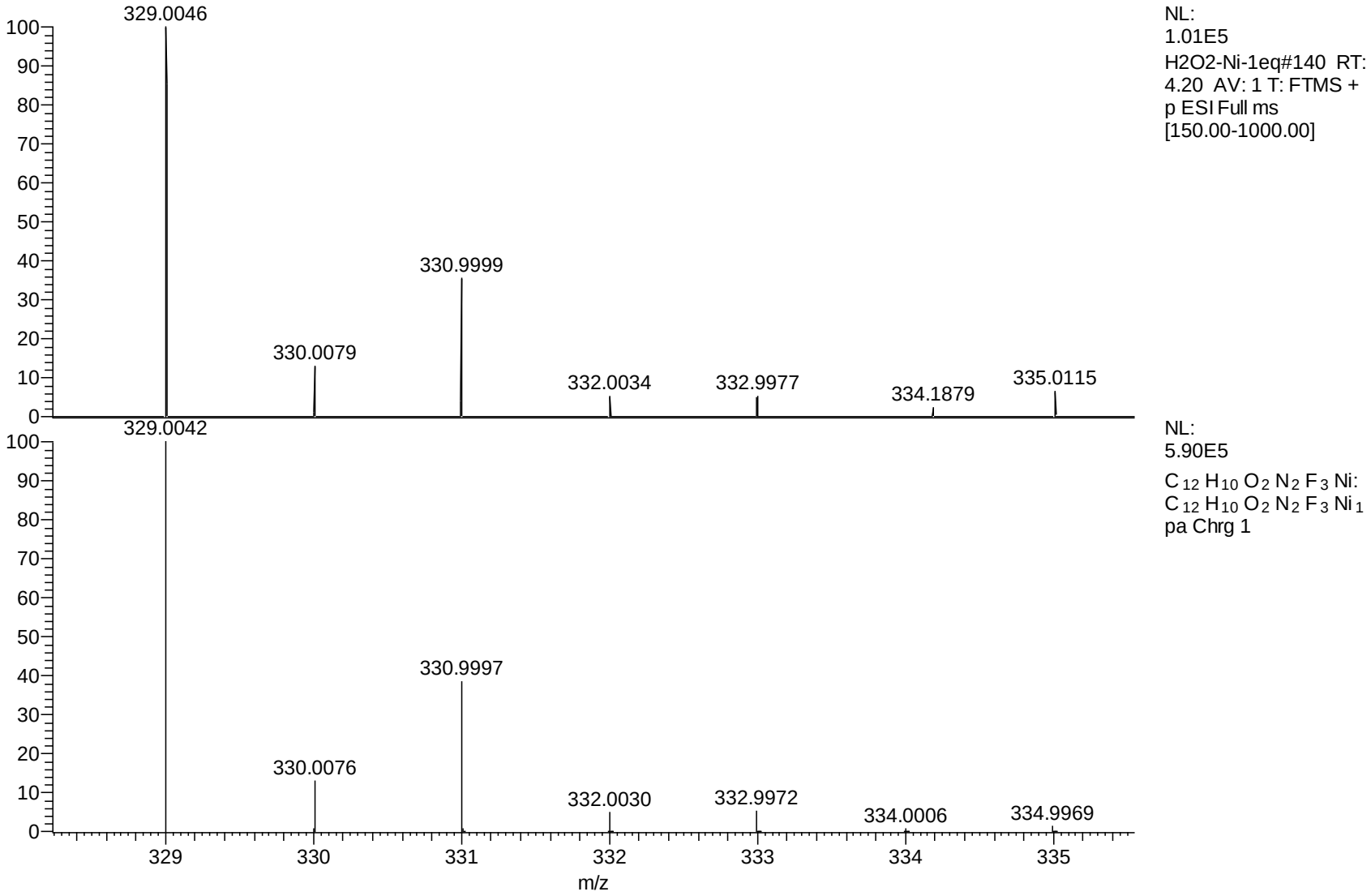

Figure S116. ESI-(HR)MS spectrum of MeOH solution of **3** after oxidation with H_2O_2 (top) and simulated spectrum of [(**L3**)Ni(CF_3COO)]$^+$, $C_{12}H_{10}O_2N_2F_3Ni$: (bottom).

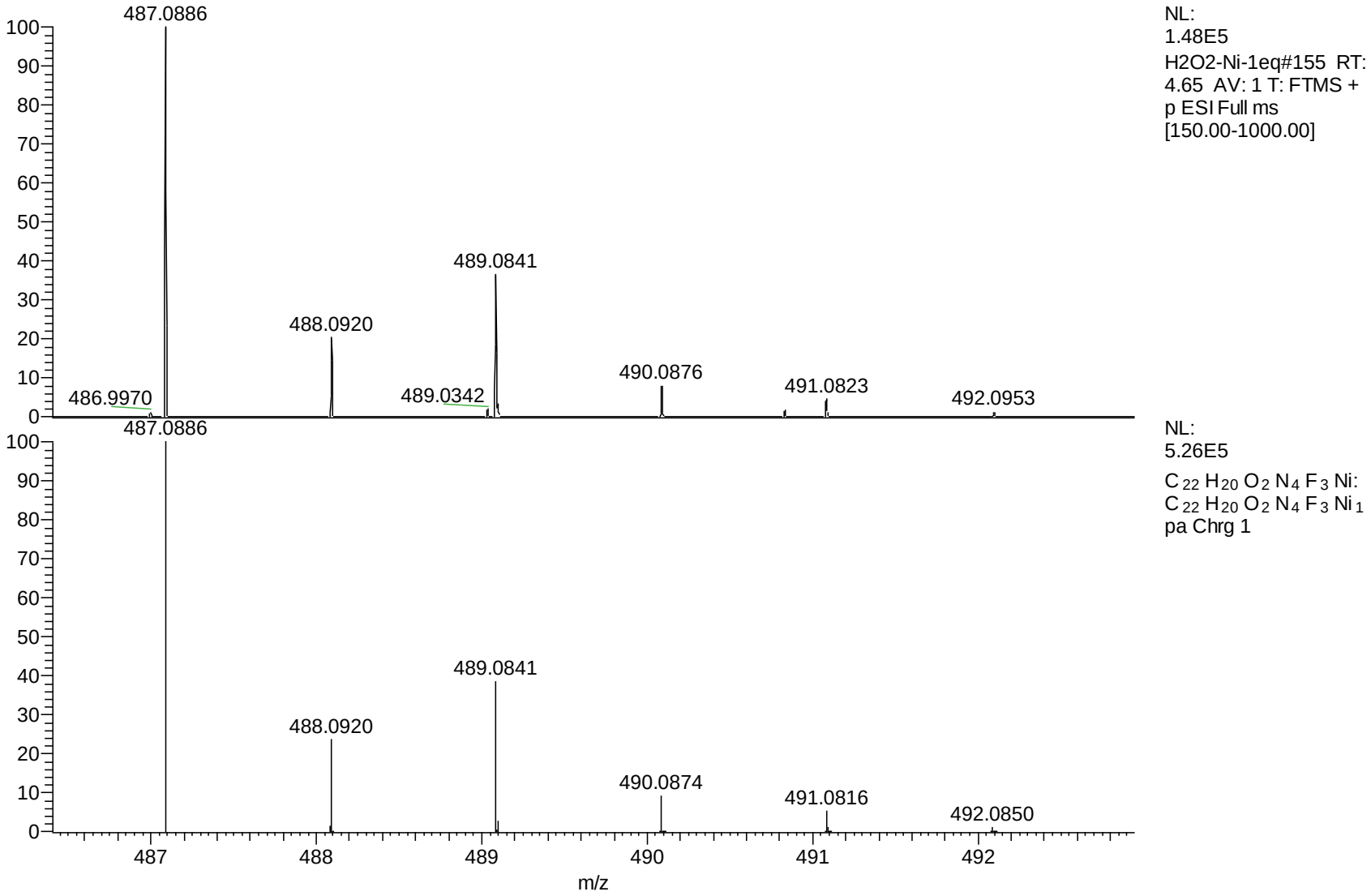

Figure S117. ESI-(HR)MS spectrum of MeOH solution of **3** after oxidation with H_2O_2 (top) (top) and simulated spectrum of $[(\mathbf{L3})_2Ni(CF_3COO)]^+$, $C_{22}H_{20}O_2N_4F_3Ni$: (bottom).

Attempted oxidation of *trans*-stilbene with peroxide oxidants

Considering possible in-situ formation of H_2O_2, we performed oxidation of *trans*-stilbene as a model substrate using a combination of peroxide-based oxidants and complex **3** as well as in the presence of a combination of O_2/conventional free radical initiator.

The attempted oxidation of *trans*-stilbene using H_2O_2 results in much less efficient oxidation as compared to the reaction under O_2, showing that Ni-mediate in-situ generation of H_2O_2 is unlikely to be responsible for the observed reactivity. Similarly, attempted oxidation by tert-butylhydroperoxide and cumene hydroperoxide gave low yields of the products. At the same time, free radical oxidation of stilbene in the presence of AIBN and O_2 (see below) results in the formation of a mixture of epoxide(s) and aldehyde, similar to the reactivity observed in the presence of **3**/O_2, although the ratio of products was different from the ratio obtained using complex **3**.

a) Attempted oxidation of *trans*-stilbene using H_2O_2 and 3

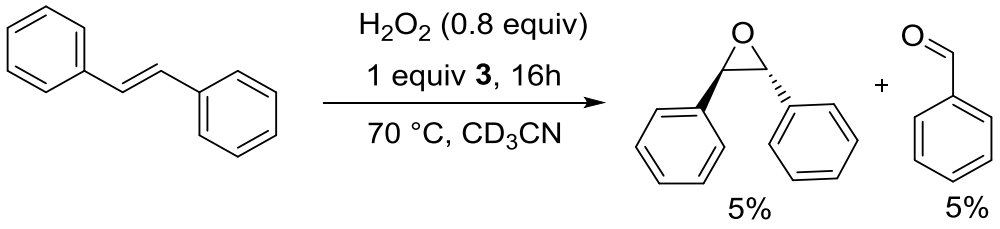

Inside the glovebox, a solution of **3** (20.6 mg, 0.0335 mmol), *trans*-stilbene (6 mg, 0.0335 mmol), hydrogen peroxide (30% wt in H_2O) (2.6 μL,0.0.025 mmol, 0.8 equiv) and mesitylene (4.6 μL, 0.0335 mmol) in anhydrous CD_3CN (0.5 mL) was placed to a J. Young NMR tube. The NMR tube was transferred to an oil bath and heated at 70 °C for 16 hours. The reaction mixture was analyzed by ^1H NMR spectroscopy, showing the formation of trans-stilbene oxide (5%), benzaldehyde (5 %) along with unreacted *trans*-stilbene.

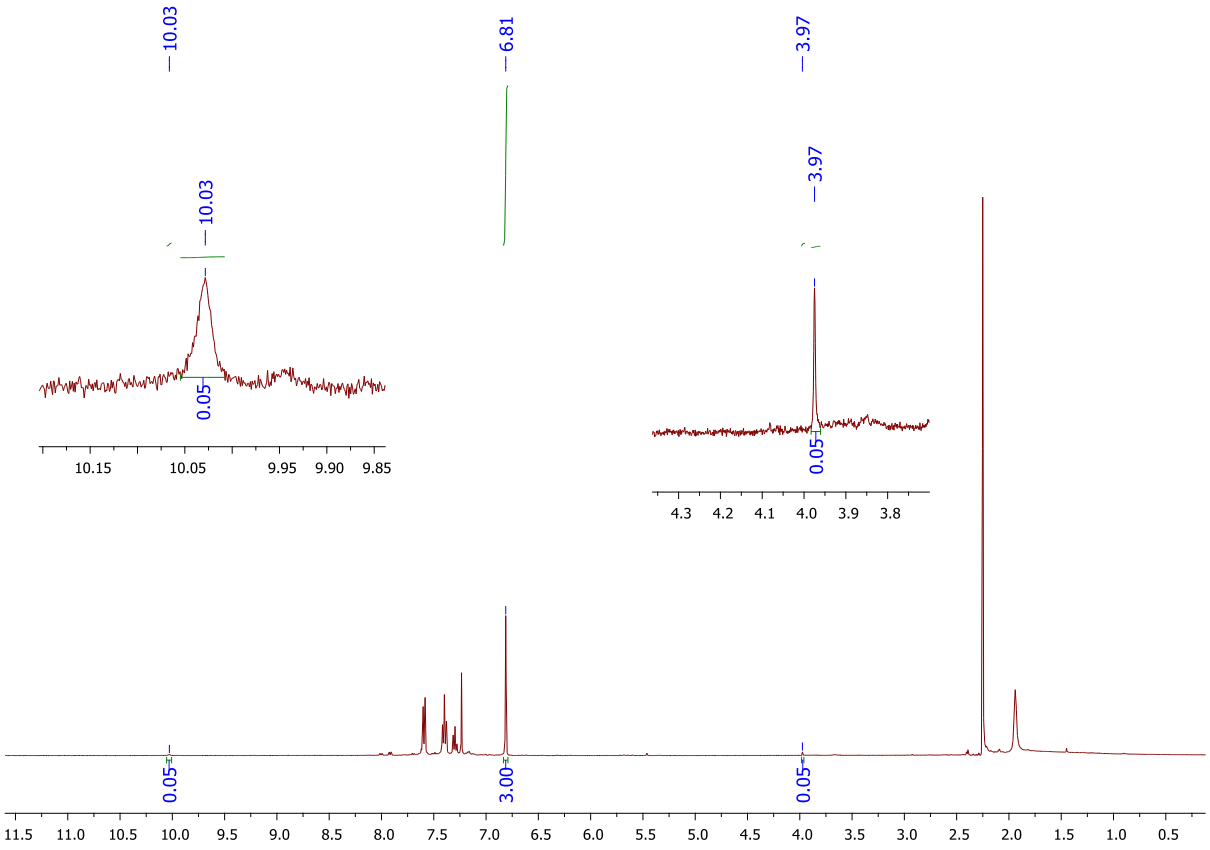

Figure S118. ^{1}H NMR spectrum of the reaction mixture after attempted oxidation of *trans*-stilbene with H_2O_2 and **3** after heating at 70 °C for 16 hours in CD_3CN.

b) Attemtted oxidation of *trans*-stilbene by using ^{t}BuOOH and 3

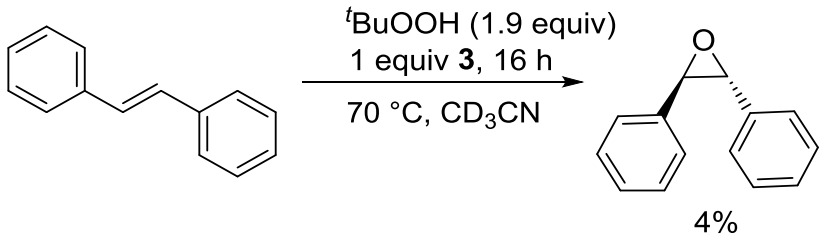

Inside the glovebox, a solution of **3** (33.2 mg, 0.0541 mmol), *trans*-stilbene (9.7 mg, 0.0541 mmol), *tert*-butyl hydroperoxide (70% in water) (14.6 µL, 0.106 mmol) and mesitylene (7.5 µL, 0.0541 mmol) in anhydrous CD_3CN (0.5 mL) was placed to a J. Young NMR tube. The NMR tube was transferred to an oil bath and heated at 70 °C for 16 hours. The reaction mixture was analyzed by ^{1}H NMR spectroscopy, showing the formation of *trans*-stilbene oxide (4%) as product along with unreacted *trans*-stilbene (95%)

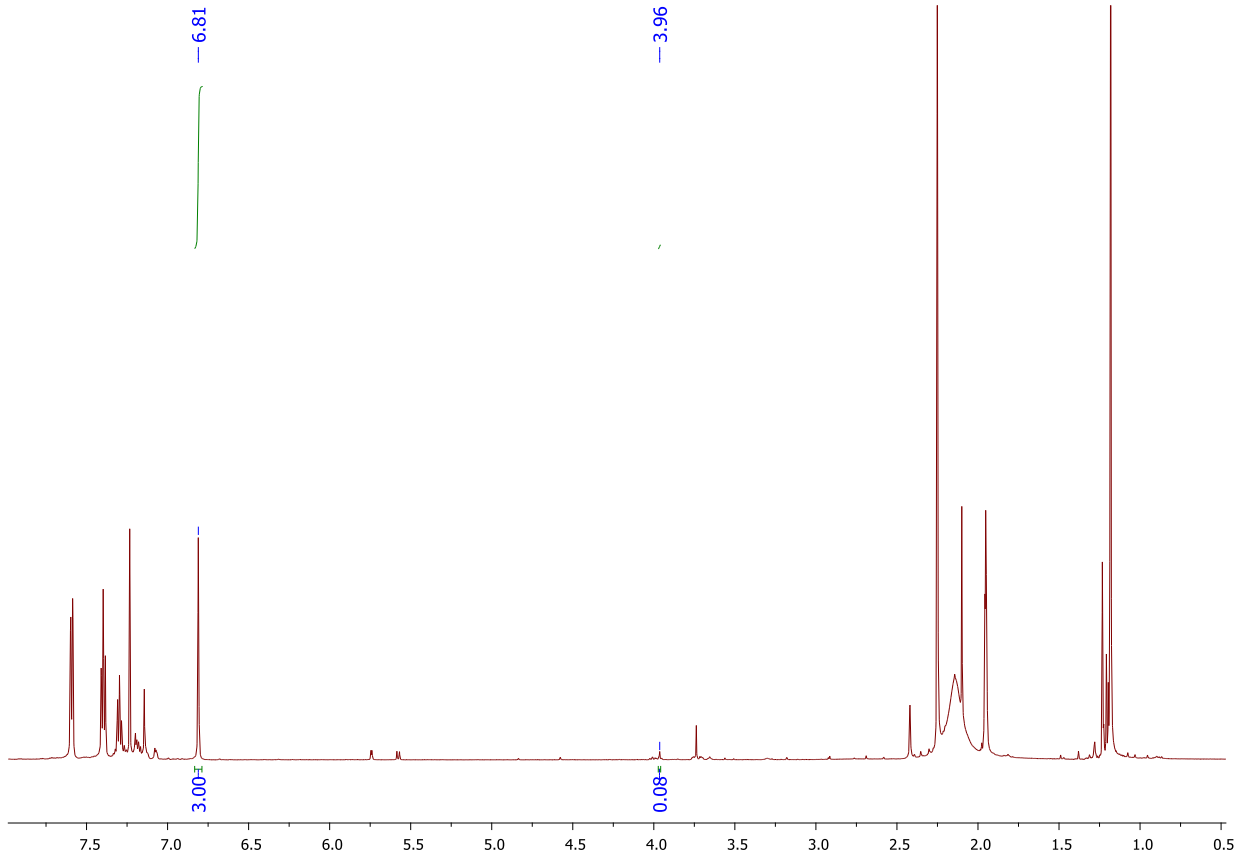

Figure S119. ^{1}H NMR spectrum of the reaction mixture after attempted oxidation of *trans*-stilbene with ^{t}BuOOH and **3** after heating at 70 °C for 16 hours in CD_3CN.

c) Attempted oxidation of *trans*-stilbene by cumene hydrogen peroxide and 3

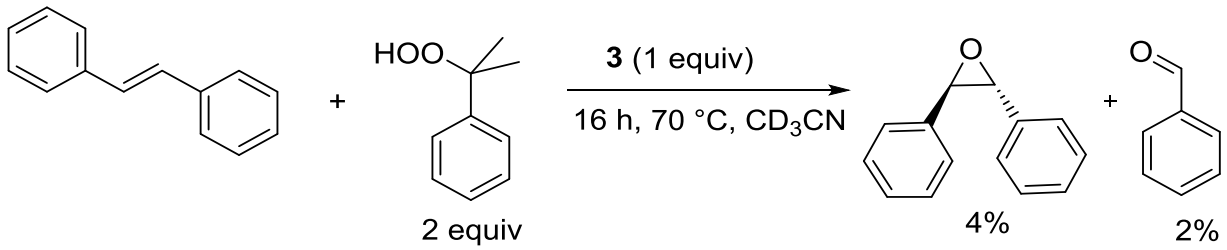

Inside the glovebox, a solution of **3** (36.2 mg, 0.0590 mmol), *trans*-stilbene (10.6 mg, 0.0590 mmol), cumene hydroperoxide (80 wt %) (22 µL, 0.118 mmol, 2 equiv) and mesitylene (8.2 µL, 0.0590 mmol) in anhydrous CD_3CN (0.5 mL) was placed to a J. Young NMR tube. The NMR tube was transferred to an oil bath and heated at 70 °C for 16 hours. The reaction mixture was analyzed by ^{1}H NMR spectroscopy, showing the formation of trans-stilbene oxide (4%) and benzaldehyde (2%) along with unreacted 90% *trans*-stilbene.

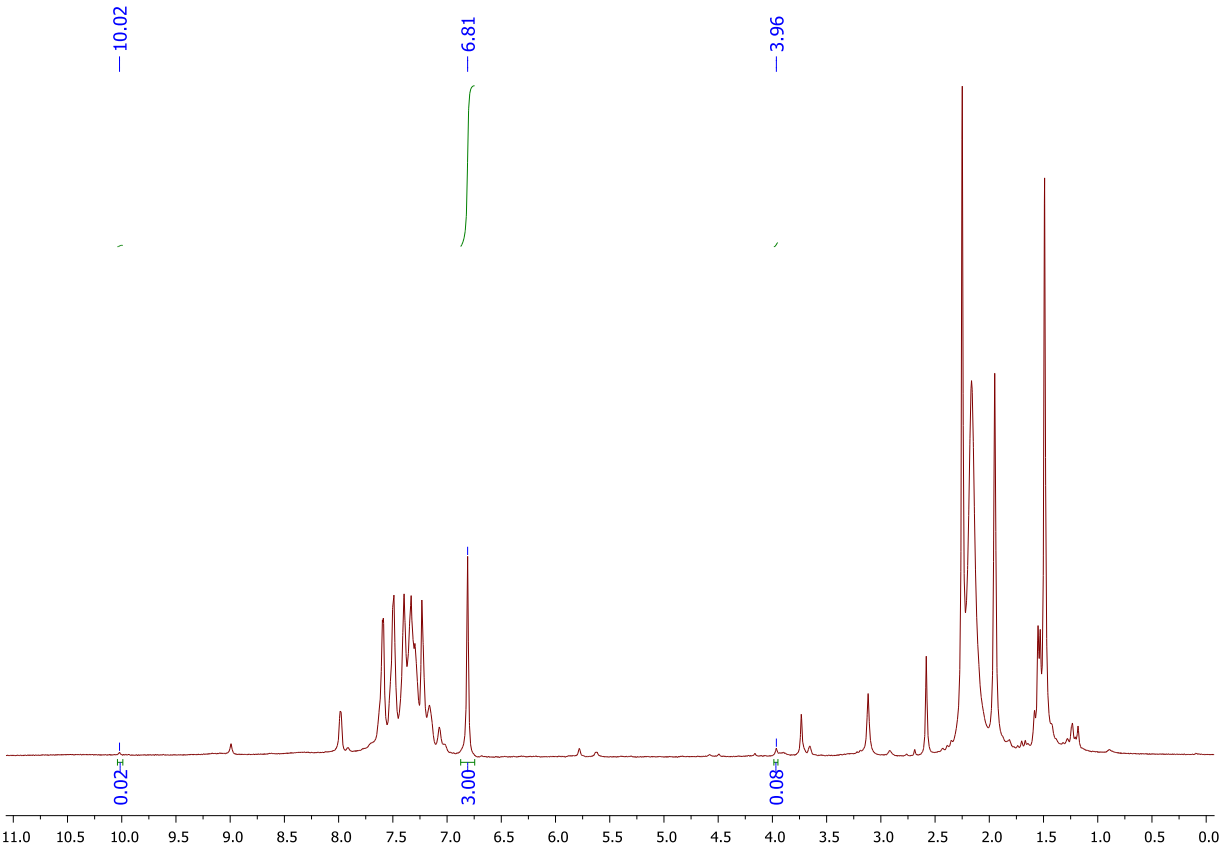

Figure S120. ^{1}H NMR spectrum of the reaction mixture after attempted oxidation of *trans*-stilbene with cumene hydroperoxide and **3** after heating at 70 °C for 16 hours in CD_3CN.

Attempted oxidation of *trans*-stilbene and alcohols under free radical conditions

To establish if free-radical reactivity in the presence of conventional radical initiators shows comparable reactivity, several model reactions were examined, oxidation of stilbenes and alcohols. Radical oxidation of stilbenes under O_2 initiated by AIBN produces a mixture of aldehyde and epoxide, although the exact ratio of epoxide:benzaldehyde is slightly different from that obtained with **3**/O_2. At the same time, oxidation of alcohols does not proceed under free-radical conditions (AIBN/O_2) suggesting that free radical pathway is not responsible for the product formation in case of alcohol oxidation mediated by **3**.

a) Oxidation of *trans*-stilbene by O_2 in the presence of AIBN

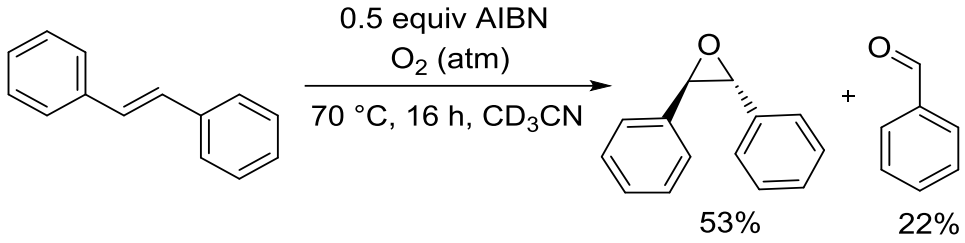

Inside the glovebox, a solution of AIBN (5.0 mg, 0.030 mmol), mesitylene (8.4 μL, 0.061 mmol) and *trans*-stilbene (10.9 mg, 0.0608 mmol) in anhydrous CD_3CN (0.5 mL) was placed to a J. Young NMR tube. The NMR tube was removed from glovebox and the reaction mixture was exposed to oxygen gas for four minutes, then transferred to an oil bath and heated at 70 °C for 16 hours. The reaction mixture was then analyzed by ^1H NMR spectroscopy, showing the formation of *trans*-stilbene oxide (53%) and benzaldehyde (22%) along with unreacted *trans*-stilbene (ca. 35%).

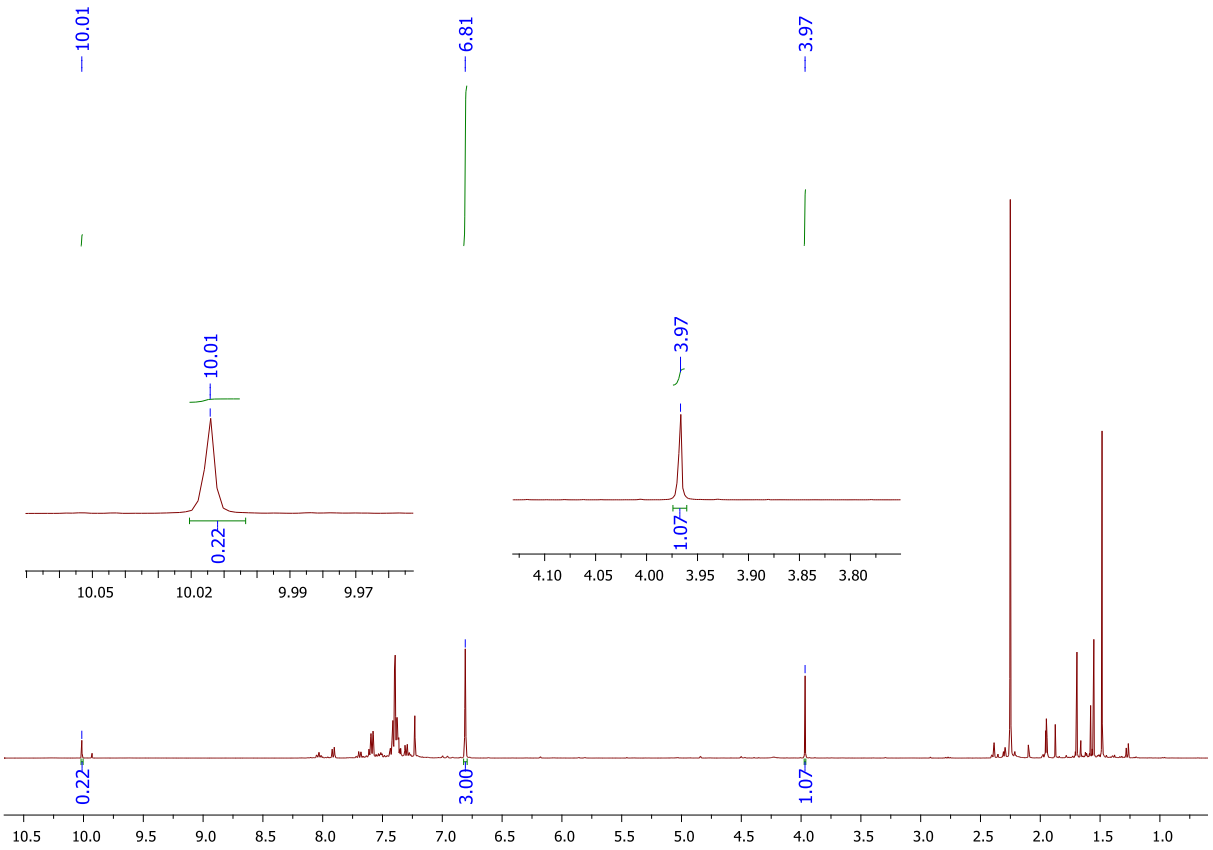

Figure S121. ^{1}H NMR spectrum of *trans*-stilbene oxidation using O_2/AIBN at 70 °C for 16 hours in CD_3CN.

b) Oxidation of *cis*-stilbene by O_2 in the presence of AIBN

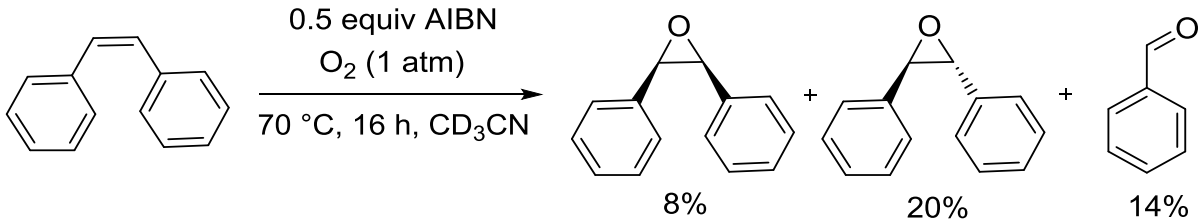

Inside the glovebox, a solution of AIBN (5 mg, 0.0304 mmol), mesitylene (8.4 µL, 0.0608 mmol) and *cis*-stilbene (10.8 µL, 0.0608 mmol) in anhydrous CD_3CN (0.5 mL) was placed to a J. Young NMR tube. The NMR tube was removed from glovebox and the reaction mixture was exposed to oxygen gas for four minutes, then transferred to an oil bath and heated at 70 °C for 16 hours. The reaction mixture was then analyzed by ^{1}H NMR spectroscopy, showing the formation of *cis*-stilbene oxide (8%), *trans*-stilbene oxide (20%), benzaldehyde (14%) and unreacted (ca. 60%) starting material.

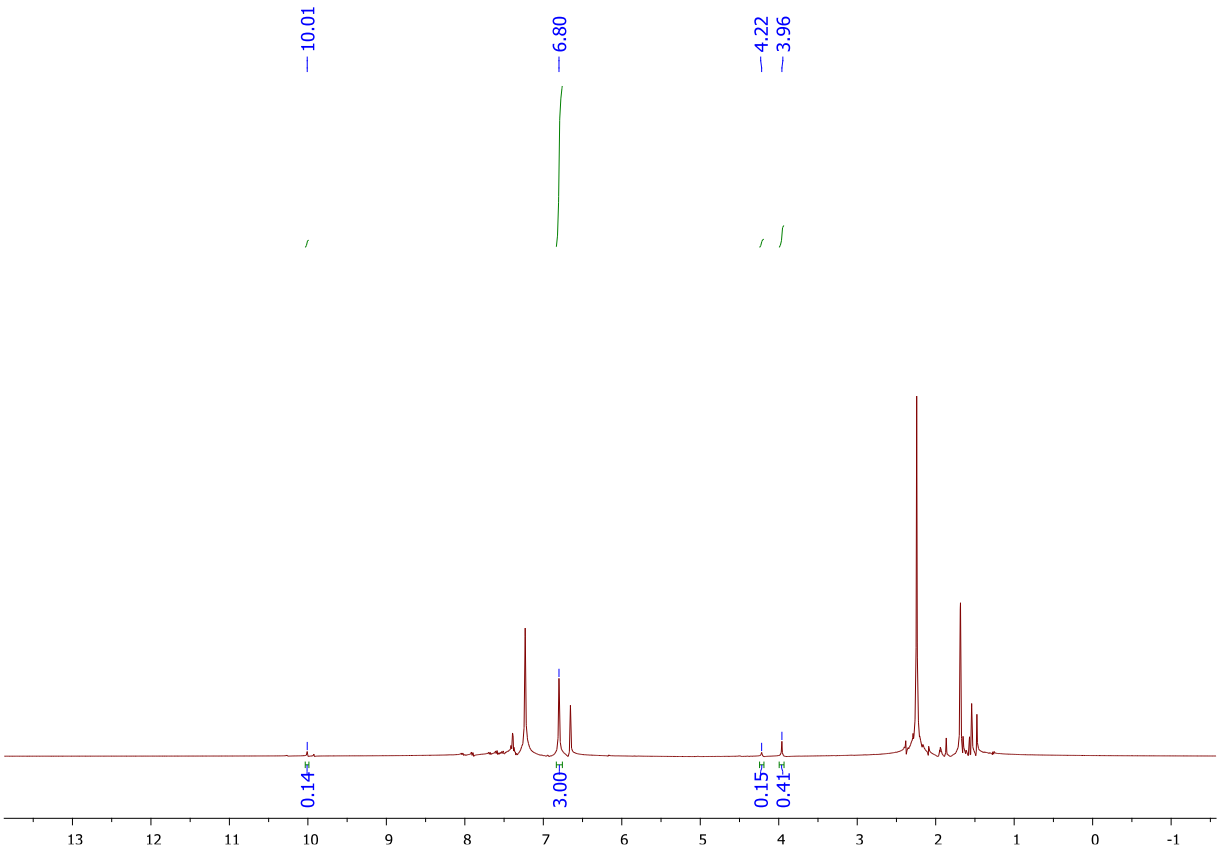

Figure S122. ^{1}H NMR spectrum of cis-stilbene oxidation using O_2/AIBN at 70 °C for 16 hours in CD_3CN.

c) Attempted oxidation of benzyl alcohol under free radical conditions

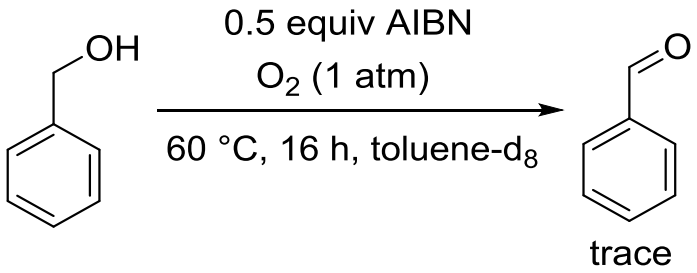

Inside the glovebox, a solution of AIBN (5.0 mg, 0.030 mmol), mesitylene (8.4 μL, 0.061 mmol) and benzyl alcohol (6.3 μL, 0.061 mmol) in dry toluene-d_8 (0.5 mL) was placed to a J. Young NMR tube. The NMR tube was removed from glovebox and the reaction mixture was exposed to oxygen gas for four minutes, then transferred to an oil bath and heated at 60 °C for 16 hours. The reaction mixture was analyzed by ^{1}H NMR spectroscopy, showing only trace amount of benzaldehyde (ca. 1%).

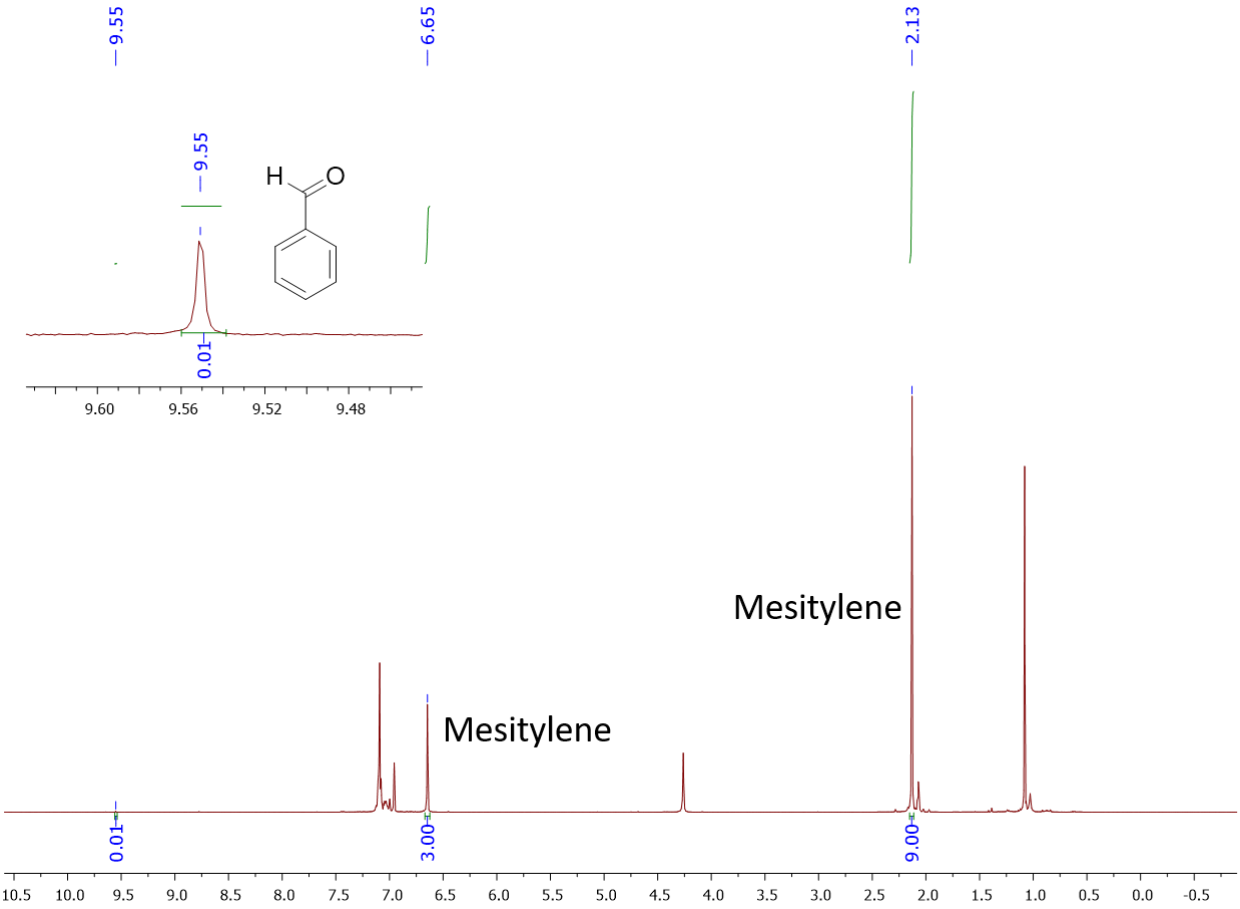

Figure S123. ^{1}H NMR spectrum of the reaction mixture containing benzyl alcohol and AIBN after heating at 60 °C under oxygen gas for 16 hours in toluene-d_8.

d) Attempted oxidation of trifluoroethanol under free radical conditions

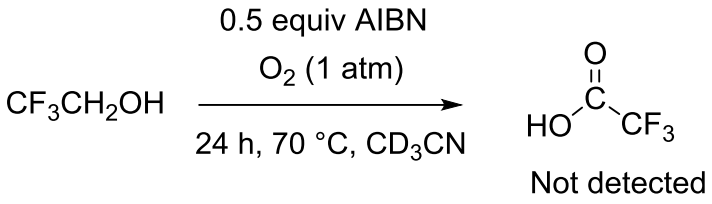

Inside the glovebox, a solution of AIBN (10 mg, 0.0608 mmol), 2,2,2- trifluoroethanol (8.7 µL, 0.1217 mmol) and α,α,α-trifluorotoluene (14.9 µL, 0.1217 mmol) in anhydrous CD_3CN (0.5 mL) was placed to a J. Young NMR tube. The NMR tube was removed from glovebox and the reaction mixture was exposed to oxygen gas for four minutes, then transferred to oil bath and heated at 70 °C for 24 hours. The reaction mixture was analyzed by ^{19}F NMR spectroscopy, confirming no formation of trifluoroacetic acid. Only unreacted starting material was present.

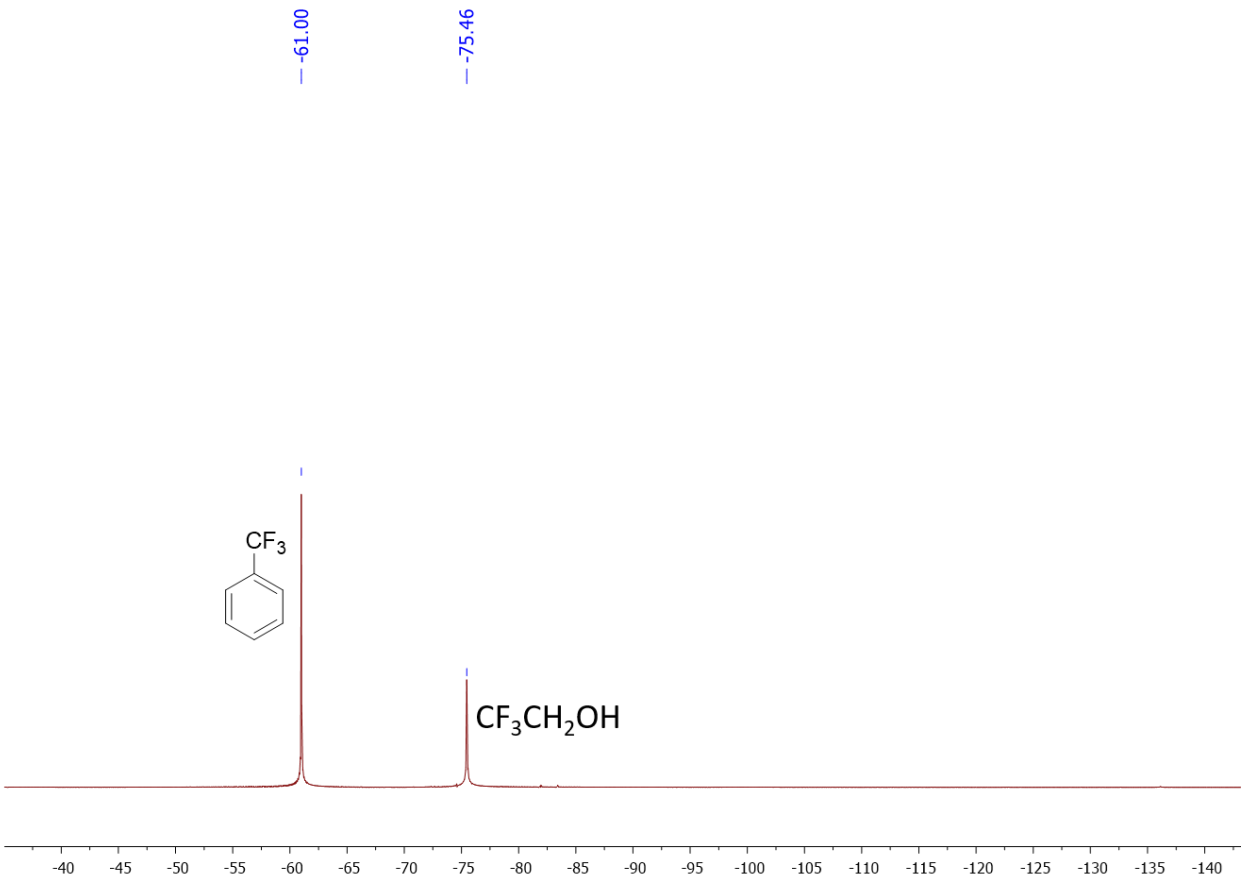

Figure S124. ^{19}F NMR spectrum of the reaction mixture containing trifluoroethanol and AIBN after heating at 70 °C under oxygen gas for 24 hours in CD_3CN.

Synthesis of 5-THF

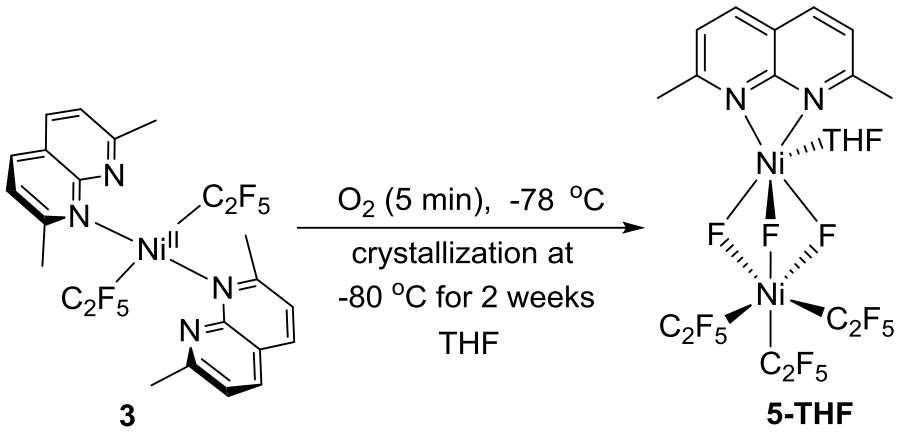

Inside the glovebox, the solution of complex **3** (10.8 mg, 0.0176 mmol), in anhydrous THF (0.4 mL) was placed to a J. Young NMR tube. The NMR tube was removed from glovebox and the reaction mixture was exposed to oxygen gas for five minutes at -78 °C, with constant shaking to ensure good mixing. During this course of time the initial yellow color of the solution changes to purple. The J. Young NMR tube cap was then sealed with a Teflon cap and another layer of electrical tape. Next, the cooled NMR tube was placed in a -78 °C cooling bath and transferred to -80 °C refrigerator without letting to warm up. Over the period of two weeks the blue color crystals appeared, which were analyzed by SC-XRD and complex **5-THF**.
Note : the crystal was stable only on cold glass slide before mounting for SC-XRD analysis.

Warming up purple solution obtained by low temperature oxidation to RT followed by crystallization under air for several days at RT afforded crystals of **3a** identified by SC-XRD.

In an independent experiment, when the purple solution obtained by low temperature oxidation of **3** (12.6 , 0.0205 mmol in 0.4 mL THF) as described above was warmed up to RT for 24 h, then mixed with equal volume of methanol (0.4 mL) and α,α,α-trifluorotoluene (5 μL, 0.04 mmol, 2 equiv to Ni) and analyzed by ^{19}F NMR in the presence of internal standard, trifluoroacetate was detected (36% yield based on total amount of C_2F_5 in the starting material). ESI-MS also showed the presence of the peaks corresponding to $[(\mathbf{L3})Ni(CF_3COO)]^+$ and $[(\mathbf{L3})_2Ni(CF_3COO)]^+$:

HRMS (ESI) calculated for $[(\mathbf{L3})Ni(CF_3COO)]^+$, $C_{12}H_{10}F_3N_2O_2Ni$: m/z calc. 329.0042; m/z found, 329.0005.

HRMS (ESI) calculated for $[(\mathbf{L3})_2Ni(CF_3COO)]^+$, $C_{22}H_{20}F_3N_4O_2Ni$: m/z calc. 487.0886; m/z found, 487.0914.

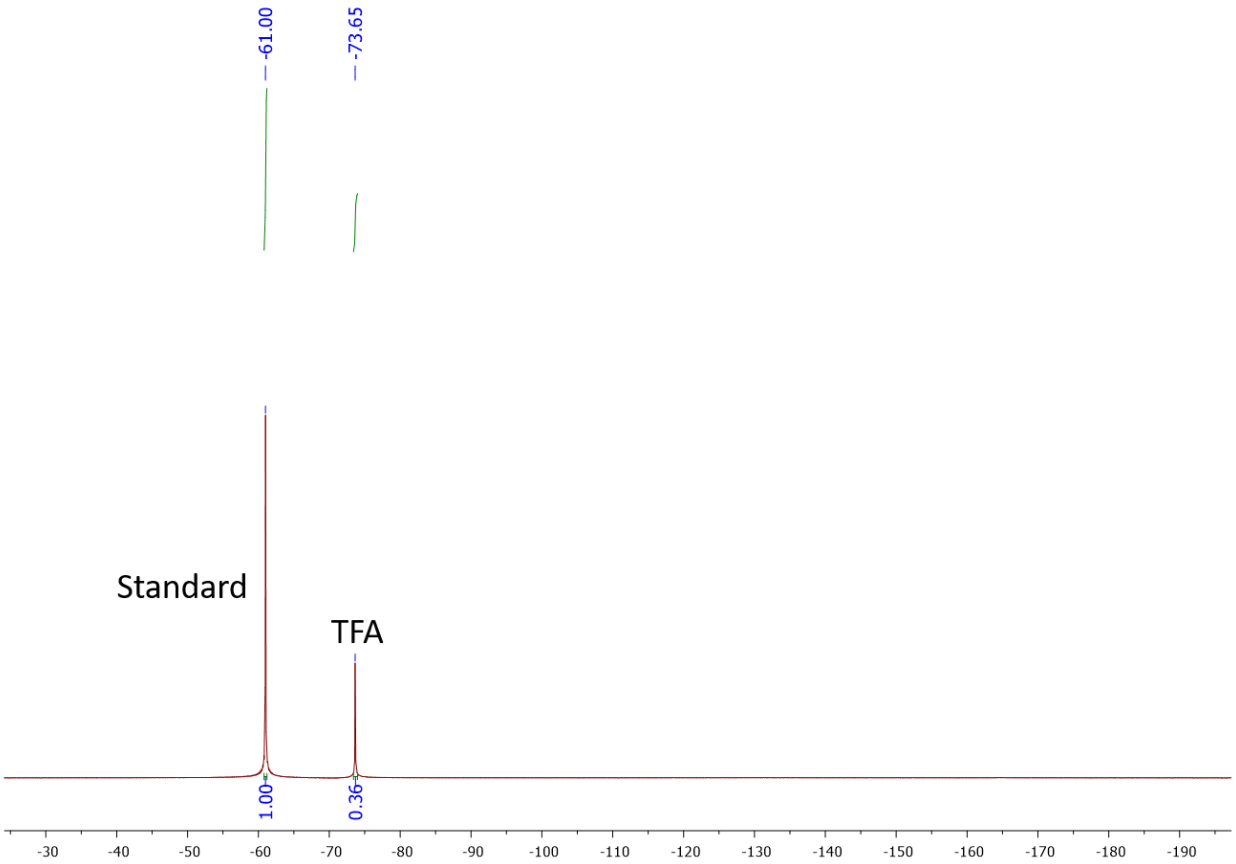

Figure S125. ^{19}F NMR spectrum of the reaction mixture of low temperature oxidation of **3** in THF after warming up to RT for 24 h and addition of MeOH.

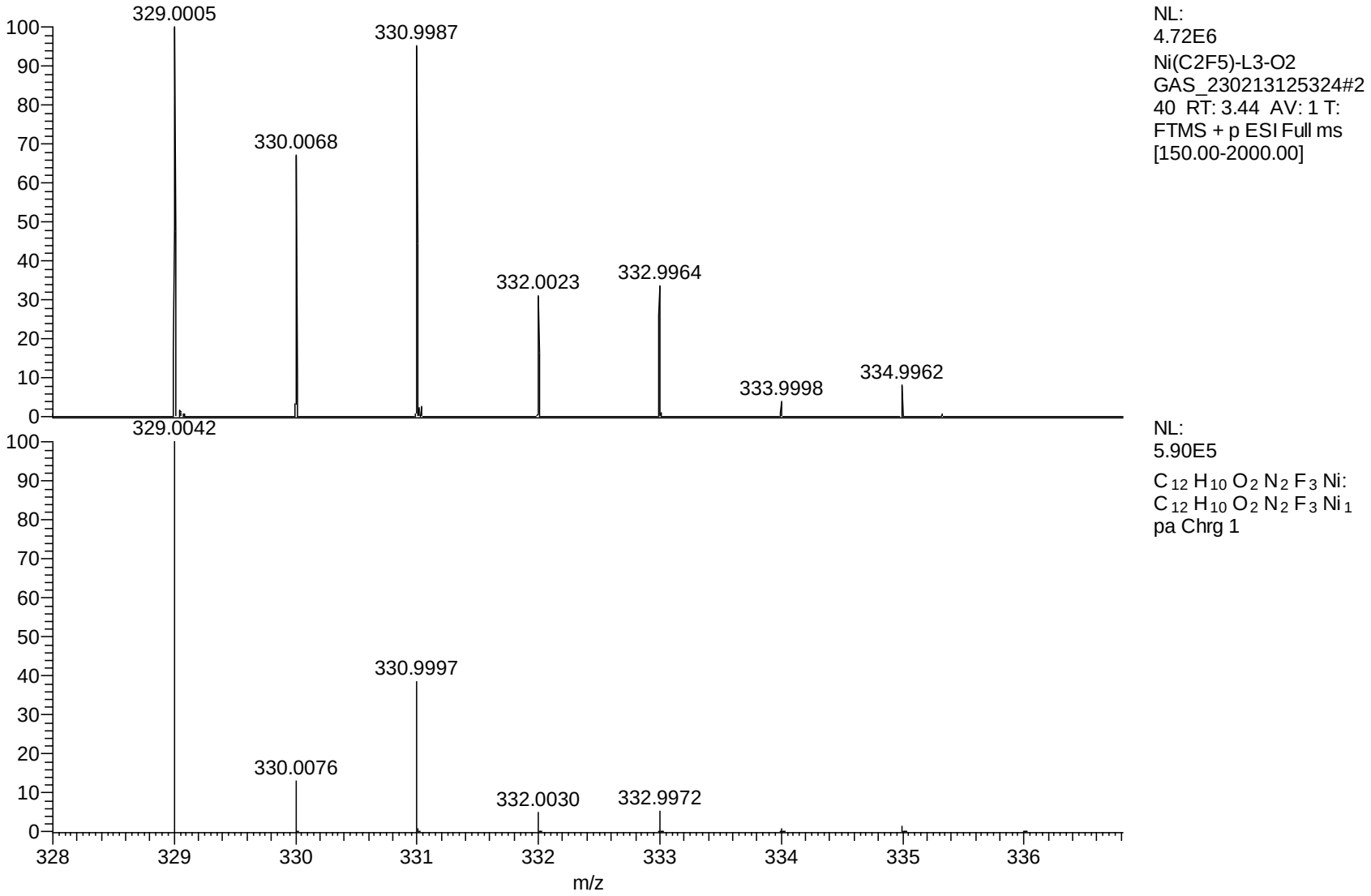

Figure S126. ESI-(HR)MS spectrum of the reaction mixture of low temperature oxidation of **3** in THF after warming up to RT for 24 h and addition of MeOH and simulated spectrum of [(**L3**)Ni(CF_3COO)]$^+$, $C_{12}H_{10}O_2N_2F_3Ni$ (bottom).

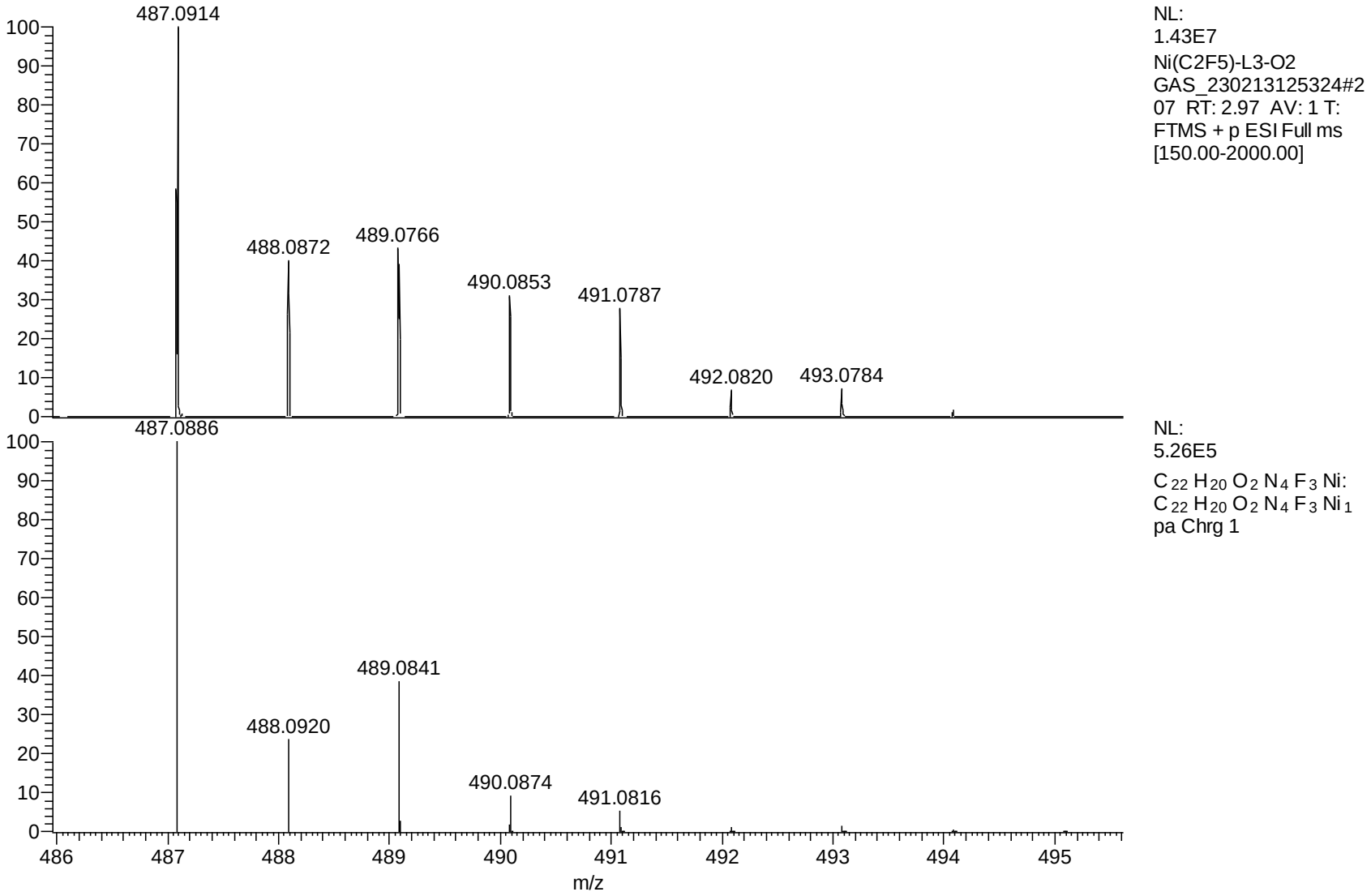

Figure S127. ESI-(HR)MS spectrum of the reaction mixture of low temperature oxidation of **3** in THF after warming up to RT for 24 h and addition of MeOH and simulated spectrum of $[(\mathbf{L3})_2Ni(CF_3COO)]^+$, $C_{22}H_{20}O_2N_4F_3Ni$: (bottom).

Synthesis of 5-MeCN

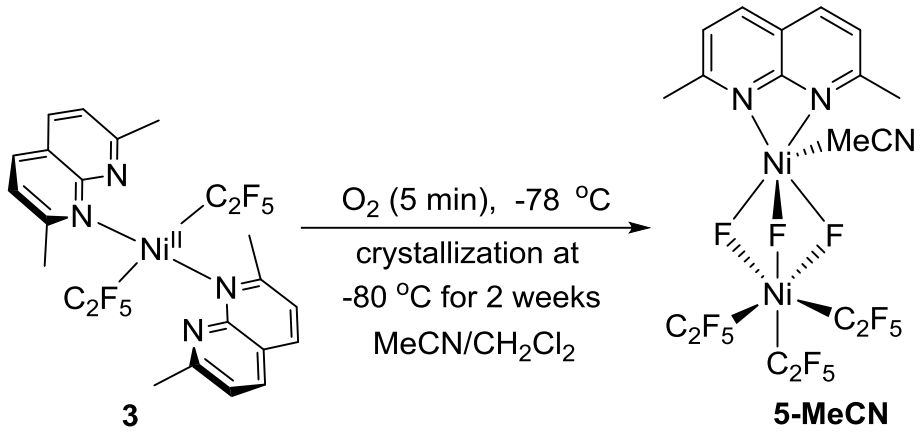

Inside the glovebox, solution of complex **3** (10.6 mg, 0.0172 mmol) in anhydrous MeCN:CH_2Cl_2 (1:1) (0.4 mL) was placed to a J. Young NMR tube. During this course of time the initial yellow color of the solution changes to purple. The J. Young NMR tube cap was then sealed with a Teflon cap and another layer of electrical tape. Next, the cooled NMR tube was placed in a -78 °C cooling bath and transferred to -80 °C refrigerator without letting to warm up. Over the period of two weeks the blue color crystals appeared, which were analyzed by SC-XRD and complex **5-MeCN**.

Note : the crystal was stable only on cold glass slide before mounting for SC-XRD analysis.

Synthesis of 6

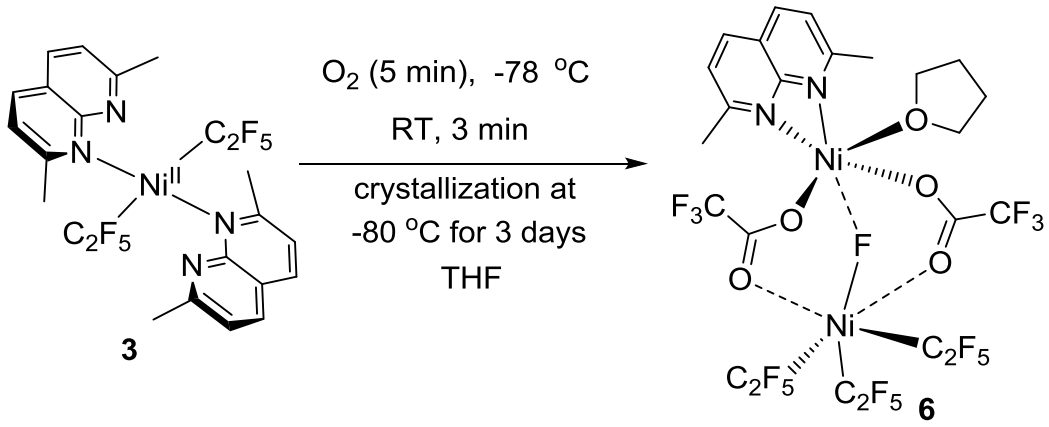

Inside the glovebox, solution of complex **3** (10.2 mg, 0.0166 mmol) in anhydrous THF (0.4 mL) was placed to a J. Young NMR tube. The NMR tube was removed from glovebox and the reaction mixture was exposed to oxygen gas for five minutes, at -78 °C, with constant shaking to ensure good mixing.
During this course of time the initial yellow color of the solution changes to purple as described above during synthesis of **5-THF**. The purple solution obtained by such method was warmed up to RT until purple color changed to yellow during the course of 3 min at RT. The yellow solution was immediately cooled down to 78 °C and crystallized at -80 °C for 3 days.

Note: the crystal was stable only on cold glass slide before mounting for SC-XRD analysis.

Reaction of 3 in presence of oxygen gas followed by UV-Vis spectroscopy

Inside the glovebox, the solution of complex **3** (5.2 mg, 0.0084 mmol) in anhydrous acetonitrile (2.5 mL) was placed to a screw-cap quartz cuvette. UV-vis spectrum was recorded before addition of oxygen. Next, then the oxygen gas was two minutesand the color changed to purple accompanied by appearance of a new band at 609 nm.
The purple solution is unstable and a 609 nm band disappears within several minutes at RT (see below)

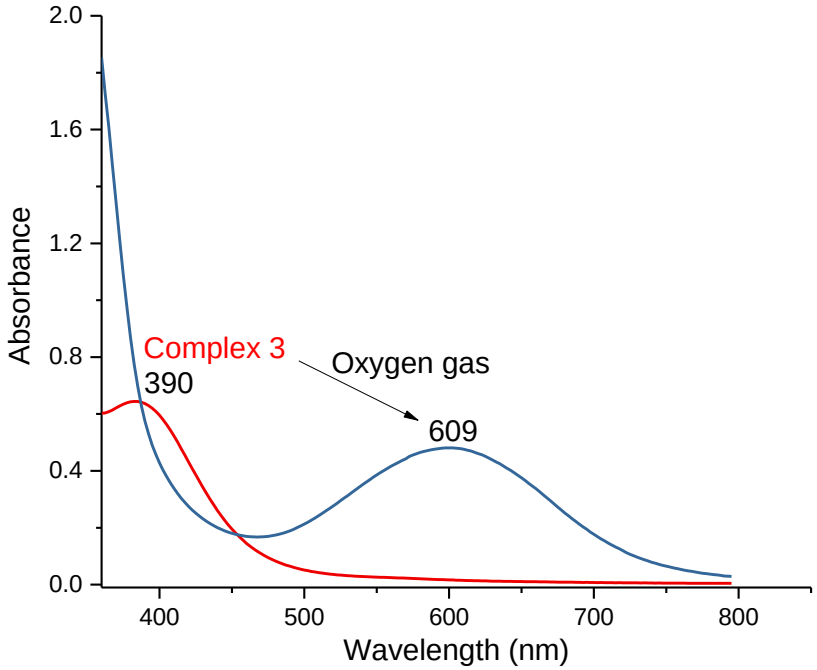

Figure S128. Comparison of UV-vis spectra of complex **3** under N_2 and immediately after passing O_2 gas in MeCN solution at RT.

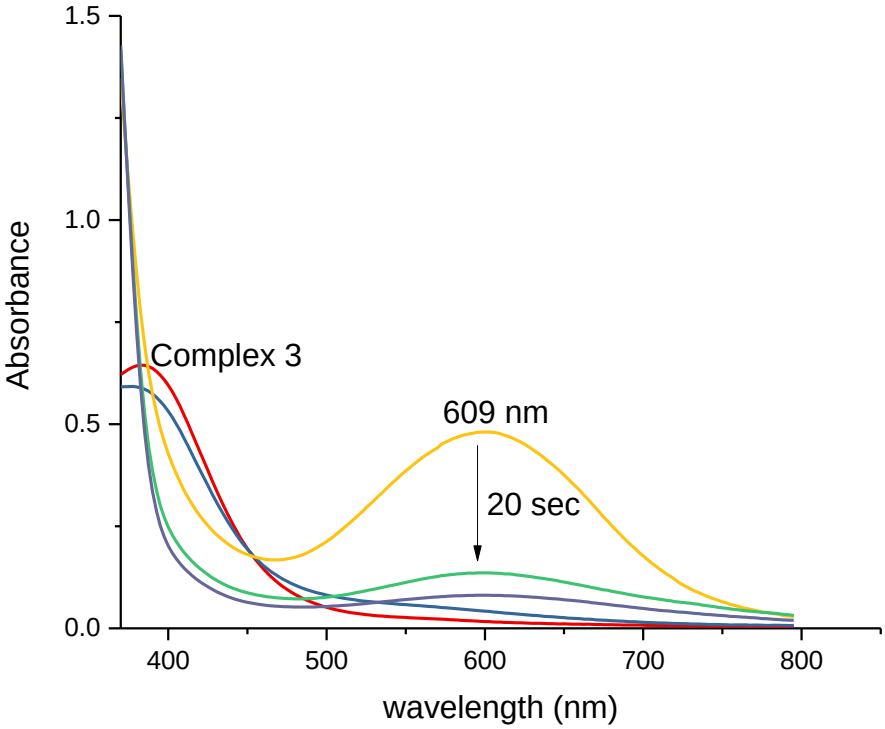

Figure S129. Time course of the disappearance of a new band at 609 nm in UV-vis spectra in MeCN solution at RT. Red line: complex 3 before addition of O_2; yellow line: UV-vis spectrum immediately after passing O_2; green line: UV-vis spectrum after 20 s at RT; purple line: UV-vis spectrum after 40 s at RT; blue line: UV-vis spectrum after 60 s at RT.

X-ray data

Data were collected using a XtaLAB AFC12 (RINC): Kappa dual offset/far diffractometer operating at T = 100 K. Data were measured using w scans with Cu K_a radiation. The diffraction pattern was indexed and the total number of runs and images was based on the strategy calculation from the program CrysAlisPro 1.171.40.54a.[28] The maximum resolution that was achieved was Q = 81.035° (0.83 Å). The unit cell was refined using CrysAlisPro 1.171.40.54a[28] on the observed reflections. Data reduction, scaling and absorption corrections were performed using CrysAlisPro 1.171.40.54a.[28] A multi-scan absorption correction was performed using CrysAlisPro 1.171.40.54a. [28] Empirical absorption correction using spherical harmonics, implemented in SCALE3 ABSPACK scaling algorithm. The absorption coefficient m of this material were applied with this wavelength (l = 1.54184Å) and the minimum and maximum transmissions are 0.811 and 1.000. The structure was solved and the space group P-1 (# 2) determined by the ShelXT 2014/5[29] structure solution program using using dual methods and refined by full matrix least squares minimisation on $\boldsymbol{F^2}$ using version 2016/6 of **ShelXL** 2016/6.[30] All non-hydrogen atoms were refined anisotropically. Hydrogen atom positions were calculated geometrically and refined using the riding model coordinated water molecules. Hydrogen atom positions were calculated geometrically and refined using the riding model. *_exptl_absorpt_process_details*: CrysAlisPro 1.171.40.54a[28] using spherical harmonics as implemented in SCALE3 ABSPACK. Graphical software and data handling was performed in OLEX2.[31]

Detailed information about crystal structure determination can be accessed via supplementary cif files. The crystallographic data for the investigated compounds have been deposited in the Cambridge Crystallographic Data Centre as supplementary publication numbers CCDC 2241818 (**1**), 2204584 (**2**), 2241816 (**3**), 2241819 (**4**), 2241821 (**2a**), 2241822 (**3a**), 2241823 (**4a**), 2241820 (**5-MeCN**), 2241817 (**5-THF**) and 2241824 (**6**). These data can be obtained free of charge via https://www.ccdc.cam.ac.uk/structures/.

Compound	**1**	**2**	**3**	**4**	**2a**
Formula	$C_{12}H_6F_{10}N_2Ni$	$C_{13}H_8F_{10}N_2Ni$	$C_{24}H_{20}F_{10}N_4Ni$	$C_{26}H_{20}F_{14}N_4Ni$	$C_{28}H_{26}F_6N_4NiO_6$
$D_{calc.}$/ g cm^{-3}	2.057	1.959	1.712	1.773	1.587
m/mm^{-1}	3.241	1.413	2.120	2.211	1.779
Formula Weight	426.90	440.92	613.15	713.17	687.24
Colour	yellow	clear yellowish	clear light yellow	clear light yellow	clear light yellow
Shape	irregular-shaped	block-shaped	plate-shaped	block-shaped	plate-shaped
Size/mm^3	0.29×0.19×0.15	0.20×0.11×0.10	0.23×0.14×0.04	0.14×0.10×0.09	0.23×0.18×0.03
T/K	100	100	100	100	100
Crystal System	monoclinic	monoclinic	monoclinic	triclinic	triclinic
Space Group	$P2_1/n$	$P2_1/n$	$P2_1/n$	P-1	P-1
a/Å	9.68610(10)	10.0066(5)	10.6069(3)	9.3627(4)	7.4720(4)
b/Å	13.95460(10)	34.6611(4)	10.0489(2)	9.4114(4)	8.6669(4)
c/Å	10.89740(10)	13.2116(7)	11.2681(3)	9.5203(3)	12.3403(6)
a/°	90	90	90	110.183(4)	99.771(4)
b/°	110.6460(10)	139.278(11)	98.067(2)	114.583(4)	105.008(4)
g/°	90	90	90	99.410(4)	105.431(4)
V/Å^3	1378.36(2)	2989.4(5)	1189.16(5)	668.08(5)	719.22(7)
Z	4	8	2	1	1
Z'	1	2	0.5	0.5	0.5
Wavelength/Å	1.54184	0.71073	1.54184	1.54184	1.54184
Radiation type	Cu K$_a$	Mo K$_a$	Cu K$_a$	Cu K$_a$	Cu K$_a$
Q_{min}/°	5.263	2.363	5.364	5.367	3.837
Q_{max}/°	79.939	33.963	80.503	72.102	80.360
Measured Refl's.	23943	133245	11676	13511	14220
Indep't Refl's	2984	11667	2506	2616	3051
Refl's I≥2 s(I)	2939	10536	2169	2361	2610
R_{int}	0.0464	0.0889	0.0762	0.0770	0.0703
Parameters	227	655	180	217	340
Largest Peak	0.638	1.110	1.099	1.124	0.639
Deepest Hole	-0.410	-0.932	-0.686	-0.437	-0.647
GooF	1.101	1.145	1.128	1.063	1.063

wR_2 (all data)	0.0850	0.1251	0.1802	0.1568	0.1329
wR_2	0.0848	0.1224	0.1748	0.1526	0.1287
R_1 (all data)	0.0344	0.0606	0.0629	0.0598	0.0551
R_1	0.0340	0.0537	0.0580	0.0544	0.0482

Compound	**3a**	**4a**	**5-MeCN**	**5-THF**	**6**
Formula	$C_{28}H_{22}F_{12}N_4Ni_2O_9$	$C_{26}H_{20}F_{10}N_4NiO_4$	$C_{19}H_{15}Cl_2F_{18}N_3Ni_2$	$C_{20}H_{18}F_{18}N_2Ni_2O$	$C_{24}H_{18}F_{22}N_2Ni_2O_5$
$D_{calc.}$/ g cm^{-3}	1.746	1.606	1.968	1.965	1.992
m/mm^{-1}	2.496	1.931	4.823	3.253	3.096
Formula Weight	903.91	701.17	815.66	761.78	949.82
Colour	yellow	clear light yellow	blue	blue	yellow
Shape	needle-shaped	block-shaped	block-shaped	needle-shaped	block-shaped
Size/mm^3	0.16×0.06×0.04	0.09×0.05×0.04	0.08×0.07×0.05	0.07×0.04×0.02	0.04×0.03×0.02
T/K	100	100	100	100	100
Crystal System	monoclinic	triclinic	monoclinic	monoclinic	triclinic
Space Group	$C2/c$	P-1	$P2_1/n$	$P2_1/n$	P-1
a/Å	20.0089(5)	8.6514(2)	11.5628(5)	10.22025(17)	12.2434(3)
b/Å	9.68800(10)	13.0136(3)	13.9251(7)	14.9324(3)	13.7951(3)
c/Å	20.2007(6)	13.6104(4)	17.4612(7)	17.5031(2)	19.1053(4)
a/°	90	88.652(2)	90	90	99.235(3)
b/°	118.582(3)	84.551(2)	101.679(4)	105.4069(17)	93.899(3)
g/°	90	71.915(2)	90	90	94.115(4)
V/Å^3	3438.62(16)	1450.02(7)	2753.3(2)	2575.21(8)	3166.45(13)
Z	4	2	4	4	4
Z'	0.5	1	1	1	2
Wavelength/Å	1.54184	1.54184	1.54184	1.54184	1.54184
Radiation type	Cu K$_a$	Cu K$_a$	Cu K$_a$	Cu K$_a$	Cu K$_a$
Q_{min}/°	4.986	3.262	4.094	3.953	3.631
Q_{max}/°	79.869	79.952	80.211	79.925	81.035
Measured Refl's.	19916	22743	27772	13634	51998
Indep't Refl's	3660	6117	5833	5157	13390
Refl's I≥2 s(I)	3475	5485	3801	4259	10553
R_{int}	0.0362	0.0321	0.0972	0.0264	0.0782
Parameters	255	519	400	390	995
Largest Peak	0.424	0.435	1.441	0.709	1.216
Deepest Hole	-0.487	-0.502	-0.824	-0.438	-1.823
GooF	1.082	1.064	1.050	1.051	1.092

wR_2 (all data)	0.0997	0.1265	0.2411	0.1317	0.2021
wR_2	0.0987	0.1232	0.2121	0.1254	0.1911
R_1 (all data)	0.0373	0.0494	0.1239	0.0518	0.0827
R_1	0.0359	0.0450	0.0832	0.0438	0.0694

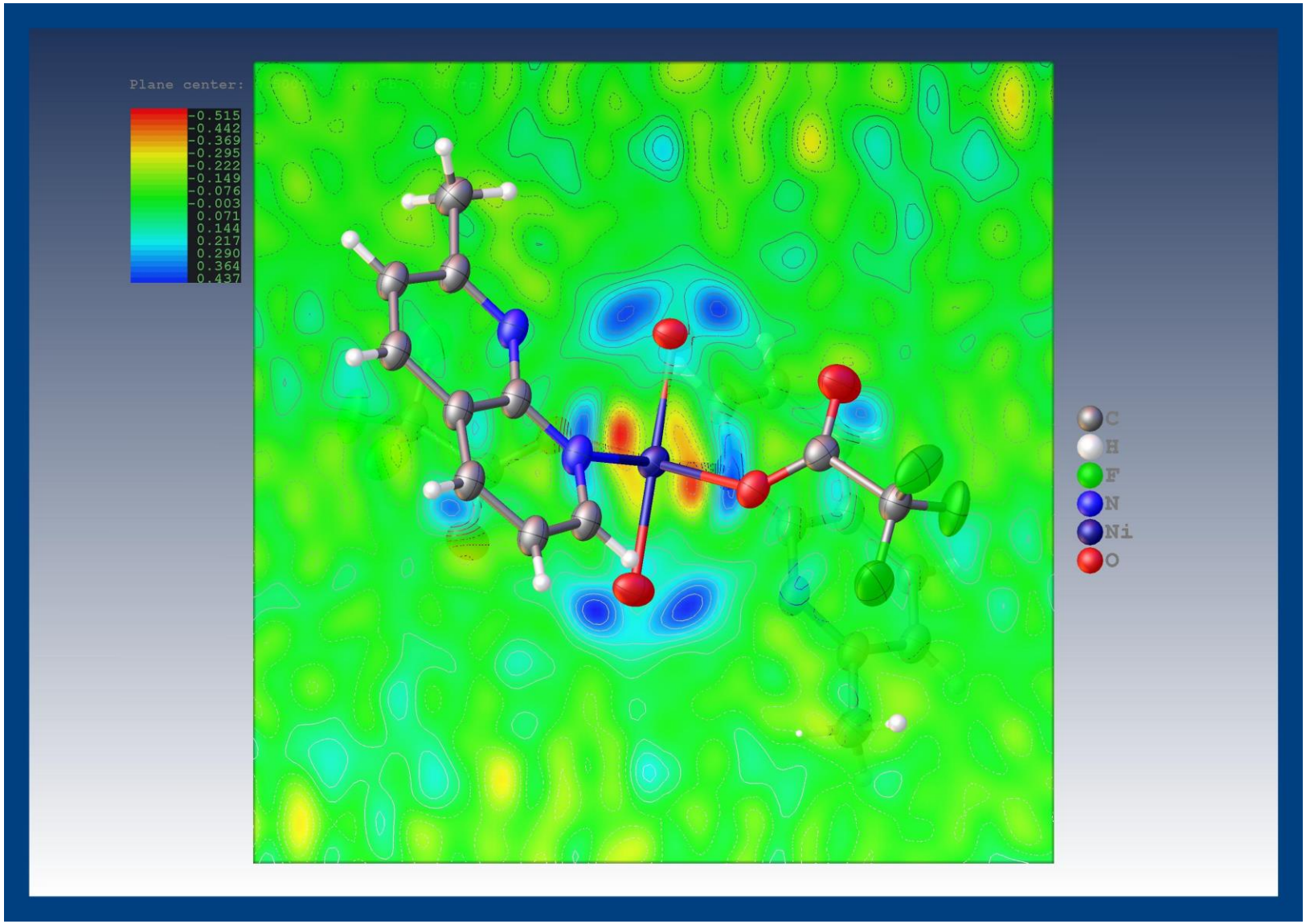

Figure S130. Electron density plot for complex **2a**.

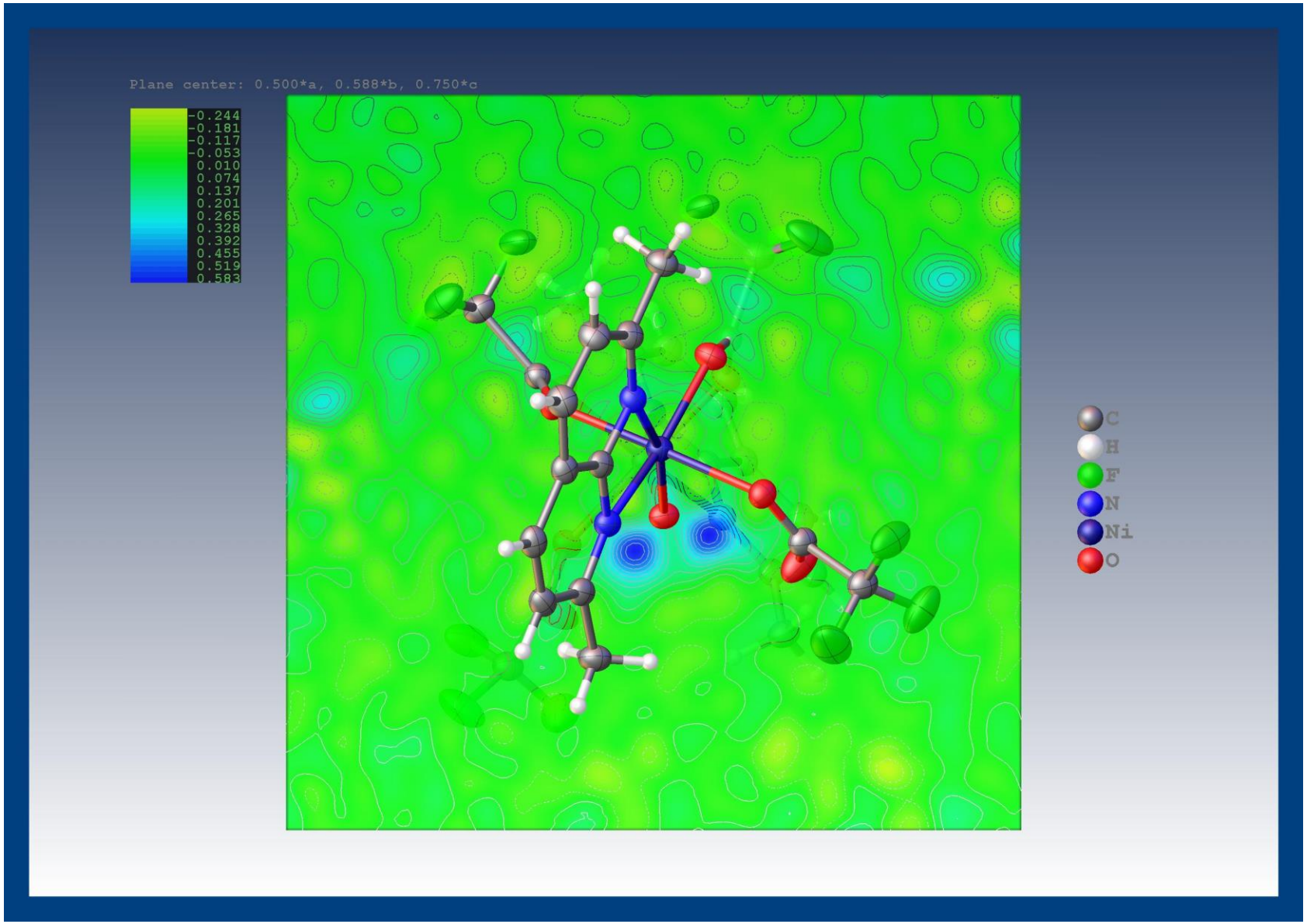

Figure S131. Electron density plot for complex **3a**.

Computational details

Comparison of spin states for complex 5-MeCN

DFT calculations were performed using ωB97XD[32] functional and def2tzvp[33] basis sets for all elements as implemented in the Gaussian 16 program package.[34] This method has previously led to good agreement of the optimized geometry for isolated $[(\mathbf{L3})_2Ni^{III}(CF_3)_2]^+$ complex with the SC-XRD structure.[14] For paramagnetic complexes, unrestricted formalism was used; wavefunction stability was checked using stable=opt job in Gaussian. Gibbs free energies are reported as the sum of electronic and thermal free energies.

The complex **5-MeCN** was optimized as a triplet using unrestricted formalism and a singlet using restricted method to model Ni^{IV}-high spin Ni^{II} vs. Ni^{IV}-low spin Ni^{II} configurations, respectively. The structures were optimized in gas phase to compare with the parameters obtained by SC-XRD. To model antiferromagnetically coupled Ni^{III}-Ni^{III} complex, the fragments were defined as follows: $Ni(C_2F_5)_3$ fragment (doublet, alpha spin, charge 0), Ni(**L3**)(MeCN) fragment (doublet, beta spin, charge +3), and three fluorines (each defined as singlet with -1 charge), and the obtained initial guess was used for geometry optimization.[35] In all cases, the wavefunction stability was verified using Stable job in Gaussian.

The comparison of electronic energies shows that the triplet state is significantly more stable than the singlet state. The singlet geometry is also significantly different from the geometry obtained by SC-XRD showing essentially monodentate binding of **L3**. The antiferromagnetically coupled state was also found significantly less stable than the triplet state.

To confirm the nature of the triplet state, population analysis was performed. The spin density was found to be localized mainly at the Ni atom of Ni(**L3**)(MeCN) fragment assigned as a high spin Ni^{II}, while no significant spin density was found on a $Ni(C_2F_5)_3$ fragment. The nature of the singly occupied orbitals was examined using population analysis using restricted open shell formalism; the two singly occupied orbitals were found to have a character of Ni(**L3**)(MeCN)-localized d_{x2-y2} and d_{z2}-orbitals, consistent with its assignment as a high-spin Ni^{II} center.

Table S3. Comparison of electronic energies for singlet (rωB97XD), triplet (uωB97XD) and antiferro-coupled (fragment guess, uωB97XD) models for geometry-optimized complex **5-MeCN**.

Speciation	E, Hartree	Relative E, kcal mol^{-1}
Triplet (uwb97xd)	-5672.416852	0
Singlet (rwb97xd)	-5672.371376	28.5
Fragment guess (uwb97xd) (antiferro coupling)	-5672.371377	28.5

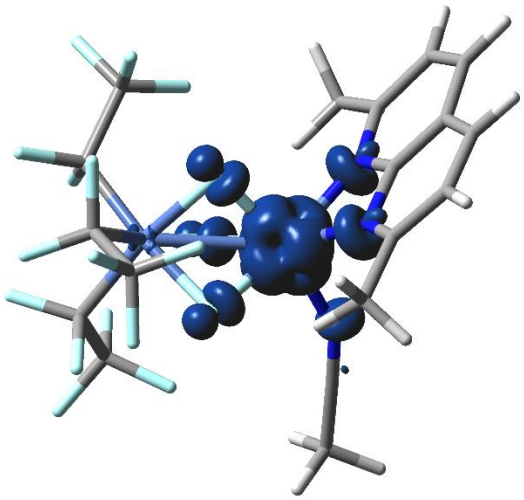

Figure S132. Spin density plot (isovalue 0.004) for geometry-optimized (triplet state) **5-MeCN**.

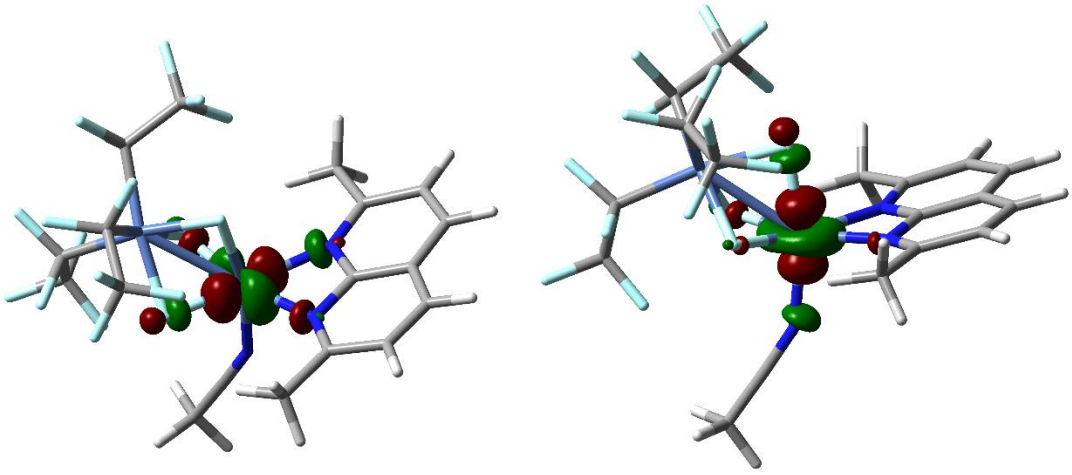

Figure S133. Two highest singly occupied orbitals (isovalue 0.06) for geometry-optimized (triplet state) complex **5-MeCN**: left – HOMO; right – HOMO-1.

Comparison of relative stability of bis-ligated *trans*- and mono-ligated *cis*-Ni(dialkyl) complexes

DFT calculations were performed using M06L functional[36-37] and def2tzvp/w06[33, 38] basis sets for all elements as implemented in the Gaussian 16 program package.[34] Geometries were optimized in solvent (acetonitrile) using the SMD solvation model.[39] This method was selected due to its reported good performance for assessing solvent-corrected organometallic thermochemistry and fast performance.[37] Analytical frequency calculations performed on the resultant geometries conformed to zero imaginary frequencies for all ground states. Gibbs free energies are reported as the sum of solvent-corrected electronic and thermal free energies. The relative free energies compared for the following general equations while varying substitution at the naphthyridine ligand (**L1** vs **L3**, eqs 1 and 2), nature of the alkyl ligand at the Ni center (C_2F_5 vs. Me vs. CF_3, eqs 1, 3 and 4) and their relative orientation (eq 5).

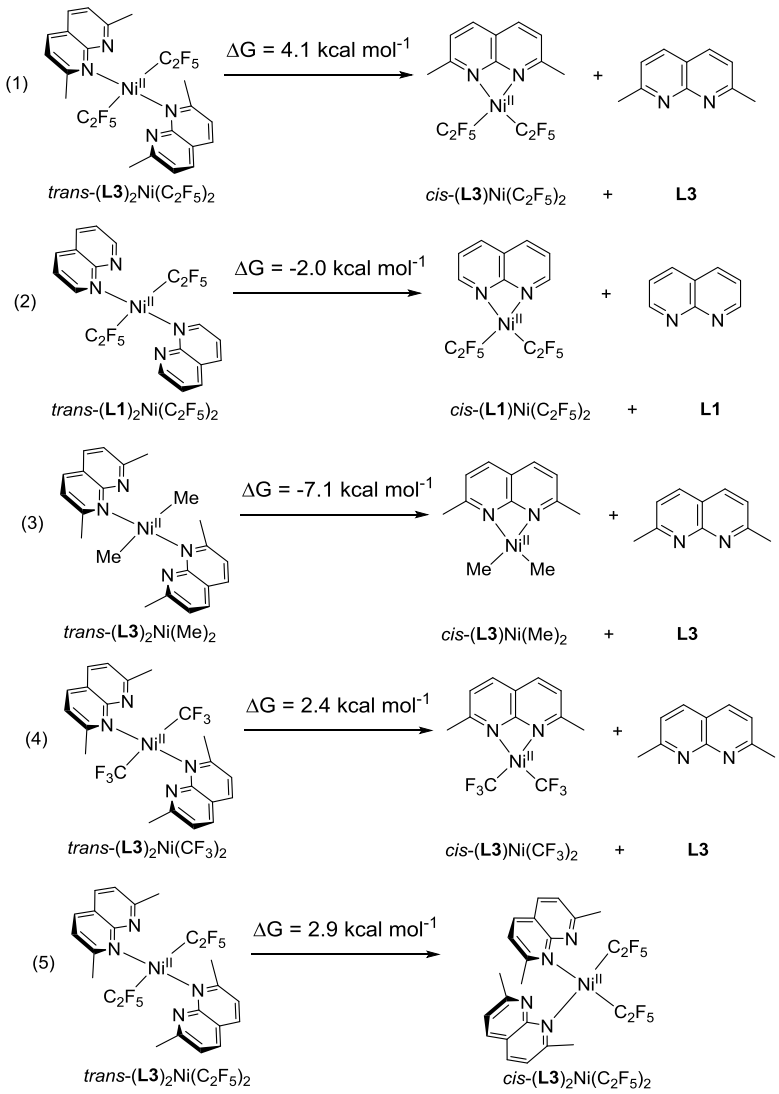

Scheme S8. Relative Gibbs free energies for bis-ligated *trans*-NiR_2 species vs. mono-ligated *cis*-NiR_2 species and a free ligand.

Table S4. Free energies for geometry-optimized structures and comparison of relative stability of bis-ligated *trans*-NiR_2 species vs. mono-ligated *cis*-NiR_2 species and a free ligand.

Speciation	ΔG (hartree)	Relative ΔG (hartrees)	Relative ΔG (kcal mol^{-1})
Equation (1):			
trans-(**L3**)$_2$Ni(C_2F_5)$_2$	-3652.687404	0	0
cis-(**L3**)$_2$Ni(C_2F_5)$_2$	-3156.089245	-	-
L3	-496.591595	-	-
cis-(**L3**)Ni(C_2F_5)$_2$ + **L3**	-3652.68084	0.006564	**4.11891**
cis-(**L3**)$_2$Ni(C_2F_5)$_2$	-3652.682832	0.004572	**2.86893**
Equation (2):			
trans-(**L1**)$_2$Ni(C_2F_5)$_2$	-3495.464048	0	0
cis-(**L1**)$_2$Ni(C_2F_5)$_2$	-3077.486513	-	-
L1	-417.9808	-	-
cis-(**L1**)Ni(C_2F_5)$_2$ + **L1**	-3495.467313	-0.00326	**-2.0487875**
Equation (3):			
trans-(**L3**)$_2$Ni(Me)$_2$	-2581.261212	0	0
cis-(**L3**)$_2$Ni(Me)$_2$	-2084.680989	-	-
L3	-496.591595	-	-
cis-(**L3**)Ni(Me)$_2$ + **L3**	-2581.272584	-0.01137	**-7.13593**
Equation (4):			
trans-(**L3**)$_2$Ni(CF_3)$_2$	-3176.997519	0	0
cis-(**L3**)$_2$Ni(CF_3)$_2$	-2680.402044	-	-
L3	-496.591595	-	-
cis-(**L3**)Ni(CF_3)$_2$ + **L3**	-3176.993639	0.00388	**2.4347**

3, *trans*-(**L3**)$_2$Ni^{II}(C_2F_5)$_2$ *cis*-(**L3**)Ni^{II}(C_2F_5)$_2$ *cis*-(**L3**)$_2$Ni(C_2F_5)$_2$

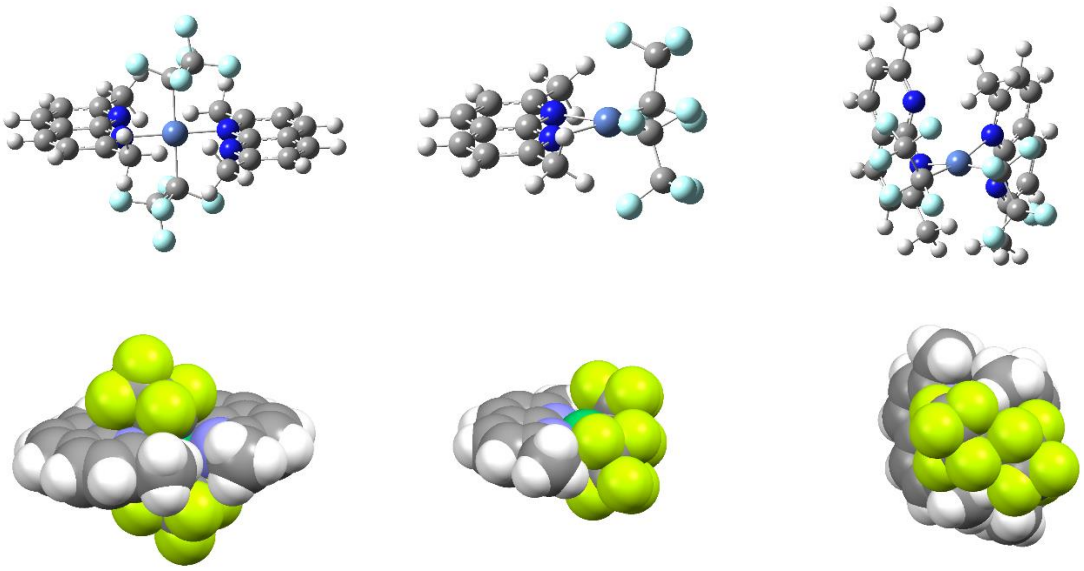

∠N-Ni-N 180.00° ∠N-Ni-C 166.76°, 166.84° ∠N-Ni-C 167.41°, 167.42°
∠C-Ni-C 180.00°

Figure S134. DFT-optimized geometries and space-filling models of **3**, *cis*-(**L3**)Ni^{II}(C_2F_5)$_2$ and *cis*-(**L3**)$_2$Ni(C_2F_5)$_2$. Deviation from the square planar geometry are present in *cis*-(**L3**)Ni^{II}(C_2F_5)$_2$ and *cis*-(**L3**)$_2$Ni(C_2F_5)$_2$ while nearly idea square-planar geometry is present in **3**.

Comparison of experimental and calculated EPR spectra for possible Ni^{III} intermediates

Several possible intermediates were geometry-optimized and their EPR spectra were calculated using ORCA.[40-41] The geometries were optimized using M06L[36-37] (unrestricted formalism) and def2tzvp[33, 38] basis set as described above using Gaussian program package. The purpose of this study is to get insight into possible coordination environment and geometry that could give rise to the observed EPR signal rather than to provide direct evidence to the exact nature of intermediate species; it also allows to exclude specific structures from consideration if they produce a clearly different splitting pattern. For comparison and to establish validity of the method, previously reported[14] stable complex $[(\mathbf{L3})_2Ni^{III}(CF_3)_2]^+$ was geometry-optimized (M06L/def2tzvp; methanol/SMD[39]) and its EPR spectrum was calculated in ORCA and compared with experimental parameters (Figure S135 and Table S5).[14] This comparison shows that calculated splitting constant A_N and overall signal pattern (nearly axial signal with splitting from two N) are in qualitative agreement with experimental data (A_N = 17.9 G showing splitting from two N), although g-values in calculated spectrum are not perfectly reproduced and tend to be shifted closer to 2.002 as compared to the experiment, which was also observed in other modeled paramagnetic Ni complexes.[17] The ORCA-calculated parameters are summarized below in Table S5.

Other intermediates were modeled as: $(\mathbf{L3})Ni^{III}$ $(trans\text{-}C_2F_5)_2(OOC_2F_5)$ (intermediate **D** in Scheme 6; x = 1), $(\mathbf{L3})Ni^{III}(trans\text{-}C_2F_5)_2(OH)$ (intermediate **E** in Scheme 6; x = 1, R = H), $(\mathbf{L3})Ni^{III}(trans\text{-}C_2F_5)_2(O_2^-)$ (superoxide adduct modeled as a triplet), and bis-ligated $(\mathbf{L3})_2Ni^{III}(C_2F_5)_2(OOC_2F_5)$ (intermediate **D** in Scheme 6, x = 2). The calculated spectra, optimized geometries and calculated EPR parameters are given below in Figures S136-137 and Table S6.

The comparison of calculated A_N parameters and signal shape shows that the bis-ligated complex $(\mathbf{L3})_2Ni^{III}(C_2F_5)_2(OOC_2F_5)$ does not reproduce experimental splitting pattern, while mono-**L3**-ligated complexes with one exogenous O-donor ligand, either $(\mathbf{L3})Ni^{III}$ $(trans\text{-}C_2F_5)_2(OOC_2F_5)$ or $(\mathbf{L3})Ni^{III}(trans\text{-}C_2F_5)_2(OH)$, show the expected pattern with splitting from only one N-atom, with A_N value closely matching the experimental A_N (16.3 G), although EPR would not allow to distinguish the nature of the exogenous O-donor ligand in these species due to significant similarity. At the same time, superoxide adduct $(\mathbf{L3})Ni^{III}(trans\text{-}C_2F_5)_2(O_2^-)$ shows much smaller calculated A_N values, presumably due to significant spin density localization on a superoxide ligand. Attempted geometry optimization of the analogous bis-ligated superoxide adduct $(\mathbf{L3})_2Ni^{III}(trans\text{-}C_2F_5)_2(O_2^-)$ led to extrusion of O_2 outside of the coordination sphere of Ni showing that such adduct is unlikely to form when both **L3** ligands are coordinated likely due to steric hindrance.

The comparison of Gibbs free energies also shows that peroxo-species **D** is expected to be more stable when only one **L3** is coordinated to Ni (x = 1), with **L3** dissociation from a bis-ligated adduct being more favorable (see Table S7). Based on this and experimentally observed splitting from only one N-atoms, it is likely that in the observed Ni^{III} intermediate, only one **L3** ligand is coordinated to a Ni center.

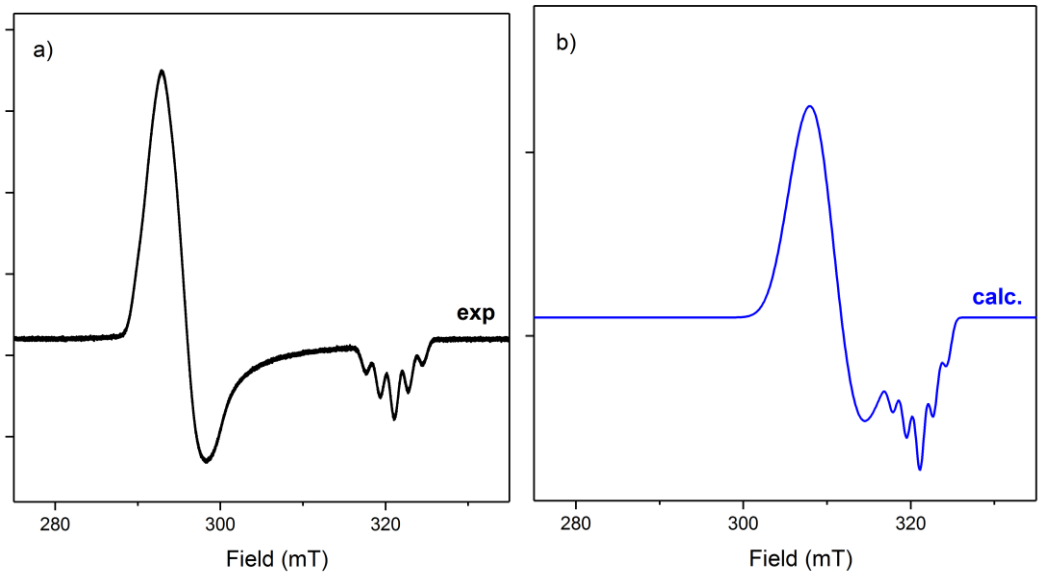

Figure S135. Comparison of (a) previously reported experimental spectrum of $[(\mathbf{L3})_2Ni^{III}(CF_3)_2]^+$ (9.076 GHz) and (b) simulated EPR spectrum visualized in EasySpin using ORCA-calculated g-tensor and A-values for DFT-optimized structure (UM06L/def2tzvp/MeOH) (HStrain parameters used for simulation: 112.996; 133.6; 20.07), same as for figures below for consistent comparison).

Table S5. Experimental and ORCA-calculated g-values and splitting parameters for previously reported $[(\mathbf{L3})_2Ni^{III}(CF_3)_2]^+$.

Complex	g_x; g_y; g_z	$A_{N,xx}$ (G)[a]	$A_{N,yy}$ (G)[a]	A_{Nzz} (G)
Experimental spectrum of $[(\mathbf{L3})_2Ni^{III}(CF_3)_2]^+$	$g_{\perp}$=2.203, $g_{//}$ =2.020,	Not resolved	Not resolved	17.86
Orca-calculated parameters for $[(\mathbf{L3})_2Ni^{III}(CF_3)_2]^+$	2.0974; 2.0939; 2.0203	19.4	16.3	15.9

[a] Splitting for g_x and g_y was unresolved experimentally and were modeled as line broadening in simulated spectrum using ORCA-calculated parameters.

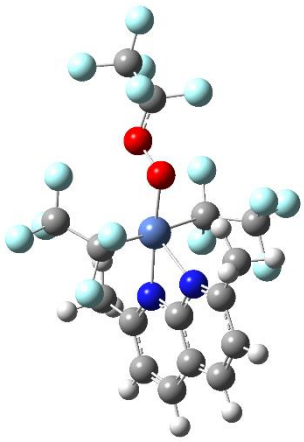

(**L3**)Ni^{III} (*trans*-C_2F_5)$_2$(OOC_2F_5) (intermediate **D** in Scheme 6; x = 1)

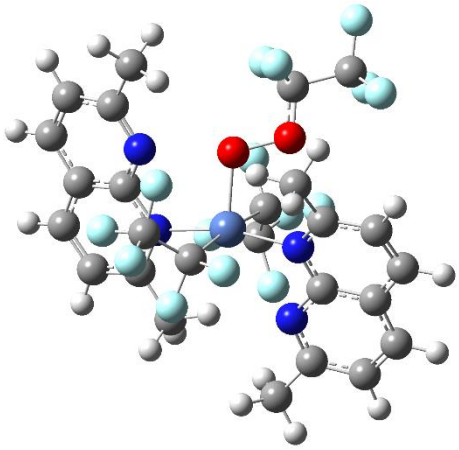

(**L3**)$_2Ni^{III}$ (*trans*-C_2F_5)$_2$(OOC_2F_5) (intermediate **D** in Scheme 6; x = 2)

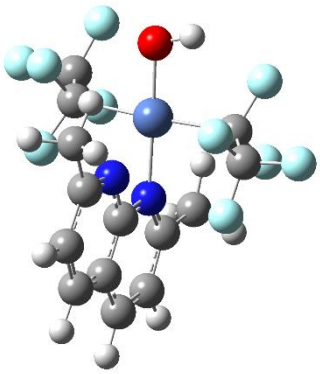

(**L3**)Ni^{III}(*trans*-C_2F_5)$_2$(OH) (intermediate **E** in Scheme 6; x = 1, R = H)

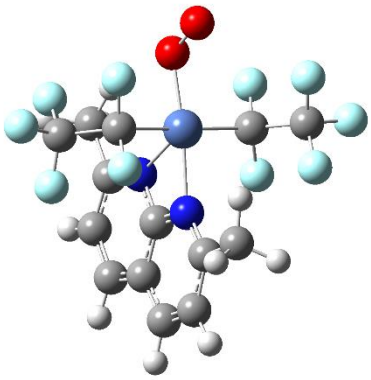

(**L3**)Ni^{III}(*trans*-C_2F_5)$_2$(O_2^-) (superoxide adduct modeled as a triplet)

Figure S136. DFT-optimized geometries for proposed intermediates used for EPR spectra calculations.

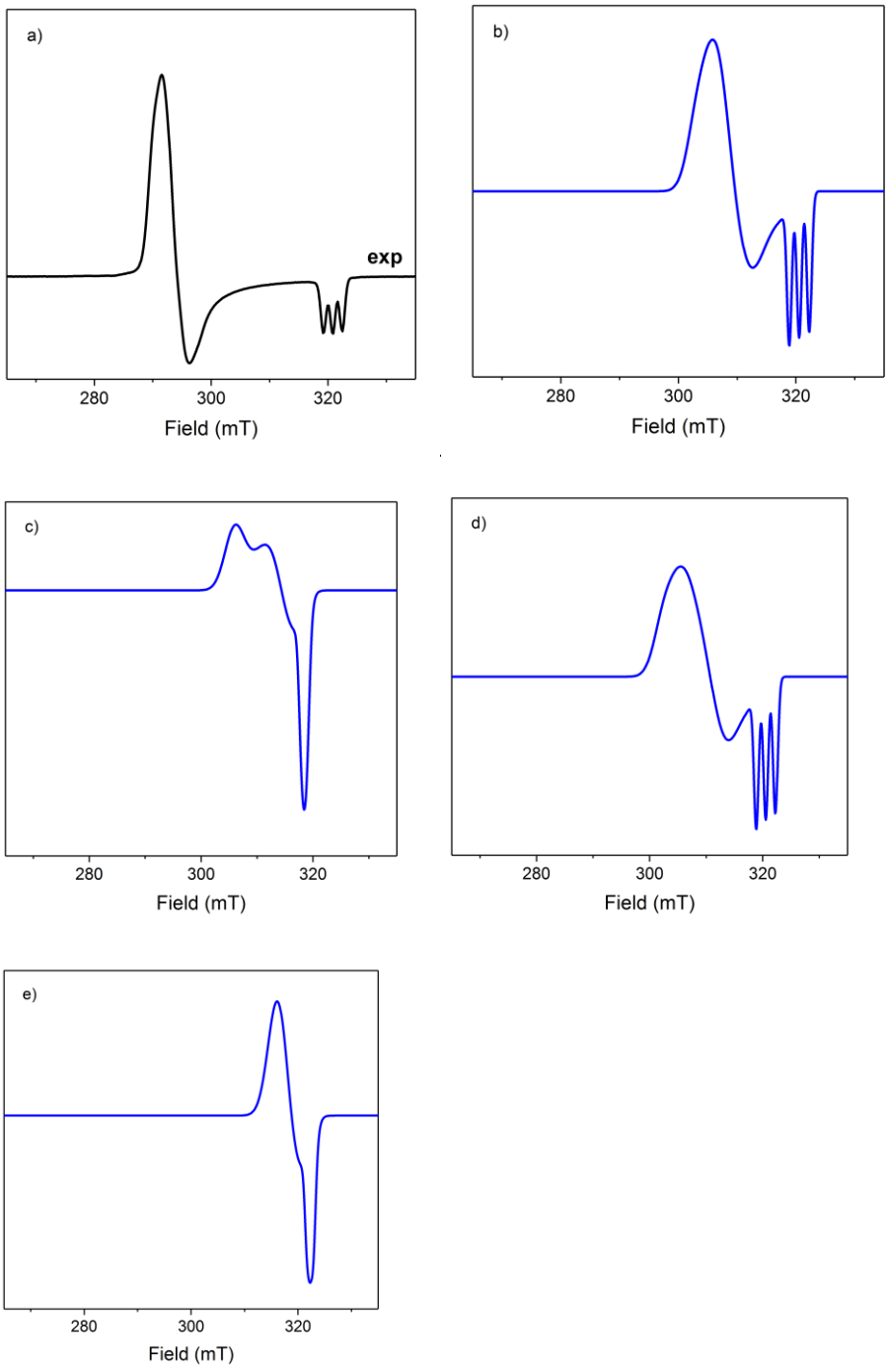

Figure S137. Comparison of (a) experimental EPR spectrum (9.082 GHz) obtained during oxidation of complex **3** with O_2 (see Figure 3 and S102) and simulated EPR spectra visualized in EasySpin using ORCA-calculated g-tensor and A-values for the following proposed intermediates: (b) (**L3**)Ni^{III} (*trans*-$C_2F_5)_2(OOC_2F_5)$, **D** (x = 1), (c) (**L3**)$_2Ni^{III}$ (*trans*-$C_2F_5)_2(OOC_2F_5)$, **D** (x = 2); (d) (**L3**)Ni^{III}(*trans*-$C_2F_5)_2$(OH), **E** (x = 1, R = H); and superoxide adduct (**L3**)Ni^{III}(*trans*-$C_2F_5)_2(O_2^-)$.

Table S6. ORCA-calculated g-values and splitting parameters for geometry-optimized intermediates considered in aerobic oxidation.

Complex	g_x; g_y; g_z	$A_{N,xx}$ (G)[a]	$A_{N,yy}$ (G)[a]	A_{Nzz} (G)
$[(\mathbf{L3})_2Ni^{III}(CF_3)_2]^+$	2.0974; 2.0939; 2.0203	19.4	16.3	15.9
(**L3**)Ni^{III} (*trans*-$C_2F_5)_2(OOC_2F_5)$, **D** (x = 1)	2.1281; 2.0968; 2.0249	21.2	17.7	17.3
$(\mathbf{L3})_2Ni^{III}$ (*trans*-$C_2F_5)_2(OOC_2F_5)$, **D** (x = 2)	2.1210; 2.0659; 2.0388	7.0	5.9	5.7
(**L3**)Ni^{III}(*trans*-$C_2F_5)_2$(OH), **E** (x = 1, R = H)	2.1341; 2.0883; 2.025	20.8	17.6	17.1
Superoxide adduct (**L3**)Ni^{III}(*trans*-$C_2F_5)_2(O_2^-)$	2.0512; 2.0414; 2.0146	8.0	6.6	6.4

[a]Experimentally observed signal during aerobic oxidation of **3**: g_x = 2.228, g_y = 2.206, g_z =2.023 (A_N = 16.3 G).
[b]Splitting along g_x and g_y was not resolved in the experimental EPR spectrum and was modeled as line broadening in simulated spectra using same HStrain parameters as used for simulation of experimental EPR spectrum in Figure S134 (112.996; 133.6; 20.07).

Table S7. Free energy comparison for bis-**L3** ligated intermediate **D** vs. mono-ligated species and a free ligand.

$$(\mathbf{L3})Ni^{III}(C_2F_5)_2(OOC_2F_5) + \mathbf{L3} \longrightarrow (\mathbf{L3})_2Ni^{III}(C_2F_5)_2(OOC_2F_5)$$

D (x = 1) → **D** (x = 2)

Speciation	ΔG, Hartree		Sum of ΔG, Hartree	Relative ΔG, kcal mol^{-1}
(**L3**)$Ni^{III}(C_2F_5)_2(OOC_2F_5)$ + **L3**	-3882.060232	-496.589422	-4378.649654	0
$(\mathbf{L3})_2Ni^{III}(C_2F_5)_2(OOC_2F_5)$	-4378.621654	-	-4378.621654	17.6

References

1. C.-P. Zhang, H. Wang, A. Klein, C. Biewer, K. Stirnat, Y. Yamaguchi, L. Xu, V. Gomez-Benitez and D. A. Vicic, *J. Am. Chem. Soc.*, 2013, **135**, 8141-8144.
2. S. Deolka, R. Govindarajan, S. Vasylevskyi, M. C. Roy, J. R. Khusnutdinova and E. Khaskin, *Chem. Sci.*, 2022, **13**, 12971-12979.
3. R. L. Peterson, R. A. Himes, H. Kotani, T. Suenobu, L. Tian, M. A. Siegler, E. I. Solomon, S. Fukuzumi and K. D. Karlin, *J. Am. Chem. Soc.*, 2011, **133**, 1702-1705.
4. J. A. Turner, *J. Org. Chem.*, 1990, **55**, 4744-4750.
5. E. Kounalis, M. Lutz and D. L. J. Broere, *Chem. Eur. J.*, 2019, **25**, 13280-13284.
6. S. Deolka, O. Rivada-Wheelaghan, S. L. Aristizábal, R. R. Fayzullin, S. Pal, K. Nozaki, E. Khaskin and J. R. Khusnutdinova, *Chem. Sci.*, 2020, **11**, 5494-5502.
7. D. A. McQuarrie, J. D. Simon, H. A. Cox and J. Choi, *Physical Chemistry: A Molecular Approach*, University Science Books, 1997.
8. S. Stoll and A. Schweiger, *J. Magn. Reson.*, 2006, **178**, 42-55.
9. MATLAB (R2016b). Natick, Massachusetts: The MathWorks Inc.
10. A. J. McNeece, K. A. Jesse, J. Xie, A. S. Filatov and J. S. Anderson, *J. Am. Chem. Soc.*, 2020, **142**, 10824-10832.
11. K. Reszka and C. F. Chignell, *Free Radical Res. Commun.*, 1991, **14**, 97-106.
12. G. R. Buettner, *Free Radical Biol. Med.*, 1987, **3**, 259-303.
13. I. Yamazaki and L. H. Piette, *J. Biol. Chem.*, 1990, **265**, 13589-13594.
14. S. Deolka, R. Govindarajan, E. Khaskin, R. R. Fayzullin, M. C. Roy and J. R. Khusnutdinova, *Angew. Chem. Int. Ed.*, 2021, **60**, 24620-24629.
15. E. Lamour, S. Routier, J.-L. Bernier, J.-P. Catteau, C. Bailly and H. Vezin, *J. Am. Chem. Soc.*, 1999, **121**, 1862-1869.
16. D. E. Hamilton, R. S. Drago and J. Telser, *J. Am. Chem. Soc.*, 1984, **106**, 5353-5355.
17. S. Lapointe, E. Khaskin, R. R. Fayzullin and J. R. Khusnutdinova, *Organometallics*, 2019, **38**, 4433-4447.
18. A. S. Brar, A. K. Goyal and S. Hooda, *J. Mol. Struct.*, 2008, **885**, 15-17.
19. V. Nikolaou, A. Anastasaki, F. Alsubaie, A. Simula, D. J. Fox and D. M. Haddleton, *Polym. Chem.*, 2015, **6**, 3581-3585.
20. J. R. Khusnutdinova, N. P. Rath and L. M. Mirica, *J. Am. Chem. Soc.*, 2012, **134**, 2414-2422.
21. M. K. Coggins and J. A. Kovacs, *J. Am. Chem. Soc.*, 2011, **133**, 12470-12473.
22. T. Matsui, S.-i. Ozaki and Y. Watanabe, *J. Am. Chem. Soc.*, 1999, **121**, 9952-9957.
23. T. Matsui, S. Nagano, K. Ishimori, Y. Watanabe and I. Morishima, *Biochemistry*, 1996, **35**, 13118-13124.
24. H. Sigel, K. Wyss, P. Waldmeier and R. Griesser, *J. Coord. Chem.*, 1974, **3**, 235-247.
25. V. S. Shivankar and N. V. J. J. o. S. Thakkar, *J. Sci. Ind. Res.*, 2005, **64**, 496-503.
26. K. A. Jesse, S. W. Anferov, K. A. Collins, J. A. Valdez-Moreira, M. E. Czaikowski, A. S. Filatov and J. S. Anderson, *J. Am. Chem. Soc.*, 2021, **143**, 18121-18130.
27. K. Żamojć, M. Zdrowowicz, P. B. Rudnicki-Velasquez, K. Krzymiński, B. Zaborowski, P. Niedziałkowski, D. Jacewicz and L. Chmurzyński, *Free Radical Res.*, 2017, **51**, 38-46.
28. CrysAlisPro (Rigaku, V1.171.40.54a, 2019) and CrysAlisPro (ROD), Rigaku Oxford Diffraction, Poland (2019).
29. G. Sheldrick, *Acta Crystallogr., Sect. A*, 2015, **71**, 3-8.
30. G. Sheldrick, *Acta Crystallogr., Sect. C*, 2015, **71**, 3-8.
31. O. V. Dolomanov, L. J. Bourhis, R. J. Gildea, J. A. K. Howard and H. Puschmann, *J. Appl. Crystallogr.*, 2009, **42**, 339-341.

32. J.-D. Chai and M. Head-Gordon, *PCCP*, 2008, **10**, 6615-6620.
33. F. Weigend and R. Ahlrichs, *PCCP*, 2005, **7**, 3297-3305.
34. Gaussian 16, Revision C.01, M. J. Frisch, G. W. Trucks, H. B. Schlegel, G. E. Scuseria, M. A. Robb, J. R. Cheeseman, G. Scalmani, V. Barone, G. A. Petersson, H. Nakatsuji, X. Li, M. Caricato, A. V. Marenich, J. Bloino, B. G. Janesko, R. Gomperts, B. Mennucci, H. P. Hratchian, J. V. Ortiz, A. F. Izmaylov, J. L. Sonnenberg, D. Williams-Young, F. Ding, F. Lipparini, F. Egidi, J. Goings, B. Peng, A. Petrone, T. Henderson, D. Ranasinghe, V. G. Zakrzewski, J. Gao, N. Rega, G. Zheng, W. Liang, M. Hada, M. Ehara, K. Toyota, R. Fukuda, J. Hasegawa, M. Ishida, T. Nakajima, Y. Honda, O. Kitao, H. Nakai, T. Vreven, K. Throssell, J. A. Montgomery, Jr., J. E. Peralta, F. Ogliaro, M. J. Bearpark, J. J. Heyd, E. N. Brothers, K. N. Kudin, V. N. Staroverov, T. A. Keith, R. Kobayashi, J. Normand, K. Raghavachari, A. P. Rendell, J. C. Burant, S. S. Iyengar, J. Tomasi, M. Cossi, J. M. Millam, M. Klene, C. Adamo, R. Cammi, J. W. Ochterski, R. L. Martin, K. Morokuma, O. Farkas, J. B. Foresman, and D. J. Fox, Gaussian, Inc., Wallingford CT, 2019.
35. J. B. Foresman and Æ Frisch, Exploring Chemistry with Electronic Structure Methods, 3rd ed., Gaussian, Inc.: Wallingford, CT, 2015.
36. Y. Zhao and D. G. Truhlar, *J. Chem. Phys.*, 2006, **125**, 194101.
37. D. G. Gusev, *Organometallics*, 2013, **32**, 4239-4243.
38. F. Weigend, *PCCP*, 2006, **8**, 1057-1065.
39. A. V. Marenich, C. J. Cramer and D. G. Truhlar, *J. Phys. Chem. B*, 2009, **113**, 6378-6396.
40. F. Neese, *WIREs Computat. Mol. Sci.*, 2012, **2**, 73-78.
41. F. Neese, *WIREs Computat. Mol. Sci.*, 2018, **8**, e1327.